STUDY OF SUN'S ROTATION AND SOLAR ACTIVITY

A Thesis

Submitted for the Degree of

DOCTOR OF PHILOSOPHY

In the Faculty of Science

BANGALORE UNIVERSITY

by

J. JAVARAIAH

INDIAN INSTITUTE OF ASTROPHYSICS

BANGALORE – 560 034

INDIA

SEPTEMBER 2000

DECLARATION

I hereby declare that the matter embodied in this thesis is the result of the investigations carried out by me in the Indian Institute of Astrophysics, Bangalore, under the supervision of Prof. M. H. Gokhale. This work has not been submitted for the award of any degree, diploma, associateship etc. of any university or institute.

[J. JAVARAIAH]

Candidate

21.9.2000

[M. H. GOKHALE]

Supervisor

Bangalore 560 034

Date: September 21, 2000

To
My Parents

Acknowledgments

I am greatly indebted to Prof. M. H. Gokhale who introduced me to this research problem, and took keen interest in all aspects of the work presented in this thesis. Without his great patience in going through the manuscript, this thesis would not have been in readable form.

I am grateful to Prof. R. Cowsik, Director, for providing excellent research facilities. My sincere thanks to Prof. N. Kameswara Rao and Prof. K. R. Sivaraman for the keen interest and moral support. I thank Prof. M. N. Anandaram for help in the University formalities.

I am thankful to Dr. H. Balthasar, Astrophysical Institute, Potsdam, for providing a magnetic tape containing Greenwich data on sunspot groups compiled during 1874–1976. I am thankful to Dr. R. F. Howard, NSO, Tucson, for providing the daily values of the differential rotation coefficients derived from Mt. Wilson Doppler measurements during 1967–1994. I am thankful to Dr. H. M. Antia, TIFR, Mumbai, for providing the values of radial variation of solar plasma rotation rate ($\Omega(r, \lambda)$) determined from BBSO helioseismic data and from GONG data. I am also thankful to Dr. R. Howe, NSO, Tucson, for providing values of $\Omega(r, \lambda)$ determined from SOHO data. I thank Dr. A. V. Raveendran for allowing me to use his MEM program.

I am thankful to Dr. R. W. Komm, NSO, Tucson, for discussion on some of the work presented in this thesis during my visit to NSO, in 1998. He is also co-author to one of my papers and the results of it are presented in Chapter III. I am grateful to Dr. John Leibacher for his support to visit to NSO and encouragement.

I thank my colleagues Mr. B. A. Varghese and Mr. J. S. Nathan for their help in the production of some of the plots using IDL Software and other help at computer.

I thankfully acknowledge many colleagues, especially Drs. K. M. Hiremath, R. Kariyappa, K. B. Ramesh, B. S. Nagabhushana, K. E. Rangarajan and R. T. Gangadhara, who encouraged me during this study.

I am thankful to library staff, for providing me all the required facilities and help in the library. I also thank Mr. P. N. Prabhakara and Mr. A. Elangovan for making xerox copies and Mr. D. Kanagaraj for making the bound volume of the thesis.

I thank my wife, Saraswathi; son, J. Nithyananda and daughter, J. Vatsala, for their cooperation and moral support.

LIST OF PUBLICATIONS

In International Journals

1. 'Sunspot activity as originating in interference of Sun's global MHD oscillations', Gokhale, M. H. and Javaraiah, J. :1990, *MNRAS* **243**, 241–251.

2. 'Global modes constituting the solar magnetic cycle I: Search for Dispersion Relations', Gokhale, M. H., Javaraiah, J., Kutty K. N. and Varghese B. A. : 1992, *Solar Phys.* **138**, 35–47.

3. 'Global modes constituting the solar magnetic cycle II: Phases, Geomagnetic eigen modes and Coupling of field behavior in different latitudes', Gokhale, M. H. and Javaraiah, J.: 1992, *Solar Phys.* **138**, 399–410.

4. 'Global modes constituting the solar magnetic cycle III : Shapes and sizes of sunspot cycle and Maintenance of MHD spectrum by Energy Cascade', Gokhale, M. H. and Javaraiah, J. : 1995, *Solar Phys.* **156**, 157–177.

5. 'Periodicities in the Solar differential rotation, Surface magnetic field and Planetary configurations', Javaraiah, J. and Gokhale, M. H.: 1995, *Solar Phys.* **158**, 173–195.

6. 'Periodicities in the north-south asymmetry of the Solar differential rotation and Surface magnetic field', Javaraiah, J. and Gokhale, M. H. : 1997a, *Solar Phys.* **170**, 389–410.

7. 'Estimation of the depths of initial anchoring and the rising-rates of sunspot magnetic structures from rotation frequencies of sunspot groups', Javaraiah, J. and Gokhale, M. H.: 1997b, *A&A* **327**, 795–799.

8. 'Short term periodicities of the Sun's 'Mean' and differential rotation', Javaraiah, J. and R. W. Komm : 1999, *Solar Phys.* **184**, 41–59.

9. 'Dependence of the meridional motions of sunspot groups on life spans and age of the groups, and on the phase of the solar cycle', Javaraiah, J. : 1999, *Solar Phys.* **189**, 289–301.

10. '22-Year periodicity in the solar differential rotation', Javaraiah, J.: 2000, accepted in *J. Astrophys. Astron.* (a special issue for proceedings of IAU Colloquium 179 held at Kodaikanal, India, during December 13–16, 1999).

In Proceedings: Refereed

1. 'Periodicities in the Sun's "Torsional MHD Oscillations" and Planetary configurations', Javaraiah, J. : 1996, in H. M. Antia and S. M. Chitre (guest eds.) Proc. of the international conf. on ' Windows On The Sun's Interior', *Bull. Astr. Soc. India* **24**, 351–354.

2. 'Short-term periodicities of solar differential rotation', Javaraiah, J. :1998a, in A. Ambastha (guest ed.) Proc. of the PRL Golden Jubilee Workshop on 'Solar Physics in India During the Next Solar Maximum and Beyond', *Bull. Astr. Soc. India* **26**, 316.

3. 'Comparison of rotation frequencies of sunspot groups with the radial gradient of Sun's plasma rotation frequency', Javaraiah, J. and Gokhale, M. H.: 1998, in A. Ambastha (guest ed.) Proc. of the PRL Golden Jubilee Workshop on 'Solar Physics in India During the Next Solar Maximum and Beyond', *Bull. Astr. Soc. India* **26**, 207–209.

4. 'Comparison of periodicities of the Sun's 'Mean' and differential rotation determined from sunspot groups and from Mt. Wilson velocity data', Javaraiah, J. : 1999, in Proc. XVIII annual meeting of Astron. Soc. of India, *Bull. Astr. Soc. India* **27**, 73–74.

5. '4-Day periodic variation in the Sun's meridional flow', Javaraiah, J.: 2000, in Proc. XIX annual meeting of Astron. Soc. of India, *Bull. Astr. Soc. India* **28**, 95–96.

In Proceedings: Unrefereed

1. 'Study of Sun's hydromagnetic oscillations using sunspot data', Gokhale, M. H., Javaraiah, J. and Hiremath, K. M. :1990, in J. O. Stenflo (ed.); Solar Photosphere: Structure, Convection and Magnetic fields, IAU Symp. No.138, 375-378.

2. 'Interpretation of the "Third Harmonic" of the solar magnetic cycle', Gokhale, M. H. and Javaraiah, J.:1990, in E. R. Priest and V. Krishan (eds.); Basic plasma process on the Sun, IAU Symp. No. 142, 119-123.

3. 'Depth dependence of periodicities in solar differential rotation', Javaraiah, J.:1998b, in S. G. Korzennik and A. Wilson (eds.) Proc. SOHO 6/ GONG 98 Workshop: Structure and dynamics of the interior of the Sun and Sun-like stars',(ESA SP-418), P. 809–812.

4. 'Depths of initial anchoring and rising-rates of sunspot magnetic structures', Javaraiah, J. and Komm, R. W.: 1999 (preliminary results presented in GONG' 99 workshop held at Tucson, USA, during March 22-24, 1999.)

ABSTRACT

The mechanism of solar activity has been investigated both from theoretical and observational points of view by many authors. It has been generally accepted that interactions of Sun's convection, rotation and magnetic field play a basic role in the generation of solar activity and solar cycle. However, the details of such an interaction are not yet fully understood (see Rosner & Weiss 1992, and references therein). The discovery of the so called 'torsional oscillations' by Howard & LaBonte (1980) and LaBonte & Howard (1982a) from the analysis of Mt. Wilson Doppler measurements during 1967–1982, stimulated further study of the spatial structure and temporal variation of the differential rotation.

Greenwich Photoheliographic Results (GPR) give a long data base for the studies of the solar activity, solar cycle, solar rotation and other properties of the motions in the solar convection zone. This data base has been used for these studies by many authors for a long time. In this thesis I present studies of solar rotation, solar meridional flow and solar activity from the analysis of the 103 yr GPR sunspot group data, 5 yr (1977–1981) NOAA/USAF sunspot group data and 26 yr Mt. Wilson velocity data (1960–1994). These studies give some interesting and potentially important clues for understanding the physical processes responsible for the solar activity and the solar cycle phenomena.

The thesis is presented in eight chapters. In Chapter I, a brief introduction is given for the present study.

In Chapter II, I present the results obtained from the Legendre–Fourier (LF) analysis of Sun's magnetic field inferred from the GPR sunspot group data during 1874–1976 (Gokhale et al. 1992; Gokhale & Javaraiah 1992, 1995). A magnetic tape of this data was kindly provided to us by Dr. H. Balthasar. From sunspot group data we inferred the rate of emergence of toroidal magnetic flux above the Sun's surface, per unit latitude interval and per unit time, using Hale's Law of magnetic polarities. Though the sunspot data came only from latitudes $< 35^{\circ}$, we found that the superposition of the main LF terms in the estimated rate of emergence of toroidal magnetic flux not only *reproduces* the butterfly diagrams, but also *predicts* the following large scale characteristics of the weak fields in latitudes $> 35^{\circ}$: (i) the migrations of neutral lines from latitudes $\sim 35^{\circ}$ *upto* $\sim 90^{\circ}$, and (ii) polar field reversals at the correct phase of the cycle. This suggests that the buoyant toroidal magnetic flux tubes, whose emergence above the Sun's surface produces 'sunspot' activity as well as the 'quiet sun' activity, may be created in the Sun by interference of 'global' MHD oscillations /waves represented by the dominant LF terms. The structure of the LF spectrum of these

oscillations/waves and its approximate 'steadiness' suggest that these oscillations are resonating with frequencies forced by some permanent sources of excitation.

In Chapter III, I present periodicities of the Sun's 'mean' and differential rotation rates determined from FFT and MEM analyses of the differential rotation coefficients derived from the 103 yr GPR sunspot group data and 26 yr Mt. Wilson velocity data (Javaraiah & Gokhale 1995; Javaraiah & Komm 1999). We computed the values of the differential rotation coefficients from sunspot group data. We have used the values of the differential rotation coefficients A, B, C derived from the Mt. Wilson velocity data, which were kindly provided by Dr. R. F. Howard. In the latter we focus on the observations obtained after 1981 with reduced instrumental noise. In the photospheric 'mean rotation' $\bar{A}$, determined from the Mt. Wilson velocity data during 1982–1994, we found the periods: 6.7–4.4 yr, 2.2 $\pm$ 0.4 yr, 1.2 $\pm$ 0.2 yr, and 243 $\pm$ 10 day (with a $\geq$ 99.9% confidence level), which are similar to the periods found in other indicators of solar activity suggesting that they are of solar origin. The 11-yr periodicity is found to be insignificant or absent in $\bar{A}$. In the differential rotation parameters $\bar{B}$ and $\bar{C}$, determined from the same data set, we found only the $\sim$ 11 yr period with a $\geq$ 99.9% confidence level. We have also found a $\sim$ 163 day periodicity in the ratio B/A determined from Mt. Wilson velocity data during 1969–1982. However, it is not found in the data during 1983–1994. Hence, whether this periodicity comes from the error in the velocity data before 1982 or due to some other reason is yet to be confirmed. The time series of $\bar{A}$ determined from the yearly sunspot group data obtained during 1879–1976 is found to be similar to the corresponding time series of $\bar{B}$. After correcting for data with large error bars (occuring during cycle minima), we have found periods of 18.3 $\pm$ 3.0 yr and 7.5 $\pm$ 0.5 yr in $\bar{A}$ and these and a few other short periods (e.g., 3.0 $\pm$ 0.1 yr, etc.) in $\bar{B}$. We found considerable differences in the periodicities of $\bar{A}$ and $\bar{B}$ determined from the velocity data and those determined from the spot group data. Reasons for these differences may be understood if the rotation rates determined from sunspot data represent the rotation rates of the Sun's deeper layers.

In Chapter IV, I present periodicities in the North-South (N-S) asymmetry of the Sun's 'mean' and differential rotation rates determined from the 103 yr GPR sunspot group data (Javaraiah & Gokhale 1997a) and 26 yr Mt. Wilson velocity data. In the N-S asymmetry of $\bar{A}$ and also that of $\bar{B}$ determined from the spot group data we have detected the periodicities : 45 $\pm$11.5 yr, 21.3 $\pm$ 4.5 yr, 13.3 $\pm$ 1.5 yr and 10.5 $\pm$ 0.5 yr. We have also found similar periodicities in the N-S asymmetry of sunspot activity. For the velocity data we have used observations obtained after 1981 with the reduced instrumental noise. The power spectrum of N-S asymmetry of $\bar{A}$ and that of $\bar{C}$ determined from the velocity data during 1982–1994, show peaks at the period 374 $\pm$ 30 day with $>$ 99.9 % confidence level. The spectrum of the N-S asymmetry of $\bar{B}$ shows peaks at the periods 374 $\pm$ 30 day, 78 $\pm$ 2 day and 49 $\pm$ 1 day with

$\geq$ 99 % confidence level. The 7°.17 inclination of the Sun's equator to the ecliptic may be responsible for the 374 day periodicity in the N-S asymmetries of the solar rotation and the differential rotation. Some of the dominant periodicities of the solar differential rotation and its asymmetry happen to match with periods of configurations of dominant planets (Javaraiah & Gokhale 1995; Javaraiah 1996). Hence, in this chapter I also include some speculations on possibility of planetary configurations providing perturbations needed for 'torsional MHD oscillations'.

In Chapter V, I present studies of dependence of the mean rotation frequency of a spot group on its age (t) and dependence of the 'initial rotation' of a spot group on its life span (τ), and compare these with the dependence of plasma rotation frequency ($\Omega(r)$) on the radial distance (r) at different latitudes (λ) as determined from helioseismology. This comparison brings out the following important possibility (Javaraiah & Gokhale 1997b) : (i) The magnetic structures of spot groups which live successively longer by 1 day are initially anchored in layers successively deeper by $\sim$ 21 Mm. (ii) Structures which yield spot groups with life spans 10–12 days are initially anchored near the base of the convective envelope. (iii) For a spot group which lives 10–12 days in latitudes $10° - 20°$ the 'anchoring layer' of its magnetic structure also rises at a rate approximately 21 Mm per day, as the spot group ages. The result (iii) is found to be more realistic for spot groups with average area $A \geq 130$ millionth of the solar hemisphere. For spot groups living 2–12 days, we find a well defined exponential dependence of the average area (A) on the life span (τ). We also find that the distribution of the number of spot groups (N) with respect to τ is nearly exponential. From these relations and the equality of the slopes in the aforementioned $r - \tau$ and $r - t$ relations we have drawn the following tentative inferences : (a) magnetic structures (flux tubes) of spot groups with $A \geq 130$ mh might be generated around base of the convection zone, (b) many of the magnetic structures may be fragmenting (branching) into smaller structures while rising through the solar convection zone, and (c) magnetic structures of spot groups (at least groups with $A < 130$ mh) might be the fragmented (branched) parts of the magnetic structures of larger spot groups. These inferences are consistent with the proposals of some theoretical models (e.g., Parker 1979b).

In Chapter VI, I present the following results obtained from the upgraded Greenwich data during 1879–1975: The equatorial rotation rate (A) is significantly larger in the odd numbered sunspot cycles (ONSCs) than in the even numbered sunspot cycles (ENSCs). The N–S asymmetry in A seems to be large in the ONSCs and less in the ENSCs. The rotation is significantly more differential in the ONSC's than in the ENSC's and the difference is mainly contributed from the southern hemisphere. In the northern hemisphere the difference is marginal. N-S asymmetry in the latitude gradient (B) of rotation is significant in the ENSCs and insignificant in ONSCs. In ONSCs the rotation is more differential in the northern hemisphere than in the southern hemisphere and it

is in opposite sense in the ENSCs. There exists a systematic cycle-to-cycle variation in B, i.e., the magnitude of B in each of the ONSCs is larger than that in its neighboring ENSCs, suggesting existence of 22-year modulation in B. Such a systematic behaviour can also be seen in the cycle-to-cycle variation of A but it is not as well defined as that of B. The trend of variation of A suggests existence of a long period of the order of 100 yr in A. Existence of $\sim$ 80-yr cycle (Gleissberg cycle) in B is seen in the cycle-to-cycle variation of B. The weak 22-year modulation in B seems to be superposed on the relatively strong 80-yr modulation. In order to determine the variations of A and B within the solar cycle, we have used the method of superposed epoch analysis (e.g., Balthasar et al. 1986). This method provides adequate samples of spot groups in different phases of the solar cycle. We found that A varies significantly only during ONSCs with amplitude $\sim 0.01\ \mu\ rad\ s^{-1}$, at minimum years. There exists a good anti-correlation between the variations of B derived from the ONSCs and ENSCs, suggesting existence of a '22-yr' periodicity in B (Javaraiah 2000). The amplitude of variation of B is $\sim 0.05\ \mu\ rad\ s^{-1}$. It seems the known Gnevyshev & Ohl rule (Gnevyshev & Ohl 1948) of solar activity is applicable also to B. The pattern of correlations of A and B with activity also suggests that the each 22-yr "episode" begin with the beginning of an even cycle and ends with the end of the following odd one, as suggested by Gnevyshev & Ohl (1948) from the analysis of sunspot numbers. It is found that in the differential rotation determined from the young groups, the dominant periodicity is '22 yr'. In the differential rotation determined from the old groups and from the short lived groups, the dominant periodicity is '11 yr'. From these results and the estimates of anchoring depths of magnetic structures of spot groups (cf., Chapter V) it is suggested that the periodicities $\sim$ 21 yr and $\sim$ 11 yr in B are dominant in the rotational perturbations in deeper layers ($r \sim 0.7R_\odot$) and shallower layers ($\sim\ r > 0.9R_\odot$), respectively (Javaraiah 1998).

In Chapter VII, I present the results of our following investigations which were made using the data on sunspot groups compiled during 1874–1981 (Javaraiah 1999). We have investigated the following: (i) dependence of the 'initial' meridional motion ($v_{ini}(\tau)$) of sunspot groups on their life span (τ) in the range 2–12 days, (ii) dependence of the mean (over life span) meridional motion ($v(t)$) of sunspot groups of life spans 10–12 days on their age (t) and (iii) dependence of the mean meridional motion of spot groups on the phase of the solar cycle (for this we use the method of superposed epoch analysis). These investigations bring out the following information: In the latitude interval $20^o - 30^o$, the forms of $v_{ini}(\tau)$ and $v(t)$ are largely systematic and mutually similar in both north and south hemispheres. In $v(t)$ there is a suggestion of existence of periodic variation in the meridional motion with period 4-day and amplitude 10–20 m s^{-1}. The meridional flows ($v_e(t)$) determined from the data during the last few days of spot groups of life spans 10–12 days are found to have magnitudes and directions similar to those of the surface meridional plasma flows determined from Dopplergrams

and magnetograms. Existence of N–S asymmetry in $v_e(t)$ is suggested. Using the anchoring depths of magnetic structures for spot groups of different τ and t estimated in Chapter V, we suggest that the patterns of $v_{ini}(\tau)$ and $v(t)$ may represent the spatial structure of the meridional flow in the Sun's convection zone, rather than its temporal variation. The mean meridional motion (v') of sunspot groups seems to vary with the phase of the solar cycle. The velocity is not significantly different from zero during the rising phase of the cycle and there is a suggestion of poleward motion (a few m s^{-1} at lower latitude and $\sim$ 15 m s^{-1} at higher latitudes) during the declining end of the cycle. Existence of N–S asymmetry in the solar cycle dependence of the mean meridional motion of sunspot groups is suggested. The strength of the asymmetry depends on the phase of the cycle. On the average, during $\frac{3}{4}$ of the cycle, the velocity seems to be poleward in the southern hemisphere and equatorward in the northern hemisphere. In latitude interval $20° - 30°$ the 'surface plasma meridional motion', $v_e(t)$, is found to be poleward around maximum years ($v_e(t) \sim 20$ m s^{-1} at 4th–5th year) and equatorward around the declining end of the cycle (about the same magnitude). There exists a reasonable correlation between the solar cycle variation of the average meridional motion v' and the differential rotation coefficients A, B and $\bar{A}$, suggesting existence of coupling in the latitudinal and longitudinal motions, somewhere in the convection zone.

In Chapter VIII, I summarize the results from Chapters II to VII and provide some overall interpretations. The main conclusions are: The LF analysis of sunspot group data presented in Chapter II suggests that the solar activity may be created in the Sun by some kind of 'slow' MHD waves constituting 'global MHD oscillations'. The periodicities in the rotation parameters, the depth dependence of the rotation of sunspot groups (and its temporal variations), and the temporal variations in the meridional motions of sunspot groups (Chapters III–VII) suggest existence of couplings between the spatial (radial, latitudinal and longitudinal) and temporal (few days to few decades) variations of Sun's magnetic field, rotation, and meridional flow. This supports the suggestion that the aforementioned oscillations are 'global MHD oscillations'. The substantial variations in the differential rotation, whose periodicities and parity suggest that these oscillations are torsional in nature. However, more work will be necessary to acquire further insight into the real mechanism of solar cycle. For this purpose we list in the end of Chapter VIII a few important investigations to be undertaken in future.

CONTENTS

Chapter I

INTRODUCTION

It is well known that Sun's radiation and solar activity have influence on the Earth's Atmosphere, Ionosphere, Magnetosphere and space environment. Although activity is observed in many distant stars and galaxies, Sun is the only star whose activity can be seen in enough detail to guide us toward understanding of its mechanism. Indeed the Sun, the nearest star, is the "nearest astrophysical laboratory", where we can learn about fundamental process in astrophysics. Solar physics is essential to give us the necessary background to understand the working of our Universe (Belvedere & Lanzafame 1997). Because of this broad appeal, solar activity and solar cycle phenomena continue to inspire a vast amount of research worldwide.

It has been generally accepted that interactions of Sun's differential rotation and magnetic field play a basic role in the generation of solar activity and solar cycle, but the exact mechanism of solar activity cycle is not yet known. In this thesis I present studies of solar rotation, solar meridional flows and solar activity which give some interesting and potentially important clues for understanding the physical processes responsible for solar activity and solar cycle phenomena.

The main conclusions of this study are as follows: Legendre Fourier (LF) analysis of magnetic field inferred from sunspot group suggests that the solar activity may be created in the Sun by some kind of 'slow' MHD waves constituting 'global MHD oscillations'. Our study of periodicities in the rotation parameters, the depth dependence of the rotation of sunspot groups (and its temporal variations), and the temporal variations in the meridional motions of sunspot groups suggest existence of couplings between the spatial (radial, latitudinal and longitudinal) and temporal (few days to few decades) variations of Sun's magnetic field, rotation, and meridional flow. This supports the suggestion that the aforementioned oscillations are 'global MHD oscillations'. We find substantial variations in the differential rotation, whose periodicities and parity suggest that these oscillations are torsional in nature.

In the next section I give plan of the thesis. In the remaining sections of this chapter I give a brief description of solar activity, solar rotation and meridional motion and review the results of some of the recent studies.

1.1. Plan of the Thesis

In Chapter II, I present our study of global modes of the Sun's MHD oscillations by LF analysis of solar magnetic field inferred from sunspot group data during 1874–1976.

In Chapter III, I present our study of periodicities in the solar differential rotation parameters using the 103 year sunspot data and the 26 year Mt. Wilson velocity data (Mt. Wilson values of coefficients A, B, C were kindly provided by Dr. R. F. Howard). The temporal variations in the differential rotation parameters represent Sun's torsional oscillations of "even-parity" (symmetric about the solar equator). Fast Fourier Transform (FFT) and Maximum Entropy Method (MEM) are used to determine periodicities in the rotation parameters.

In Chapter IV, I present our study of periodicities in the north–south asymmetry of the differential rotation coefficients determined from the spot group data and the Mt. Wilson velocity data. The temporal variations in the north–south asymmetries of the differential rotation parameters represent 'odd–parity' torsional oscillations (i.e., they are anti-symmetric about the solar equator). We also comment on the matching of dominant periodicities of solar differential rotation with periods of configurations of dominant planets.

In Chapter V, we determine the dependence of the rotation of sunspot groups on their life span and age, and compare these dependences with the radial variation of the angular velocity of Sun's rotation. From this we determine the depths of initial anchoring and the rate of radial rise of sunspot magnetic structures. In this chapter, we also study the relation between area and life span of sunspot groups, and the distributions of the number of spot groups (N) with respect to their life span. The importance of the area-life span relation in connection with anchoring depths and rising rates of sunspot magnetic structures is pointed out.

In Chapter VI, using the upgraded Greenwich spot group data during 1879–1975 we determine the following: (i) cycle–to–cycle modulations of the differential rotation parameters and (ii) variations of these parameters during the solar cycle. In the same chapter, we also study the periodicities in the differential rotation by determining it separately from well defined data samples of 'long lived' young and old sunspot groups.

In Chapter VII, from the data on sunspot groups compiled during 1874-1981 we investigate the following: (i) dependence of the 'initial' meridional motion ($v_{ini}(\tau)$) of sunspot groups on their life span (τ) in the range 2–12 days, (ii) dependence of the mean meridional motion ($v(t)$) of sunspot groups of life spans 10–12 days on their age (t) and (iii) dependence of the mean meridional motion of spot groups, (with and without inclusion of second and subsequent appearances of recurrent spot groups), on the phase of the solar cycle.

In Chapter VIII, first I summarize the conclusions from Chapters II to VII and then provide some overall interpretations of the results in Chapters II–VII. More work will be necessary to acquire further insight into the real mechanism of solar cycle. For this purpose I list, in the end, important investigations I plan to undertake in near future.

1.2. Solar Activity

The term "solar activity" applies to a large variety of structures and phenomena in Sun's atmosphere created by interaction of Sun's magnetic field with ionized gases on a variety of length scales and time scales. For example, sunspots, flares, active prominences, which occur in low latitudes and spicules, bright chromospheric emission along the supergranule boundaries, ephemeral bipolar regions, X-ray bright points, etc. which occur at any latitudes in Sun's atmosphere.

Sunspots are the earliest observed solar phenomenon of solar activity. The earliest known records of sunspots observed by naked eye were found in Chinese documents that go back 2,000 years (Wittmann & Xu 1987; Li 1999). Sunspots are essentially small dark areas on the Sun's visible surface (the photosphere). They appear within 35° solar latitudes on either side of the Sun's equator. A sunspot may last from a few hours to several weeks depending on the maximum size it attains. The area of a sunspot is measured in a unit called a millionth of solar hemisphere - briefly, mh ($\approx 3 \times 10^6$ km^2). The typical sizes of sunspots ranges from $\sim$ 10 mh to 10^3 mh. Those exceeding 25 mh generally have a dark core called an umbra occupying the central 15 to 20 per cent of the spot's area. This is surrounded by a less dark region called the penumbra which contains hundreds of radially oriented, densely packed long, thin, dark and bright structures called penumbral filaments. Small dark regions resembling small sunspot umbra without a penumbra are also observed and are called pores. These have lifetimes of few hours to few days only.

Sunspots appear dark because they are only 10 to 20 per cent as bright as the surrounding photosphere. The gases in the umbra and the penumbra have temperatures of about 4000°–5000° K respectively while that of the normal photosphere is about 6000° K. It is believed that sunspots are 'cool' because of their strong magnetic fields, about 3000 G (with magnetic fluxes in the range of 10^{20}–10^{22} Mx), which are thousands of times stronger than the average field in the normal photosphere. Pores have field strengths of 2000–2500 G, with fluxes in the range of 10^{19}–10^{20} Mx.

Although individual sunspots are frequent, most sunspots occur in groups. Spot groups are often large and complex. Depending on their size and complexity spot groups can be classified into number of classes (see Bray & Loughhead 1964). Spots of each group are spread over a generally elongated area called the active region. Most active

regions are bipolar, with two main spots and either surrounding plages of opposite magnetic polarities or a single plage covering both. The main westward spot is called the leading spot and the main eastward spot is called follower spot. The line segment joining the two spots is tilted with respect to the east–west direction making a small angle with the local latitude (on the Sun) such that the leading spot is nearer to the equator. Careful examination of the sunspot data also reveals that the magnitude of this tilt with respect to the east–west direction increases with heliocentric latitudes, from 4° for sunspot pairs located near the equator to 10° at $\sim$ 35° latitude (see also Gilman & Howard 1986; Wang & Sheely 1989). This result is usually known as Joy's Law.

Sunspots are associated with a number of other remarkable solar activity phenomena, such as flares, prominences, filaments, plages etc. (detailed descriptions of solar activity phenomena are given in Zirin 1966; Gibson 1973; Priest 1982).

1.2.1. THE ELEVEN-YEAR SUNSPOT CYCLE

During the years 1826–1851 a German amateur astronomer, Heinrich Schwabe, noted that the yearly number of sunspots systematically decreased and increased alternatively during the periods 1826 to 1830, 1831 to 1837, 1838 to 1843, 1844 to 1848 and 1849 to 1851. He thus discovered " the $\sim$ 11-year sunspot cycle" (which is commonly known as solar activity cycle or solar cycle). Soon after, Wolf (1852) defined the "relative sunspot number" and extended knowledge of its value more than a century into the past by assembling old records. Since then a careful tradition at Zurich has maintained the long term uniformity of this solar activity index (Waldmeier 1961). Detailed information on the solar activity cycle is obtained from a variety of sources. Sunspot observations provide many important details and are available for more than 20 sunspot cycles. In recent decades sunspot observations have been augmented with direct observations of the Sun's magnetic field and we now have nearly continuous observations of the photospheric velocity field as well. These data sets are supplemented by synoptic observations of the Sun's outer layers at wavelengths ranging from the radio to hard x-rays (Hathaway 1998), which include observation at important optical lines Ca II K and H-alpha. Figure 1.1(a) shows the presence of a cycle with an average period of about 11-yr in yearly sunspot numbers from 1870 to the present. The cycles vary in amplitudes, duration or period (cycle length) and shape. The length of a sunspot cycle varies from 9 to 14 years. Most cycles are asymmetric with a rapid rise in numbers from sunspot minimum and a slower decline in numbers from sunspot maximum. Larger cycles tend to rise faster and reach maximum in a shorter time than the smaller cycles (Waldmeier effect).

Sunspot positions reveal additional details about the activity cycle. Such measurements have been routinely obtained at many observatories including Greenwich, Mt.

Wilson, Kodaikanal, and the USAF/NOAA SOON network (cf., http://wwwssl .msfc .nasa .gov /ssl /pad /solar /greenwch.htm). Before the sunspot number of any cycle reaching minimum, sunspots of the new cycle appear at latitude 35° on either side of the equator, and then onwards the mean latitude of sunspots activity systematically migrates towards the equator (Figure 1.1(b), 'Butterfly Diagram'). The equatorward migration of the active latitude bands and the overlaps of cycles near minima are both important features of the activity cycle. The solar activity also shows long–term variation, such as a modulation of about 90 years, called 'Gliesberg cycle'. A large number of minor periodicities in sunspot activity have also been reported (Wolf 1976; Carbonell & Ballester 1992). Many of the periodicities in solar activity happens to coincide with periodicities in planetary configurations (e.g., review by Seymure et al. 1992). Existence of a small north–south asymmetry in the activity is also known. Some authors also reported existence of $\sim$ 11-year periodicity and a few other periodicities in the north–south asymmetry (see e.g., Carbonell et al. 1993 and references therein).

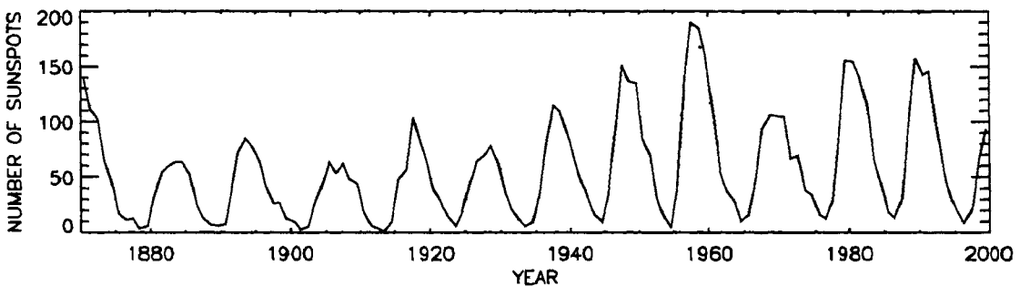

Figure 1.1(a). Yearly sunspot numbers from 1870 to the present (cf., http://www.astro.cma.be /SIDC /DATA /yearssn.dat).

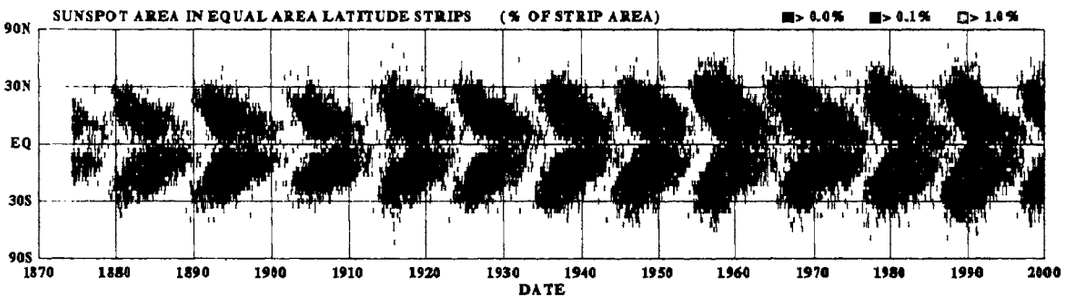

Figure 1.1(b). A Butterfly diagram showing the latitudinal distribution of area of sunspots from 1870 to the present (cf., http://wwwssl.msfc.nasa.gov /ssl /pad /solar /images /bfly.gif).

Periods of suppressed activity like the *Maunder minimum* from 1645 to 1715 and the *Spörer minimum* in the 15th century as well as periods of increased activity such as *current Modern Maximum* and *Medieval Maximum* in the 12th century are known to

have occured. As deduced combining, where available, sunspot and aurora occurrence reports, paleoclimatic and paleomagnetic data and ^{14}C concentration in tree ring, there probably existed ten similar solar activity minima and eight maxima in total since 5300 BC, with significant impact on Earth's climate and geomagnetic activity (Maunder 1922; Eddy 1976, 1978; Ding Youji 1978; see also reviews by Rosner & Weiss 1992, Nesme-Ribes et al. 1996; Polygiannakis et al. 1996). However, even during the Maunder Minimum there are indications that the 11-yr cycle was still at work (Ribes & Nesme-Ribes 1994; Merzlyakov 1997 and references therein).

Several different approaches have been made for understanding, (and predicting, if possible), the short and long-term evolution of the sunspot cycle, through spectral, statistical and morphological studies of sunspot activity (see Polygiannakis et al. 1996, Li 1997 and references therein).

There are several other measures that can be used for studying solar cycle: for example the 10.7-cm radio flux, which comes primarily from the higher levels in solar atmosphere; Mount Wilson magnetic plage strength index (MPSI), Kitt Peak magnetic index (KPMI); and UVI, a measurement of the solar UV variability as determined by the Mg II 280 nm core-to-wing ratio (also visit http://www.sunspotcycle.com).

1.2.2. SOLAR MAGNETIC CYCLE

Photospheric magnetic field measurements reveal the magnetic nature of sunspots and the solar activity cycle. During each sunspot cycle, the magnetic polarity of the leading spots in the north hemisphere is the same as that of the weak field near the Sun's north pole at the beginning of that cycle. A similar rule holds good in the southern hemisphere, wherein polarities are opposite to those in the northern hemisphere. The weak fields in the polar regions themselves reverse their polarities within one or two years after the year of maximum sunspots. Polarity orientations of spot groups in each hemisphere reverse from one sunspot cycle to the next, which was first demonstrated by Hale and his collaborators (Hale et al. 1919). This is known as Hale's Polarity Law. Thus, the Sun's magnetic properties constitute a 22-yr cycle (consisting of two consecutive sunspot cycles) called the 'solar magnetic cycle'.

1.2.3. THE EXTENDED SOLAR CYCLE

The 'butterfly diagrams' show overlap of the old and the new sunspot cycles, near sunspot minima. This has been well known for several years. In view of this and from analyses of coronal green line emission, ephemeral active regions and torsional oscillation signal, Wilson et al. (1988) concluded that sunspot activity is simply the main phase of what they call 'an extended-cycle' (also see Altrock 1997). This 'extended-cycle' begins at high latitudes before the maximum of a sunspot cycle and progress

towards the equator during the next 18–22 year. However, according to Stenflo (1992) the concept of an extended cycle is superfluous and leading to confusion.

1.2.4. THEORY

There are two main approaches for explaining the mechanism of solar cycle, viz., one is based on a turbulent dynamo operating in or immediately below the solar convective envelope and the other is on large scale oscillation superposed on a fossil magnetic field in the radiative core. The dynamo theory has been very well studied by many authors (Parker 1979a, 1993; Roberts 1972; Cowling 1981; Stix 1981, 1991; Dikpati & Charbonneau 1999; see also reviews by Deluca & Gilman 1991; Rosner & Weiss 1992) and the models based on this theory agree with many observed features of solar magnetic activity. With regard to the hydromagnetic oscillator, clear and complete mechanism explaining the large-scale oscillations of the magnetic field has not been found (Piddington 1976; Layzer et al. 1979; Dicke 1979; also review by Rosner & Weiss 1992).

Turbulent Dynamo: Basic idea of the turbulent dynamo theory is that the solar magnetic fields are generated and maintained by complicated nonlinear interactions between the solar plasma and magnetic fields. For a complete solution to this highly nonlinear dynamo problem, it is necessary to solve the full magnetohydrodynamic equations and demonstrate that : (i) there is a velocity field (v) which can maintain an oscillating magnetic field ($\mathbf{B}$); and (ii) this velocity field is itself maintained by the available forces, such as those exerted by convective turbulence and Lorentz force. These two steps involve solving the induction equation and the equation of motion, respectively, under suitable assumptions. Solving both equations simultaneously is extremely difficult. Most work was restricted to the first step alone, which is referred to as the *kinetic dynamo problem* (see Priest 1982).

With a turbulent kinetic dynamo the global properties of the solar magnetic field can be reasonably well described. Such a dynamo consists of two basic elements: (a) differential rotation, which produces a toroidal field (east–west component) by continuously winding up a poloidal field (ω effect), and (b) the 'α-effect' which is induction effect of cyclonic turbulence that regenerates the poloidal (north–south component) field component, and (c) enhancement of diffusion by turbulence. The 'α-effect' effect is crucial in turbulent dynamo models.

Though the models based on turbulent dynamo theory agree with many observed features of the solar cycle, a sufficiently detailed and realistic model of the dynamo process to account for all the different aspects of solar magnetism is not yet available. The available turbulent dynamo models have several difficulties: for example, in such models the role of the differential rotation in the cyclic variation of the solar activity is

not clear (e.g., Gilman 1992). The turbulent dynamo theory requires angular velocity increasing radially inward (e.g., Stix 1981; Parker 1987) whereas helioseismical data show that the angular velocity in the equatorial latitudes is either constant or slightly decreases radially inward throughout the convection zone except in a thin layer at the top (e.g., Brown et al. 1989; Libbrecht 1989; Dziembowski et al. 1989; Goode at al. 1991; Tomezyk et al. 1995; Antia & Chitre 1996; Dalsgaard & Thompson 1999, see also Section 1.3.5). This theory is developed by averaging over turbulent fluctuations. The 'first order smoothening approximation' used in the models of Mean-Field Electrodynamics may not valid on the Sun (for more detail see Priest 1982; Rosner & Weiss 1992).

Oscillator Models: The basic idea of magnetic oscillator models is to consider the observed oscillating large-scale solar poloidal and toroidal field as effects of periodic amplification of primordial fields due to oscillations in the differential rotation rate of the solar interior. The main difficulty in the oscillator models is regarding energetics. No oscillator model offers means of maintaining the oscillations against dissipation of velocity and magnetic fields. There is no observational evidence for the ambient field about which oscillations are claimed to occur or for variations in angular velocity with a 22-year period. Many solar physicists suspect that the Sun is too old and has had too much convection to have fossil field in its radiative core (see review by Rosner & Weiss 1992).

1.3. Sun's Rotation

Study of solar rotation rate and its variation with latitude (the differential rotation) and time is extremely important for understanding the Sun's internal dynamics and solar magnetic activity cycle. The study of solar rotation dates back to the first telescope observation of sunspots and solar rotation is the most studied of solar motion fields. However, the dynamics that produces the differential rotation are still not understood. The well known reviews on theoretical back ground of solar rotation are written by Gilman (1974, 1976) and Dicke (1970) and discussed in detail the theories of the differential rotation, various fluid dynamical models.

Solar rotation has been investigated by a variety of techniques which fall basically in three categories: (i) Doppler-shift measurements of particular spectral lines, (ii) tracking of tracers (like sunspots, sunspot groups, faculae, small magnetic elements, plages, filaments, etc.), and (iii) helioseismical measurement of the Sun's internal rotation. Methods (i) and (ii) are less accurate than the method (iii). But methods (i) and (ii) enable us to study Sun's rotation in the past.

Doppler and tracers measurements agree within a 5% accuracy level, but they do not at 1% level. At this level of accuracy the measured rotation rate depends not only

upon whether Doppler or tracer methods are applied but also upon the choice of line (in Doppler method) and what types of tracers and what characteristic properties (size, age, etc.) of tracers are used. Obviously, the Doppler measurements yield rotation of surface layers. Because of magnetic origin of all solar features their rotation is more likely to represent rotation of deeper layers where the magnetic fields of the features anchored (e.g., Foukal 1972; Schüssler 1987). However, the reason for the discrepancy in the results derived from tracers and from Doppler measurements, and also in the results obtained from different tracers, is not yet clear (e.g., D'Silva & Howard 1994). There are several other significant pitfalls in both Doppler and tracer methods (e.g., see Schröter 1985).

There are several good reviews in the literature on the topic of solar rotation. (e.g., Gilman 1974, 1980; ; Howard 1978, 1984, 1996a; Paternó 1978; Schröter & Wöhl 1978; Schröter 1985, Bogart 1987; Howard et al. 1991, Libbrecht & Morrow 1991; Snodgrass 1992) In the following subsections, I present only a very brief review of studies of solar rotation.

1.3.1. PHOTOSPHERIC DOPPLER VELOCITY MEASUREMENTS

Several observatories have synoptic programs, where full disk velocity measurements are performed daily: Mt. Wilson, Stanford, Kitt Peak, Crimea, etc.. Synoptic programs provide consistent and high accuracy measurements over an extended period of time. For example, Mt. Wilson rotation measurements cover more than three 11-yr cycles from 1967 to the present. Doppler velocity measurements are now routinely obtained by several instruments including those of GONG and those on the SOHO satellite. These observations provide spatial and temporal coverage of the photospheric flows (Hathaway et al. 1996; Hathaway 1996, 1998). Limitations and sources of systematic errors in Doppler measurements are discussed in detail by Schröter (1985).

Livingston (1969) was the first who published comprehensive measurement of solar rotation taken at the Kitt Peak Observatory, covering the period 1966-1968. He obtained the value $13^{\circ}.74$ day^{-1} for the equatorial rotation rate. Subsequently, a number of authors published the values of the rotation rate and the differential rotation rate determined from modern Doppler method (see Table I in the review by Schröter (1985)). The practice of making polynomial fits to the full-disk maps of Doppler data in daily Mount Wilson Magnetograms was started by Howard & Harvey (1970). They fitted the Mt. Wilson data from 350 magnetograms (or Doppler grams) obtained during 1966 1968 to the following form: $\omega(\lambda) = A + Bsin^2\lambda + Csin^4\lambda$, where $\omega(\lambda)$ is the solar rotation at latitude λ, the parameter A represents the equatorial rotation rate, B and C measure the latitude gradient of the rotation rate with B representing mainly low latitudes and C representing largely higher latitudes. They obtained $A = 13.76$, $B = -1.74$ and $C = -2.19$. The units are degrees ($^{\circ}$) day^{-1} sidereal.

1.3.2. ROTATION MEASUREMENTS FROM MAGNETIC STRUCTURES AS TRACERS

Determination of solar rotation using magnetic structures as tracers can be done by tracking relatively stable and long-lived individual magnetic structures, such as sunspots, faculae, plages, which are relatively scarce. When the features are sufficiently plentiful, for example, the small magnetic features in a magnetogram, the rotation can be determined by correlation methods (Wilcox & Howard 1970; Wilcox et al. 1970; Stenflo 1974, 1977, 1989; Sheely et al. 1992; Snodgrass 1983, 1991; Komm et al. 1993a). Sunspots are relatively good tracers of rotation and other motions at the surface in the sense that they are small, relatively well defined and unchanging, and often live for several days or more. Sometime sunspots live long enough to cross the central meridian more than once. An important drawback is that sunspots are confined to low latitude belts.

Heliographic coordinates are an obvious choice for determining accurately the Sun's rotation and meridional motion (north–south motion of solar plasma) by tracer method (Schröter 1985). The accuracy in determination of heliographic coordinates of mass center of a sunspot group is $\sim$ 0°.5 and therefore error in the calculations of daily velocity values is about 1° day^{-1} (1.4×10^4 cm s^{-1}) (Balthasar & Wöhl 1980; Zappalá & Zuccarello 1991; Paternó et al. 1991, Zuccarello 1993). However, error in determination of the mean velocity is inversely proportional to the square root of the number of observations (N) used, it is 0°.07 day^{-1} (9.9×10^2 cm s^{-1}) for $N = 200$.

Carrington (1863) showed, using sunspots as tracers for the first time, that sun has a differential rotation, i.e, the rotation is fastest at the equator and decreasing gradually towards the pole, in both the northern and southern hemispheres. Of all the tracers, sunspots are the most extensively used in the studies of the solar rotation and the solar meridional motion.

Greenwich Photoheliographic Results (GPR) compiled during 1874–1976 give a long data base for the studies of solar activity and the solar cycle, the solar rotation and other properties of motions in solar convection zone. This data has been extensively used by several authors for a long time to determine the solar rotation and the differential rotation (e.g., Newton & Nunn 1951; Ward 1965a; 1966; Godoli & Mazzucconi 1979, Balthasar & Wöhl 1980; Arévalo et al. 1982; Lustig & Dvorak 1984; Balthasar et al. 1986; Tuominen & Virtanen 1987). The other large data sets are Mount Wilson sunspot data set covering the time period 1917-1985 (Howard et al. 1984) and Kodaikanal data set covering the time period 1906–1987 (Sivaraman et al. 1993; Gupta 1994, Howard et al. 1999). Measurements of these data were made using the same technique. Some other data bases are: sunspot drawings of Kanzelhöhe Observatory, data of digitized Ca II K spectroheliograms recorded at Meudon Observatory (Ribes et al. 1985), Solar patrol data of the Catania Observatory (e.g., Ternullo et al. 1981) and sunspot draw-

ings obtained at the National Astronomical Observatory of Japan during 1954–1976 (Kambry & Nishikawa 1990; Yoshimura & Kambry 1993). A distinct advantage of the Mount Wilson and Kodaikanal data sets is that besides positions of spot groups, individual sunspot positions and areas have also been measured. Hence, the rotation and other motions of individual spots, besides spot groups, are also studied from the Mount Wilson and Kodaikanal data sets. The studies based on Meudon Observatory refer to rotation of sunspots. Studies based on Greenwich data generally refer to rotation of sunspot groups.

Newton & Nunn(1951) using the data on long-lived and recurrent sunspots during the years 1978–1944 derived a historic law of the differential rotation,

$$\omega(\lambda) = A + Bsin^2\lambda,$$

where the equatorial rotation rate $A = 14.368 \pm 0.004$ and the latitude gradient of the rotation rate $B = -2.69 \pm 0.04$ (see Schröter 1985). The units are degrees (°) day^{-1} sidereal and λ is heliographic latitude.

In general, most of the previous authors in their statistical studies had only considered recurrent phenomena, whereas Ward (1964, 1965a, b, 1966) also included the young and short-lived non-recurrent sunspots. He found a slight higher equatorial rotation rate and somewhat steeper $\omega(\lambda)$–profile than those found by previous authors. From his studies it also emerged, for the first time, that the solar rotation rate determined from sunspots depends on certain characteristics of the sunspots used. Since then, several attempts have been made by a number of authors to derive the rotation rate accurately using large data sets and to study the rate of rotation of sunspots by classifying the spots according to their classifications, such as, single, bipolar, follower, leader, complex structures, and characteristics, such as, area, life span, age (young and old spots or spot groups), angles of inclinations, etc (see Howard 1984, 1996a; Schröter 1985). These studies yielded several vital clues for the understanding of the dynamics of flows in the solar convection zone and the cyclic activity of the solar magnetic field.

Figure 1.2 (adopted from Snodgrass 1992), shows time-averaged rotation profiles determined using various photospheric indicators that are available. The rotation rate from Doppler measurements is significantly lower than the magnetic and sunspot rates. The slowest rate is coming from the photospheric plages (see also, Snodgrass 1992; Howard 1984; Schröter 1985). It is difficult to establish rotation as a function of height or depth, since it is difficult to establish accurately the height or depth of tracers (Schröter 1985).

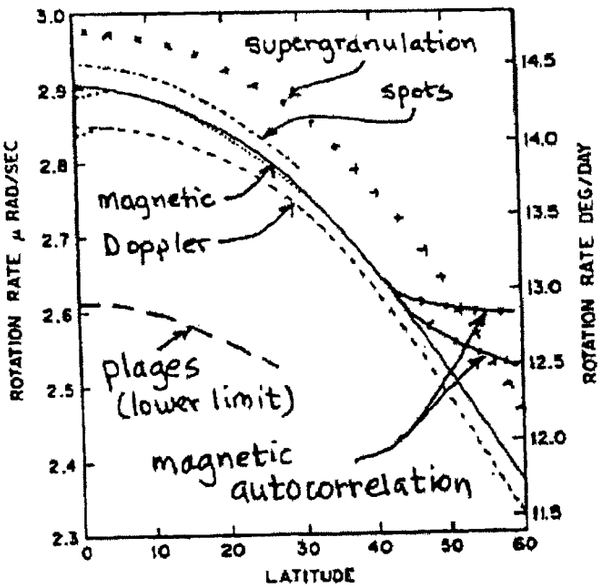

Figure 1.2. Solar rotation profiles using various indicators (adopted from Snodgrass 1992).

1.3.3. NORTH-SOUTH ASYMMETRY IN THE ROTATION OF OUTER LAYERS

Existence of north-south asymmetry in solar activity is shown by several statistical studies for most of the activity phenomena (see Carbonell et al. 1993 and references therein). Small hemispheric difference in the solar rotation is also known (Howard & Harvey 1970; Schröter et al. 1978; Godoli & Mazzucconi 1979; Arévalo et al. 1982; Lustig 1983; Howard et al 1984; Howard & Gilman 1986; Balthasar et al. 1986; Hathaway & Wilson 1990). Antonucci et al. (1990) performed a Fourier analysis of large-scale photospheric features on magnetograms, in different latitude bands, and detected a strong north-south asymmetry. Meunier et al. (1997) analyzed photospheric faculae data over cycle 19 and found existence of a strong north-south asymmetry in the mean rotation rate of faculae. Recently, existence of slight north-south asymmetry in the differential rotation rate is shown also by time-distance helioseismic measurements (Duvall et al. 1998; Giles & Duvall 1998). Hathaway & Wilson (1990) analyzed rotation rate of sunspots from Mt. Wilson sunspot data for individual sunspots during 1923-1975 and found that the southern hemisphere, having fewer spots, rotates faster (by $0.016 \pm 0.004^{\circ}$ day^{-1}) than the northern hemisphere.

1.3.4. TIME DEPENDENCE OF THE ROTATION OF OUTER LAYERS

Since differential rotation plays a important role in producing solar activity, the study of temporal variations in solar rotation might provide vital clue for the mechanism of solar cycle. Many attempts to study the cycle dependence of solar rotation have been made (see Howard 1984 and Schröter 1985 for reviews). The most extensive studies are based upon long time series of sunspots and sunspot groups covering several solar cycles. An 11-year pattern of changes in rotation related to the activity cycle is shown by a number of authors using sunspot data. An increase in the equatorial rotation rate is found at solar minimum (Tuominen & Kyrölaninen 1982; Arvalo et al. 1982; Lustig 1983; Gilman & Howard 1984; Balthasar et al. 1986; Kambry & Nishikawa 1990). The discovery of the so called 'torsional oscillations' by Howard & LaBonte (1980) and LaBonte & Howard (1982a) from the analysis of Mt. Wilson Doppler measurements during 1967–1982, stimulated further study of the spatial structure and temporal variation of the differential rotation. The observed 'torsional oscillations' consist of alternating bands of rotation faster (or slower) than average, and moving in each hemisphere, from high latitudes towards the equator in $\sim$ 22 years (see Figure 1.3). In a given latitude the velocity of torsional oscillation changes its direction from east to west and *vice versa* during 11 years with amplitude of about 3 m s^{-1}. It has also been suggested that the Sun's rotation may be different during the extended minimum periods, such as Maunder minimum (Ribes et al. 1987). However, there is, at present time, no uncontroversial evidence for long term, or secular, changes in the solar rotation rate (Howard et al 1991).

Howard & LaBonte (1980) and LaBonte & Howard (1982a) argued in favor of rotation combined with other convective phenomena driving the dynamo and that the observed torsional oscillations pattern is a direct manifestation of this causal connection. Theoretical models attempt to explain the torsional oscillations pattern by linking it to the equatorward propagation of dynamo waves associated with the activity cycle. Yoshimura (1981) and Schüssler (1981) calculated a pattern by considering the Lorentz force back-reaction of bands of toroidal magnetic field on the surface plasma. Kliorin & Ruzmaikin (1984) show that the Lorentz force from a subsurface dynamo wave could produce the pattern and refute arguments against this model made by LaBonte & Howard (1982a). Rüdiger & Kichatinov (1990) consider the influence of large-scale magnetic fields on Reynolds and turbulent stresses, and find that Lorentz stress is dominated by the microscale feedback due to Reynolds stresses. In this model, the torsional oscillation is a real oscillation associated with the changing viscosity tensor in the presence of the azimuthal magnetic field of the dynamo wave. The authors do not discuss how the pattern produced in this fashion matches the observed torsional pattern. Wilson (1987) and Snodgrass & Wilson (1987) suggest, based on observations, that the torsional pattern is the surface signature of the link between the polar fields

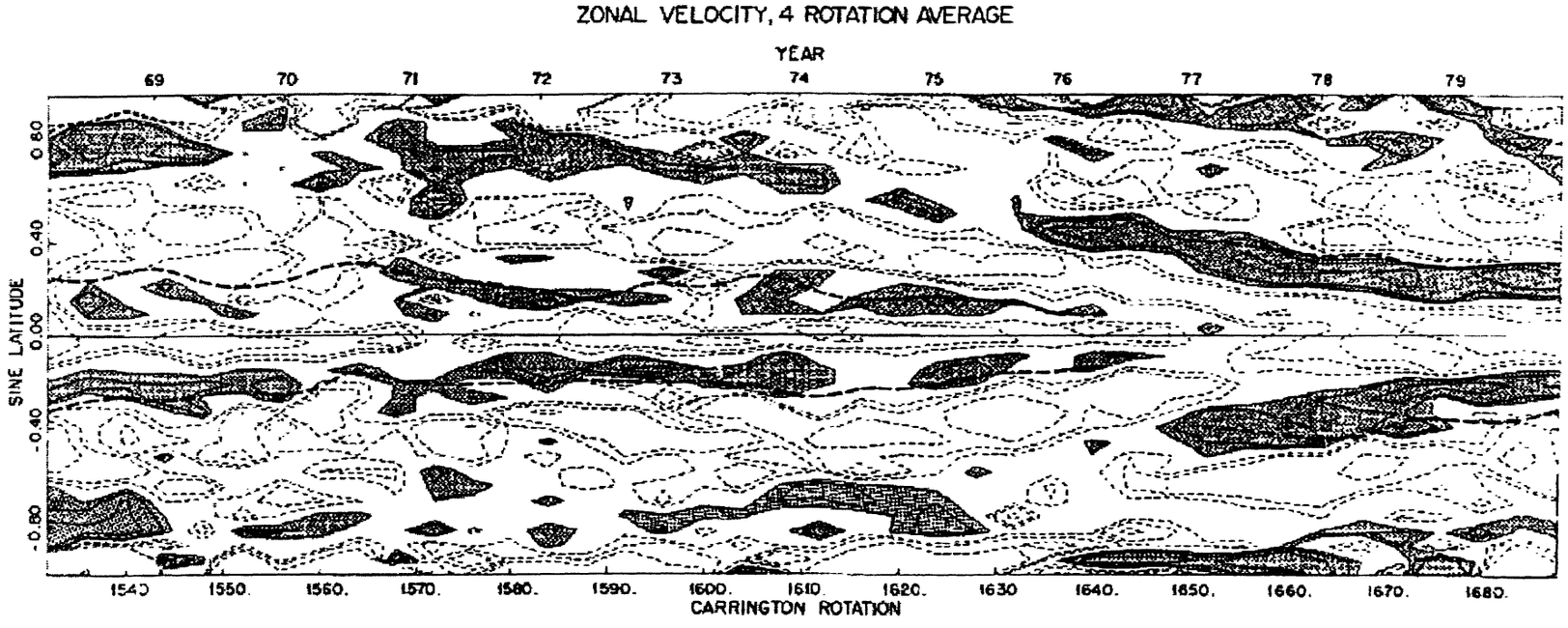

Figure 1.3. Counter plot of the zonal-excess rotation velocity. The zonal excess is the zonal rotation velocity minus a smooth curve fitted to each of 34 independent zones of equal width in sine latitude. The daily values have been averged over independent intervals of four Carrington rotations (109.1012 days) to reduce the random solar noise level. Contour levels are 1.5, 3, and 6 m s^{-1}. Solid contours represent regions of faster rotation (westward flow): dashed contours, slower rotation (eastward motion). Regions of faster rotation have been shaded to render the latitude drift of the velocity bands obvious. The heavy dashed lines mark the latitudes of the maxima of the magnetic flux distribution, observed simultaneously with the velocity data (adopted from Howard & LaBonte 1980).

and the active-region fields. In this model, the zone of enhanced shear is produced by the Coriolis force due to a downflow either from an azimuthal convective pattern or from convergence of meridional flows. A more detailed discussion of this model is presented in Snodgrass (1992). Gilman (1992) proposes that the torsional oscillations are a secondary flow arising from the thermal and mechanical disturbance caused by solar activity and the subsurface toroidal field at certain latitudes.

1.3.5. HELIOSIESMIC MEASUREMENT OF THE SUN'S INTERNAL ROTATION

Helioseismology is a branch of solar physics, in which one uses the knowledge of oscillations of the Sun for probing the Sun's internal structure. Since last two decades this powerful technique has been used to study radial gradient of plasma rotation and other internal properties of the Sun through the study of the solar acoustic modes. The observed frequencies of the solar acoustic (p) modes are used for determining the internal rotation. The observed oscillations are called five-minute oscillations because they have periods in the vicinity of five minutes. The modes of the observed oscillations are distinguished not only by their different frequencies, but also by their different patterns on the surface of the Sun. The p-modes are identified by the radial order n and the spherical harmonic degree l and azimuthal order m, with $2l+1$ possible m values, from $-l$ to $+l$. $|m|$ indicates the number of node circles crossing a line of latitude, while $l-|m|$ gives the number of node circles crossing a line of longitude. Modes of the same l and m but different n have different frequencies, with the spacing between modes of adjacent n being related to the inverse of sound speed. In the absence of rotation the frequencies of the modes of the same n and l are independent of m, owing to absence of any prefered axis. However, rotation breaks this symmetry and remove the degeneracy of the frequencies. Thus the splitting due to the rotation as given by observations is

$$\delta\nu_{nlm} = \nu_{nlm} - \nu_{nl} \quad ,$$

where ν_{nlm} is the frequency of an individual mode and ν_{nl} is the central frequency of the multiplet. For the sake of convenience, the angular frequency $\omega_{nlm} = 2\pi\nu_{nlm}$ can be used instead of ν_{nlm}. The quantity $L = \sqrt{l(l+1)}$ is also commonly used, and ν_{nlm}/L is monotonically related to the lower turning point radius of the (n,l,m) mode. The observed splittings related to the internal rotation in the following way (e.g., Di Mauro et al. 1998)

$$\delta\omega_{nlm} = \int_0^{R_\odot}\int_0^{\pi} K_{nlm}(r,\theta)\Omega(r,\theta)rdrd\theta \quad ,$$

where r is the radial distance from the center and θ is the colatitude. $K_{nlm}(r,\theta)$ are the kernels functions which depend on the equilibrium model quantities and oscillation eigen functions. Thus by knowing observationally determined rotational frequency

splittings and theoretical eigen functions, the internal rotation can be determined. The dependence of splittings on angular velocity can be used in a 2-dimensional inverse problem to probe the Sun's internal differential rotation.

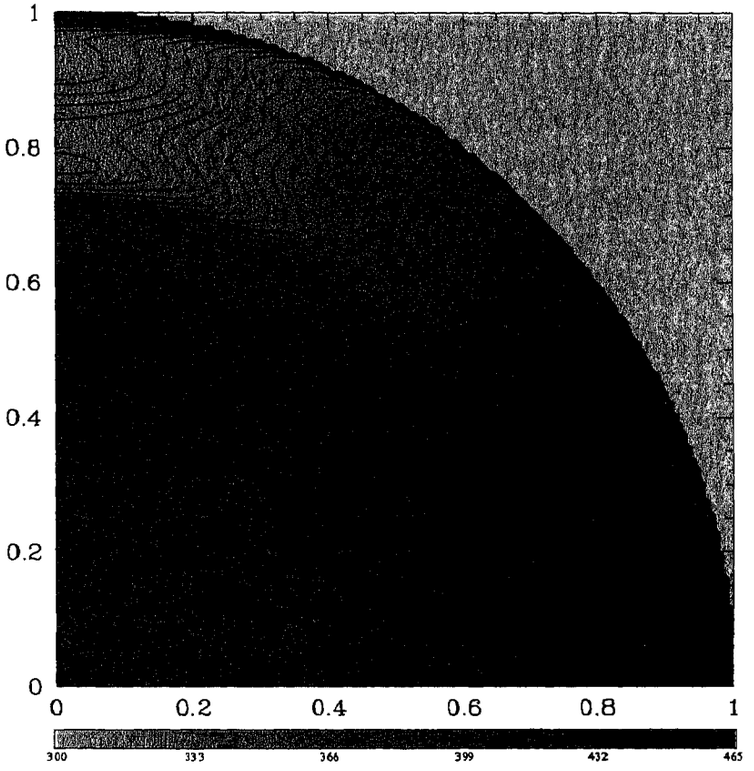

Figure 1.4. A contour diagram of the solar rotation rate as obtained by the 1.5D inversion technique using GONG months 4–14 data. Due to the symmetry of the inversion results, the rotation rate has been shown for just one quadrant only. Contours are drawn at intervals of 5 nHz. The highest level near the equator around $r = 0.9 - 0.95$ is 465 nHz. The red lines are at interval of 5 nHz and blue ones at 20 nHz. The x-axis represents the solar equator while the y-axis represents the rotation axis (curtsey H. M. Antia).

A typical internal rotation profile inferred from heliosismological data is given in Figure 1.4 (kindly provided by H. M. Antia). Note that, the differential rotation exist down to base of the convection zone. The rotation is not constant on cylinders aligned with the rotation axis, as was predicted by simulations in the early 1980s. There is a transition to latitudinally independent rotation near the base of the convection zone, in a layer which has become known as the tachocline (see Kosovichev 1996, Hill 1998). This layer is of interest as it is now thought that the dynamo is located there. Recently, F. Hill reviewed solar cycle dependence of all areas of global helioseismology which

considers oscillations that provide longitudinally-averaged information (Hill 1998).

Some inversions of the odd splitting coefficients appear to show an equatorial rotation rate that does evolve as the cycle phase changes (e.g. Goode & Dziembowski 1991; Woodard & Libbrecht 1993b). Other analyses either conclude that there is no change (e.g. Woodard & Libbrecht 1993a, Schou 1990; Antia et al. 1996) or that the evidence is weak (Gough & Stark 1993b). Recently, using GONG and SOHO data over 4.5 yr time span, Howe et al. (2000a) have detected changes in the rotation near the base of the convective envelope, including a prominent variation with a period of 1.3 yr at low latitudes. Using splitting measurements of the f mode from SOI data, Kosovichev & Schou (1997) and Schou (1998, 1999) have inferred the latitudinal variation of angular velocity. They find some agreement between the features seen in the f-mode inversion and those seen in a measurement of the surface torsional oscillation pattern from GONG data (Hathaway et al. 1996). Using the GONG and SOHO data, Howe et al. (2000b) have shown that the torsional oscillation pattern extend downward at least 60 Mm.

Local helioseismology, in which sections of the solar surface are studied, now provides information on the cellular patterns below the surface (e.g. Hill 1990, Duvall et all. 1997). While supergranulation is readily observed, giant cell convective motion still remain unresolved with these techniques (Hathaway 1998).

1.4. Meridional Circulation

Models of solar activity cycle and solar differential rotation suggest that there might exist solar meridional motion and might play an important role in generation of solar activity cycle and in the maintenance of solar differential rotation (see Schröter 1985). Some of the observed properties of solar activity also suggest existence of meridional motion : for example, the equatorward shift of average activity latitude bin and the observed poleward migration of unipolar magnetic field regions and polar filaments bands, over the solar cycle (Howard et al. 1991). Tracking of tracers (like sunspots, sunspot groups, faculae, plages, prominences, small magnetic features) and direct Doppler measurements are the two principle methods used to measure the meridional flow. Because the magnitude of the meridional flow is at least two order smaller than the rotation speed, it is relatively more difficult to measure (Howard 1996a). Though the existence of meridional flow is confirmed observationally, its magnitude and direction is not clear. Meridional motions derived by using sunspots as tracers generally lead to smaller amplitudes of a few ms^{-1} (see, for example, Balthasar et al. 1986; Howard & Gilman 1986; Lustig & Wöhl 1991), whereas a majority of Doppler measurements suggest a poleward flow of 10–20 ms^{-1} (for example, Duvall 1979; LaBonte & Howard 1982b; Ulrich et al. 1988; Hathaway 1996).

Chapter II

LEGENDRE FOURIER ANALYSIS OF THE SOLAR MAGNETIC FIELD INFERRED FROM SUNSPOT GROUPS

2.1. Introduction

A number of observations suggest that the solar activity may be originating in 'waves'. For example, the well-known 'butterfly diagrams' show that the sunspot activity originates in waves with periods 11-yr (or multiples there of), which propagate from middle latitudes in each solar hemisphere towards the solar equator (Becker 1955, references therein). The observed pattern of so called 'torsional oscillation' is of the form of waves in each hemisphere traveling from high latitudes to the equator in about 22 years with an amplitude of a few ms^{-1} (Howard & LaBonte 1980; LaBonte & Howard 1982a; Snodgrass 1985; Komm et al. 1993a). Poleward migration of weak magnetic field (Howard 1974), prominence belts and polar faculae (Makarov & Sivaraman 1983, 1986) can also be seen to be waves of one-way migrations. It could be that all these waves are in fact global, but appear confined to certain latitudes in their manifestations in the respective observations. Supposing this is true, each wave contributing to the overall pattern would be equivalent to a set of at least approximately stationary global oscillations of the Sun with appropriate phase differences. The following questions would then arise: (i) which set of oscillation modes contributes with appreciable amplitudes; (ii) what are the amplitudes and phases of these modes, (iii) how do the amplitude and phases vary in time, (iv) what is the physical nature of these oscillations, and so on. We discuss these questions in the present chapter.

We inferred sunspot 'occurrence probability' and a rough measure of the underlying 'toroidal magnetic field' during 1874-1976 using Greenwich sunspot group data (kindly provided by H. Balthasar) and Hale's Law of magnetic polarities (Section 1.2.2 of Chapter I). From spherical-harmonic-Fourier (SHF) analysis of these sunspot 'occurrence probability' and 'toroidal magnetic field' we showed that the butterfly diagrams could be a consequence of the near constancy of amplitudes and phases of axisymmetric odd-degree oscillations of period $\sim$ 22 yr in the Sun's magnetic field (Gokhale & Javaraiah 1990a; Gokhale et al. 1990). The amplitude spectrum of these oscillations for degree up to $l = 13$ was shown to be similar to that derived by Stenflo & Vogel (1986) and Stenflo (1988) from magnetogram data during 1960–1985. We have also tentatively inferred that the third harmonic of the 22-yr magnetic cycle might be an artifact of some non-linearity between the field magnitude and the sunspot occurrence

probability (Gokhale & Javaraiah 1990b).

We extended the above study of global modes in the solar magnetic fields, (Gokhale et al. 1992; Gokhale & Javaraiah 1992, 1995), with a refined analysis of the data. The Legendre-Fourier (SHF order $m = 0$) analyses were carried out with the highest temporal frequency resolution ($\sim 1/103$ yr^{-1}) allowed by the length of the whole sequence, and over an extended area of the $\nu - l$ plane, viz., up to $l = 36$ and $\nu = 55/107$ yr^{-1}, where l is the spherical harmonic degree and ν is the temporal frequency. In this chapter I present the results of these extended studies.

In Section 2.2 we describe the data and the method of analysis. In Section 2.3 we present the LF amplitude spectrum of the 'inferred magnetic field', $B_{inf}(\theta, \phi, t)$, as perspective plots, and in Section 2.4 using grey-level representation. In Section 2.5 we identify coherent oscillations in the 'main power ridges'. In Section 2.6 we describe the physical reality of the coherent oscillation modes. In Section 2.7 we compare the results found by us from the sunspot data with the results from the magnetogram data (Stenflo 1988). In Section 2.8 we model the variation of the annual measure of sunspot activity. In Section 2.9 we identify four dominant modes of stationary oscillations. In Section 2.10 we conjecture a phenomenology for maintenance of the Legendre Fourier (LF) spectrum and production of activity. In Section 2.11 we draw conclusions and briefly discuss them.

The mathematical formulation of the SHF analyses of sunspot data (Gokhale & Javaraiah 1990) is given in Appendix 2A.

2.2. Data and Method of Analysis

2.2.1. THE DATA

We have used the data from Ledgers I and II of the Greenwich photographic results (GPR). A magnetic tape of this data for the years 1874-1976 was kindly provided by H. Balthasar. From this data we chose the heliographic coordinates i.e., latitude (λ) and longitude (ϕ), and the time of observation (t) for each day observation of each sunspot group.

2.2.2. DEFINITION OF SUNSPOT OCCURRENCE PROBABILITY

For each time interval (T1, T2) chosen for analysis (e.g., a sunspot cycle or a sequence of years/cycles) we have defined 'sunspot occurrence probability' $p(\mu, \phi, \tau)$ as

$$p(\mu, \phi, \tau) = \begin{cases} \frac{1}{N}\delta(\mu - \mu_i, \phi - \phi_i, \tau - \tau_i) & \text{at } (\mu_i, \phi_i, \tau_i),\ \text{i} = 1, 2, ..., \text{N}, \\ 0 & \text{elsewhere in } (\mu, \phi, \tau) \text{ space.} \end{cases}$$

where $\tau = (t - T_1)/(T_2 - T_1)$, $\mu = cos\theta$, $\theta = 90^\circ - \lambda$, δ represents a delta function in

(μ, ϕ, τ), $N = N(T_1, T_2)$ is the number of data points during the interval (T_1, T_2), and t is the time of observation (in days, including the fraction of the day of the observation) from the *zero* hour of the first day of the interval (T_1, T_2).

Owing to the non-zero (though small) spreads and uncertainties in μ_i, ϕ_i, and τ_i, the delta functions here must be considered as mathematical idealizations of properly normalized 'physical' delta functions of large finite values over small finite domains.

2.2.3. DEFINITION OF 'NOMINAL TOROIDAL FIELD' INFERRED FROM SUNSPOT DATA

A strong toroidal field is essential for production of sunspot activity in general. The toroidal field is not directly measurable, but from the generally bipolar nature of the fields associated with activity, it is believed that the emerging flux is toroidal. Hence, using Hale's laws of magnetic polarities, we define a 'nominal toroidal field', $B_\phi(\theta, t)$, in the following manner (we thank Professor M. Stix for this suggestion):

$$B_\phi(\theta, t) = \begin{cases} \pm p(\theta, t) & \text{in the northern solar hemisphere} \\ \mp p(\theta, t) & \text{in the southern solar hemisphere,} \end{cases}$$

the upper signs being taken during the 'even numbered' sunspot cycles and the lower ones during the 'odd numbered' cycles.

2.2.4. DEFINITION OF THE 'INFERRED MAGNETIC FIELD' IN TERMS OF THE 'FIRST DAY DATA'

Earlier, (Gokhale & Javaraiah 1990a; Gokhale et al. 1990; Gokhale & Javaraiah 1990b), we used the above definitions for sunspot occurrence probability and inferred magnetic field. Later, (Gokhale et al. 1992; Gokhale & Javaraiah 1992, 1995), we modified the definition of the occurrence probability $p(\theta, \phi, t)$ during a time interval (T_1, T_2) as

$$p(\theta, \phi, t) = \begin{cases} \frac{n_k}{N} \delta(\mu - \mu_k, \phi - \phi_k, \tau - \tau_k) & \text{at } (\mu_k, \phi_k, \tau_k) \\ 0 & \text{elsewhere,} \end{cases} \tag{2.1}$$

where θ, ϕ, τ, t and δ have the same meanings as explained in Section 2.2.2. Here the arguments of the delta function $\mu_k = cos\theta_k$, θ_k, ϕ_k and t_k are the values of (μ, ϕ, t) given by the *first day's* observation of the kth spot group, n_k is the overall life span of the kth spot group, in days, and

$$N = \sum_{k=1}^{K} n_k, \tag{2.2}$$

K being the total number of all the sunspot groups observed during the interval (T_1, T_2).

In this modified definition, each spot group is considered as a phenomenon occuring at the heliospheric position where it was *first* observed. As a result, the scatter due to its subsequent proper motions gets eliminated.

Moreover, in this definition the statistical weight of a spot group is proportional to its lifespan rather than the number of days of its observation. Thus, the statistical weights of spot groups get corrected for the gaps in the observations. These corrections are particularly important for the recurrent spot groups.

Similar to the magnetic field defined in Section 2.2.3, the 'inferred' magnetic field $B_{inf}(\theta, \phi, t)$ is then defined here as

$$B_{inf}(\theta, \phi, t) = \pm p(\theta, \phi, t),$$

where the sign, plus or minus, is chosen according to Hale's laws of magnetic polarities of bipolar sunspot groups. Care is taken to separate the data from the old and the new sunspot cycles during the periods of overlaps of successive cycles (next subsection). We find that these refinements improve the accuracy of our results by a few percent.

Another measure of the 'inferred' magnetic field, $B^*_{inf}(\theta, \phi, t)$ is defined by replacing the life spans n_k in Equations (2.1) and (2.2) by the maximum observed areas $A_{max,k}$ of the spot groups as statistical weights of the probability distribution $P(\theta, \phi, t)$.

Resulting Modifications in the Formulae for Computing LF Amplitudes and Phases

The definition of the inferred magnetic field above has led to the following modified formulae for computing the LF amplitudes $A(l, \nu)$ and phases $\varphi(l, \nu)$ of the axisymmetric modes in $B_{inf}(\theta, \phi, t)$ during any specified time interval (T_1, T_2) (for determining the phases of the various modes, the time interval must be at least as long as the period of oscillation):

$$A(l, \nu) = [P_c^2(l, \nu) + P_s^2(l, \nu)]^{1/2} \tag{2.3}$$

and

$$\varphi(l, \nu) = tan^{-1}[P_c(l, \nu)/P_s(l, \nu)] \tag{2.4}$$

(to be chosen 0° and 360° so that $sin\varphi$ and $cos\varphi$ have the correct signs), where

$$P_c(l, \nu) = \frac{C(l, \nu)}{N} \sum_k n_k P_l(\mu_k) cos(2\pi\nu t_k), \tag{2.5a}$$

$$P_s(l, \nu) = \frac{C(l, \nu)}{N} \sum_k n_k P_l(\mu_k) sin(2\pi\nu t_k), \tag{2.5b}$$

where

$$C(l, \nu) = \begin{cases} (2l+1)/2\pi & \text{if } \nu \neq 0, \\ (2l+1)/4\pi & \text{if } \nu = 0. \end{cases} \tag{2.6}$$

2.2.5. SEPARATION OF THE DATA FROM SUCCESSIVE SUNSPOT CYCLES DURING THE PERIODS OF THEIR OVERLAPS

Earlier, (Gokhale & Javaraiah 1990a; Gokhale et al. 1990), we had separated the data of successive sunspot cycles by treating the data before and after the specified dates of sunspot minima as belonging respectively to the old and the new cycles. This had caused wrong signs to be attached in determining B_{inf} from the new cycle data before the dates of minima (and from the old cycle data after the dates of minima), during the few years of overlaps of the successive cycles. In later analyses, (Gokhale et al. 1992, Gokhale & Javaraiah 1992, 1995), we have drawn, in the latitude-time plane, straight lines in the "butterfly wings" which separate completely the data belonging to the old and the new cycles, and have attached signs strictly in accordance with Hale's laws of sunspot magnetic polarities.

2.2.6. THE UNIT OF FREQUENCY (ν_0)

The length of the full data set allows a frequency resolution $\sim 1/103$ yr^{-1}. However, from the drift rates of phases of the axisymmetric modes we have found the mean frequency of these modes to be $1/21.4$ yr^{-1}. Hence, we have taken its integral quotient nearest to $1/103$ yr^{-1}, viz., $\nu_0 = 1/107$ yr^{-1}, as the unit of frequency.

2.3. The LF Amplitude Spectrum of $B_{inf}(\theta, \phi, t)$

2.3.1. THE PERSPECTIVE PLOTS

In Figures 2.1(a) and 2.1(b) we give perspective plots of the SHF amplitudes of the odd and the even degree axisymmetric modes in $B_{inf}(\theta, \phi, t)$ with respect to l and ν up to $l = 36$ and $\nu = 55\nu_0$.

2.3.2. THE SPECTRUM FOR THE ODD DEGREE MODES

It is clear that most of the LF power is concentrated in the odd degree modes with frequencies within $\pm\nu_0/2$ on either side of $\nu_* = 5\nu_0$. (This corresponds to periods in the range 19.8 yr and 23.3 yr.) In this narrow frequency band the spectrum forms a smooth 'ridge' which has a 'main hump' over $l = 1 - 11$, with a high peak at $l = 5, 7$ and a 'tail' for $l > 19$.

There are low, 'subsidiary' ridges along $\nu = 3\nu_*$, $5\nu_*$ and $9\nu_*$. The power concentration in the ridge along $\nu = 3\nu_*$ is expected in view of the asymmetry of the sunspot cycle (e.g., Bracewell 1988). It was shown earlier (Gokhale & Javaraiah 1990b) that the amplitudes and phases of the modes with $\nu = \nu_*$ are correlated to those of the modes of the same l with $\nu = 3\nu_*$. This indicates that the secondary ridge at $\nu = 3\nu_*$ could be a mathematical artifact of some nonlinear dependence of the 'inferred field' on the

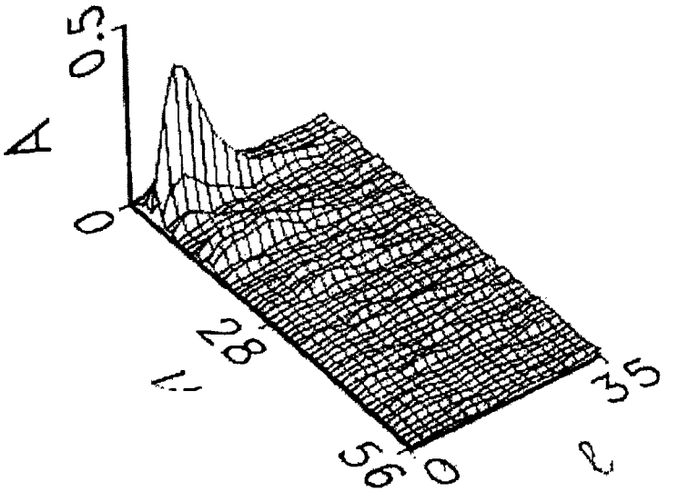

Figure 2.1(a)

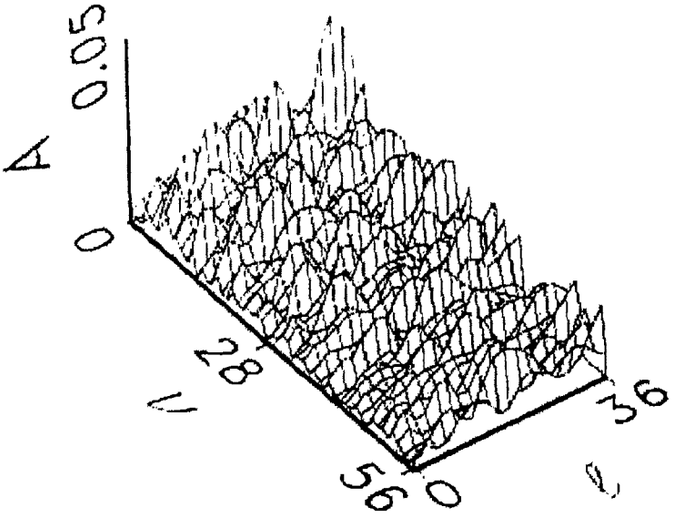

Figure 2.1(b)

Figure 2.1. Perspective plots of the LF amplitude (A) of the modes of (a) odd and (b) even degree, as a function of frequency ν and degree l, in the magnetic field $B_{inf}(\theta, \phi, t)$ as inferred from the sunspot data during 1874–1976 using Equation (2.1). The unit of frequency is 1/107 yr^{-1}. The vertical scales of (a) and (b) are different.

variable representing the basic physical oscillations with frequency ν_*. Alternatively it could also result from common excitation by a single forcing oscillation. These possibilities may be true even for the other subsidiary ridges which seem to represent the set of the higher odd harmonics of ν_*.

It is important to note that in Figures 2.1(a) and 2.1(b), there is no evidence for existence of any general $\nu - l$ relation (free oscillation modes) as hinted from magnetogram data (Stenflo & Vogel 1986). On the contrary power concentration in ridges along specific frequencies suggest 'forced' oscillations.

(The amplitude spectrum of the odd degree modes in the inferred field $B^*_{inf}(\theta, \phi, t)$ obtained by taking in Equation (2.1) statistical weights proportional to the 'maximum observed areas of sunspot groups' instead of their 'life spans' is found to be noisier than the one obtained from $B_{inf}(\theta, \phi, t)$. Thus, the lifespan of a sunspot group gives a clearer information on the global nature of solar cycles than that given by the maximum area.)

2.3.3. THE SPECTRUM FOR THE EVEN DEGREE MODES

The amplitude spectrum for the even degree modes is noisy and the level of power is comparable to that of the noise level in the spectrum for the odd degree modes. There are no power ridges to suggest any $\nu - l$ relation.

2.4. The Grey-Level Representation of the Spectra

For determining whether the local power concentrations in the LF spectra are aligned along any curves in the $\nu - l$ plane, we made image-processed grey-level representations of the power spectra corresponding to the amplitude spectra given in Figure 2.1 using the standard method of hodograph equalization. These representations are shown in Figures 2.2(a) and 2.2(b). Needless to say, equal intensities do not represent equal amplitudes in these figures.

2.4.1. 'APPARENT' EXISTENCE OF $\nu - l$ RELATIONS

These grey level representations indicate a possibility that in each of the power spectra of the odd and the even degree modes, the peaks may lie along a set of curves in the $\nu - l$ plane. One such set of curves, drawn subjectively, is illustrated in the right-hand side panel in each figure. Incidentally, these sets of curves are reminiscent of a similar looking set in the power spectra of the acoustic modes.

The following peculiarities raise doubts about the reality of the existence of the $\nu - l$ relations indicated by the 'curves' in Figures 2.2(a) and 2.2(b):

(i) The power distribution does not give continuous ridges along these curves, and

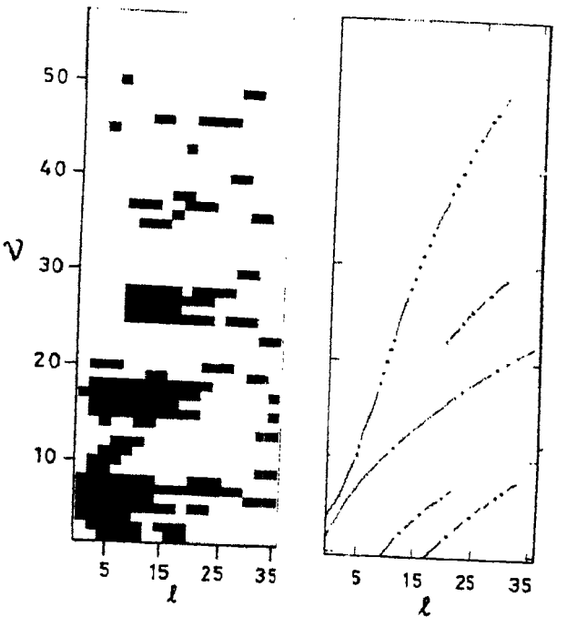

Figure 2.2(a)

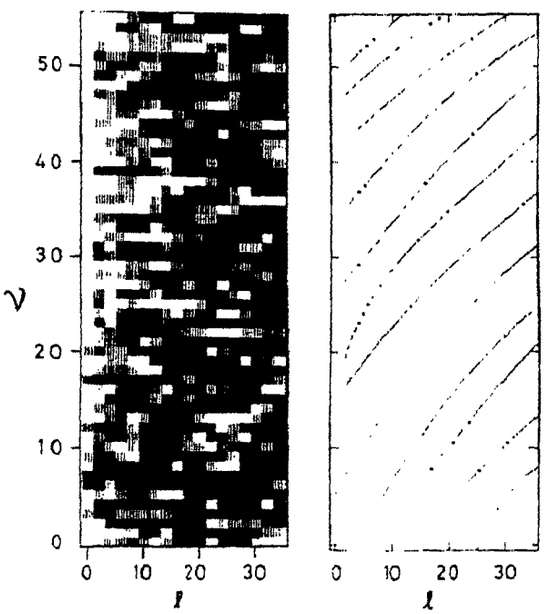

Figure 2.2(b)

Figure 2.2. Image-processed grey-level diagrams representing the LF power spectra corresponding to the amplitude spectra in Figures 2.2(a) and 2.2(b), respectively. The panel on the right side of each diagram shows a set of curves along which the LF power 'appears' to be aligned.

(ii) The curves cannot be drawn unambiguously in an objective manner. In fact some power concentrations can alternatively be considered to be lying along a set of curves with negative slopes.

2.4.2. SPECTRA OBTAINED FROM TWO 'PARTLY RANDOM' SIMULATED DATA SETS

In order to determine whether the apparent alignments of the power concentrations in the SHF spectra have any real significance, we compare these spectra with those obtained from two 'partly random' simulated data sets. In both the simulated data sets, the epochs and the lifetimes of the 'sunspot groups' were assumed to be the same as those in the real data, but the latitudes of sunspot groups 'occurring' during each year and within each butterfly wing, were redistributed within the width of the wing in a random way. Thus, the simulation is random on scales $l \geq 13$ in odd parity.

In doing so, the wings given by the new cycle data in each hemisphere, during the years of overlaps, were treated separately. Hence, the simulations are random on all scales ($l \geq 0$) in the even parity.

In simulation 'I' the latitudes were re-distributed with *Gaussian* probability distributions, with means and standard deviations the same as those in the real data.

In simulation 'II' the redistributions were made with *uniform* distributions over the full widths defined by the yearly minimum and the maximum latitudes of the real data in the respective wings.

Amplitude Spectra Given by the Simulated data sets

Both the simulated data sets SI and SII yield perspective plots of LF spectra similar to those given by the real data and, hence, those plots are not reproduced here. They are low and noisy for the even degree axisymmetric modes and show high, smooth ridges at $\nu = \nu_* = 5\nu_0$, peaking at $l = 5$, 7 (and also low ridges along a few odd harmonics of $\nu = \nu_*$) for the odd degree axisymmetric modes. The ridges given by data sets SI and SII simulate the ridge in Figure 2.1(a) up to $l = 21$ and $l = 35$, respectively. This shows that the distribution of sunspot activity within the butterfly wings is closer to reality in the *uniform probability distribution* than in the Gaussian probability distribution. For odd degree modes with $l \leq 11$, the similarity in the spectra of the real and the simulated data sets are a consequence of the fact that both the simulated data sets have exactly the same temporal distribution as that of the real data and also simulate the butterfly wings in the latitude time distribution.

Grey-Level Representations of the Spectra Given by the Simulated Data Sets

Power concentrations were found to be aligned along several curves even in the grey-

level representations of the spectra obtained from the simulated data sets 'SI' and 'SII'. The presence of power alignments like those seen in 2.2(a) are expected in the region $l < 13$ of the $\nu - l$ plane for odd degree modes since on these scales and in odd parity the simulated data sets retain the systematic properties of the butterfly diagram of the real data. But the power alignments are also reproduced for $l \geq 0$ in even modes and also for $l \geq 13$ in odd modes, on which scales the latitudes are randomly distributed in 'SI' and 'SII'. Hence, the alignments in Figure 2.2 cannot be taken as evidence for any physical relation between the ν and l of the modes in the real data.

2.5. Coherent Oscillations in the 'Main Power Ridges'

2.5.1. VARIATIONS IN THE RELATIVE PHASES OF MODES IN THE 'MAIN POWER RIDGE'

We determined the phases φ_l of the modes l = 1–35 in the 'main power ridge', ($\nu = \nu_* = 1/21.4$ yr^{-1}), during the eighty two intervals (during 1874–1976) each of 22 yr length and displaced by one year relative to the previous interval. As expected from the earlier somewhat cruder analysis (Gokhale et al. 1990), the relative phases $\delta_l (= \varphi_l - \varphi_5)$ are approximately constant. For quantitative comparison of their constancy, we give in Table 2.1 the mean values (δ_l) and the standard deviations ($\Delta\delta_l$) of δ_l for the field inferred from the real data set ('R') and also for fields derived from the two simulated data sets 'SI' and 'SII'.

The data samples during the successive 22-yr intervals are not statistically independent (since they overlap) and, hence, it may be thought that the r. m. s. variations should have been computed from a set of four or five non-overlapping intervals during 1874–1976. However, the mean values and the r. m. s. variations computed from the 82 intervals are equivalent to those computed from non-overlapping intervals with uniform weighting in time. Moreover, we have verified that the r.m.s. variations computed from non-overlapping intervals are actually smaller than those from the eighty-two intervals.

2.5.2. THE STATIONARY, APPROXIMATELY STATIONARY, AND NON-STATIONARY MODES

From Table 2.1 we see that for each data set, the modes in the main ridge fall automatically into three categories:

(1) Stationary Modes : viz., modes with constant phases ($\Delta\delta_l \leq 15°$),

(2) Approximately Stationary Modes: viz., modes with approximately constant phases ($\Delta\delta_l \leq 30°$),

(3) Non-Stationary Modes: viz., modes with large phase variations ($\Delta\delta_l \gg 30°$).

In Table 2.2 we list the modes of each category in the data sets R, SI and SII.

Table 2.1: Mean values $\bar{\delta}_l$ (in degrees) and standard deviations $\Delta\delta_l$ (in degrees) of the relative phases $\delta_l(=\varphi_l - \varphi_5)$ of the LF odd degree modes (SHF order $m = 0$) of frequency $1/21.4$ yr^{-1}, in the magnetic field inferred from real data set R and the simulated data sets SI and SII.

l	R		SI		SII	
	$\bar{\delta}_l$	$\Delta\delta_l$	$\bar{\delta}_l$	$\Delta\delta_l$	$\bar{\delta}_l$	$\Delta\delta_l$
1	7.7	1.4	9.5	4.3	7.9	1.57
3	-174.5	1.0	-173.5	3.2	-174.7	1.12
5	0.0	0.0	0.0	0.0	0.0	8.0
7	170.4	2.1	167.4	8.6	169.3	2.8
9	-27.3	6.0	-30.5	21.8	-32.3	10.0
11	123.0	10.3	139.6	27.9	112.9	16.9
13	93.2	9.6	-35.8	44.7	-99.8	11.5
15	55.4	9.1	-	$\gg 30.0$	75.5	31.9
17	-155.5	10.6	-	-	-87.3	77.4
19	-9.6	14.5	-	-	-	$\gg$30.0
21	142.3	23.1	-	-	-	-
23	-49.2	32.7	-	-	-	-
25	132.2	35.2	-	-	-	-
27	-10.5	25.0	-	-	-	-
29	190.9	27.5	-	-	-	-
31	-4.1	70.4	-	-	-	-
33	147.1	97.6	-	-	-	-
35	92.0	77.9	-	-	-	-

2.5.3. PRESENCE OF FOUR MODES OF 'COHERENT GLOBAL OSCILLATIONS'

Using the complex amplitude A_l (determined in Section 2.3) and relative phases δ_l we have computed the mean relative real amplitudes $a_l(= A_l cos\delta_l)$ and $b_l(= A_l sin\delta_l)$ of the sine and cosine (temporal) phases of the stationary and approximately stationary modes in the field inferred from the real data ('R') and that inferred from the simulated data set 'SII' (the set that simulates the real data more closely : Section 2.4.2). These are given in Table 2.3. In the same table, we also give the r. m. s. variations Δa_l and Δb_l of a_l and b_l. It can be seen that in each phase, there are groups of terms characterized by a range of l in which the respective 'phase-amplitude', a_l or b_l, is maximum near the center and falls off to the noise level (i.e, ≤ 0.04) at both ends. The signs of the successive phase-amplitudes in each group are alternately positive and negative, and this rule breaks at the ends of the respective l-ranges. The level of the r. m. s. variations Δa_l or Δb_l within each group are mutually similar, and different from those in the other groups.

From Table 2.3 it is clear that the field inferred from the real data contains four

Table 2.2: List of modes of each category in the three data sets

Category	R (real data)	SI (Gaussian)	SII (box)
$\Delta\delta_l \leq 15°$	$l = 1 - 9$	$l = 1 - 7$	$l = 1 - 13$
$\Delta\delta_l \leq 30°$	$l = 21 - 29$	$l = 9 - 11$	$l = 15$
$\Delta\delta_l \gg 30°$	$l \geq 31$	$l \geq 13$	$l \geq 17$

independent geometrical modes of *coherent global oscillations* defined by the following expressions:

$$B_1 = \left[\sum_{l=1}^{11} a_l P_l(\mu)\right] sin(2\pi\nu_* t), \quad B_2 = \left[\sum_{l=3}^{17} b_l P_l(\mu)\right] cos(2\pi\nu_* t),$$
$$B_3 = \left[\sum_{l=15}^{29} a_l P_l(\mu)\right] sin(2\pi\nu_* t), \quad B_4 = \left[\sum_{l=21}^{25} b_l P_l(\mu)\right] cos(2\pi\nu_* t). \tag{2.7}$$

Pending identification of the physical nature of these oscillation modes, we call them '*geometrical eigenmodes*'.

2.5.4. ABSENCE OF B_3 AND B_4 IN SIMULATED DATA SETS

The simulated data sets 'SI' and 'SII' do not yield even approximately constant phases for modes beyond $l = 11$ and 15, respectively (see Table 2.1). It is obvious that the field inferred from these data sets cannot contain the geometrical eigenmodes B_3 and B_4. These data sets contain eigenmodes B_1 and B_2 in truncated forms, as illustrated for 'SII' in Table 2.3.

2.5.5. GEOMETRICAL REALITY OF THE MODES $B_1, .., B_4$ IN DISTRIBUTION OF $B_{inf}(\theta, t)$

The simulated data set 'SI' and 'SII' are only illustrative. However, the following points emerge from the above results.

(i) The presence of B_1 and B_2, though in their truncated forms, in the simulated data sets 'SI' and 'SII' is due to the incorporation of approximately real butterfly diagrams in these data sets through prescription of the real annual means and standard deviations for latitudes of sunspot groups within each wing.

(ii) The absence of the 'higher degree' oscillations B_3 and B_4 in SI, and even in the more realistic simulation SII, illustrate the fact that these two oscillations are not

Table 2.3: Mean values (a_l, b_l) and r.m.s. variations (Δa_l, Δb_l) of the amplitudes of the sine and cosine components, respectively, of the LF modes of odd degrees and 21.4-yr periodicity in the magnetic field inferred from two data sets. Groups of a_l and b_l printed in bold (separated by mean values below – or nearly equal to – the level of variation together with the breaks in the alternation of the signs) represent independent coherent global oscillations (denoted by B_1, B_2, B_3, B_4 in text).

l	Real data set				Simulated data set 'SII'			
	a_l	Δa_l	b_l	Δb_l	a_l	Δa_l	b_l	$\Delta b_l a$
1	**0.247**	0.014	0.033	0.008	**0.249**	0.038	0.035	0.019
3	**-0.718**	0.026	**-0.065**	0.014	**-0.724**	0.069	-0.067	0.036
5	**1.00**[a]	0.028	**0.000**[a]	–	**1.000**[a]	0.070	0.000[a]	–
7	**-0.945**	0.081	**0.157**	0.024	**-0.916**	0.249	**0.169**	0.061
9	**0.636**	0.112	**-0.318**	0.035	**0.568**	0.374	**-0.334**	0.087
11	**-0.264**	0.095	**0.390**	0.031	**-0.184**	0.311	**0.385**	0.098
13	0.017	0.056	**-0.345**	0.036	-0.042	0.117	0.298	0.153
15	**-0.152**	0.047	**0.219**	0.044	0.077	0.183	0.142	0.160
17	**-0.171**	0.052	**-0.081**	0.039				
19	**0.137**	0.045	-0.018	0.028				
21	**-0.097**	0.047	**0.064**	0.024				
23	**0.069**	0.057	**-0.066**	0.022				
25	**-0.061**	0.052	**0.044**	0.018				
27	**0.061**	0.035	-0.013	0.019				
29	**0.060**	0.037	0.010	0.024				
31	0.052	0.060	0.015	0.028				

[a] By virtue of definition

present in the simulated data sets since the 'distribution of sunspot activity within the wings of the butterflies is totally random.

We conclude that the distribution of the real sunspot activity even within the wings of butterflies is not random. At least down to scales $l = 29$, it is defined systematically by superposition of the stationary and approximately stationary LF modes of the inferred field.

From the foregoing discussion it follows that the coherent oscillations B_1, B_2, B_3 and B_4 are geometrically significant.

2.6. Physical Reality of the Coherent Oscillation Modes

In this section we see how the observed global latitude-time behaviours of the Sun's various 'magnetic' features, considered as measures of $B(\theta, t)$, can be reproduced by superposition of B_1, B_2, B_3, and B_4 not only in the sunspot or 'low' ($\leq 30°$) latitudes

but also in the 'medium' ($30° - 75°$) and the 'high' ($\geq 75°$) latitudes.

2.6.1. THE LATITUDE-TIME DISTRIBUTION OF $B(\theta,t)$ GIVEN BY B_1+B_2: BUTTERFLY DIAGRAMS AND THE FIELD IN HIGH LATITUDES

We plotted $B(\theta,t)$ as given by

$$B(\theta,t) = B_1(\theta,t) + B_2(\theta,t).$$

We found that in latitudes $\leq 30°$ this produces a butterfly diagram. To some extent this is expected since B_1 and B_2 are obtained from the dominant LF modes in $B(\theta,t)$ which is defined as $\pm P(\theta,t)$ and $P(\theta,t)$ has the form of the butterfly diagrams. However, it is important to note that the butterfly diagram produced by this is *more realistic* than the one obtained by superposing the dominant LF modes (*even degrees* and '11 yr' periodicity) in $p(\theta,t)$ itself, (Gokhale & Javaraiah 1990a), in the following respects:

(i) the shape and the extent of the wings is more realistic,

(ii) the overlaps between the successive sunspot cycles near the sunspot minima are present and are of the right order (viz., $\sim$ 3 yr).

In addition, we notice that moderate flux concentrations in the high latitudes, which may be responsible for the polar facular activity reach maxima near the 'sunspot minima' (i.e., minima of $|B(\theta,t)|$ in the low latitudes), and *vice versa* (Makarov & Sivaraman 1989).

Further, these high latitude field concentrations, considered collectively in latitudes above 70°, change signs around the 'sunspot maxima', i.e., at about the same time as (and also by same sense as) the observed polar fields do.

Thus the LF modes B_1 and B_2 in the inferred magnetic field '$B_{inf}(\theta,t)$' give a more realistic and more global description of the solar cycle phenomenon than that given by the dominant modes in the 'sunspot occurrence probability'.

2.6.2. THE LATITUDE TIME DISTRIBUTION OF $B_1+B_2+B_3$: MIGRATION OF NEUTRAL LINES

In the latitude-time diagram given by $B_1(\theta,t)+B_2(\theta,t)$ (described in previous section) we have found that the 'magnetic neutral lines' do not seem to migrate up to the poles as seen in the analysis of H_α spectroheliograms by Makarov & Sivaraman (1989). Instead in the polar region, the migrations were found to be away from the poles.

The latitude-time diagram given by

$$B(\theta,t) = B_1(\theta,t) + B_2(\theta,t) + B_3(\theta,t).$$

gives all the afore-mentioned properties of the $\theta - t$ distribution of $|B_1 + B_2|$ which

agree with the observed global behaviour of the surface distribution of solar magnetic field. In addition, this also produces migrations of 'magnetic' neutral lines from the middle latitudes to poles in a way similar to those deduced by Makarov & Sivaraman (1989). To migrate from $\sim 35°$ to poles these neutral lines take 15 yr, i.e., same as the real neutral lines.

2.6.3. THE LATITUDE TIME DISTRIBUTION OF $B_1 + B_2 + B_3 + B_4$

In Figure 2.3 we show the $\theta - t$ diagram given by

$$B(\theta, t) = B_1(\theta, t) + B_2(\theta, t) + B_3(\theta, t) + B_4(\theta, t).$$

This figure keeps all the 'good' properties of the $\theta - t$ distribution of $|B_1 + B_2 + B_3|$. In addition, it yields, in years around sunspot minima, a somewhat higher ratio of the polar field to the field in the middle latitudes. This is necessary to account for the presence, during such years, of facular activity in high latitudes without its presence in middle latitudes.

Figure 2.3 does not produce the detailed real trajectories of the neutral lines in the $\theta - t$ diagrams as determined by Makarov & Sivaraman (1989). However, the agreement with the observed behaviour of the neutral lines is quite satisfactory, taking into consideration: (i) the uncertainties in the amplitudes and the phases, (ii) the uncertainties in determining the global neutral lines using the H_α spectroheliograms, (iii) the omission of the 'non-stationary' and the higher harmonic LF modes as well as of the small-amplitude even degree modes which are also actually present in the inferred magnetic field, and (iv) the fact that the figure represents a mean pattern over all the 9 sunspot cycles since it uses amplitudes and phases averaged over 103 years.

Thus, all the four eigenmodes B_1 through B_4 are necessary and sufficient to produce a fairly satisfactory 'cleaned image model' of the observed "mean" latitude–time behaviour of the Sun's real magnetic field over nine cycles.

It is important note that this pattern in all latitudes is obtained by superposing LF terms given by spot group data which comes only from low latitudes.

2.7. Comparison with Results from the Magnetogram data

The amplitude and the relative phases of the LF modes $l = 1$–13 determined from the sunspot data are generally similar to those obtained by Stenflo (1988) from the magnetogram data during 1960–1985, which had also given a reasonably good synthetic butterfly diagram. However, the sunspot data have enabled us to study the variations or constancy of the relative phases over the 103 years. Moreover, there are some important differences. (i) The relative amplitude of the mode $l = 1$ is higher (and that of $l = 3$ is

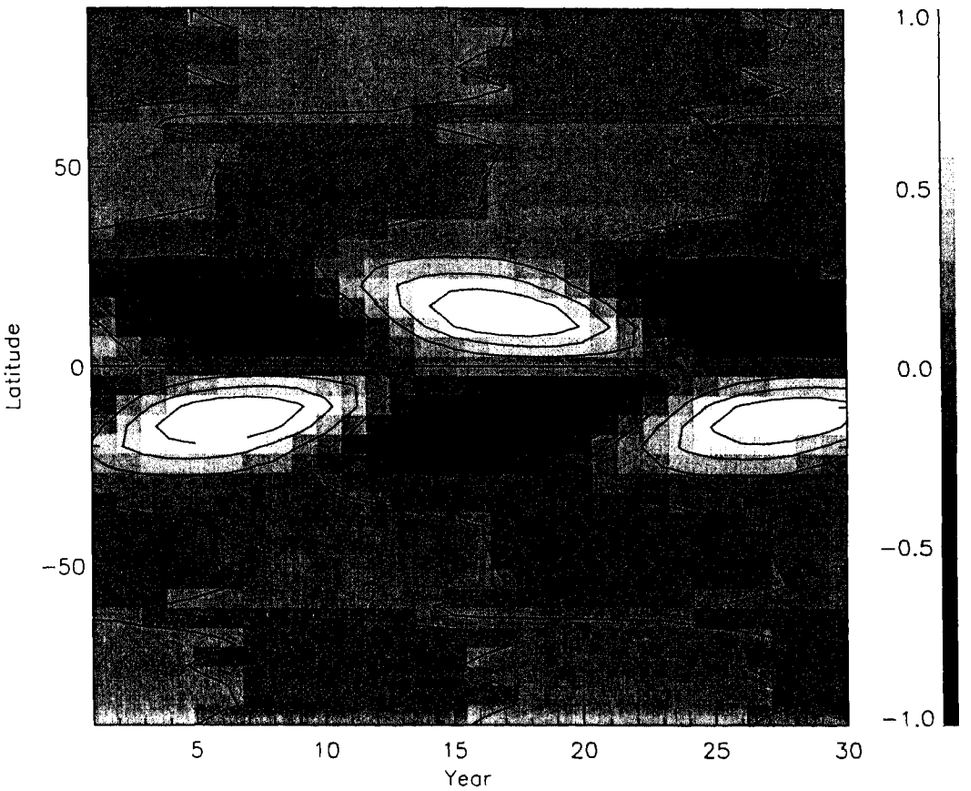

Figure 2.3. Grey level representation of the latitude-time distribution of $B = B_1 + B_2 + B_3 + B_4$ (cf., Section 2.6.3). The different levels of magnitude of B (in arbitrary units) are represented by the different levels of shades (and contours represented by continuous curves) as indicated by the right-hand-side vertical scale. The negative latitudes represent southern hemisphere.

lower) in the fields observed at the surface than in the fields inferred from the sunspot data. We attribute this difference to the fact that, on the surface, a considerable amount of magnetic flux from the 'following' polarities of the active regions spreads into the middle latitudes, thereby transferring 'SHF power' from $l = 5$ and 3 to $l = 3$ and 1, respectively. (ii) In Stenflo's synthetic butterfly diagram the synthesized 'field strength' at the high latitudes is (unrealistically) of the same order as that in the low latitudes. In contrast, the field in the high latitudes in our butterfly diagrams is (realistically) of the same order as, or only slightly stronger, than the weak field in the middle latitudes. This is because the LF modes with $l > 13$, which are present in our synthesis, provide larger degree of interference even in the higher latitudes.

2.8. Modeling the Variation of the Annual Measure of Sunspot Activity

2.8.1. THE 'FLUX EMERGENCE RATE', $Q(\theta,t)$, INFERRED FROM DATA, AND ITS LEGENDRE-FOURIER ANALYSIS

So far the sunspot occurrence probability during any given time interval was normalized to the total amount of activity in that time interval (Section 2.2). Thus the unit of B_{inf} varied from cycle to cycle, depending upon the 'size' of the cycle. This is fine for studying the latitude-time distribution of activity during any single time interval irrespective of the total amount of activity during that interval. However, for modeling the *variation in the rate of production* of sunspot activity the total probability in any given time interval should be proportional to the total measure of activity in that time interval. Hence, we revise the renormalization of sunspot occurrence probability in the following manner.

Consider length scales large compared to the dimensions of the spot groups and time scales large compared to the life spans of the spot groups but small compared to the durations of the sunspot cycles (e.g., length scales $\geq 10^4$ km and time scales $\geq$ a few months). On such scales we define the sunspot occurrence probability, as a function of latitude and time, as follows:

$$\wp(\theta,t) = \begin{cases} \tau_k \delta(\theta-\theta_k, t-t_k) & \text{at } (\theta_k, t_k) \\ 0 & \text{elsewhere,} \end{cases}$$

where θ_k, t_k are the values of θ and 't' for the spot group 'k', τ_k is the life span of the spot group 'k', and δ represents the Dirac delta function. As required, the integral of $\wp(\theta,t)$ over the unit sphere during any time interval is proportional to the measure of sunspot activity during that interval.

This probability function is related to the sunspot occurrence probability function $p(\theta,t)$ of Section 2.2.4 in the following way:

$$\wp(\theta,t) = (\sum_k \tau_k) p(\theta,t),$$

where the summation $\sum_k$ extends over all the spot groups observed during a given time interval, or during a given sunspot cycle.

We take τ_k as a measure of the amount of magnetic flux which emerges above the photosphere (and eventually leaves the Sun), in association with appearance (and disappearance) of the spot group 'k'. From the generally bipolar nature of the fields associated with activity, it is believed that the emerging flux is toroidal.

In analogy to $B_{inf}(\theta,t)$ in Section 2.2.4, we then define a quantity $Q(\theta,t)$ as

$$Q(\theta,t) = \pm\wp(\theta,t), \tag{2.8}$$

where the signs $\pm$ are chosen strictly according to Hale's laws of magnetic polarities with care described in Section 2.5.5. Clearly, on time scales $\geq$ a few months and length scales $\geq 10^4$ km, $Q(\theta,t)$ represents a measure of '*the amount of the toroidal magnetic flux emerging above the photosphere at* (θ,t), *per unit latitude interval per unit time*'. Equation (2.8) can also be written as

$$Q(\theta,t) = (\sum_k \tau_k) B_{inf}(\theta,t).$$

Amplitudes and Phases of Legendre-Fourier Terms during Each Sunspot Cycle

Using the method given Section 2.2.4, we have determined the amplitudes $q(l,n)$ and the phase $\alpha(l,n)$ of the LF terms of odd degrees, $l = 1$ to 29, and frequencies $\nu = n\nu_*$ ($n = 1, 3, 5, 7$) in $Q(\theta,t)$, during each of the nine sunspot cycles between 1879 and 1976. During each cycle, the spectrum of the *relative amplitudes* in 'Q' is similar to (but not the same as) that during the whole sequence of the 103 years. Owing to the above relation between Q and B_{inf}, the latter spectrum is the same as the *relative amplitude* spectrum of B_{inf} Figure 2.1 (Section 2.3.1) during the 103 years.

2.8.2. A MODEL OF TOROIDAL FLUX EMERGENCE AS PROVIDED BY INTERFERENCE OF TORSIONAL MHD OSCILLATIONS

(a) Formation of Toroidal Flux Tubes and Their Emergence

Consider a set of axi-symmetric MHD oscillations (e.g., torsional), each represented, during each cycle, by a set of LF terms, and described collectively by the sets $\{l\}$ and $\{n\}$ of the values of l and n, respectively. The toroidal magnetic field B_ϕ at a point (r,θ), at an instant 't' during a cycle 'i', can be written as

$$B_\phi(i;r,\theta,t) = \sum_{\{l\}}\sum_{\{n\}} b(i;l,n) f_{l,n}(r) \times P_l(\mu) sin[2\pi n\nu_* t + \epsilon(i;l,n)], \tag{2.9}$$

where $b(i;l,n)$ and $\epsilon(i;l,n)$ represent the amplitudes and the 'initial' phases of the terms (l, n) in 'B_{inf}', during the cycle 'i', $f_{l,n}(r)$ is the radial eigenfuction for the mode (l,n) and $\mu = cos\theta$.

At θ and 't' where the interference creates a toroidal flux bundle whose magnetic buoyancy overcomes its magnetic tension, the flux bundle will emerge above the photosphere.

(b) The rate of Emergence of Toroidal Flux

Let τ_{max} be the maximum time required for any such toroidal flux bundle, after its creation, to emerge above the photosphere at all longitudes. Since the large-scale meridional flows in the Sun's radiative core are negligible, the amount of toroidal flux across any meridional section of the radiative core must remain constant. Hence, on time scales $> \tau_{max}$, and less than the diffusion time scales, the amount of the toroidal flux $Q(\theta,t)$, emerging above the photosphere per unit time across a latitude interval $d\theta$, will be given by

$$Q(\theta,t) = \partial \left[\int_0^R B_\phi(r,\theta,t) r d\theta dr \right] / \partial t,$$

where $r = R_{bc}$ is the radius of the base of the convective envelope. Hence, for modeling the sunspot cycles, the flux emergence rate $Q_{mod}(i;\theta,t)$ during any cycle 'i' can be written, using Equation (2.9), as

$$Q_{mod}(i;\theta,t) = \sum_{\{l\}} \sum_{\{n\}} b(i;l,n) g_{l,n}(R_{bc}) \times 2\pi n \nu_* P_l(\mu) cos[2\pi n \nu_* t + \epsilon(i;l,n)], \qquad (2.10)$$

where

$$g_{l,n}(R_{bc}) = \int_0^R f_{l,n}(r) r dr.$$

(c) Relations between the LF Terms in 'Q' and Those in 'B_ϕ

Equation (2.10) can be rewritten as

$$Q_{mod}(i;\theta,t) = \sum_{\{l\}} \sum_{\{n\}} q(i;l,n) \times P_l(\mu) cos[2\pi n \nu_* t + \alpha(i;l,n)],$$

where

$$q(i;l,n) = 2\pi n \nu_* b(i;l,n) g_{l,n}(R_{bc}) \qquad (2.11a)$$

and

$$\alpha(i;l,n) = \epsilon(i;l,n) + \pi/2. \qquad (2.11b)$$

It follows that according to this model, (i) the sets of terms $\{l\}$ and $\{n\}$ of appreciable amplitudes in the LF spectrum of B_ϕ will be same as those obtained through the LF analysis of 'Q', but (ii) owing to the factor $g_{l,n}$ in Equation (2.11a), the ratios of amplitudes ('b's) of different LF terms in 'B_ϕ' may not be same as those of the amplitudes ('q's) of the corresponding terms in 'Q', and (iii) the temporal variations and relative differences in the phases of LF terms in B_ϕ will be same as those in the phases of the corresponding terms in $Q(\theta,t)$.

(d) The Torsional MHD Nature of the Oscillations

The only observed large-scale flows that can, in principle, create toroidal fields are the 'torsional waves' of '11-yr' periodicity (LaBonte & Howard 1982a), or '22-yr' periodicity (Javaraiah & Gokhale 1995; Javaraiah & Komm 1998; Javaraiah 1998; see Chapters III and VI) detected in the photospheric rotation. Rotational perturbations on time scales of years seem to exist even in the solar interior (Dziembowski & Goode 1991). In the presence of even a very weak but sufficiently long-lived poloidal field with $l = 1$ and 3 (e.g., Mestel & Weiss 1987; Spruit 1990; Gokhale & Hiremath 1992; Hiremath 1995; Hiremath & Gokhale 1995), such perturbations would constitute torsional MHD waves.

Thus, if the LF terms in 'B_ϕ' represent global oscillations/waves, then these must be 'torsional' MHD in nature.

2.8.3. METHOD TO MODEL THE 'SHAPES' AND 'SIZES' OF THE INDIVIDUAL SUNSPOT CYCLES BY RECOMBINING ANY PRESCRIBED SET $\{l, n\}$ OF LF TERMS IN 'Q'

It follows from Equation (2.8) that the sunspot occurrence probability *per latitude interval of unit photospheric area per unit time*, at colatitude 'θ', at time 't', will be given by

$$\wp_{mod}(\theta, t) = \mid Q_{mod}(\theta, t) \mid . \tag{2.12}$$

Hence, in a model combining a prescribed set $\{l, n\}$ of LF terms the sunspot occurrence probability, $\wp_{mod}$, at the central epoch 't_{ijk}' of the kth 'month' in the jth year of the ith cycle can be written as

$$\wp_{mod}\{l\}, \{n\}; i, j, k) = T \int_{45^\circ}^{135^\circ} |Q_{mod}(i; \theta, t_{ijk})| sin\theta d\theta$$

$$= 2T \int_{45^\circ}^{90^\circ} | \sum_{\{l\}} \sum_{\{n\}} q(i, l, n) P_l(\mu) sin[2\pi n \nu_* t_{ijk} + \alpha(i, j, k)]| sin\theta d\theta. \tag{2.13}$$

Here the term 'month' means any given 1/12 part of a year and 'T' is its length.

The limits of integration with respect to the colatitude are chosen so as to exclude the low-level flux concentrations outside the sunspot zone which are not strong enough to be seen as sunspot activity (see Section 2.6), and the symmetry of the integrand is used for changing the limits of the integral.

The annual measure of the sunspot occurrence probability is

$$s_{mod}(\{l\}, n, i, j) = \sum_{k=1}^{12} \wp_{mod}(\{l\}, \{n\}; i, j, k). \tag{2.14}$$

The variation of $s_{mod}(\{l\}, \{n\}; i, j)$ with 'j' gives the 'reconstructed shape' of the sunspot cycle 'i' for a given choice of $\{l\}$ and $\{n\}$.

The 'size' of the cycle 'i' in the reconstructed model will then be given by

$$S_{mod}(\{l\},\{n\},i) = \sum_j s_{mod}(\{l\};\{n\},i,j). \tag{2.15}$$

2.8.4. IDENTIFICATION OF THE SET OF SIGNIFICANT LF TERMS IN 'Q' THAT ACCOUNT FOR MOST OF THE OBSERVED SUNSPOT ACTIVITY

According to Parceval's theorem, the size $S_{mod}(i)$ of a sunspot cycle 'i' in the recombination model must be proportional to the total LF power in the set $[\{l\},\ \{n\}]$ of terms taken in Equation (2.13). Thus

$$P(i;\{l,n\}) = \sum_{\{l\},\{n\}} [q(i;l,n)]^2.$$

Starting from a set of lowest l and n, the correlation between $P(i;\{l,n\})$ and the observed size of the cycle i, viz., $S_{obs}(i)$, first increases with inclusion of terms with higher and higher l and n. a stage comes when the correlation starts dropping down due to larger relative errors in the amplitudes of the higher terms. From the maximum correlation we have identified $\{l = 1,\ 3,\ ...,13;\ n = 1,\ 3,\ 5\}$ as the set of LF terms in 'Q' which are significant in modeling by recombination of LF terms. The high ($\sim$ 99.98%) correlation assures that the significant set is adequate to account for most of the observed sunspot activity.

2.8.5. COMPARISON BETWEEN THE MODELED AND THE OBSERVED 'SHAPES'

For each cycle 'i' we have modeled the 'shape' $s_{mod}(i)$ with various choices of $\{l\}$ in the range 1 to 13 and $\{n\}$ in the range 1, 3, 5. This must be compared with the 'observed shape'.

For determining the 'shape' of a cycle 'i' we take the sum $s_{obs}(i,j)$ of the life-spans (in days) of all the spot groups born during the jth year of the cycle 'i' as the measure of the sunspot activity during that year.

For each of several choices of the sets $\{l\}$ and $\{n\}$, we have computed the coefficients of correlation between $s_{mod}(\{l\},\{n\};i,j)$ and $s_{obs}(i,j)$ during each cycle 'i'. We have also computed the correlation between $S_{mod}(\{l\},\{n\},i)$ and $S_{obs}(i)$ for $i = 1$ to 9. The results are given in the next two subsections.

Importance of The Terms with $n = 1,\ 3,\ 5$

We have found that during each cycle 'i' the correlation between the modeled 'shape' $s_{mod}(\{l\},\{n\};i,j)$ and the observed 'shape' $s_{obs}(i,j)$, for $j = 1$ to 11, is $> 80\%$ for any choice of $\{l\}$ in the range $l = 1$ to 13 with $n = 1$. As expected from the asymmetries

of the sunspot cycles (Bracewell 1988), inclusion of corresponding terms with $n = 3$ increases the correlations substantially (e.g., by > 4%). Still further improvement by inclusion of higher terms ($n > 7$) will be negligible since their amplitudes are quite small. Thus, terms of l = 1,....,13 and n = 1, 3 (or n = 1, 3, 5), are adequate for modeling the shapes of the cycles.

The Optimal Set $\{l, n\}$ That Give the best Correlation

Among the high correlations given by the different choices of $\{l, n\}$ with l in the range l = 1,...,13, and n = 1, 3, the subset $\{l = 3;\ n = 1,\ 3\}$ or $\{l = 3,\ 5;\ n = 1,\ 3\}$ gives the highest correlation ($\sim 0.97\%$) between s_{mod} and s_{obs} during each of the nine cycles. The latter subset gives the highest average correlation between the observed and the modeled shapes over the whole sequence of the nine cycles (see Figure 2.4). However, the differences between the correlations given by the two subsets seem too small to be significant (see Table 2.4).

Hence, during every cycle the shape consisting of the eleven observed points (*ten relative values*) can be equally well reproduced by specifying *only four parameters*, viz., the amplitudes and phases of $\{l = 3;\ n = 1,\ 3\}$.

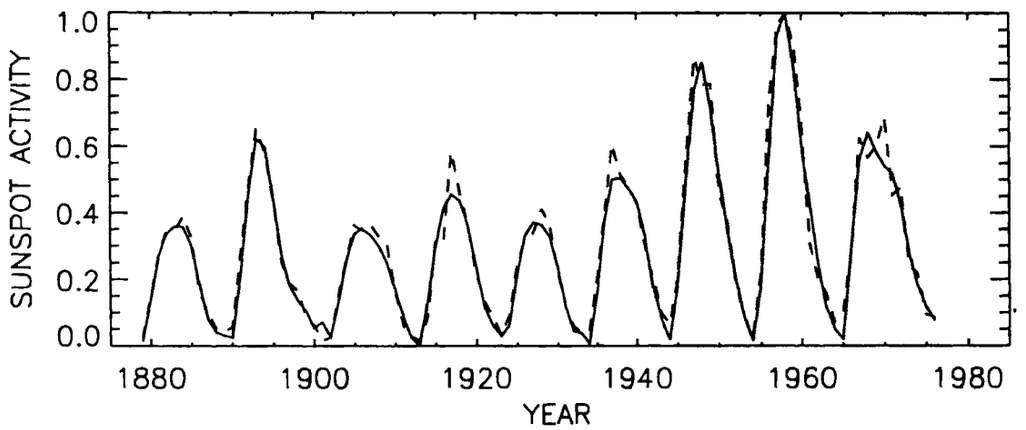

Figure 2.4. Variation of $s_{obs}(i, j)$ (dashed curve), and that of $s_{mod}(i, j)$ (continuous curve), both normalized to their values in 1958, during sunspot cycles i = 12 to 20. For each cycle the model uses amplitudes and phases of only $\{l = 3,\ 5;\ n = 1,\ 3\}$. Agreement from the model using $\{l = 3;\ n = 1,\ 3\}$ only will be almost equally good (see Section 2.8.5).

Table 2.4: The coefficients of correlations between the observed 'shapes' of the cycle (Waldmeier number) $i = 12,\ 13, ..., 20$, and those reconstructed using sets $\{l = 3,\ n = 1,\ 3\}$ and $\{l = 3,\ 5;\ n = 1,\ 3\}$.

Cycle No.	$\{l = 3;\ n = 1,\ 3\}$	$\{l = 3,\ 5;\ n = 1,\ 3\}$
12 (1879-1889)	0.973	0.980
13 (1890-1901)	0.984	0.983
14 (1902-1912)	0.968	0.976
15 (1913-1922)	0.959	0.959
16 (1923-1933)	0.968	0.981
17 (1934-1943)	0.966	0.973
18 (1944-1953)	0.983	0.979
19 (1954-1964)	0.993	0.991
20 (1965-1976)	0.939	0.954
Average	0.970	0.975

2.9. The Stationary Oscillations

2.9.1. HIGH MUTUAL CORRELATIONS BETWEEN THE AMPLITUDES AND PHASES OF TERMS WITH DIFFERENT l BUT SAME n

The high correlations between the modeled and the observed shapes for subset $\{l\} = \{1,\ 3, ...,\ 13\}$ noted in Section 2.8.5 suggest the presence of high mutual correlations among the amplitudes and phases of the LF terms in this range of l for each n. Such high mutual correlations are indeed seen in Figures 2.5 and 2.6 showing, for $n = 1$, the variations in amplitudes $q(l, n)$ and phases $\alpha(l, n)$ respectively, determined from 11-yr intervals successively displaced by 1 yr.

2.9.2. EXISTENCE OF RESONANT AND APPROXIMATELY STATIONARY GLOBAL OSCILLATIONS IN B_ϕ

In view of Equation (2.11b), the phase variations in Figures 2.6 and 2.7 can be considered also as the variations in the phases $\epsilon(l, n)$ of LF terms in B_ϕ.

Further, we see in Figures 2.6 and 2.7 that the terms $l = 1,\ 3, ...,\ 15$, $n = 1,\ 3$ form four separate groups ($l = 1,\ 3,\ 5,\ 7;\ n = 1$), ($l = 9,\ 11,\ 13,\ 15;\ n = 1$), ($l = 1,\ 3,\ 5,\ 7;\ n = 3$), and ($l = 9,\ 11,\ 13,\ 15;\ n = 3$), such that terms within each group $\approx \pm 180°$, and a certain common degree of 'phase constancy'.

Hence, the expression on the right-hand side of Equation (2.9) can be written as four sums, each collecting the terms in each group, and representing a stationary global

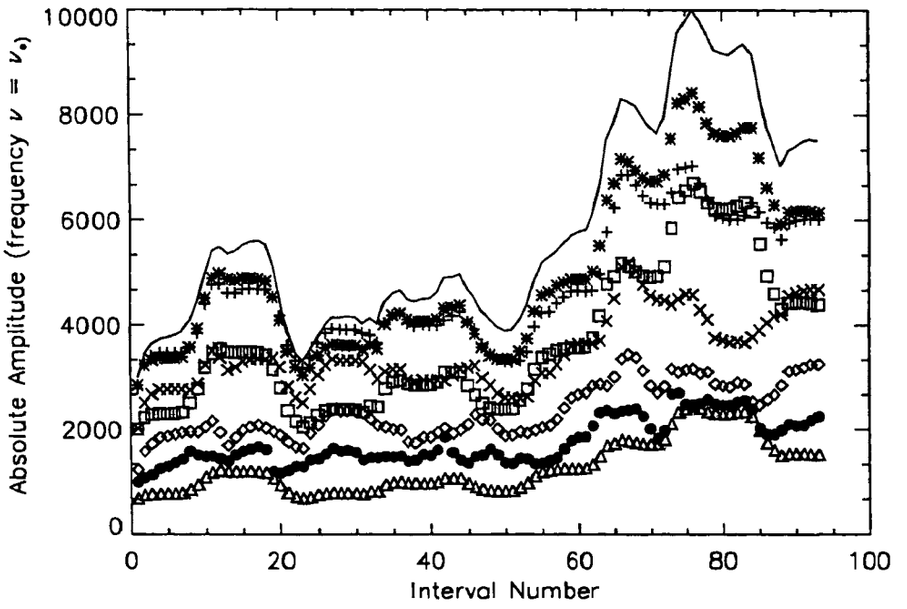

Figure 2.5. Temporal variation of the amplitude $q(l,\ n)$, for $n = 1$, as represented by values during 11-yr intervals successively displaced by 1 yr. The symbols $\triangle$, $\square$, $*$, $+$, $\times$, $\diamond$, and $\bullet$, represent $l = 1, 3, 5, 7, 9, 11$ and 13, respectively. The continuous curve represents the values of the amount of observed sunspot activity (S_{obs}) during the respective intervals.

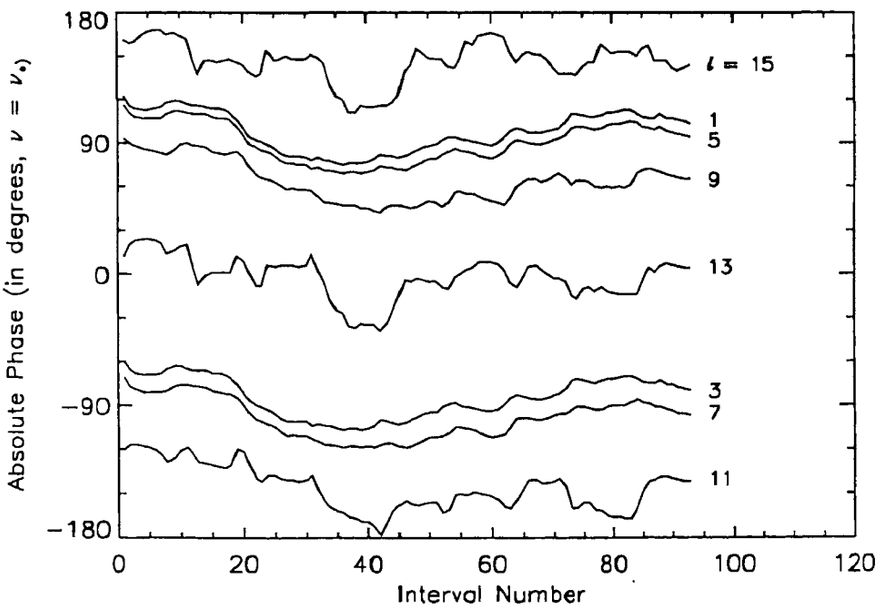

Figure 2.6. Temporal variation of the phases $\alpha(l,\ n)$, or $\varepsilon(l, n)$ of the terms $l = 1, 3,...,15$, all with $n = 1$, during the 11-yr intervals successively displaced by 1 yr.

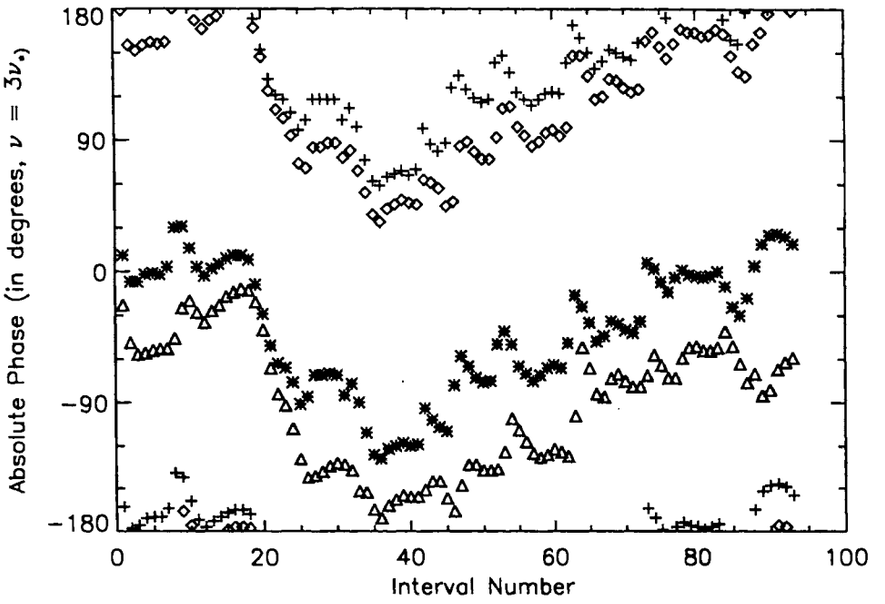

Figure 2.7(a).

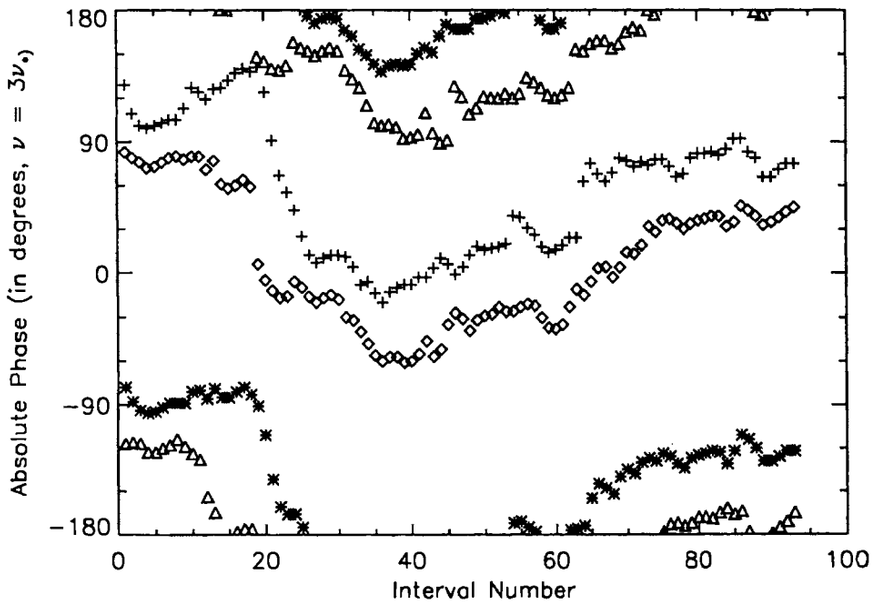

Figure 2.7(b).

Figure 2.7a-b. Temporal variation of the phases $\alpha(l,\ n)$ or $\varepsilon(l,\ n)$, of the third harmonic ($n = 3$) terms as represented by values during 11-yr intervals successively displaced by 1 yr. In (a), symbols $+$, $*$, $\diamond$, and $\triangle$ represent $l = 1$, 3, 5 and 7, respectively. In (b) they represent $l = 9$, 11, 13, and 15, respectively.

oscillation in 'B_ϕ'.

Mutual correlations are also seen in the similarly determined variations of the phase $\alpha(l, n)$ of the terms of different l for $n = 3$ shown in Figures 2.7(a) and 2.7(b).

2.10. A possible Phenomenology for Maintenance of the LF Spectrum and Production of Activity

Here I present a phenomenology which we conjectured for understanding the above results.

2.10.1. POSSIBILITY OF EXISTENCE OF CASCADE OF ENERGY IN THE LF SPECTRUM

In the Sun, the density falls rapidly near the photosphere. The intensity of the background field may not vary much (e.g., Gokhale & Hiremath 1993). Hence, if torsional MHD waves are excited inside the Sun, their phase speed would increase rapidly as they approach the photosphere traveling along the field lines. Therefore the waves will be trapped inside the sun by total internal reflections at the photosphere. In general the angles of incidence will be non-zero, and hence the reflected waves will have different values of l than the incident waves. This transfer of energy will continue during successive reflections provided there is a continued supply of energy at the original 'l'. In the whole process, appreciable energy will be stored only in the normal modes of global oscillations (for which higher l corresponds to higher ν). Since the dissipation occurs at high l and ν, the overall transfer of energy will constitute a cascade from modes of lower l, ν to those of higher l, ν.

2.10.2. EVIDENCE FOR EXISTENCE OF CASCADE OF ENERGY IN THE LF SPECTRUM

There are high correlations among the phases (and also among the amplitudes) of LF terms of low and high values of l (Section 2.9.1) and among the terms of low and high values of n (Gokhale & Javaraiah 1990b).

If we examine Figure 2.6 carefully, we find *increments* and *decrements* of the *initial phases* of terms in $n = 1$ occuring during intervals of lengths ~ 7 yr and ~ 4–5 yr. These variations imply *decelerations* and *accelerations*, respectively, in the phase speeds of the waves of the frequency ν_* on time scales corresponding to $3\nu_*$ and $5\nu_*$. Accelerations and decelerations in the phase speeds of the terms in $\nu = 3\nu_*$ in Figure 2.7 are also seen to occur during exactly the same intervals of time. Thus, the correlations which exist for each l in the phase variations of the lower and the higher n (e.g., $\sim$ 85-90% between $n = 1$ and 3; Gokhale & Javaraiah 1990b), seem to be due to the simultaneous phase accelerations and phase decelerations of the waves of the lower and the higher n. So, the phase variations in Figures 2.6 and 2.7 indicate transfer of energy from LF terms

of $3\nu_*$ and $5\nu_*$.

Similarly the mutual correlations between the amplitudes and phases of LF terms of different l, and same n, imply transfer of energy from waves of lower 'l' to those of higher l, with the same ν.

Whenever the flux bundles formed by interference of MHD waves emerge above the photosphere by the process envisaged in Section 2.8.2, they will be seen as 'surface fields'. The dissipation of the emerged flux bundles in the atmosphere will produce 'activity' of various types on various scales.

The 'toroidal flux bundles' given by interference of the waves with non-random phase variations will be regularly distributed in latitude and time. Thus the modes with $\nu = \nu_*$, $3\nu_*$, and $5\nu_*$, would yield the observed 'photospheric fields' and 'activity' that are distributed regularly in latitudes and in time, viz., (i) sunspot activity distributed in 'butterfly diagrams', (ii) 'weak' fields appearing to migrate towards the poles, and (iii) the 'reversing' polar fields. (This is already shown, up to the terms in ν_* alone, for $l = 1$ to 13 by Stenflo (1988), and for $l = 1$ to 29 by us in Section 2.6.)

Since the waves with $n > 5$ have random phases (Section 2.10.3), the flux tubes formed by their interference may be producing the small-scale fields and activity distributed randomly on the surface, and in time (may be , e.g., 'bright points' in X-ray and EUV emissions).

The emergence of flux tubes as in Section 2.8.2 implies sudden removal of energy, viz., the magnetic energy of the flux tubes, from the interfering waves. Since this occurs on time scales (τ_{max} : Section 2.8.2) much shorter than the wave periods, this would lead to 'shifts' in the phases of the respective terms in the LF spectrum.

We have determined the cycle-to-cycle 'shifts' in the phase, ϵ_{ln}, from changes in α_{ln}, using Equation (2.11b). These are $< 30°$ for $n = 1$, $\sim 30° - 90°$ for $n = 3$, and $90° - 120°$ for $n = 5$. For $n > 5$ the phase changes are $> 120°$ and hence, essentially random.

For each LF terms, the observed cycle-to-cycle phase change will be the net result of the energy received from terms of lower l, n, energy contributed to the emerging flux tubes, and energy passed on to the terms of higher l, n.

The foregoing discussion suggests that the LF spectrum of the global oscillations is a net result of (i) input of energy at some low l, ν, (ii) cascade of energy from lower l, ν to higher l, ν, and (iii) intermittent removal of energy from the waves in the form of toroidal flux tubes formed by interference.

The dominant LF Terms in the Basically Excited Oscillation and the Approximate Balance Between Inputs and Outputs of Energy

In Figure 2.5 we also see that the amplitudes $q(l,n)$ for $n = 1$ and $l = 1$–13 determined from 11-yr long time intervals successively displaced by 1 yr show high correlations with the measure of sunspot activity, S, during those intervals. Actually, these correlations are expected from the definition of $q(l,n)$. However, among these, the best correlation is given by amplitudes of $l = 3$ and 5 not by the largest two amplitudes in 'Q', viz., of $l = 5$ and 7 (see Figure 2.1). Thus, the energy in $\{l = 3,\ 5;\ n = 1\}$ seems to control the variation of the amount of sunspot activity even on time scales ≥ 11 yr. This, along with the result of 2.10.3, shows that $\{l = 3,\ 5;\ n = 1\}$ may be the dominant terms in the basically excited waves.

The same correlation also suggests that on time scales > 11 yr there may be a fairly good balance between the rate of energy input into ($l = 3, 5$; $n = 1$) and that of energy disposal through sunspot activity. [Evidence for the Associated 'Torsion' : It may be noted that the terms $\{l = 3,\ 5;\ n = 1\}$ belong to the mode $\{l = 1,\ 3,\ 5,\ 7;\ n = 1\}$ in B_ϕ which corresponds to $\{l = 2,\ 4,\ 6;\ n = 1\}$ in the rotational angular velocity (i.e., the 'torsional oscillation' of '22-yr periodicity'). In the analysis of surface rotation the presence of such an oscillation is indicated by that of 22-yr periodicity in the coefficient of $sin^2\theta$ (Javaraiah & Gokhale 1995, see Chapters III and VI).]

2.10.3. VERIFICATION OF THE PHENOMENOLOGY

Correlation Expected between the 'Cycle Size' and the 'Phase-Changes'

Since the changes in the phases of LF terms with $n = 1$ and 3 are not large (see Section 2.10.3), these phase changes can serve as measures of the net effect of the gains and losses of energy by these terms. Hence, according to the foregoing model of energy cascade and production of activity (Sections 2.10.2 and 2.10.3), the following correlations should exist.

Test 1: the size of a sunspot cycle should be proportional to the amount of energy by all those waves whose interference creates the sunspot activity during that cycle. Hence, $S_{obs}(i)$ should be correlated to the phase changes of the corresponding LF terms from cycle '$i-1$' to cycle 'i'.

Test 2: also, the change in the cycle size from one cycle to the next cycle should be correlated to the phase shifts of the terms representing those waves of $n = 1$ into which the energy is input during some earlier cycles.

Verification of the 'Test 1'

For verifying *Test 1* we have determined the coefficients of correlations of $S_{obs}(i)$ with the sums of the changes $\Delta\epsilon_{l,n}(i-1,\ i)$ in the phases of the terms (l, n), taken in different combinations, during the cycle '$i-1$' to those during the 'i'.

We find the correlations between

$S_{obs}(i)$ and $\sum_{n=1,3,5} \Delta\epsilon_{5,n}(i-1,\ i)$ equal to 90%,

$S_{obs}(i)$ and $\sum_{l=1,3,5,7} \Delta\epsilon_{l,5}(i-1,\ i)$ equal to 94%,

where the combination given in the summation is the one that gives the *maximum* correlation (of the value given).

Thus, we find: (a) the size of a sunspot cycle is highly correlated to the energy *lost* by a set of waves during the current cycle, and (b) the maximum correlation is with the energy lost by the wave corresponding to the term $l = 5$ through $n = 1, 3, 5$, and also to the energy lost by the waves corresponding to the terms $l = 1, 3, 5, 7$ through $n = 5$.

Verification of the 'Test 2'

For verifying *Test 2* and identifying the terms of the fundamental frequency in which the energy is input, we have determined the correlations between the changes in the cycle size:

$$\Delta S_{obs}(i-1,\ i) = S_{obs}(i) - S_{obs}(i-1)$$

and the sums of phase shifts, in combination of terms with $n = 1$, occuring between the previous one or two cycles.

In the notation used earlier, the maximum correlations are:

$\Delta S_{obs}(i-1,\ i)$ and $\Delta\epsilon_{5,1}(i-1,\ i)$: 87%

and

$\Delta S_{obs}(i-1,\ i)$ and $\Delta\epsilon_{11,1}(i-2,\ i-1)$: 90%.

Thus the change in the cycle size from '$i-1$' to 'i' is well correlated with the amounts of energy input into the waves of frequency ν_* during the cycles '$i-2$', '$i-1$', and the maximum correlations are with energy inputs into : (a) the wave $[l = 5,\ n = 1]$ during either '$i-1$' or cycle 'i', (b) the wave $[l = 11,\ n = 1]$ during the cycles '$i-2$' and '$i-1$'. [*Note:* the above correlations imply that the time lapse between the input of energy and its loss through interference is longer for $l = 11$ than for $l = 5$. This means that the phase difference between $l = 5$ and $l = 11$ seen in Figure 2.7 should not be considered as *lag* of 240° for $l = 11$ rather than a lead of 120°. This is to point out

that the result '(b)' need not be interpreted as energy-input in $l = 11$ occuring earlier than in $l = 5$.]

Scope for Forecasting the 'Cycle Size'

In Figure 2.8 we compare the observed cycle sizes S_{obs} with those 'predicted' using the second correlation. It is clear that such a forecast can be satisfactory.

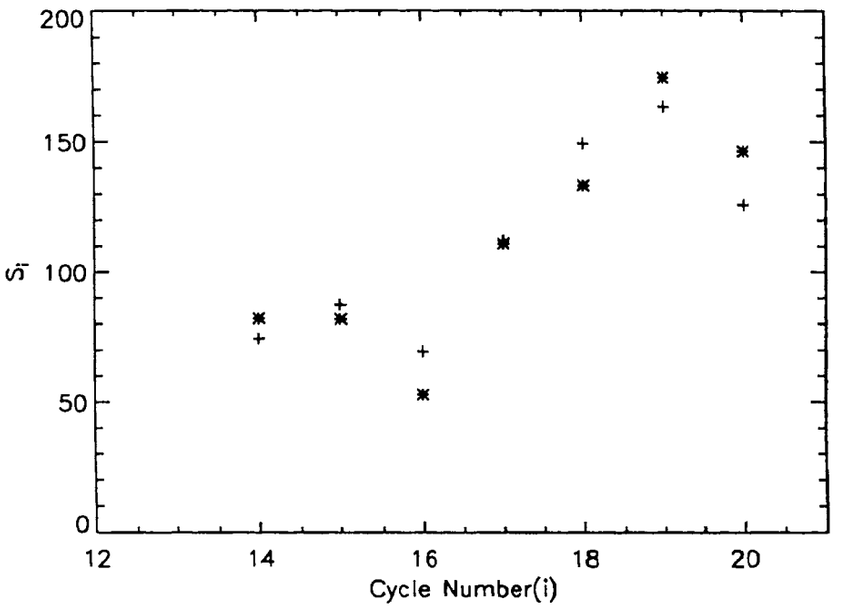

Figure 2.8. The observed cycle sizes $S_{obs}(i)$, represented by '+' and those 'predicted' ('*') on the basis of the 90% correlation of $S_{obs}(i)$ to $\Delta\varepsilon_{11,1}(i-2,\ i-1)$ (see Section 2.10.3).

2.11. Conclusions and Discussion

Conclusions:

The refined analysis of the Sun's magnetic field 'inferred' from the sunspot data, we draw the following conclusions (interpretations of the results):

(1) This study confirm the earlier result (Gokhale & Javaraiah 1990a; Gokhale et al. 1990) that the sunspot data can be used to study, even quantitatively, the global behaviour of the solar magnetic field during several cycles before the beginning of the regular magnetogram observations, at least on large scales.

(2) There is no convincing evidence for existence of any relation between the frequency (ν) and the degree (l) of either odd or even degree axisymmetric modes, whatever be the physical nature of the modes.

(3) The narrow band widths of the ridges at ν_*, $3\nu_*$, $5\nu_*$, etc. in Figure 2.1(a) provide the following clues for the theoretical modeling. One possibility is that the internal thermal and magnetic field of the Sun are so structured that the frequencies of all the admissible modes lie in band widths $\sim \nu_0$ around ν_* ($\sim 1/21.4$ yr^{-1}), $3\nu_*$, $5\nu_*$,...,etc. The other, simpler interpretation of Figure 2.1(a) is that the basic oscillations may be 'forced' (e.g., through boundary conditions imposed on the 'dynamo' by some 'clock' in the deep solar interior as suggested by Dicke 1979). The approximate constancy of the band width of the 'ridges' at ν_*, $3\nu_*$, etc. in Figure 2.1(a) suggests that the band width of the 'forcing frequency' is much less than ν_0, i.e., $\ll 1/107$ yr^{-1} ($\ll 0.3$ nHz), if the high frequencies are harmonics of ν_* and not independent forcing frequencies.

(4) The modes in the 'main power ridge' of the SHF spectrum of the Sun's magnetic field as inferred from sunspot data constitute at least four independent distinct coherent global oscillations $B_1....B_4$. Superposition of all the four modes, $B_1....B_4$, is *necessary* and *sufficient* to reproduce important observed properties of the latitude-time distribution of the real solar magnetic field, not only in the 'sunspot zone' (from where the data comes), but also in the middle ($35° - 75°$) and the high ($\geq 75°$) latitudes, with appropriate relative orders of magnitudes and phases (Section 2.6). Thus, $B_1....B_4$ seem to represent really existing global oscillations in the Sun's magnetic field.

(5) As an interpretation of the results of analysis in Sections 2.8, 2.9, and 2.10.1–2.10.2 we have suggested in Sections 2.10.3 and 2.10.4 the following phenomenological model for production of sunspot activity and maintenance of the 'approximately steady' LF spectrum of the global MHD waves.

(i) The primary input of fresh energy into an existing spectrum of torsional MHD waves occurs mainly at $l = 3,\ 5;\ \nu = \nu_*$ (by some unidentified forcing process),

(ii) This energy cascades to the waves of higher spatial and temporal frequencies, maintaining the oscillations described in Section 2.9.2, and the waves of higher l, n (presumably due to reflections of the waves at the boundaries such as the photosphere and the base of the convective envelope).

(iii) The cascading energy keeps on leaking out intermittently in the form of critical buoyant toroidal flux bundles (created by superposition of waves) whose emergence produces surface fields and activity on various scales (e.g., sunspot activity from interference of waves represented by $\{l = 1,\ 3, ..., 13;\ \nu = 1,\ 3,\ 5\}$, and 'non-sunspot activity' at higher l and n).

(iv) 'Inferred rate' does yield relative amplitudes and phases for LF terms, at least up to = 13 (Section 2.7), similar to those derived from the directly 'observed' poloidal flux distribution at the photosphere (Stenflo & Vogel 1986; Stenflo 1988). This is expected from model in Section 2.10 if, on the time scales and length scales of the model, the 'instantaneously' observed photospheric poloidal field at $(\theta,\ t)$ is proportional to $Q(\theta, t)$, the '*rate of emergence* of the toroidal flux per unit latitude interval per unit time'.

Discussion:

Section 2.8.5 presents one possible model of sunspot cycle as arising from superposition of the LF terms in the 'rate of emergence of toroidal magnetic field', not only qualitatively in terms of the latitude-time distribution, but also quantitatively in terms of the shapes and sizes of the successive sunspot cycles.

Here the rate of emergence of magnetic field is not directly measured but is inferred from the sunspot data itself. However, Conclusion (4) shows that the phenomenological model in Section 2.10 is not based on a trivial consequence of the forward and the backward LF transforms.

This brings us back to the questions : (a) what is the physical nature of these waves and oscillations ?, (b) what kind of steady field in the Sun's interior can sustain such oscillations ?

The answers to these questions can hardly be expected purely from a data analysis. However, for the sake of completeness of the model, on the grounds given in Sections 2.8.2 and 2.10.4 it is expected that the LF terms in 'B_ϕ' represent the toroidal magnetic component of the 'torsional MHD oscillations'. As for the question (b), we note that in a recent model of the 'steady' part of the Sun's internal poloidal field, 'the best fit' for its *iso-rotation* with the helio-seismologically determined internal rotation of the Sun is given by terms only up to $l = 3$ (Gokhale & Hiremath 1993; Hiremath 1995; Hiremath & Gokhale 1995). This model of the 'steady' field is constrained to an

asymptotically uniform finite field at large distance. The alfvén travel time along all field lines is nearly same so that the model can provide the necessary 'steady framework' for the oscillations. The strength of this 'steady' field (required for the '22-yr' periodicity of the torsional MHD oscillation) is $\sim 10^{-2}$ G, which would not be detectable in the presence of the periodically reversing surface fields produced by emergence of toroidal flux tubes (2.10.3 to 2.10.3). Hence, the presence of the necessary 'steady' background field of primordial origin, is not ruled out.

It is also shown in Hiremath (1995) that the 'residuals' of the fit indicate the presence of *deviation from isorotation* (i.e., time-dependent perturbations) with $l = 5$ as the dominant term and with a time scale in the range 1–100 yr. These properties of the 'deviation from isorotation' are in agreement with the present analysis and interpretation.

The phenomenological model in Section 2.10.3 describes a possible way in which toroidal magnetic flux tubes could be produced. The time scales of their rise to the surface are assumed to be smaller than the smallest ($\sim$ 1 yr) resolution used in modeling the 'shapes' of the cycles. This is in accordance with computations by Choudhury & D'Silva (1990) for radial travel of flux tubes and with the observational estimate of Howard & LaBonte (1981), and the rising rates of sunspot magnetic structures estimated by us (Chapter V). However, a detailed mathematical modeling of torsional MHD waves (e.g., in a steady' field such as in the model mentioned above), and their interference, will be necessary for (i) ascertaining the reality of the phenomenology developed in this study and for (ii) exploring the possibility of sound predictions of the 'shapes' and 'sizes' of future sunspot cycles. It will be important to model the emergence of the toroidal flux bundles, especially the separation of their identities from the ambient field and their distribution in longitude.

The phenomenological model of the energy cascade indicates that the overall sunspot cycle phenomenon resembles a 'relaxation oscillation' (mentioned by Bracewell, 1988). Here the 'negative damping' corresponds to the energy input into the waves of $\nu = \nu_*$ and the 'positive damping' to the loss of energy in the form of flux tubes leaving the main body of the Sun and dissipating in the atmosphere. Therefore, the most important task will be to model the process that *perpetually excites* the waves at $\nu = \nu_*$.

At present the only mechanism of *perpetual excitation* at frequencies near ν_* which we can think of is a resonance coupling to the Sun's motion about the center of mass of the solar system. These torques will depend upon the orbital motions of the planets, whose configurations are known to have some dominant periodicities common to sunspot activity (e.g., review by Seymure et al. 1992) and to the solar differential rotation (see Chapter IV). However, the energetics of such a mechanism need to be worked out.

APPENDIX 2A.

2A.1 Formulae for SHF components

The harmonic components $H_{cc}(l,m,n,\backslash T_1,T_2)$, $H_{cs}(l,m,n,\backslash T_1,T_2)$, $H_{sc}(l,m,n,\backslash T_1,T_2)$, $H_{ss}(l,m,n,\backslash T_1,T_2)$ in the expansion

$$p(\mu,\phi,\tau) = \sum_{\alpha,l,m,n} H_\alpha(l,m,n\backslash T_1,T_2) \times P_l^m(\mu)_{sin}^{cos}(m\phi)_{sin}^{cos}(2\pi n\tau) \qquad (2A.1)$$

during the interval (T_1,T_2) are given by

$H_\alpha(l,m,n \setminus T_1,T_2)$

$$= C(l,m,n)\int_0^1 d\tau \int_0^{2\pi} d\phi \int_{-1}^{+1} d\mu p(\theta,\phi,\tau) \times P_l^m(\mu)_{sin}^{cos}(m\phi)_{sin}^{cos}(2\pi n\tau) \qquad (2A.2)$$

$$= \frac{C(l,m,n)}{N}\sum_i P_l^m(\mu)_{sin}^{cos}(m\phi)_{sin}^{cos}(2\pi n\tau), \qquad (2A.3)$$

where α is a symbol representing the subscript 'cc', 'cs' 'sc' or 'ss', depending upon the combination of the cosines or sines of $(m\phi)$ and $(2\pi n\tau)$ in the respective term, and

$$C(l,m,n) = \Lambda\frac{(l-m)!(2l+1)}{(l+m)!\pi}$$

with

$$\Lambda = \begin{cases} 1 & \text{for } m \neq 0 \; n \neq 0, \\ \frac{1}{2} & \text{if m} = 0 \text{ or n} = 0, \\ \frac{1}{4} & \text{if m} = 0 \text{ and n= 0} \end{cases}$$

2A.2. Determination of Amplitudes and Phases

2A.2.1. REFERRED TO $t = T_1$ AS ZERO EPOCH

The amplitudes $A_c(l,m,n)$ and $A_s(l,m,n)$ of the modes $P_l^m(cos\theta)cos(m\phi)e^{2\pi in\tau}$ and $P_l^m(cos\theta)sin(m\phi)e^{2\pi in\tau}$ during (T_1, T_2) are given by

$$A_c(l,m,n) = [H_{cc}^2(l,m,n) + H_{cs}^2(l,m,n)]^{1/2},$$
$$A_s(l,m,n) = [H_{sc}^2(l,m,n) + H_{ss}^2(l,m,n)]^{1/2}. \qquad (2A.4)$$

We also define the rms amplitude of $P_l^m(\mu)$ term as

$$A_l(l,m,n) = [A_c^2(l,m,n) + A_s^2(l,m,n)]^{1/2}.$$

For $m = 0$: $A(l, m, n) = A_c(l, m, n)$.

By phases $\varphi_c(l, m, n)$ and $\varphi_s(l, m, n)$ of the above modes during (T_1, T_2) 'referred to $t = T_1$ as the zero epoch' we mean the values of φ in their time dependence expressed as

$sin[2\pi\nu(t - T_1) + \varphi]$, where $\nu = n/(T_1 - T_2)$.

These phases are given by

$$\varphi_c(l, m, n) = tan^{-1}[H_{cc}(l, m, n)/H_{cs}(l, m, n)] + 0 \text{ or } \pi$$

and

$$\varphi_s(l, m, n) = tan^{-1}[H_{sc}(l, m, n)/H_{ss}(l, m, n)] + 0 \text{ or } \pi, \qquad (2A.5)$$

where 0 or π is chosen to ensure the correct signs for the sine and cosines.

For axisymmetric ($m = 0$) modes φ_s and the symbol φ_c will be replaced by φ.

2A.2.2. AMPLITUDES AND PHASES REFERRED TO OTHER ZERO EPOCHS

It can be shown that the above formulae also give the amplitudes and phases referred to any epochs T_0 other than T_1 as zero epoch if in equation (2A.3) one takes

$\tau = (t - T_0)/(T_2 - T_1)$ instead of $(t - T_1)/(T_2 - T_1)$.

In such a shift of zero epoch, the amplitudes remain invariant and the phases shift by $2\pi\nu(T_1 - T_o)/(T_2 - T_1)$.

Chapter III

PERIODICITIES IN THE SUN'S SURFACE ROTATION

3.1. Introduction

In the previous chapter, we showed that the Legendre-Fourier analysis of the Sun's inferred magnetic field from sunspot data during 1874–1976 strongly suggests that the solar activity may be originating in the interference of Sun's global magnetic oscillations with frequencies $\sim 1/21.4$ yr^{-1} and a few odd harmonics of it. If these oscillations are torsional magnetohydrodynamic (MHD) in nature then the solar rotation also should have oscillations with aforementioned frequencies. In this chapter we discuss the periodicities in Sun's rotation (Javaraiah & Gokhale 1995; Javaraiah & Komm 1999).

Attempts were made in the past by a number of authors to investigate variations of solar surface rotation by different ways and using different data. The solar cycle dependence of the differential rotation (B) was discovered by Balthasar & Wöhl (1980). Balthasar & Wöhl analyzed the Greenwich data during 1940–1968 and found that the equatorial rotation (A) is faster during the sunspot minima than during the maxima. A similar pattern of variation was found by a number of authors using different sets of data on sunspots (Arévalo et al. 1982; Lustig 1983; Gilman & Howard 1984; Balthasar et al. 1986; Kambry & Nishikawa 1990). Tuominen & Kyröläinen (1981) found in the variation of A, a significant dip from cycle 13 to cycle 14. Gilman & Howard (1984) noticed a cycle-to-cycle difference in the yearly values of the residual rotation rates of sunspots. Lustig (1983) and Balthasar et al. (1986) found that there were no systematic variations in the yearly values either of A or of B. Kambry & Nishikawa (1990) found that the smaller the amplitude of the solar cycle, the larger is the value of A. Yoshimura & Kambry (1993) found a monotonic increase in the value of A from cycle 17 to cycle 20. Paternó et al. (1991) analyzed Greenwich data on spot groups of age ≥ 3 days during the years 1874–1976 and obtained 16.1-yr and 6.2-yr periodicities in A. Komm (1995) calculated the Hurst exponent for daily A, B, and C coefficients deduced from Mt. Wilson velocity data during 1967–1992 and noticed persistent behavior in the temporal variations of the solar rotation rate on time scales from 20 days to 11 yr.

LaBonte & Howard (1982a) analyzed Mt. Wilson velocity data during 1967–1980 and found that the ratios B/A and C/A of the differential rotation coefficients A, B and C vary with the phase of the solar cycle. LaBonte & Howard called these solar cycle variations of B/A and C/A as 'torsional oscillations' of period 11-year and wave number 1 hemisphere^{-1}. They used the ratios B/A and C/A instead of B and C

to avoid systematic effects in the Mt. Wilson velocity data. The so-called 'torsional oscillation', discovered by Howard & LaBonte (1980) consists of alternating bands of faster (or slower) than average rotation moving from high latitudes towards the equator in $\sim$ 22-yr time. Howard & LaBonte (1983) also noticed a trend of $\sim$ 11-yr cyclic variation of north-south asymmetry in the solar equatorial rotation rate A, determined from the data in the two hemispheres. They called this a 'torsional oscillation' of period $\sim$ 11-yr and wave number 0.5 hemisphere^{-1}. Snodgrass & Howard (1985), using Mt. Wilson magnetograms (1967–1983), Ulrich et al. (1988) using Mt. Wilson Doppler measurements (1967–1987) and Komm et al. (1993a) using NSO Kitt Peak magnetograms (1975–1991), confirmed the existence of a torsional oscillation pattern.

It has been claimed that the torsional pattern is present in sunspot motions (Godoli & Mazzucconi 1982; Tuominen et al. (1983) although in both cases the result is marginally significant, judging from the errors. Tuominen et al. (1983) analyzed longitudinal and latitudinal motions of recurrent sunspot groups using Greenwich data during 1874–1976. Although their time resolution was course, they found some evidence for the 11-yr oscillation in the sunspot zones with an amplitude of a few m s^{-1}. Gilman & Howard (1984) and Balthasar et al. (1986) observed faster and slower bands, but with no clear migratory character. Ternullo (1990) discovered evidence of equatorward moving bands of torsional oscillation through a very careful study of the sunspot drawings made during cycle 21 at Catania Astrophysical Observatory. Ternullo used only the data of old spot groups, i.e., for each spot group only the data collected from the 4th day of observation until the last observation available have been taken into account. Recently, Meunier et al. (1997) analyzed the rotation of photospheric faculae obtained at Meudon throughout cycle 19 (1954–1964) and found bands of faster and slower rotation rates with an amplitude of a few meters per second similar to the torsional oscillations. Makarov et al. (1997) studied the long-term variations of the differential rotation of the solar large-scale magnetic field using synoptic Hα maps in the latitude zone from $+45°$ to $-45°$ in the period of 1915–1990. In each solar cycle, they find a band of faster or slower than average rotation moving from high to low latitudes. The slow band roughly corresponds to the location of magnetic activity. A long term variation of about 55 years is also observed in the torsional oscillation pattern.

In Section 3.2 of this chapter, we describe the data sets and the parameterization of solar differential rotation used in our studies of variations in the differential rotation. In Section 3.3, we show the temporal variation of the parameters of differential rotation, and in Section 3.4, we derive periodicities and their significance levels from Fast Fourier Transform (FFT) power spectrum analysis. In Section 3.5 we confirm the periodicities of the order of solar cycle period by binning the sunspot group data into longer than 1 yr intervals and from analyzing simulated time series. In this section we also check the effects of latitudinal distribution of sunspot activity and age of the groups. In

Section 3.6 we compare the results from sunspot and the velocity data. In Section 3.7.1 we compare periodicities in differential rotation determined from sunspot data with those in the solar magnetic cycle. In Section 3.8 we summarize the work and briefly discuss the results.

3.2. Data Analysis

3.2.1. POLYNOMIAL EXPANSION

The Sun's differential rotation can be determined from full disc velocity data using the 'standard' polynomial expansion:

$$\omega(\lambda) = A + B\sin^2\lambda + C\sin^4\lambda, \tag{3.1}$$

while for sunspot data, it is sufficient to use only the first two terms of the expansion:

$$\omega(\lambda) = A + B\sin^2\lambda, \tag{3.2}$$

where $\omega(\lambda)$ is the solar rotation rate at latitude λ, the parameter A represents the equatorial or 'mean' rotation rate, B and C measure the latitude gradient of the rotation rate with B representing mainly low latitudes and C representing largely higher latitudes.

As pointed out by several authors (see Snodgrass 1984 and references therein), due to the non-orthogonality of the fit functions, the coefficients A, B, and C, have crosstalk which affects their temporal behavior. Snodgrass & Howard (1985) used the so-called Gegenbauer Polynomials as a set of disk-orthogonal fit functions with $T_1^0(\sin\lambda) = 1$, $T_2^1(\sin\lambda) = 5\ \sin^2\lambda - 1$, and $T_4^1(\sin\lambda) = 21\sin^4\lambda - 14\sin^2\lambda + 1$, which leads to the following expansion:

$$\omega(\lambda) = \bar{A} + \bar{B}(5\sin^2\lambda - 1) + \bar{C}(21\sin^4\lambda - 14\sin^2\lambda + 1). \tag{3.3}$$

The coefficients $\bar{A}$, $\bar{B}$, and $\bar{C}$ are free of crosstalk; $\bar{A}$ represents the 'rigid body' (or 'mean') component in the rotation, $\bar{B}$ and $\bar{C}$ are the components of the differential rotation. If the polynomial expansion is terminated at $\bar{C}$ (or C), the coefficients, $\bar{A}$, $\bar{B}$, and $\bar{C}$, are related to the standard A, B, and C coefficients as follows:

$$\bar{A} = A + (1/5)B + (3/35)C, \quad \bar{B} = (1/5)B + (2/15)C, \quad \bar{C} = (1/21)C. \tag{3.4}$$

In this case, the temporal variation of C is identical to that of C.

Pierce & Lopresto (1984), Snodgrass (1992), and Komm et al. (1993) used Legendre polynomials as a set of orthogonal functions and describe the differential rotation as follows:

$$\omega(\theta) = DP_0 + EP_2(\cos\theta) + FP_4(\cos\theta), \tag{3.5}$$

where θ is the co-latitude and P_0, P_2, and P_4 are Legendre polynomials. If the expansion is truncated at the third term, the coefficients D, E, and F are related to the coefficients A, B, C in equation (1) as follows:

$$D = A + (1/3)B + (1/5)C, \quad E = (2/3)B + (4/7)C, \quad F = (8/35)C. \tag{3.6}$$

Generally, the ω and the coefficients of differential rotation (A, B, C, etc.) are expressed in degrees (°) day^{-1} or μ *rad* s^{-1} and ω is considered as the sidereal angular velocity. The rotation rate is also discussed in terms of km s^{-1} or m s^{-1} and simply in rotation periods. The ω is also expressed in rotation frequency and the unit nanohertz (nHz) is used whenever comparison is needed with helioseismically determined Sun's rotation frequency $\Omega(r)$. One can easily convert the rotation rate expressed in one unit to another unit using the conversion factors in Table 3.1, compiled by Dr. R. W. Komm.

Table 3.1., Conversion Factors (compiled by Dr. R. W. Komm)

to convert from	multiply by
deg/day to microrad/sec	0.20201
deg/day to m/sec	140.596 cos(latitude)
deg/day to nanohertz	32.150
to convert from	**add**
Synodic to sidereal rotation (Earth's orbital motion)	0.9856 deg/day (averaged over a year)

3.2.2. DETERMINATION OF $\bar{A}$, $\bar{B}$ and $\bar{C}$ FROM Mt. WILSON VELOCITY DATA

Dr. R. F. Howard kindly provided us the daily values of the A, B, C coefficients (recall Equation (3.1)) derived from Mt. Wilson velocity data for the time period 1967-1994. To reduce the influence of gaps in the daily data, we binned the daily data into 19-day consecutive intervals (the data during 1967–1968 were not used) which leads to time series close to a power of two in length leading with 497 19-day intervals. However, even after re-binning the data, gaps are found between the 8th and the 13th interval, and between the 176th and 178th interval, hence the statistics are poor in some intervals. We filled these gaps with average values from the adjacent intervals. We converted the coefficients to the corresponding Gegenbauer polynomial coefficients, $\bar{A}$, $\bar{B}$, and $\bar{C}$, (Equation (3.4)) and Legendre polynomial coefficients, D, E, and F, (Equation (3.6)). Since both Gegenbauer and Legendre polynomials are orthogonal, we expected the results to be the same and did this mainly as a consistency check. We found that the temporal variation and the resulting power spectra of the D, E, and F

values are indeed nearly identical to the ones of $\bar{A}$, $\bar{B}$, and $\bar{C}$ and that the corresponding spectra of A, B, C are very similar to the ones of $\bar{A}$, $\bar{B}$, $\bar{C}$ except the spectrum of B which is noisier than either one of $\bar{B}$ or E. Therefore, here we show only the results of the Gegenbauer polynomials in order not to duplicate the figures. Owing to the spectrograph modification (see Howard et al. 1983), there is a substantial difference in the data obtained before and after 1982. We carried out a power spectrum analysis for the whole data set of 1969–1994 and for the two subsets covering 1969–1981 and 1982–1994.

3.2.3. DETERMINATION OF $\bar{A}$ AND $\bar{B}$ FROM SUNSPOT GROUP DATA

The sunspot group data compiled from the Greenwich Photoheliographic Results (GPR) of 1874–1976 which was provided to us by Dr. H. Balthasar. The data consist of the observation time (the date and the fraction of the day), heliographic latitude (λ) and longitude (ϕ) for each spot group on each day of its observation. For the period 1940–1976, there are no data available for spot groups on days where the absolute value of central meridian longitude ($|CML|$) exceeds 58°. Hence, for the sake of uniformity such data are omitted also from the data during the period 1874–1939. The sidereal rotation velocities (ω) have been computed for each pair of consecutive days in the life of each spot group. For each yearly average, we computed a least-square fit using the first two terms of a Gegenbauer polynomial expansion:

$$\omega(\lambda) = \bar{A} + \bar{B}(5\sin^2\lambda - 1). \tag{3.7}$$

This equation does not include $\bar{C}$, because it is negligibly small in the fit for sunspot data. Hence, the variation of $\bar{B}$ is identical to that of B ($\bar{B} = \frac{1}{5}B$), and $\bar{A} = A + (1/5)B$, where A and B are the coefficients in Equation (3.2).

We have also computed the coefficients D and E by fitting the data to Legendre polynomials (Equation (3.6)). Again, only the first two terms are used and D and E are related to A and B in Equation (3.2) by $D = A + (1/3)B$ and $E = (2/3)B$ (cf., Balthasar et al. 1986). As for the velocity data, we found that the temporal variation and the resulting power spectra of the D and E are very similar to those of $\bar{A}$ and $\bar{B}$ and are not shown here.

We fitted the rotation rates obtained from sunspot group data to Gegenbauer polynomial expansion, Equation (3.7) above, mainly for the sake of comparing the short-term periodicities in $\bar{A}$ and $\bar{B}$ determined from the sunspot data and velocity data. This might also be necessary for comparing the temporal behaviour of one parameter to that of another (as suggested by the anonymous referee of one of our paper, Javaraiah & Gokhale 1997a) because this fit eliminates the crosstalk among the parameters. However, the sunspot data is confined only low and middle latitudes. Hence, fitting of sunspot data to Gegenbauer or Legendre polynomial expansion may not help much.

Dr. R. F Howard and Dr. H. Balthasar also expressed similar views (personal communications). We have also studied temporal variations and periodicities in the ratio B/A determined from the spot group data (Javaraiah & Gokhale 1995). Let $\Delta(A)$ and $\Delta(B)$ be the uncertainties in A and B, respectively. Then the uncertainty of the ratio B/A will be $\Delta(B/A) \sim [A\Delta(B) - B\Delta(A)]/A^2 \sim \Delta(B)/A < \Delta(B)$, since $\Delta(A) < \Delta(B)$ and $|A| > |B|$. Consequently, the variation in B/A are easier to detect than those in A and B. However, we found that periodicities in B and B/A are the same.

Data corresponding to 'abnormal' motions, viz, displacements exceeding 3° day^{-1} in longitude or 2° day^{-1} in latitude were excluded from the least-squares fits. This reduces the data sample by about 3% but guards against recording errors including those in identifying small spot groups from one day to the next (Ward 1965a, 1966). This leads to a considerable reduction in the uncertainties in rotation parameters. In Table 3.2 we give the values of the parameters A, B and their uncertainties ΔA, ΔB derived from the data in the northern and the southern hemispheres separately and in combination, during the whole period 1874–1976. In the same table we also give the number of data points (N) from the respective hemispheres and from the whole Sun. Comparing with the corresponding values of N, A, and B derived by Balthasar et al. (1986), we find the following:

(1) Our number of data points N is less by about 3%.

(2) Our values of A are slightly smaller, but the uncertainties, ΔA, are much smaller (by about 17%).

(3) Our absolute values of B are smaller by about 3% but the uncertainties, ΔB, are smaller by about 23%.

(4) The north-south differences of A and of the amount of activity N remain the same. The amount of activity is about 6% higher in the northern hemisphere. The value of A is little higher in the southern hemisphere than that expected from the anticorrelation between A and N (Sakurai 1976; Kambry & Nishikawa 1990).

(5) The absolute value of B is slightly larger in the southern hemisphere than in the northern hemisphere. The last result agrees with the result obtained by Hathaway & Wilson (1990) from the data for individual sunspots. However, in our analysis the north south difference in B is smaller than the uncertainty in B.

3.3. Temporal Variations of the Rotation Coefficients

Figure 3.1(a) shows the variations of $\bar{A}$, $\bar{B}$, and $\bar{C}$, binned into 19 day intervals of the Mt. Wilson velocity data (1969–1994). This figure shows a striking difference in the temporal behaviour of coefficients $\bar{A}$, $\bar{B}$, $\bar{C}$ determined before and after the year

Table 3.2. The values of the parameters A and B (in degrees day^{-1}) and their uncertainties $\Delta(A)$ and $\Delta(B)$ derived from the data during the entire period 1874-1976. N is the number of data points gone in each determination.

	A	$\Delta(A)$	B	$\Delta(B)$	N
Northern hemisphere	14.524	±0.006	-2.757	±0.063	42482
Southern hemisphere	14.544	±0.007	-2.797	±0.067	39926
Whole sphere	14.533	±0.005	-2.772	±0.046	82448

1982. The data in the first 250 intervals (before 1982) are much noisier and show a greater variation than after 1982. As mentioned earlier, the spectrograph change in 1982 resulted in reduced instrumental noise in the data from the year 1982 onward. For this reason, we concentrate mainly on the second half of the data set, after 1982, and include the variation in $\bar{A}$, $\bar{B}$ and $\bar{C}$ during 1982-1994 as a separate figure (Figure 3.1(b)).

Figure 3.2 shows the temporal (yearly) variations of $\bar{A}$ and $\bar{B}$ derived from the spot group data during the years 1879-1976. The error bars are ± 1 σ (standard deviation) values. The rotation rates of the spot groups during the years 1874-1878 have been omitted because of their large uncertainties. Large deviations from the average value together with large error bars appear periodically and coincide with solar cycle minima. The large errors are due to the reduced number of sunspot groups during cycle minima and reflect the resulting increased uncertainty. Therefore, after first analyzing the data without correction, we repeated the analysis excluding all data points with an estimated error larger than three times the median error. For a spectral analysis, it is rather difficult to correct for these 'outliers' due to their periodic occurrence. After some testing, we choose to replace them with the average over adjacent values. The solid line in Figure 3.2 connects the 'corrected' data and the dotted line the original uncorrected data.

As seen in Figures 3.1(b) and 3.2, the average values are $\bar{A} = 2.700 \pm 0.022\,\mu$ rad s^{-1}, $\bar{B} = -0.136 \pm 0.004\,\mu$ rad s^{-1}, and $\bar{C} = -0.023 \pm 0.004\,\mu$ rad s^{-1} determined from Mt. Wilson velocity data of 1982-1994 and $\bar{A} = 2.83 \pm 0.03\,\mu$ rad s^{-1}, and $\bar{B} = -0.11 \pm 0.04\,\mu$ rad s^{-1} determined from the corrected sunspot group data. The uncorrected sunspot data lead to the same averages of $\bar{A}$ and $\bar{B}$ but with slightly larger deviation for $\bar{A}$ and more than 50% larger deviation for $\bar{B}$. These values agree well with previously published results by LaBonte & Howard (1982a) and Snodgrass et al. (1984) for Mt. Wilson Doppler data and by Howard et al. (1984) and Balthasar et al. (1986) for sunspot groups. The average value of $\bar{A}$ determined from the velocity data is slightly lower than the average $\bar{A}$ derived from the corrected sunspot group data, while the average value of $\bar{B}$ determined from the velocity data is slightly larger than the average $\bar{B}$ of the sunspot group data.

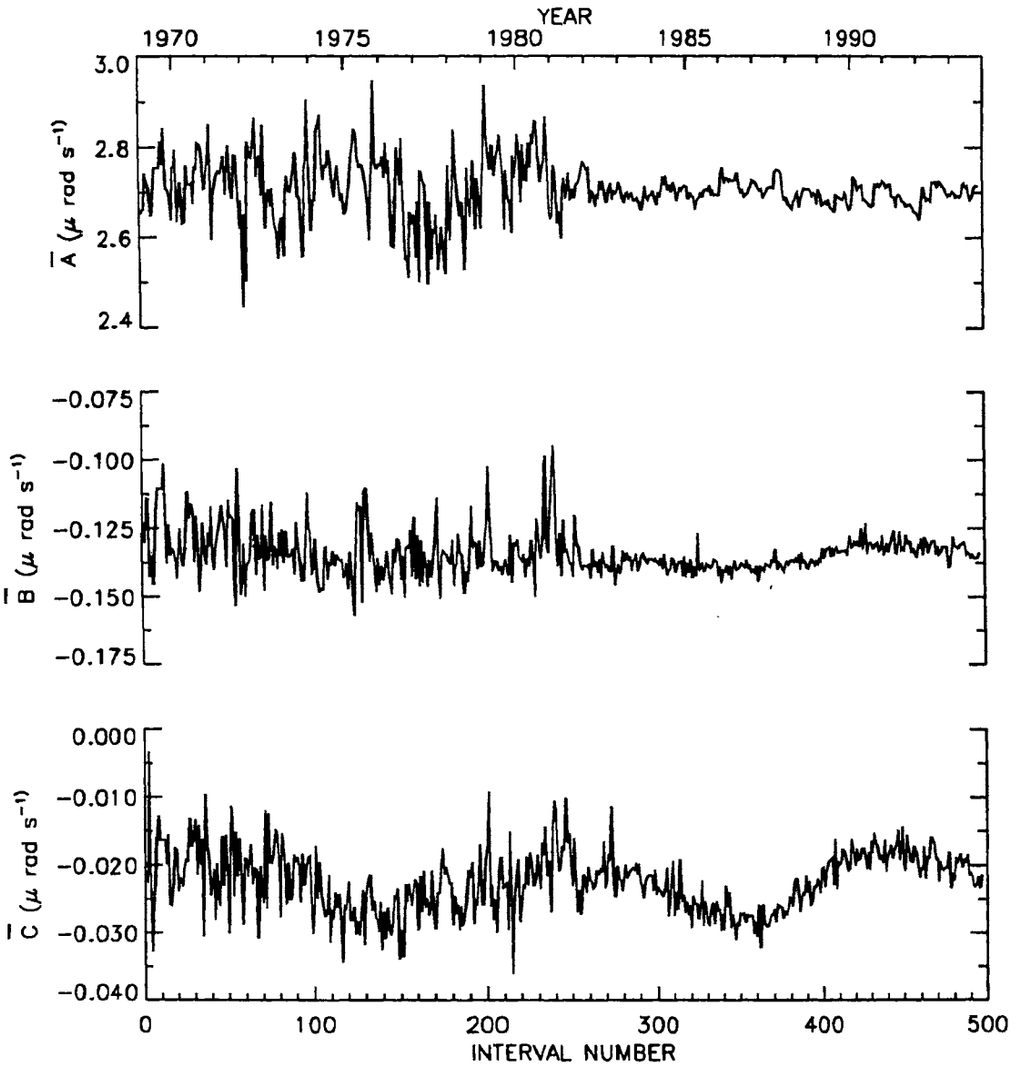

Figure 3.1(a). Variation of the coefficients A, B and C (Equation (3.3)) determined from Mt. Wilson velocity data during 1969–1994 rebinned into consecutive 19-day intervals.

Figure 3.2 shows that the temporal variation of $\bar{A}$ determined from the sunspot group data resembles the corresponding variation of $\bar{B}$ leading to a rather large positive correlation of 0.87 between the two time series. The velocity data show a small anticorrelation of 0.29–0.30 between $\bar{A}$ and $\bar{B}$ and $\bar{A}$ and $\bar{C}$ (Figure 3.1(b)). The parameters $\bar{B}$ and $\bar{C}$ of the velocity data show a positive correlation of 0.60. This agrees with Snodgrass & Howard (1985) who noticed existence of resemblance in the long term trends of $\bar{B}$ and $\bar{C}$ determined from the velocity data obtained before 1982. The corresponding Legendre polynomials show a correlation of similar magnitude and same sign, while B and C of the conventional non-orthogonal representation are anticorrelated.

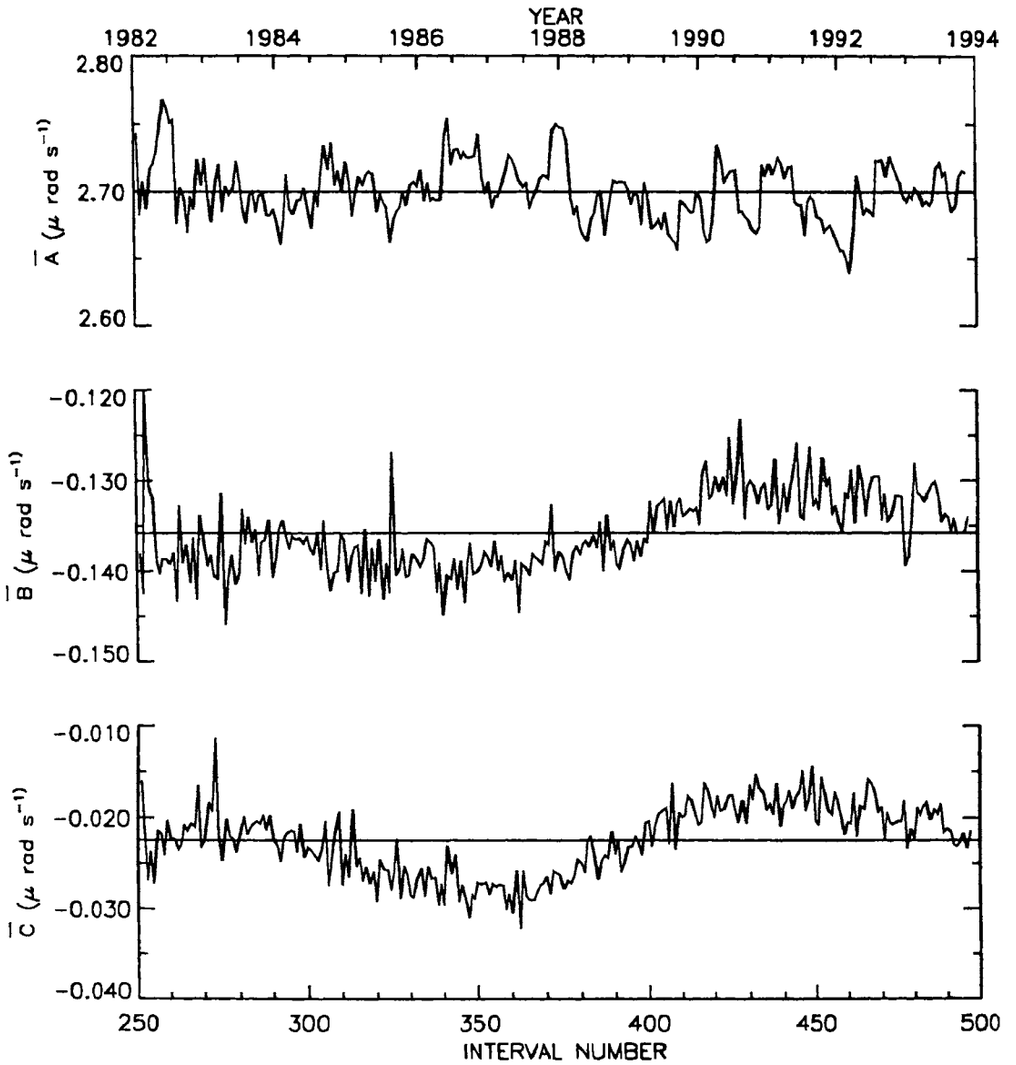

Figure 3.1(b). The same as in Figure 3.1(a) but for the time period 1982-1994. The horizontal lines represent the average values.

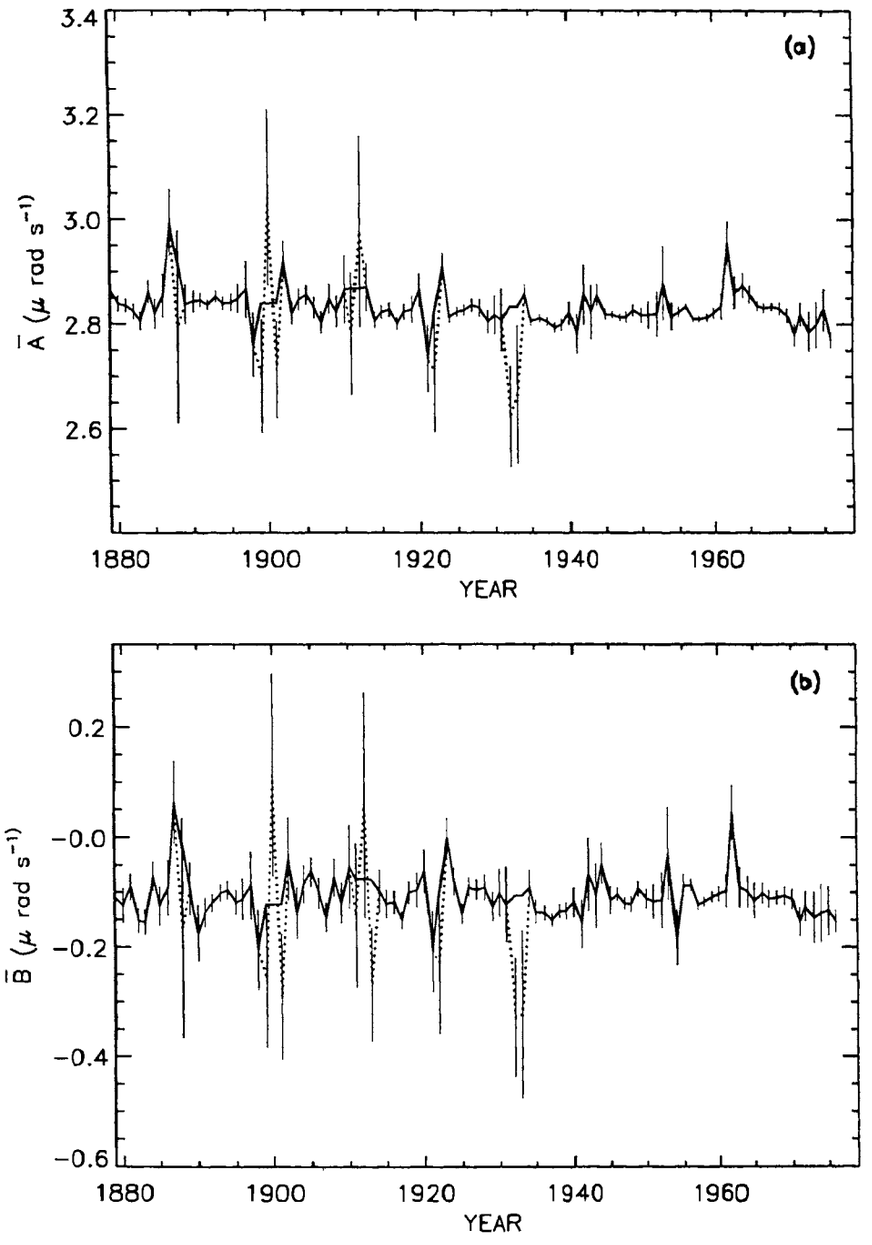

Figure 3.2a b. Annual variation of the coefficients $\bar{A}$ and $\bar{B}$ (Equation (3.7)) determined from sunspot group data during 1879 1976. The solid and dotted curves represent 'corrected' and 'uncorrected' data respectively.

3.4. Periodicities in the Rotation Coefficients

3.4.1. PERIODICITIES IN THE Mt. WILSON VELOCITY DATA

We computed power spectra of the time series of $\bar{A}$, $\bar{B}$, $\bar{C}$. We subtracted a first-order polynomial fit from each time series, apodized it with a 10% cosine taper, which detrends the sequence and removes the leakage between the repeated data segments (e.g., Brault & White 1971), and zero-padded each time series to the next power of 2 before we calculated the spectra. For each power spectrum, we determined the level of significance for individual peaks in units of standard deviation (σ) of the values of the power over the whole frequency range (2.0σ - 3.0σ correspond to confidence levels of 95%–99.7%). Figures 3.3(a-c) and 3.4(a-c) show the power spectra of $\bar{A}$ and $\bar{B}$ determined from the whole data set 1969–1994, and for the two subsets 1969–1981 (intervals 1–250) and 1982–1994 (intervals 251–497). Figure 3.5 shows the power spectrum of $\bar{C}$ determined from the whole dataset 1969–1994; the spectra of the two subsets, not shown here, also show just a single peak related to the 11-yr solar cycle. Due to the reduced noise, the amplitudes are smaller in the spectra of the second subset by about one order of magnitude for $\bar{A}$, and a factor of about three for $\bar{B}$.

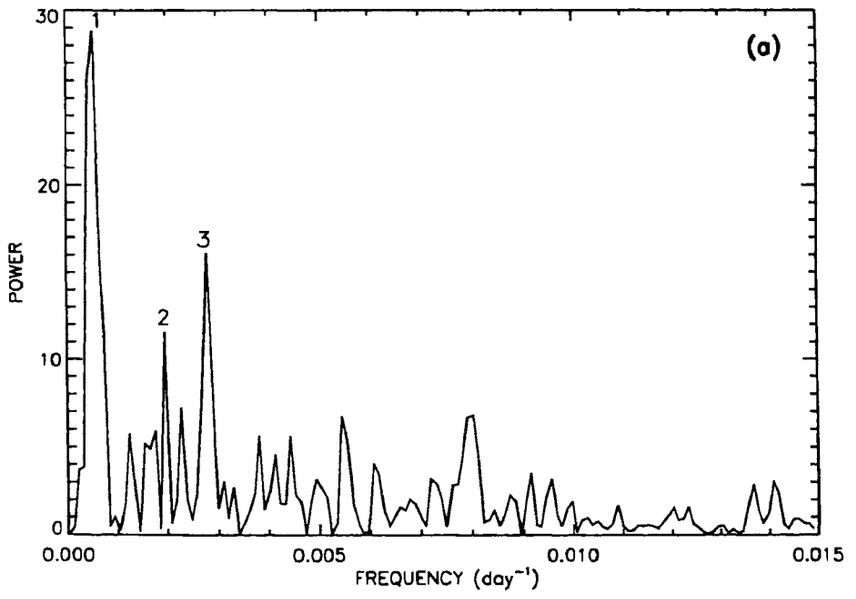

Figure 3.3(a).

Figure 3.3a-c. Power spectra of $\bar{A}$ determined from Mt. Wilson velocity data for (a) the whole period 1969-1994 and two subsets (b) 1969-1981 and (c) 1982–1994. The serial numbers of periodicities given in Table 3.3 are marked near the top of each peak.

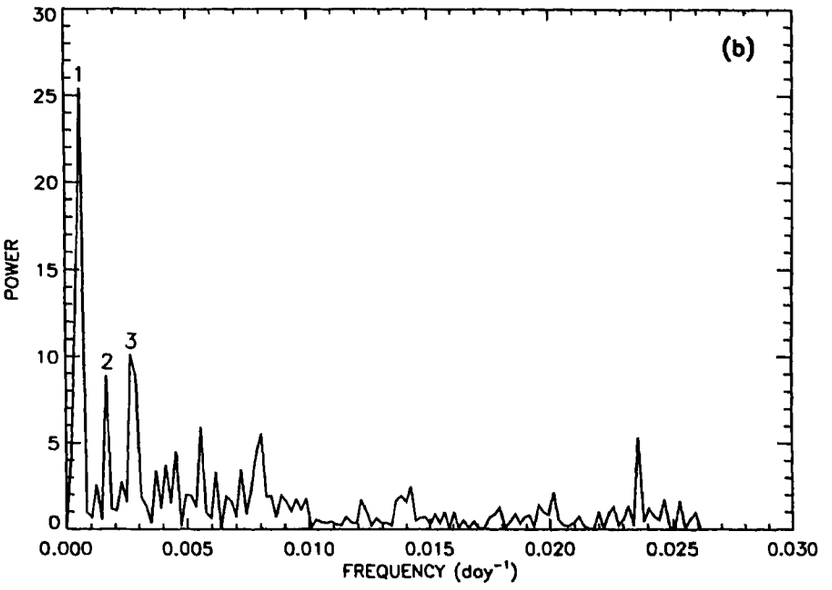

Figure 3.3(b).

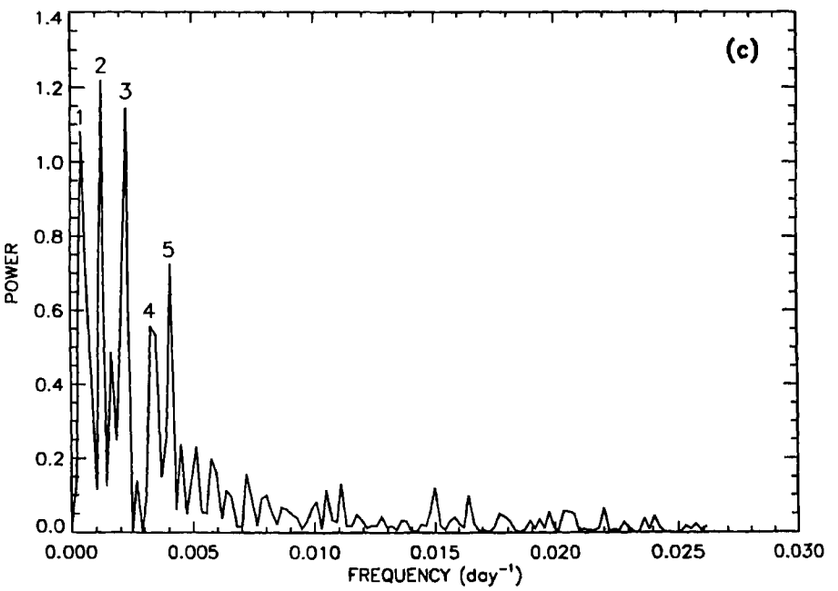

Figure 3.3(c).

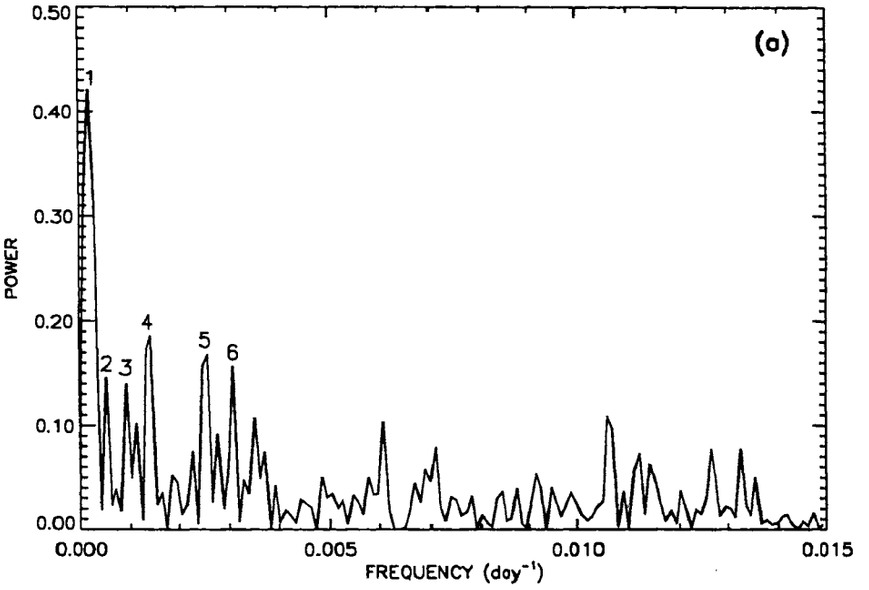

Figure 3.4(a).

Figure 3.4a-c. Power spectra of $\bar{B}$ determined from Mt. Wilson velocity data: (a) 1969–1994, (b) 1969–1981 and (c) 1982–1994. The serial numbers of periodicities given in Table 3.3 are marked near the top of each peak.

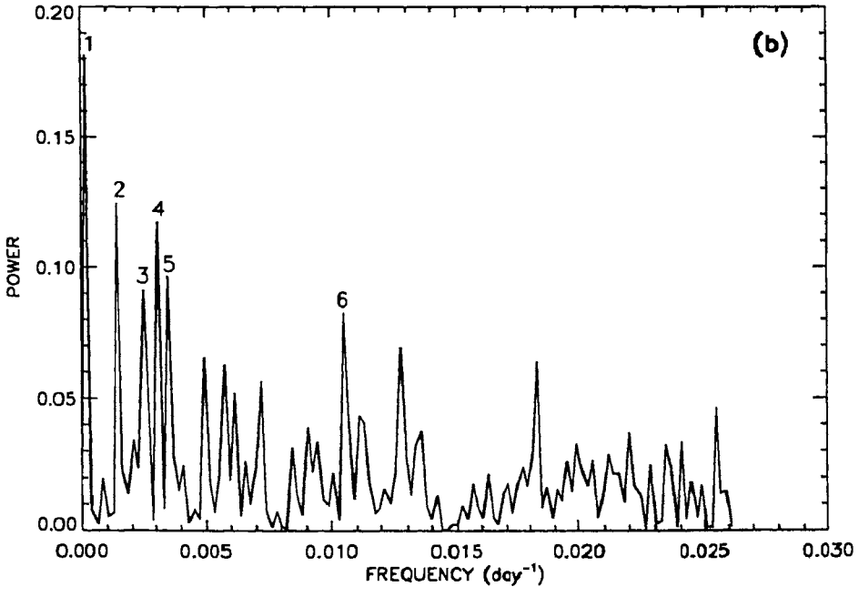

Figure 3.4(b).

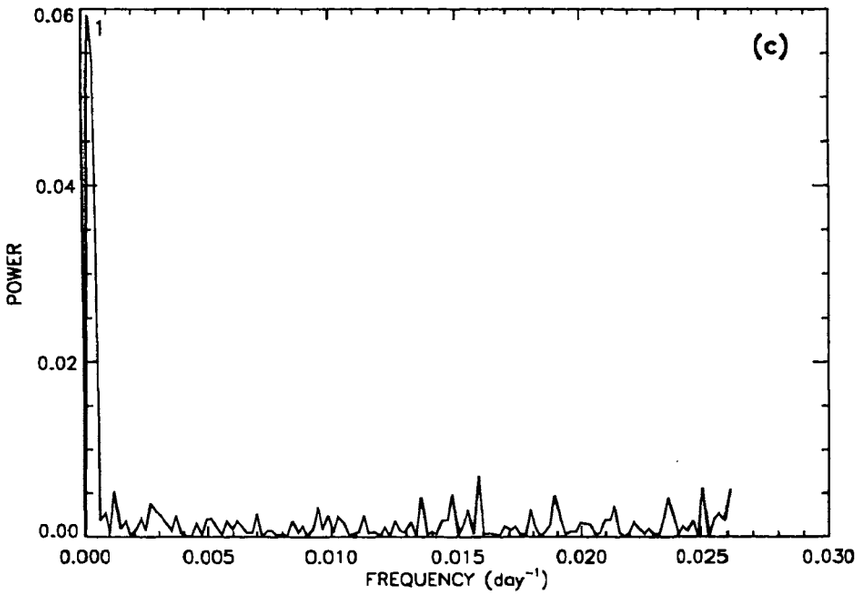

Figure 3.4(c).

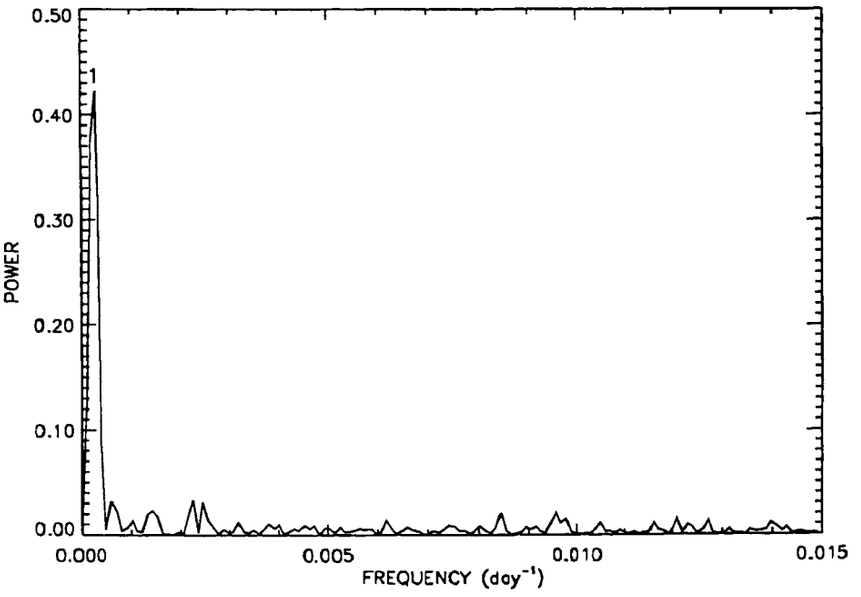

Figure 3.5. Power spectrum of C determined from Mt. Wilson velocity data during the whole period 1969–1994.

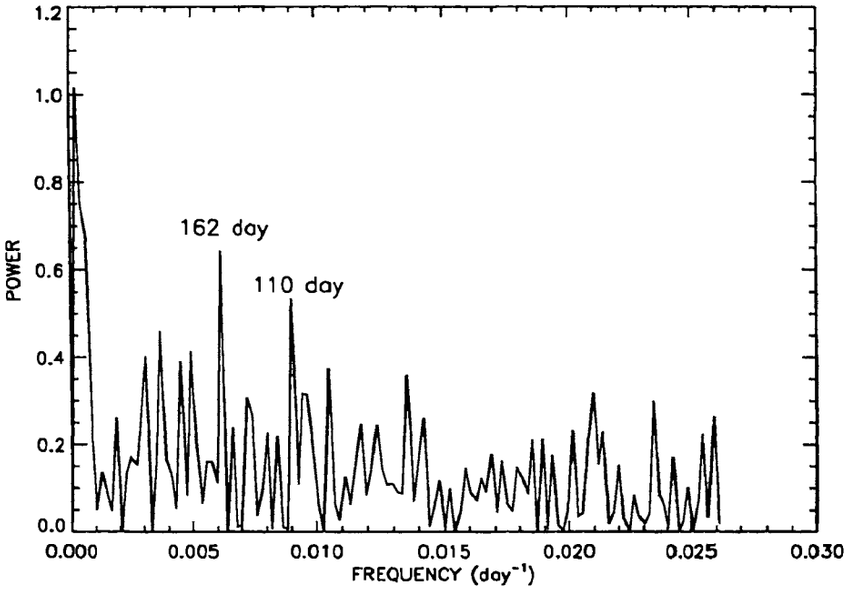

Figure 3.6. Power spectrum of the ratio B/A of the differential rotation coefficients A and B determined from the Mt. Wilson velocity data during 1969-1981.

Table 3.3 shows the periodicities with a significance level greater than 2σ (or 95%). Note that the frequency bin is $\Delta\nu = 2.0559 \times 10^{-4}\mathrm{day}^{-1}$ for the subsets, thus the first few points in the subset power spectra represent periods of 13.3, 6.66, 4.44, 3.33 years and so on, while the frequency bin of the whole data set is half this size. We follow the rule (cf. Thomson 1990) that in order to be considered significant and not just due to sampling fluctuations the 'confidence level' of a peak has to be equal or greater than $1 - \frac{1}{N}$ in a data set of length N. Therefore, we discuss only periodicities with $\sigma \geq 3.0$.

For $\bar{A}$, we find that the time series 1969-1994 is dominated by the data before 1982 leading to the same periods in the complete data set and in the first subset. In 1982-1994, the 11-yr solar cycle is absent, but we find higher harmonics such as a period at half the solar cycle. In addition, we find periodicities with 2.2 ± 0.4 yr, 1.2 ± 0.2 yr, and 243 ± 10 day with a ≥ 3.0 confidence level in the subset 1982–1994.

For $\bar{B}$, we find a variety of periods in the complete data set and the first subset, however they do not appear in the second subset 1982-1994. To reduce uncertainties, we repeated the analysis for the ratio B/A. Figure 3.6 shows power spectrum of B/A determined from first subset (1969-1981). In this spectrum in addition to the dominant 11 yr period, the periodicities of 110 ± 3 day and 162 ± 6 day are present with a significance of 2.4σ and 3.1σ. The periods shown in Table 3.3 for $\bar{B}$ of this subset are also present in B/A at a smaller level of significance. The spectrum (figure is not

shown) of the ratio B/A of the second subset (1982–1994) shows only the 11-yr period, as $\bar{B}$ in Table 3.3. Therefore, the shorter than 11-yr periodicities of $\bar{B}$ in the first subset might be due to instrumental noise. The spectrum of $\bar{C}$ shows only the solar cycle period in the whole data set as well as any of the two subsets. Thus, the two parameters, $\bar{B}$ and $\bar{C}$, characterizing differential rotation vary with the solar cycle and show no other significant short-term periodicity.

Table 3.3. The periodicities in $\bar{A}$, $\bar{B}$, and $\bar{C}$ determined from a spectral analysis of Mt. Wilson velocity data obtained during the period 1969–1994 and the two subsets of 1969–1981 and 1982–1994. The serial numbers, identifying the peaks in Figures 3.3–3.5, and the levels of significance (in units of σ) are also given.

	Sl. No.	1969–1994 Period	σ	1969–1981 Period	σ	1982–1994 Period	σ
$\bar{A}$:							
	1	5.3 ± 1.3 year	8.4	4.4 ± 1.0 year	8.2	6.7-4.4 year	4.6
	2	1.4 ± 0.1 year	3.0	1.7 ± 0.2 year	2.5	2.2 ± 0.4 year	5.3
	3	360 ± 30 day	4.5	374 ± 30 day	2.9	1.2 ± 0.2 year	4.9
	4					304 ± 30 day	2.2
	5					243 ± 10 day	3.0
$\bar{B}$:							
	1	∼ 13.3 year	8.5	∼ 13.3 year	6.0	∼ 13.3 year	8.2
	2	5.3 ± 1.3 year	2.5	1.9 ± 0.3 year	3.9		
	3	3.0 ± 0.5 year	2.4	1.1 ± 0.1 year	2.6		
	4	1.9 ± 0.3 year	3.4	324 ± 20 day	3.6		
	5	1.1 ± 0.1 year	3.0	286 ± 16 day	2.8		
	6	324 ± 10 day	2.7	95 ± 2 day	2.3		
$\bar{C}$:							
	1	∼ 13.3 year	10.0	∼ 13.3 year	10.6	∼ 13.3 year	8.6

3.4.2. PERIODICITIES IN THE ROTATION PARAMETERS DETERMINED FROM SUNSPOT GROUP DATA

Figure 3.7 shows the annual sunspot rotation rates (×) according to their year relative to the nearest sunspot minimum (1923, 1934, 1944, 1955, 1965, 1975, 1986) to search for a solar cycle variation, as done by Gilman & Howard (1984) and Balthasar et al. (1986). We excluded two years data (1932 and 1933) which have errors larger than three times the median error, as discussed above, and we mark the data of the year 1962 with a different symbol (□) since it shows a positive $\bar{B}$ value and a rather large deviation from the average $\bar{A}$ and $\bar{B}$ values. The solid line connects average values, excluding 1962, and the displayed error bars are the corresponding standard deviations. The grand average is included as dotted line. We find a variation with the cycle in $\bar{A}$ such that $\bar{A}$

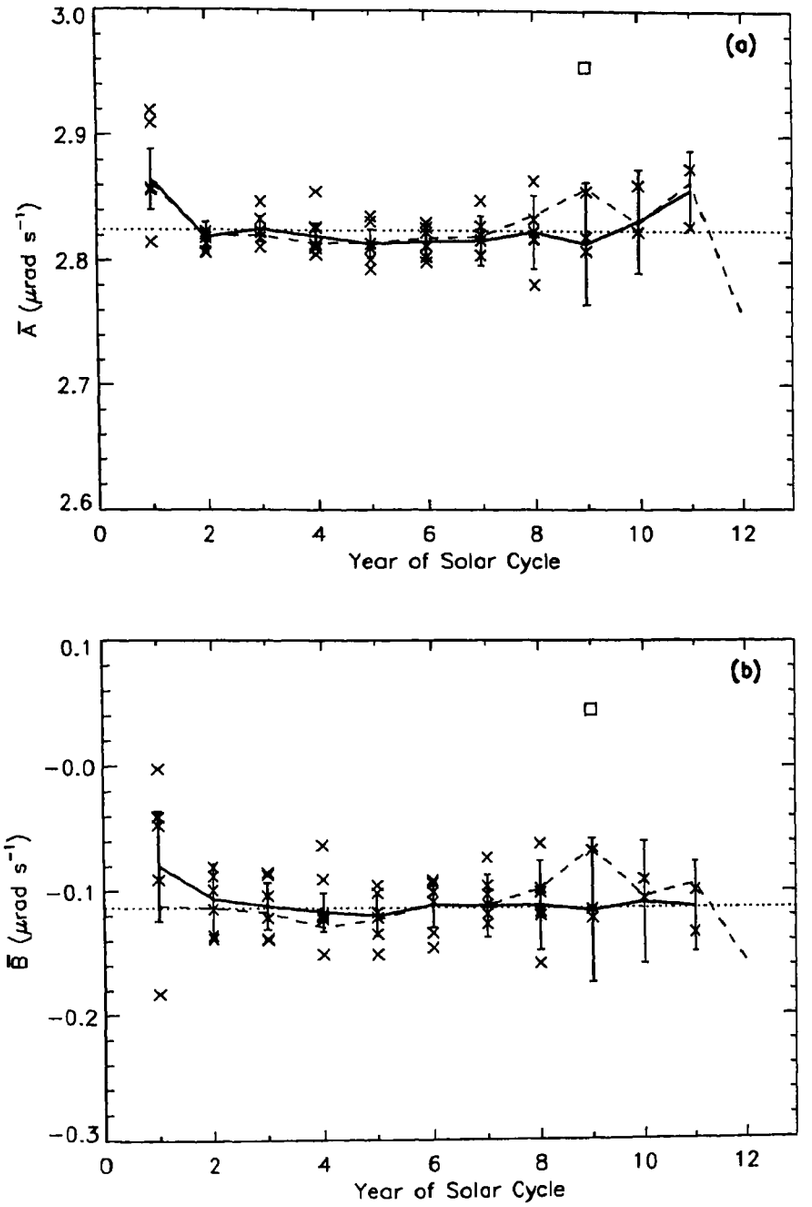

Figure 3.7a-b. $\bar{A}$ and $\bar{B}$ determined from the 'corrected' sunspot group data as a function of the year of the solar cycle. Cycle minimum corresponds to year 1, the individual values are shown as (×), the average value for a given year as solid line, and the grand average values as dotted lines. The results by Balthasar et al. (1986) are included as dashed line.

is slightly larger than average during cycle minimum and slightly smaller than average during cycle maximum. The difference between maximum and minimum is about two standard deviations. We find no comparable cycle variation in $\bar{B}$. The variations in $\bar{A}$ and $\bar{B}$ are very similar to the ones reported by Balthasar et al. (1986), included as dashed line, with the exception of year nine where they found a strong increase. We can reproduce this increase by including the year 1962. Thus the value of year nine hinges on the reliability of a single data point.

We then calculated power spectra of the yearly sunspot group data. Table 3.4 shows all periods with a significance level above 1.8σ for the original time series and the one corrected for outliers; Figure 3.8 shows the corresponding spectra of $\bar{A}$ and $\bar{B}$ of the corrected data. According to the $1 - \frac{1}{N}$ rule (cf. Section 3.4.1), we should only consider periodicities as being significant with a $\geq 2.6\sigma$ level.

Table 3.4. The periodicities in $\bar{A}$ and $\bar{B}$ determined from a spectral analysis of sunspot group data; the original data and corrected for measurements with error bars larger than three times the median error. The serial numbers, identifying the peaks in Figure 3.8, and the levels of significance (in units of σ) are also given.

	Sl.	original		corrected	
	No.	Period	σ	Period	σ
$\bar{A}$:					
	1	$\sim$ 64 year	2.8	$\sim$ 64 year	2.4
	2	8.5 $\pm$ 0.5 year	1.9	18.3 $\pm$ 3.0 year	3.1
	3	3.1 $\pm$ 0.1 year	2.1	10.7 $\pm$ 1.8 year	1.8
	4	2.6 $\pm$ 0.1 year	2.8	7.5 $\pm$ 0.5 year	2.7
$\bar{B}$:					
	1	18.3 $\pm$ 3.0 year	2.1	18.3 $\pm$ 3.0 year	4.2
	2	8.5 $\pm$ 0.5 year	1.9	7.5 $\pm$ 0.5 year	2.1
	3	3.9 $\pm$ 0.3 year	2.1	3.0 $\pm$ 0.1 year	2.4
	4	3.1 $\pm$ 0.2 year	2.1		
	5	2.6 $\pm$ 0.1 year	1.9		
	6	2.1 $\pm$ 0.1 year	2.3		

As expected from the similar time series and the large correlation coefficient of $\bar{A}$ and $\bar{B}$ (cf. Section 3.3), some periodicities are present in both data sets. The corrected $\bar{A}$ and $\bar{B}$ spectra show periods of 18.3 years and 7.5 years. In addition, we find the 11-yr solar cycle period in $\bar{A}$ and a 3-yr period in $\bar{B}$ which is most likely a higher harmonic of the solar cycle. The 64 yr period in $\bar{A}$ indicates the existence of a longer periodicity, probably the Gleissberg cycle, but the time series is too short to adequately resolve this period.

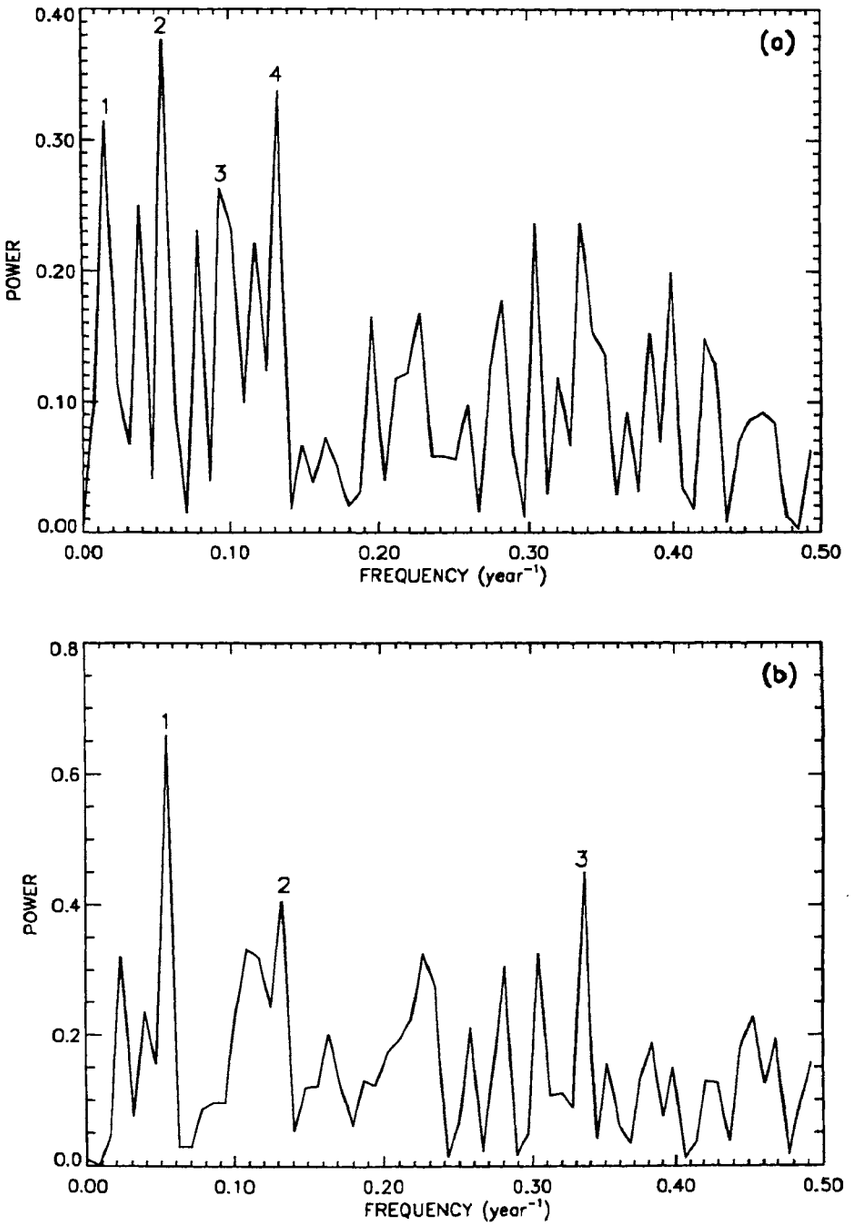

Figure 3.8. (a) Power spectrum of $\bar{A}$ and (b) that of $\bar{B}$ determined from the 'corrected' sunspot group data. The serial numbers of periodicities given in Table 3.4 are marked near the top of each peak.

When, in addition, we exclude the years 1887 and 1962, the significance of the 11-yr period in $\bar{A}$ increases from 1.8 to 3.4σ, while the significance level of all other periodicities decreases on average by 0.5 for $\bar{A}$ and 0.9 for $\bar{B}$. Though the level of significance changed considerably, the periodicities remain the same.

The spectra of the original data show the same periods as the corrected data but with different (lower) significance levels. For example, the 18.3-yr period is present with a significance level of 1σ in $\bar{A}$ and 2.1σ in $\bar{B}$. In addition, the spectra of the original data show two more periods in $\bar{A}$ of 3.1 and 2.6 years and three more in $\bar{B}$ of 3.9, 2.6, and 2.1 years. If we use only the data points with an estimated error larger than three times the median error (i.e., data during the minimum years) and set the other data points to the average value, we get similar power spectra with the same periods. Thus, these additional periodicities are clearly related to the variation during solar cycle minimum. It is difficult draw a definite conclusion on these periodicities, which either represents a 'true' solar variation during cycle minimum or the effect of uncertainties. However, the comparison of original and corrected sunspot data allows us to distinguish between solar cycle related periodicities and cycle minimum related ones. All the periodicities determined from corrected data are solar cycle related periodicities.

3.5 Confirmation of the Periodicities of the Order of the Solar Cycle Period

3.5.1. CONFIRMATION FROM TIME SERIES OF INTERVALS OF LENGTH LONGER THAN ONE YEAR

We computed the rotation parameters during non-overlapping intervals of length 2 yr (2-yr NOI) and during the moving time intervals (MTI) of lengths 2-yr successively shifted by 1 yr (2-yr MTI), and also during the 3-yr MTI, 4-yr MTI and 5-yr MTI. Figures 3.9(a) and 3.9(b) show the variations in the values of the parameters A and B during 5-yr MTI. The successive intervals 1879–1883, 1880–1884, ..., 1972-1976 are denoted by the intervals numbers 1, 2, ..., 94, respectively, and they are shown in the bottom scale. The middle years of these intervals are shown in the top scale. In these figures it can be seen that the uncertainty bars are sufficiently small for determining the variations in A and B on time scales ≥ 5 yr.

Continuous curve in the Figure 3.10 represents the FFT power spectra of the temporal variation of B in 5-yr MTI. The spectra of the ratio B/A were found to be same as that of B. In Table 3.5, we give the results obtained from the power spectra of the time series of the ratio B/A computed for 2-yr NOI, 2-yr MTI, 3-yr MTI, 4-yr MTI and 5-yr MTI (Javaraiah & Gokhale 1995).

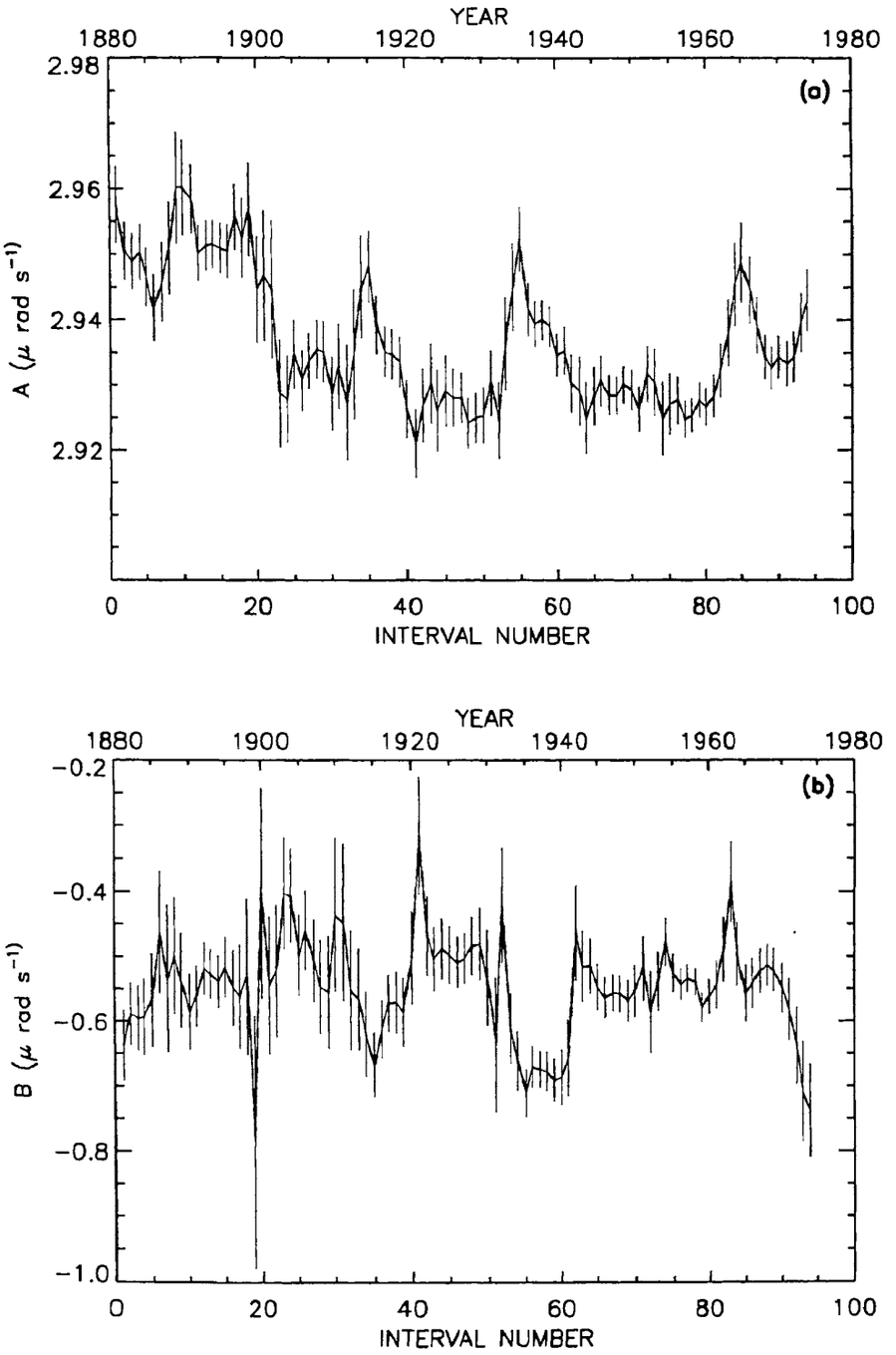

Figure 3.9a-b. Variations of the Sun's equatorial rotation rate A and the latitudinal gradient of the rotation rate B during 5-yr MTI. (The successive intervals 1879-1883, 1880-1884, ..., 1972-1976 are denoted by the intervals 1, 2, ..., 94, respectively, and they are shown in the bottom scales. The middle years of these intervals are shown in the top scales.)

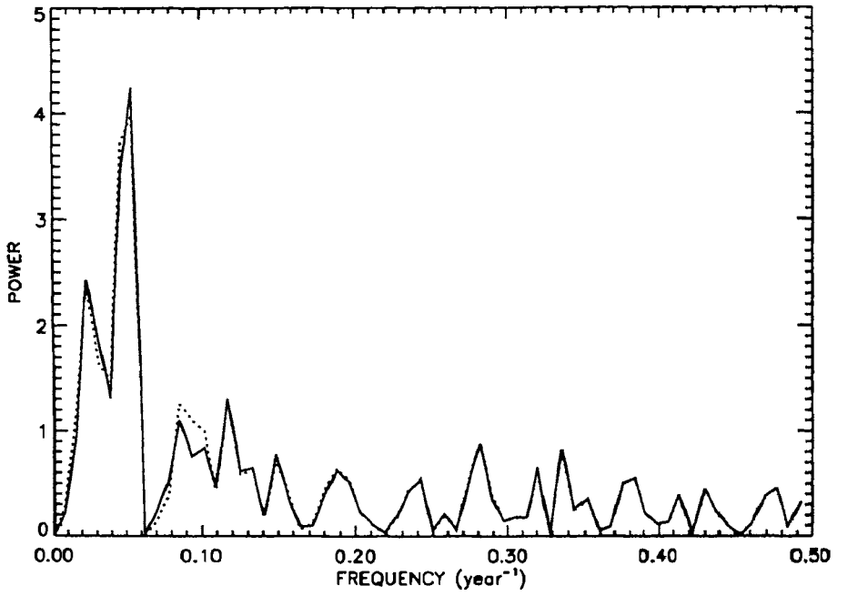

Figure 3.10. Continuous curve represents the power spectrum of B determined from sunspot group data during 5-yr MTI. The spectrum of corresponding simulated variation B' is represented by dotted curve.

Table 3.5. Periods of B/A (or B or $\dot{B}$) with their uncertainties derived from FFT analysis of temporal variations represented by values during different sequences of >1 yr intervals of the spot group data . Below the value of each period the level of significance, in units of standard deviation (σ), is given in brackets.

The sequences of	Periods (in years) and levels of significance				
2-yr NOI	18.3 $\pm$ 3.0	7.5 $\pm$ 1.0	4.6 $\pm$ 1.0		
	(3.6)	(1.7)	(2.5)		
2-yr MTI	43 $\pm$ 10	18.3 $\pm$ 2.0	8.5 $\pm$ 1.0		
	(1.9)	(5.6)	(3.3)		
3-yr MTI	$\sim$ 43	$\sim$ 32	18.3 $\pm$ 2.0	8.5 $\pm$ 1.0	
	(2.5)	(1.0)	(5.7)	(3.3)	
4-yr MTI	$\sim$ 43	$\sim$ 32	$\sim$ 21	18.3 $\pm$ 2.0	8.5 $\pm$ 1.0
	(1.8)	(1.3)	(1.5)	(6.2)	(2.3)
5-yr MTI	$\sim$ 64	$\sim$ 43	$\sim$ 32	$\sim$21	18.3 $\pm$ 2.0
	(1.1)	(1.5)	(2.3)	(2.9)	(5.8)
	$\sim$ 12	8.5 $\pm$ 1.0			
	(1.1)	(1.0)			

It should be noted here that as the interval length increases, the uncertainties in the derived parameters reduces. However, in the power spectrum derived from larger interval lengths, the peaks corresponding to the higher frequencies are washed out, and the peaks at lower frequencies get broader.

3.5.2. CONFIRMATION FROM SIMULATED TIME SERIES

To check whether the positions and significance levels of the peaks in the power spectra of B are reliable in spite of the uncertainties in the values of A and B, we used the following method. We generated simulated time series B' of B, where in each interval the value of B' is a random number between $B - \Delta B$ and $B + \Delta B$. The dotted curve in Figure 3.10 represents the FFT spectrum of the simulated time series B'. The positions of the peaks in the spectrum of simulated time series (dotted curves) are the same (within the uncertainty limits) as in the spectrum of original time series (dotted curve). Thus, if the 'true' values of d B are anywhere within the respective uncertainty range, the positions of the peaks are the same. This is also true for the spectrum of simulated time series B'/A' of the ratio B/A, where in each interval the value of A' is a random number between $A - \Delta A$ and $A + \Delta A$. This indicates that the periodicities in Table 3.5 are not artifacts of errors in the values of A and B.

3.5.3. DETERMINATION OF PERIODS FROM MAXIMUM ENTROPY METHOD

To determine the values of the periodicities with better accuracy, we have computed the spectra of B/A by maximum entropy (MEM) analysis for autoregressive (AR) process order $p = n/2$ and $p = n/3$, where n is the number of intervals in the analyzed series (Ulrych & Bhishop 1975). The MEM power spectra showed presence of peaks at the positions where the FFT spectra show. In addition, in the MEM spectra the peaks were found to be well defined (Javaraiah & Gokhale 1995) .

3.5.4. CHECKING THE EFFECTS OF VARIATION IN THE LATITUDE DISTRIBUTION OF SUNSPOT ACTIVITY

Near the latitude of 35°, sunspots appear only in the beginning of the solar cycle and the mean latitude of all sunspots is $\sim 15°$. Hence, as in Balthasar et al. (1986), we have fitted the rotation values to the form

$$\omega(\lambda) = G + H(sin^2\lambda - sin^2 15°).$$

Obviously $H = B$ and $G = A + Hsin^2 15°$. As in their work, we find that the variation and uncertainties in G are slightly smaller than those in A. We find that the periodicities in H/G are same as those in B/A. Thus, the periodicities in B/A are not artifacts of the variation in the latitudinal distribution of the spot groups.

3.5.5. CHECKING FROM THE DATA OF YOUNG AND OLD GROUPS

Balthasar et al. (1986) pointed out that the variation of the rotation rate during the 11-yr sunspot cycle comes from the variation in the rotation rates of young groups (and not from the variation in the percentage of the young groups in the whole sample). We find that the periodicities in the differential rotation derived from the sunspot group data are not due to the variations in the relative contributions to the data from the young (age $\leq$ 3 days) or the old (age $>$ 3 days) groups. This point is addressed in the Chapter VI from the analysis of the well defined samples of the data of young and old groups.

3.6. Comparison of the Periodicities Determined From Velocity and Sunspot Data Sets

We can compare only periods longer than 2 years, because the temporal resolution and length of the two data sets are different, as described in Sections 3.2.2 and 3.2.3, leading to different frequency bin sizes and Nyquist frequencies in the resulting power spectra. Moreover, the spot group data are limited to $\pm 35°$ in latitude and the rotation rate depends on the type of spot groups used (see Chapter V).

Tables 3.3 and 3.4 show that there are considerable differences in the periodicities (and/or their level of significance) of $\bar{A}$ and $\bar{B}$ determined from sunspot and velocity data. There is a variation with the 11-yr solar cycle in $\bar{A}$ of the sunspot data but not in the velocity data, which instead show a period of about half the 11-yr cycle absent in the sunspot data. The spectrum of $\bar{B}$ of the velocity data shows the 11-yr solar cycle, while $\bar{B}$ of the sunspot data shows a period almost twice that long ($\sim$ 22-yr magnetic cycle) which is also present in $\bar{A}$ of the sunspot data and which has no correspondence in the velocity data. The sunspot data show additional harmonics of the solar cycle which have no counterpart in the velocity data. On the other hand, the $\bar{A}$ of velocity data show some shorter periods which are absent in the sunspot data.

3.7. Comparison of Periodicities in the Solar Differential Rotation With Those of Surface Magnetic Field.

The 18.3 ± 3.0 yr periodicity in the differential coefficient B determined from the spot group data matches with the '22-yr' band of the surface magnetic field determined by Stenflo & Vogel (1986) from the Spherical harmonic Fourier analysis of magnetogram data during 1960-1985, and determined by us from the Legendre Fourier analysis of distribution of magnetic field inferred from sunspot data (Chapter II). The 7.5 ± 1.0 yr periodicity of B approximately matches with the $\sim$ 22/3-yr period, viz., the 'third harmonic of the 22-yr band, determined by Bracewell (1988) from the analysis of annual

mean sunspot numbers with signs attached, and by us (cf., Chapter II) in the magnetic field inferred from the sunspot data. The 3.9 $\pm$ 0.4 and 2.6$\pm$ 0.2 year periods of B (original data), match with the 4.19 and 2.55 year periods found in the photospheric magnetic field by Csada (1974) using the magnetograms (1959–1967).

Since the differential rotation is essentially a torsion, the agreement between the periods in the magnetic field and in the differential rotation coefficient, B, strongly suggest that the 'solar magnetic cycle' essentially consists of 'torsional MHD oscillations' as suggested by LaBonte & Howard (1982a), (though the torsional oscillations which they found have 11-yr periodicity), and argued by us in Chapter II.

3.8. Conclusions and Discussion

Conclusions:

From the study of the temporal variations in the differential rotation parameters deduced from Mt. Wilson velocity data during 1969-1994 and from GPR sunspot group data during 1879-1976, we have drawn the following conclusions.

(1) There are considerable differences in the temporal behaviour of $\bar{A}$, $\bar{B}$, and $\bar{C}$ determined from velocity data before and after 1982 when the instrument was substantially improved.

(2) The temporal variation of $\bar{A}$ determined from velocity data during 1982–1994, have periodicities of 6.7-4.4 yr, 2.2 $\pm$ 0.4 yr 1.2 $\pm$ 0.2 yr, and 243 $\pm$ 10 day with $\geq 3\sigma$ confidence level.

(3) In the variation of $\bar{B}$ determined from the velocity data during 1982-1994, the $\sim$ 11 yr periodicity is dominant and no other significant short periodicity is found. Including velocity data prior to 1982 leads to additional periodicities with $\geq 3\sigma$ confidence level which are most likely of instrumental origin.

(4) In the variations of $\bar{C}$ determined from the velocity data obtained before the year 1982 and also from the year 1982 onward, the $\sim$ 11 yr periodicity dominates and no other significant periodicity is found.

(5) There are considerable differences in the temporal behaviour of $\bar{A}$ and $\bar{B}$ determined from sunspot and spectroscopic velocity data.

(i) The 11-yr solar cycle is absent in $\bar{B}$ of the sunspot data, while it appears to be present in $\bar{A}$. This is the opposite to the behavior of $\bar{A}$ and $\bar{B}$, obtained from spectroscopic data.

(ii) The sunspot data show higher (than second) harmonics of the solar magnetic cycle which are not present in the spectroscopic data.

(iii) There exists a large positive correlation between $\bar{A}$ and $\bar{B}$ determined from the spot group data, while $\bar{A}$ and $\bar{B}$ from the spectroscopic data show a small anticorrelation. In sunspot data, $\bar{A}$ is slightly larger than average during cycle minimum and slightly smaller during cycle maximum.

Discussion:

The difference in the temporal variation of rotation determined from velocity and from sunspot measurements are understandable if the sunspot rotation is representative of rotation at some depth in the convection zone, while the velocity measurements represent the surface rotation (Foukal 1972). In Figure 3.11, we show the radial variation of the Sun's rotation frequency ($\Omega(r)$) at latitude 15° (continuous curve) provided by Dr. H. M. Antia, who determined it from the Big Bear Solar Observatory (BBSO) helioseismic data (Woodard & Libberecht 1993) using the inversion method of Antia & Chitre (1996). The surface rotation frequency at this latitude, determined from Mt. Wilson velocity data during 1982–1994, is included as '+' and the rotation frequency, determined from the entire sunspot group data during 1874-1976, is included as '×'. We find that the average sunspot rotation frequency equals the rotation frequency at radius $r \sim 0.93 R_{\odot}$, which is rather close to the solar surface. However, this is an average over all sunspot data, while it is well-known that sunspots of different size and age show different rotation rates (Howard et al. 1984; Balthasar et al. 1986; Javaraiah & Gokhale 1997b; cf., Chapter V). D'Silva & Howard (1994) attribute the higher rotation rate of sunspots to an interaction between magnetic buoyancy and drag coupled with the Coriolis force acting on rising flux tubes. The validity of this assumption is discussed in Javaraiah & Gokhale (1997b), where we inferred 'anchoring' depths for the sunspot groups of different life spans and age using the rotation frequency as a function of depth determined from helioseismic studies (described in Chapter V). In Chapter VI we discuss the periodicities in differential rotation determined from the well defined young and old groups.

The periodicities found in the sunspot velocity data are related to the solar cycle, and the spectroscopic velocity data show the 11-yr cycle in $\bar{B}$ and $\bar{C}$ and no other significant periods. This leaves only the short-term periodicities in $\bar{A}$ of the velocity data unexplained. For this reason, we compare these short-term periodicities with periods found in other indicators of solar activity which might have a physical significance rather than being a coincidence. The '1.2 -1.5 yr' periodicity in $\bar{A}$ is also found in solar flare activity (Ichimoto et al. 1985) and in solar neutrino flux and in several solar-terrestrial phenomena (see Liritzis 1995). However, Walther (1998) argues that the correlation between solar neutrinos and sunspots were based on a statistical fallacy. Interestingly, Howe et al. (2000a) have detected 1.3 yr periodicity in the rotation of the Sun near the base of its convective envelope at low latitudes, using GONG and SOHO helioseismic data over a 4.5 yr time span (from May 1995 to November 1999). Other

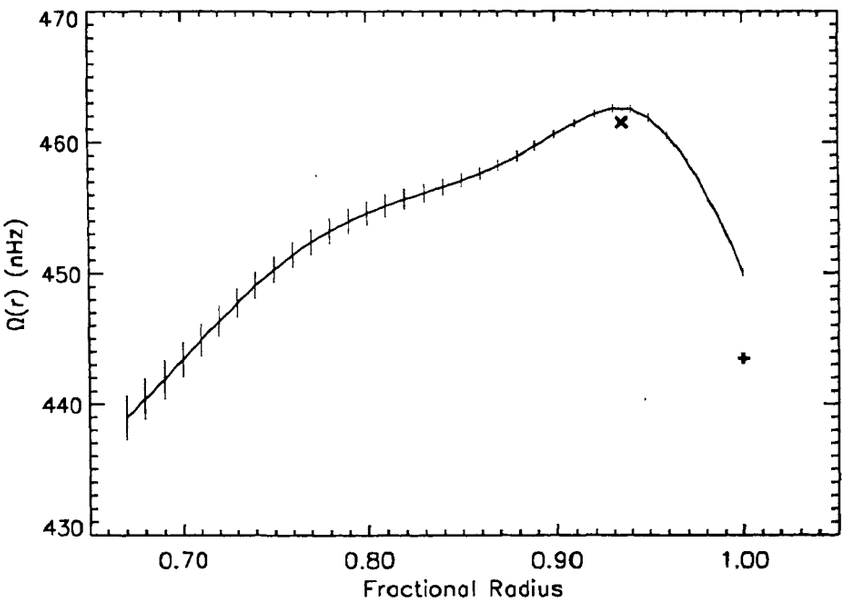

Figure 3.11. The radial variation of the Sun's angular frequency ($\Omega(r)$) at latitude 15° provided by Dr. H.M. Antia. The surface rotation at this latitude, determined from Mt. Wilson velocity data during 1982-1994, is included as '+' and the rotation frequency, determined from the entire sunspot group data during 1874-1976, is included as '×'.

short-term periodicities (2.66 yr, 1.96 yr, 330.7 day) were detected in measurements of solar diameter variation during 1975-1984 (Delache et al. 1985). A number of authors have shown the existence of a 150-158 day periodicity in flare activity and flare related data, solar neutrino flux variation, solar diameter variation and daily sunspot area (see Carbonell & Ballester 1992 and references therein) which is insignificant or absent in the present analysis. The short-term periods in $\bar{A}$ are similar to periods found in other indicators of solar activity suggesting that they are of solar origin. However, we cannot completely rule out that they are due to some subtle instrumental effect. To clearly establish the origin of these short-term periods in $\bar{A}$, we need good velocity rotation measurements for at least another solar cycle. Furthermore, there probably exist short-term variations which are episodic in nature (e.g., Bai & Sturrock 1991; Bai 1994; Oliver & Ballester 1995).

Chapter IV

PERIODICITIES IN THE NORTH–SOUTH ASYMMETRY OF THE SUN'S SURFACE ROTATION

4.1. Introduction

In previous chapter I presented periodicities in the Sun's 'mean' rotation rate $\bar{A}$ and in differential rotation coefficients $\bar{B}$ and $\bar{C}$ determined form Mt. Wilson Doppler velocity data, and the periodicities in $\bar{A}$ and $\bar{B}$ determined from sunspot group data. The periodicities in $\bar{B}$ and $\bar{C}$ represent even-parity modes of the Sun's torsional oscillations which are symmetric about the equator. In this chapter we discuss periodicities in the north–south (N–S) asymmetries of $\bar{A}$ and $\bar{B}$ (Javaraiah & Gokhale 1997a), which may represent the odd-parity modes of Sun's torsional oscillations (Howard & LaBonte 1983; Snodgrass & Howard 1985).

Existence of N-S asymmetry in the solar activity is shown by several statistical studies for most of the solar activity phenomena (see e.g., Carbonell et al. 1993 and references therein), but the cause of the N–S asymmetry of solar activity is not known so far (e.g.,see Sokoloff & Ribes 1994). Existence of $\sim$ 11 yr and a few other periodicities in N–S asymmetries of various indices of solar activity were also shown by a number of authors (for reference see Table I in Duchlev & Dermendjiev 1996). Even-parity modes in the Sun's global magnetic oscillations which might correspond to N–S asymmetry in the differential rotation are also known to exist, but with relatively smaller amplitudes (Stenflo & Vogel 1986; Gokhale & Javaraiah 1990a; cf., Chapter III). Existence of N–S asymmetry in the differential rotation rate is shown by a number of authors (e.g., Balthasar et al. 1986; Gilman & Howard 1984; Hathaway & Wilson 1990; cf., Chapter III). However, its relation to the solar activity in general and to the N–S asymmetry of solar activity in particular is not yet clear. Study of the temporal variations in the N–S asymmetry of the differential rotation rate is therefore important.

In Section 4.2 of this chapter we describe the spot group data and determine values of A, B and $\bar{A}$ in the N and S hemispheres and their N–S asymmetries. In Section 4.3 we show the temporal variations of A and B in the N and S hemispheres. In the same section we also show the temporal variations of the N–S asymmetries of A, B, $\bar{A}$, and of amount of activity, and discuss these variations briefly. In Section 4.4 we determine the periodicities in the N–S asymmetries of A, B and $\bar{A}$ using fast Fourier transform (FFT) analysis and confirm the presence of the periodicities in the asymmetries of A, B and $\bar{A}$ from similar analysis of a simulated series. In the same section we also determine the

values of the periodicities in the asymmetries of A, B and $\bar{A}$ from MEM analysis and confirm the periodicities from the young and the old spot groups data. In Section 4.5 we determine short-term periodicities in the N-S asymmetries of the differential rotation coefficients from Mt. Wilson velocity data. In Section 4.6 we suggest the existence of a relation between the asymmetric global modes in the solar magnetic field and those in the asymmetries of A, B, and $\bar{A}$. We then compare the periodicities in the N–S asymmetry of sunspot activity with those in the asymmetries of A, B, and $\bar{A}$. In Section 4.7 we comment on matching of some dominant periodicities of the rotation coefficients with the periods of configurations of major planets. In Section 4.8 we summarize the conclusions and briefly discuss their interpretations.

4.2. Data and Analysis

The data and the method of analysis used here are same as described in Sections 3.2.2 and 3.5.1 of the previous chapter.

The N–S asymmetry (ζa) of a measure of a solar phenomenon (ζ) can be defined as:

$$\zeta a = (\zeta n - \zeta s)/(\zeta n + \zeta s), \tag{4.1}$$

where ζn and ζs are the measures of ζ in the N and S hemispheres respectively.

Using the method of least-square fit to the well-known formula of the differential rotation, (Equation (3.2), Chapter III): $\omega(\lambda) = A + Bsin^2\lambda$, we computed An, Bn, As and Bs, during moving time intervals (MTI) of lengths 3-yr successively shifted by 1 yr (3-yr MTI) and also during the 5-yr MTI. Here An (Bn) and As (Bs) are the values of A (B) derived from the data in the N and S hemispheres respectively. (The samples given by MTI shorter than 3 years are inadequate to determine the variations.) All the least-square fits were computed by excluding the data corresponding to the 'abnormal' motions viz. displacements exceeding 3^o day^{-1} in longitude or 2^o day^{-1} in latitude. This helps us to reduce the uncertainties in the values An, Bn, As and Bs considerably (cf., Section 3.2.3 of Chapter III).

Using Equation (4.1) above, we determined the values of the N–S asymmetry Aa of A and Ba of B, during the 3-yr MTI and 5-yr MTI. For the sequences of these values of Aa and Ba, FFT and MEM analyses were used to determine the periodicities in Aa and Ba.

Due to non-orthogonality of the fit functions, the coefficients A and B may have a crosstalk which affects their temporal behaviors. Hence, as suggested by an anonymous referee of our paper Javaraiah & Gokhale (1997a), we determined, in each hemisphere, values of the coefficients $\bar{A}$ and $\bar{B}$ in the Equation (3.7) (cf., Section 3.2.3):

$$\omega(\lambda) = \bar{A} + \bar{B}(5sin^2\lambda - 1).$$

As already mentioned in the previous chapter, since C obtained from sunspot data is small, the variation of $\bar{B}$ is identical to that of B. Thus the variations and periodicities in the N–S asymmetry of B shown in the present analysis hold good for the N–S asymmetry ($\bar{B}a$) of $\bar{B}$ also. Each periodicity in the temporal variation of the N–S asymmetry Ba (or $\bar{B}a$) represents an odd parity mode of torsional oscillation. Each periodicity in the temporal variation of the N–S asymmetry ($\bar{A}a$) of the 'mean' rotation $\bar{A}$, mainly represents an odd parity mode of torsional oscillation whose spherical harmonic degree is lower than that of $\bar{B}a$.

The coefficient A is not actually the equatorial rotation rate. In each hemisphere, it is an approximate measure of the mean rotation rate over a small range of latitudes near the equator (e.g., Howard & LaBonte 1983). For completeness we show the variations and periodicities of Aa besides those of Ba and $\bar{A}a$. (Note: In the determination of the periodicities in Aa, Ba and in $\bar{A}a$, the rotation rates of spot groups during the years 1874–1878 have been omitted because of their large uncertainties mentioned in Chapter III.)

4.3. Temporal Variations in An, As, Bn, Bs, Aa, Ba and $\bar{A}a$

Solar rotation rate deduced from sunspot data depends on the type of the spot group used. Also, spots are limited to $\pm 35^\circ$ latitudes. These properties of the data may cause systematic effects in the variations of A and B (Howard & LaBonte 1983). Moreover, as a result of variation in the amount of data, the uncertainties in A and B are large during the sunspot minima and small during the sunspot maxima. The uncertainty in the ratio B/A is smaller that of B (cf., Section 3.2.2). Similarly, if $\Delta(An)$ and $\Delta(As)$ are the uncertainties in An and As respectively and $\Delta(An) \sim \Delta(As) = \xi$ (say), then it can be shown that the $\Delta(Aa) \sim \xi/(2As\sqrt{m})$, where m is the number of data points in either hemisphere. Similar expressions also hold for $\Delta(Ba)$ and $\Delta(\bar{A}a)$. Consequently, the variations Aa, Ba and $\bar{A}a$ are easier to detect than those in A, B and $\bar{A}$.

Figures 4.1(a), 4.1(b), 4.2(a) and 4.2(b) show the variations in An, As, Bn and Bs respectively during 5-yr MTI. The successive intervals 1879–1883, 1880–1884,....,1972–1976 are denoted by the interval numbers 1, 2,...,94 respectively and they are shown in the bottom scale. The middle years of these intervals are shown in the top scale. In these figures it can be seen that the uncertainty bars are sufficiently small for determining the variations in An, As, Bn and Bs on time scales $\geq$ 5-yr.

Figures 4.3(a), 4.3(b) and 4.3(c) show the variations in Aa, Ba and $\bar{A}a$ respectively derived from the 3-yr MTI (dotted curve) and 5-yr MTI (dashed curve). In these figures it can be seen that the average amplitude of Ba is substantially larger than that of Aa. There exists a good resemblance in the patterns of variations in Aa and Ba, though the relative amplitudes of their variations are not proportional. However, there exist cross

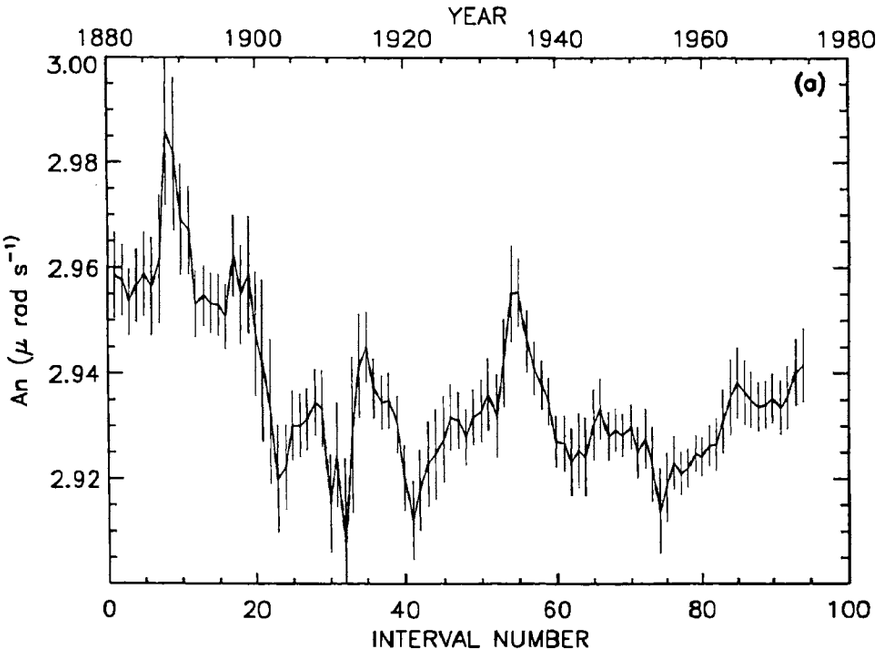

Figure 4.1(a).

Figure 4.1a–b. Variations of the Sun's equatorial rotation rates An and As in the (a) N- and (b) S-hemispheres during 5-yr MTI. (The successive intervals 1879–1883, 1880–1884,....,1972–1976 are denoted by the interval numbers 1, 2,...,94 respectively and they are shown in the bottom scales. The middle years of these intervals are shown in the top scales.)

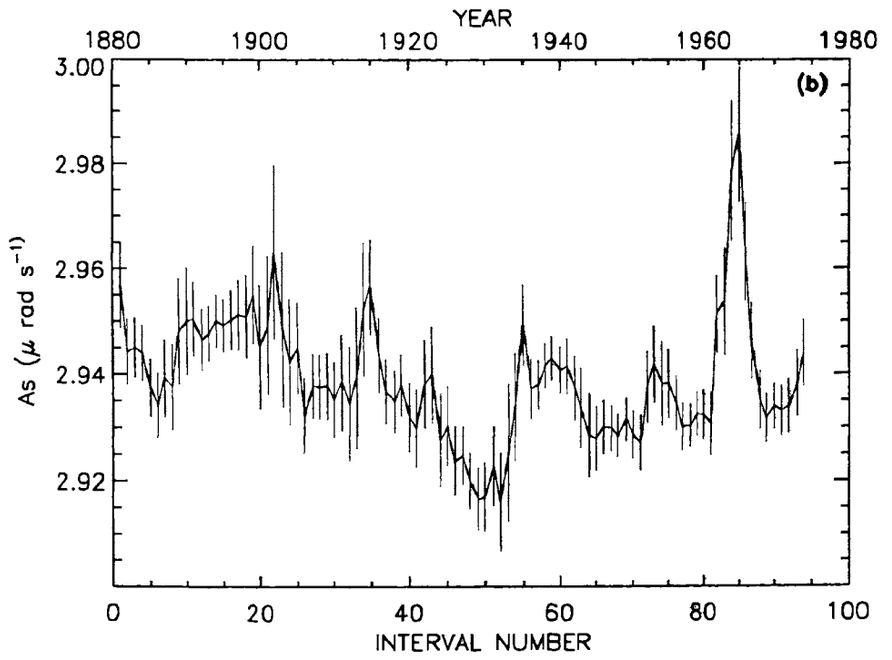

Figure 4.1(b).

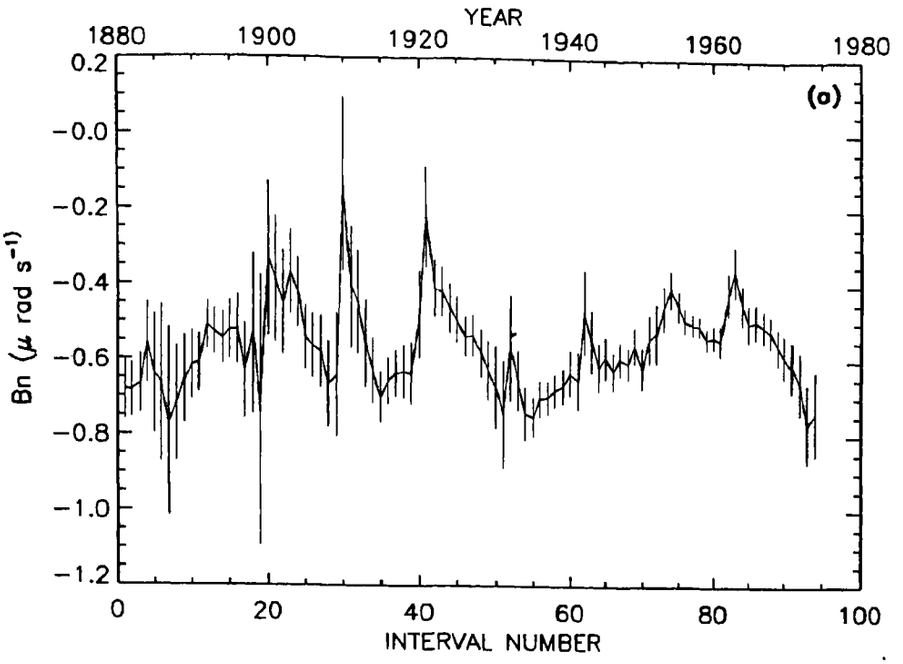

Figure 4.2(a).

Figure 4.2a-b. Variation of the latitudinal gradients, Bn and Bs of the Sun's rotation rate in the (a) N- and (b) in the S-hemispheres during 5-yr MTI. (The bottom and the top scales have the same notations as in Figure 4.1.)

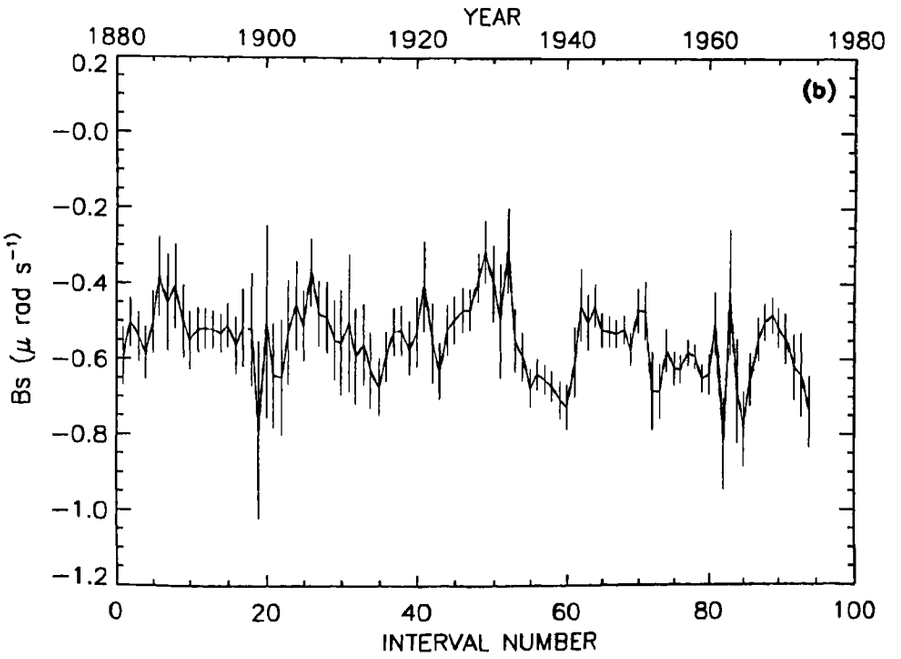

Figure 4.2(b)

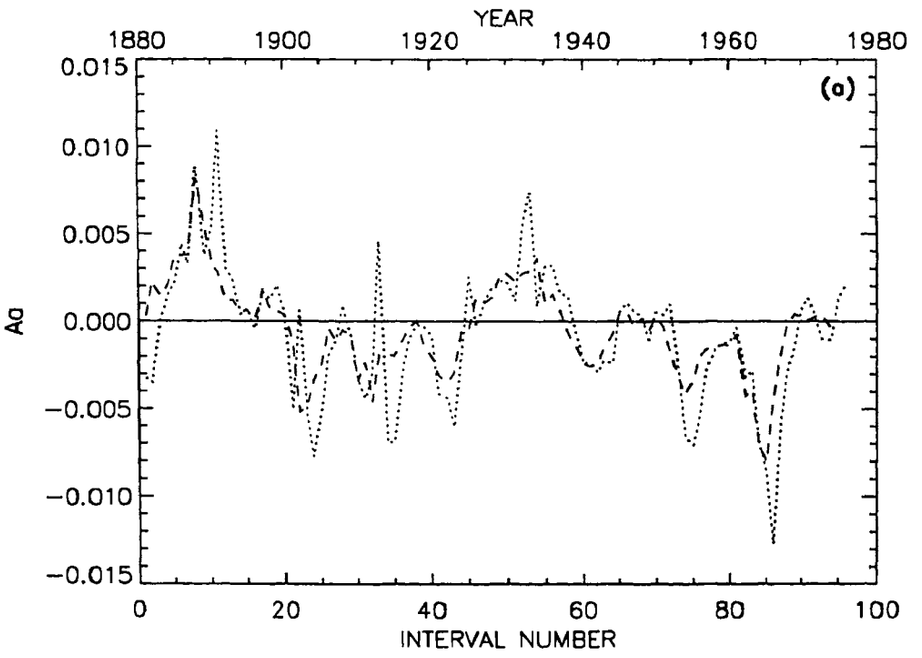

Figure 4.3(a).

Figure 4.3a-c. Variations of the N-S asymmetries Aa, Ba and $\bar{A}a$ respectively, calculated during 3-yr MTI (dotted curve) and 5-yr MTI (dashed curve). (The bottom and the top scales have the same notations as in Figure 4.1). Error bars are not shown here since they are quite small (see Section 4.3).

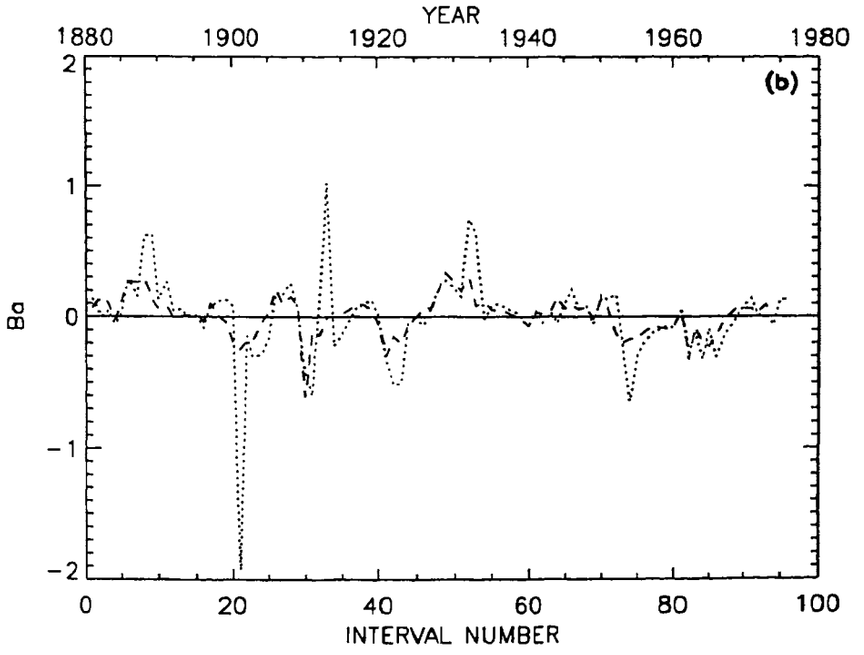

Figure 4.3(b).

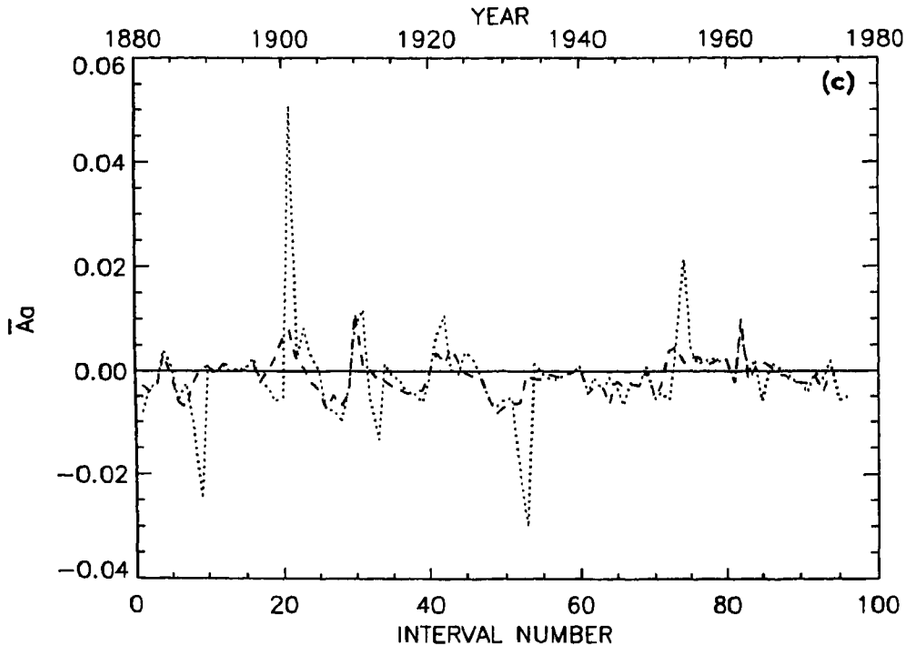

Figure 4.3(c).

talks between An and Bn, and between As and Bs. Hence, the resemblance between Aa and Ba may not have a physical meaning. In fact the variation in $\bar{A}a$ is much more similar in character to the variation in Ba, except for the opposite sign. [This is expected from the definition of $\bar{A}$ (see Section 2.2.1 of Chapter III) because in each hemisphere, the amplitudes of variations in B are much larger than those of A (see Figures 4.1 and 4.2).]. This anticorrelation of $\bar{A}a$ and Ba might be having a physical meaning.

The values of Ba are positive in the interval numbers 1–20 (corresponding to the period 1882–1893) and 46–57 (corresponding to the period 1924–1939). Thus, during these periods the N-hemisphere rotated more differentially than the S-hemisphere. During the former period the solar activity in the S-hemisphere was on the average higher than that in the N-hemisphere and during the latter one, there was no significant difference in the amounts of activities in the two hemispheres (e.g., see White & Trotter 1977; Yi 1992). Except during the former period, there is no definite anticorrelation between the N–S asymmetry of the amount of activity and that of the differential rotation on time scales '3–5 yr'. In order to verify this we computed the correlations of Aa, Ba and $\bar{A}a$ to Xa, the N–S asymmetry of sunspot activity X (say). In Figure 4.4 we show the variation of Xa during 3-yr MTI (dashed curve). In the same figure we also show the variation of X during 3-yr MTI (dotted curve). (Here the number of data points gone in the determinations of A, B, $\bar{A}$ during a given interval is taken as the measure of sunspot activity during that interval.) The correlations between the Aa and

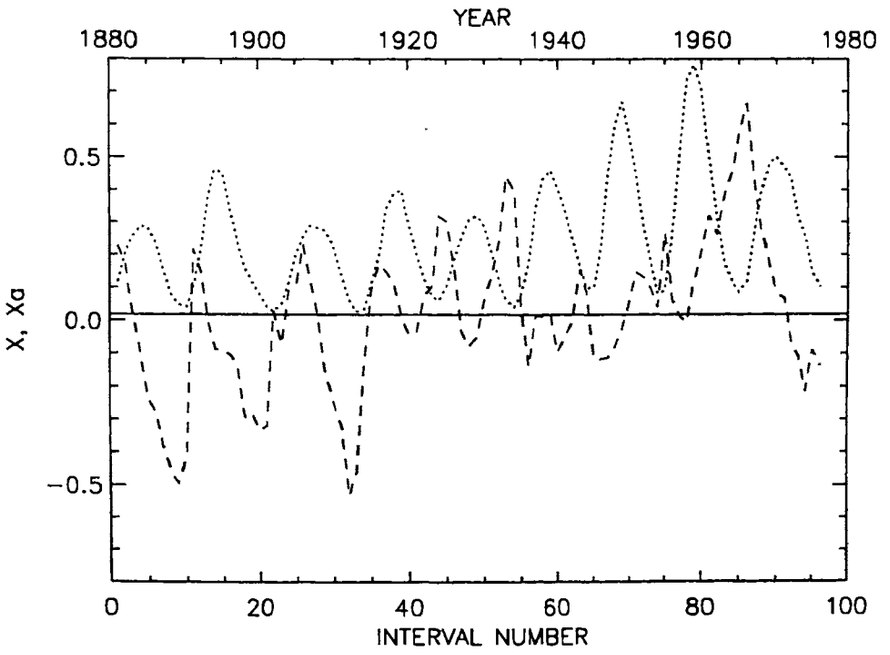

Figure 4.4. Variations of sunspot activity X (dotted curve) and of N–S asymmetry Xa (dashed curve) of X during 3-yr MTI (cf. Section 4.3). The horizontal line represents the average value of Xa.

Xa for 3-yr MTI and 5-yr MTI is found to be only -3.6% and -4.8% respectively. The correlations between the Ba and Xa of 3-yr MTI and 5-yr MTI are merely -1% and -2% respectively. The correlations between $\bar{A}a$ and Xa of 3-yr MTI and 5-yr MTI are also only 3.6% and 3.1% respectively. Thus, it seems the N–S asymmetries of rotation parameters have no relation with the N–S asymmetry of activity on time scales ≤ 5 yr.

In Figure 4.4 one can see that the average value of Xa of the first 45 intervals (before the year around 1925) has a sign (negative) opposite to that of the later intervals. The average value of the amount of activity (X) of the first 45 intervals is some what lower than that of the later intervals. In general, there exists a good anticorrelation between Xa and X suggesting existence of the periodicities $\sim$ 11-yr and $\sim$ 100 yr (e.g., Verma 1993) in Xa also as in X. The anticorrelation suggests that relative contribution from northern hemisphere is larger for the larger activity X.

4.4. Periodicities in Aa, Ba and $\bar{A}a$

4.4.1. FFT ANALYSIS

We have computed FFT (fast Fourier transform) power spectra of the sequences of values of Aa, Ba and $\bar{A}a$ for 3-yr MTI and 5-yr MTI. While computing the FFT of any sequence of values, a first-order polynomial fit obtained from the whole sequence of the values is first subtracted from each value. Next the first and the last 10% of the data is apodised by using a cosine bell function and then the size of the sequence is extended to the next power of 2 by taking an adequate number of zero values. This detrends the sequence and removes the leakage between the repeated data segments (e.g., Brault & White 1971).

It should be noted here that as the interval length increases, the uncertainties in the parameters An, As, Bn, and Bs reduce. However, in the power spectrum derived from larger interval lengths, the peaks corresponding to the higher frequencies are washed out, and the peaks at lower frequencies get broader.

For each FFT spectrum we have determined the mean ('m') and the standard deviation ('σ') over the whole frequency range. The standard deviation 's' is determined after omitting the values which are greater than $m + 2.5\sigma$ in the spectrum. The FFT spectra are discussed below.

Periodicities in Aa

The continuous curve in Figure 4.5(a) represents the FFT power spectrum of the temporal variations in Aa obtained from sequences of 3-yr MTI. This spectrum shows a very large power peak at 42.7^{+20}_{-10} yr, and another peak at 21.33^{+4}_{-3} yr, which are significant at 5.8σ and 3.2σ respectively. This spectrum also shows a broad power hump at 8 -14-yr with possible peaks at $\sim$ 14.2-yr, $\sim$ 9.8-yr and at $\sim$ 8.5-yr, which are significant at 3.8s, 2.5s and 2.3s respectively. There are also small peaks at $\sim$ 6.4-yr, $\sim$ 5.6-yr and $\sim$ 3.7-yr, whose levels of significance are in the range $\sim$ 1.0–1.5s. (Here the 2σ corresponds to 95% confidence for $n-1$ degrees of freedom and the 2s level corresponds to 95% confidence for $n-3$ degrees of freedom, where $n = 64$ is the total number of frequency values in the spectrum.)

In the FFT power spectrum of Aa obtained from the sequence of 5-yr MTI, we found the same peaks, (within the uncertainty limits), with the same significance levels as in Figure 4.5(a). Hence, this spectrum is not shown here.

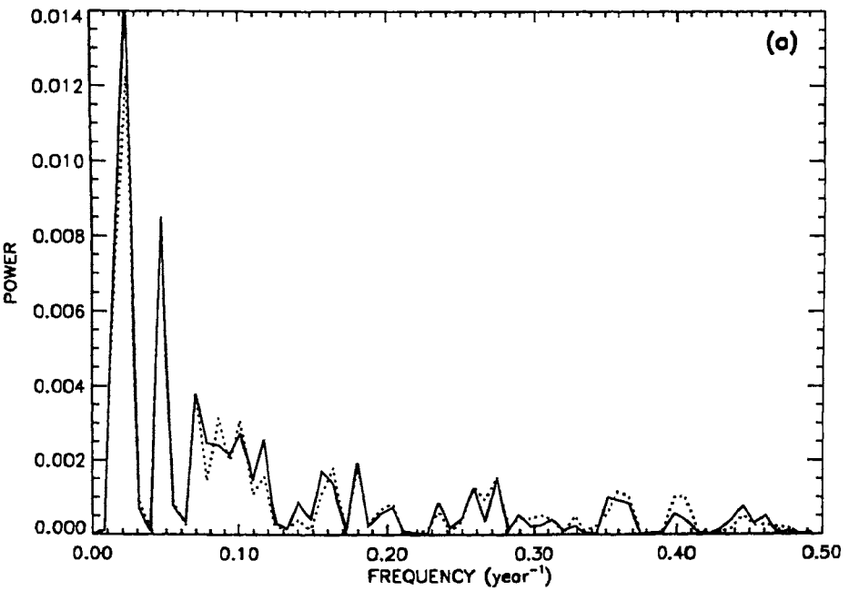

Figure 4.5(a).

Figure 4.5a–c. FFT power spectra of Aa, Ba and of $\bar{A}a$ are represented by continuous curves. The spectra of corresponding simulated variations Aa', Ba' and $\bar{A}a'$ are represented by dotted curves. (a): The spectra of Aa and Aa' are obtained from the values of 3-yr MTI. (b): The spectra of Ba and Ba' are obtained from the values of 5-yr MTI. (c): The spectra of $\bar{A}a$ and $\bar{A}a'$ are obtained from the values of 5-yr MTI.

Periodicities in Ba

The continuous curve in Figure 4.5(b) represents the FFT power spectrum of Ba obtained from the sequence of 5-yr MTI. This spectrum shows a dominant but broad peak corresponding to periods in the range '42–64-yr' which is significant at $\sim 3.5\sigma$ level. There are peaks at 21.33^{+4}_{-3} yr, 14.2 ± 1 yr, and at 10.6 ± 1 yr which are significant at levels 2.7σ, 2.3σ (4.8s) and 3.4σ respectively. This spectrum also shows the possibility of existence of periodicities in Ba at $\sim$ 8.5-yr, $\sim$ 6.1-yr and at $\sim$ 5.3-yr with $\sim$ 1.0s levels. (Here the 2σ level corresponds to 95% confidence for the $n-1$ degrees of freedom and the 2s level corresponds to 95% confidence for $n-4$ degrees of freedom.)

The FFT spectrum of Ba obtained from the sequence of 3-yr MTI is found to be quite similar to that of the 5-yr MTI. Therefore (and for another reason given in Section 4.4.2) this spectrum is not shown here.

Periodicities in $\bar{A}a$

The continuous curve in Figure 4.5(c) represents the FFT power spectrum of $\bar{A}a$ ob-

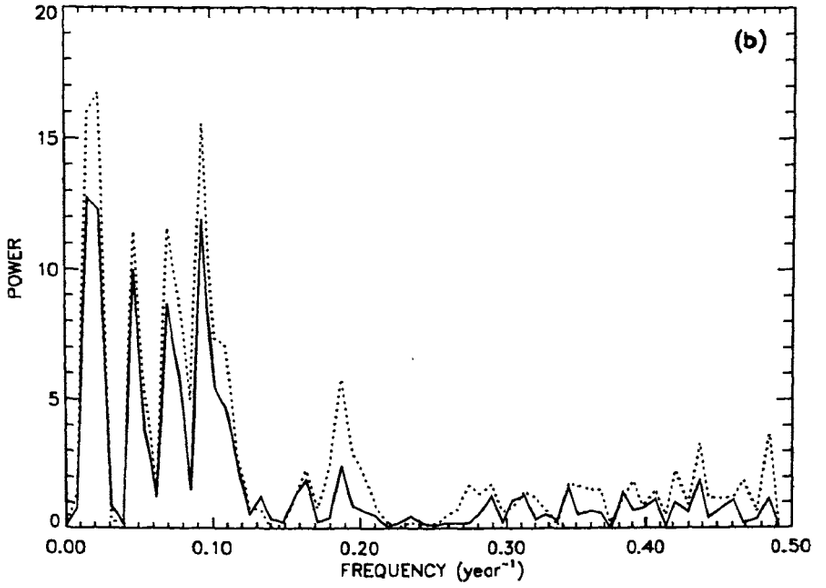

Figure 4.5(b).

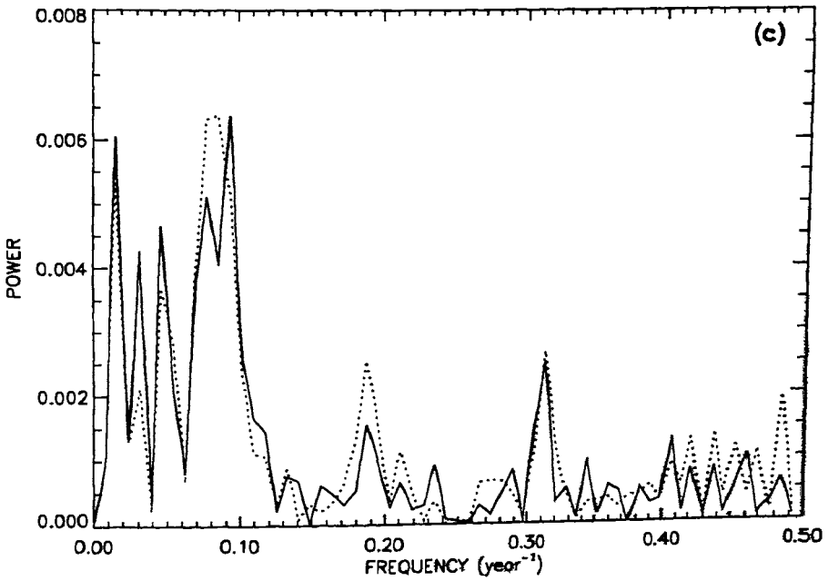

Figure 4.5(c).

tained from the sequence of 5-yr MTI. As expected (see Section 4.3), the positions and the levels of significance of the main peaks in this spectrum are almost same as those of the peaks in the FFT spectrum of *Ba*. However, the spectrum of $\bar{A}a$ shows relatively larger amount of power in the range '7-14' yrs. This spectrum also shows a peak at '32-yr' which is significant at 2.1σ (or 3.2s) level. The peak at '6.1-yr' is weaker and the one at 3.1-yr is much stronger than the corresponding peaks in the spectrum of *Ba*.

The FFT spectrum of $\bar{A}a$ obtained from 3-yr MTI (not shown here) is similar to that obtained from 5-yr MTI except for a much higher noise level.

4.4.2. CONFIRMATION FROM SIMULATED TIME SERIES OF *Aa*, *Ba* AND $\bar{A}a$

To check whether the periodicities in *Aa*, *Ba* and $\bar{A}a$ determined in Section 4.4.1 are correct in spite of the uncertainties in the values of *An*, *As*, *Bn* and *Bs*, we used the following method, which we have already used in Section 3.5.1 of Chapter III. We generated 'simulated' time series *An'* by varying each value of *An* in the time series by adding to it a random number whose magnitude is equal to or less than the uncertainty in that value. Similarly, we generated the 'simulated' series *As'*, etc.. From these series we construct the simulated series *Aa'*, *Ba'* and $\bar{A}a'$ respectively for *Aa*, *Ba* and $\bar{A}a$. We then computed the Fourier analysis of *Aa'*, *Ba'* and $\bar{A}a'$.

The dotted curves in the Figures 4.5(a-c) represent the FFT spectra of the time series *Aa'*, *Ba'* and $\bar{A}a'$. The positions and the level of significance of peaks in these spectra are the same (within the uncertainty limits) as those of peaks in the corresponding spectra (continuous curves) of the real time series of *Aa*, *Ba* and $\bar{A}a$. This shows that even if the 'correct' value of *An*, *Bn*, etc. were anywhere within the respective uncertainty range, the periodicities would be the same as those found in Section 4.4.1. Hence, the periodicities found in Section 4.4.1 are present in the true variations of *Aa*, *Ba* and $\bar{A}a$.

[In the FFT spectrum of *Ba'* obtained from 3-yr MTI, large disagreements in the positions of peaks are found in comparison with the positions of the peaks in the spectrum of *Ba*. This discrepancy is due to large uncertainties in the values of *Bn* and *Bs* during some intervals around the periods of solar minima. Thus, the periodicities in *Ba* obtained from 3-yr MTI are not reliable. Therefore the FFT spectrum of *Ba* obtained from 3-yr MTI is not shown in Section 4.4.1]

4.4.3. MAXIMUM ENTROPY ANALYSIS

To determine the values of the periodicities in *Aa*, *Ba* and $\bar{A}a$ with better accuracy, we have computed the power spectra of *Aa*, *Ba* and $\bar{A}a$ by MEM choosing various values for the order m of an autoregressive (AR) process in the range $(n/3, n/2)$ as suggested in Ulrych & Bishop (1975), where n is the total number of intervals in the analyzed

series. The MEM Fortran program was provided to us by Dr. A. V. Raveendran.

Periodicities in Aa from MEM *analysis*

In Figure 4.6(a) we show the MEM power spectra of Aa for $p = n/2$ obtained from the sequences of 3-yr MTI. The continuous and dashed curves represent the MEM power spectra of Aa and Aa' respectively. The MEM power spectra show the existence of '45 yr', '21.3 yr', '13.3 yr', '10.5 yr', '8.8 yr', '6.5 yr' and '5.6 yr' periodicities in the variations of Aa. In this figure, the positions of all the peaks in the continuous and in the dashed curves coincide. (The same behavior is found also in the MEM spectra of Aa and Aa' obtained from 5-yr MTI, hence we have not shown these spectra.) This confirms the reality of the above-mentioned periodicities in the variation of Aa.

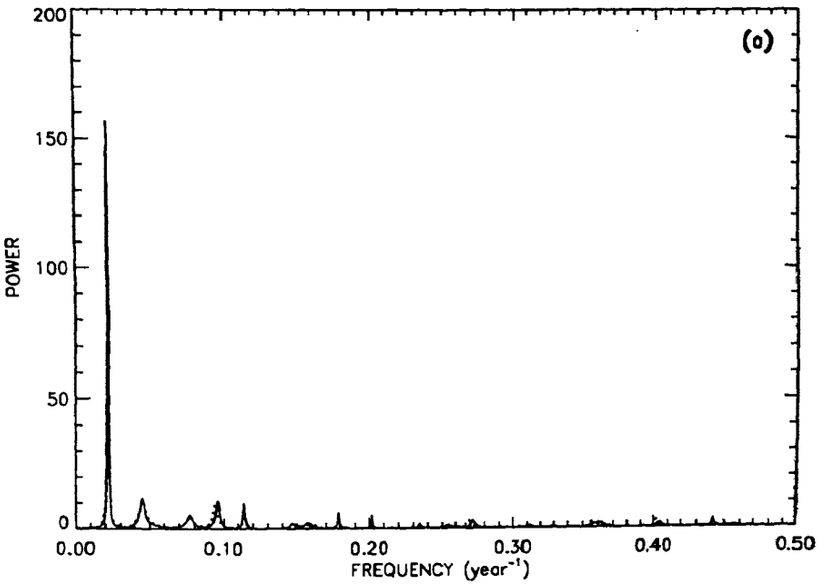

Figure 4.6(a).

Figure 4.6a-c. MEM power spectra of Aa, Ba and of $\bar{A}a$ (for autoregressive process of order $p = n/2$, where n is the length of the time series) are represented by continuous curves. The spectra of corresponding simulated variations Aa', Ba' and of $\bar{A}a'$ are represented by dotted curves. (a): The spectra of Aa and Aa' are obtained from the values of 3-yr MTI. (b): The spectra of Ba and Ba' are obtained from the values of 5-yr MTI. (c): The spectra of $\bar{A}a$ and $\bar{A}a'$ are obtained from the values of 5-yr MTI.

Periodicities in Ba from MEM *analysis*

In Figure 4.6(b) we show the MEM power spectra of Ba (continuous curve) and Ba' (dotted curve) for $m = n/2$ obtained from the sequence of 5-yr MTI. These MEM

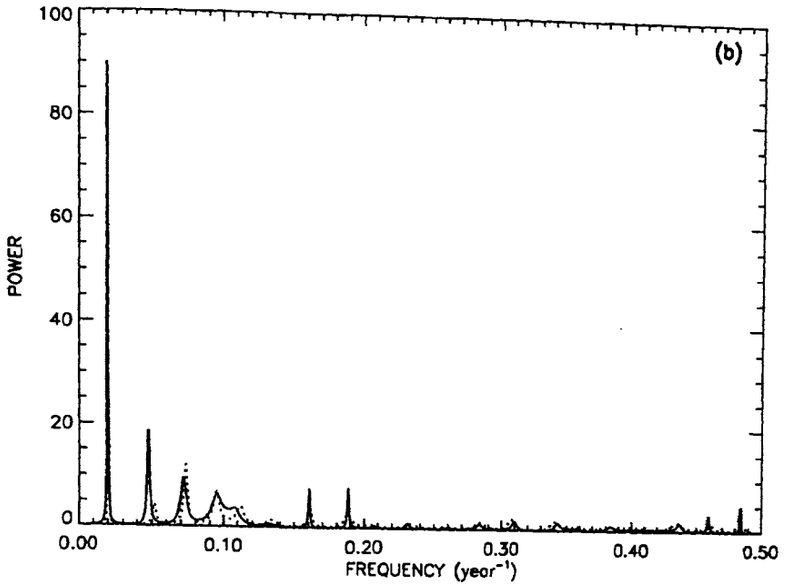

Figure 4.6(b).

power spectra show the existence of '50 yr', '20.8 yr', '13.9 yr', '10.5 yr', '9.3 yr', '6.25 yr' and '5.32 yr' periodicities in *Ba*. In this figure also the locations of the peaks in the continuous and dashed curves almost coincide. This confirms the reality of all the above-mentioned periodicities in the variation of *Ba*.

Periodicities in $\bar{A}a$ from MEM *analysis*

In Figure 4.6(c) we show the MEM power spectra of $\bar{A}a$ (continuous curve) and $\bar{A}a'$ (dotted curve) for $p = n/2$ obtained from the sequence of 5-yr MTI. These MEM power spectra show the existence of '55 yr', '19.6 yr', '13.2 yr', '10.5 yr', '9.0 yr', '6.29 yr' and '5.29 yr' periodicities in $\bar{A}a$. Surprisingly, even the spectrum obtained by 5-yr MTI shows the existence of a very dominant periodicity at '3.22 yr'. This periodicity is significant (though not dominant) in the FFT spectrum also. (A reason for the absence or insignificance of this periodicity in the spectrum of *Ba* may be that $\bar{A}a$ depends more on the rotation in the deeper layers of the Sun.) The positions of the peaks at all the above-mentioned periodicities in the continuous and the dashed curves almost coincide. This confirms the reality of all the above-mentioned periodicities in the variation of $\bar{A}a$. The spectrum of $\bar{A}a$ also shows the possibility of existence of the following periodicities: '30.3 yr', '4.29 yr', '3.52 yr', '2.44 yr', and '2.17 yr', but these periodicities are not reproduced by the $\bar{A}a'$. Hence, their significance is doubtful.

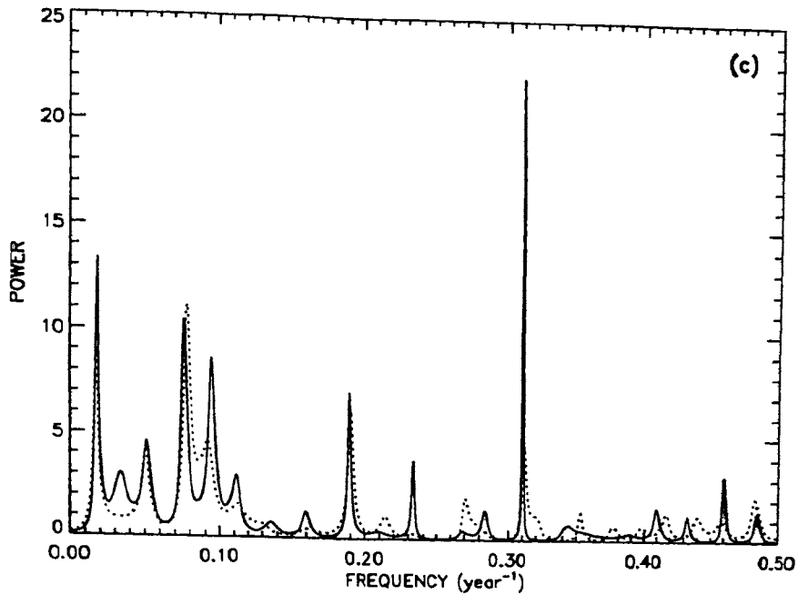

Figure 4.6(c).

4.4.4. CHECKING FROM THE ROTATION RATES OF THE YOUNG AND THE OLD SPOT GROUPS

To determine whether the periodicities seen in Sections 4.4.1 and 4.4.3 are due to the variations in the relative contributions to the data from the young and the old spot groups, we have analyzed separately the data corresponding to the spot groups of age ≤ 3 days and those of age > 3 days.

Figures 4.7(a-c) show the FFT spectra of Aa, Ba and $\bar{A}a$ obtained from data corresponding to the young groups (continuous curve) and the old groups (dotted curve) for the sequence of 5-yr MTI. It can be seen in Figures 4.7(a) and 4.7(c) that the positions of the peaks in the power spectra of Aa and $\bar{A}a$ obtained from the young groups and the old groups taken separately are almost the same, (within the limits of their uncertainties), as the peaks in the corresponding spectra obtained from the combined data (Figures 4.5(a) and 4.5(c)). This suggests that the periodicities in Aa and $\bar{A}a$ determined in Sections 4.4.1 and 4.4.3. are present in the real variations of Aa and $\bar{A}a$, and are not coming from the variations in the relative contributions to the data from the young and the old groups.

In Figure 4.7(b) it can be seen that except for the absence of a peak at '21.3 yr', the positions of the remaining peaks in the power spectra of Ba obtained from the young groups and the old groups taken separately are almost the same (within the limits of their uncertainties) as the peaks in the corresponding spectra obtained from

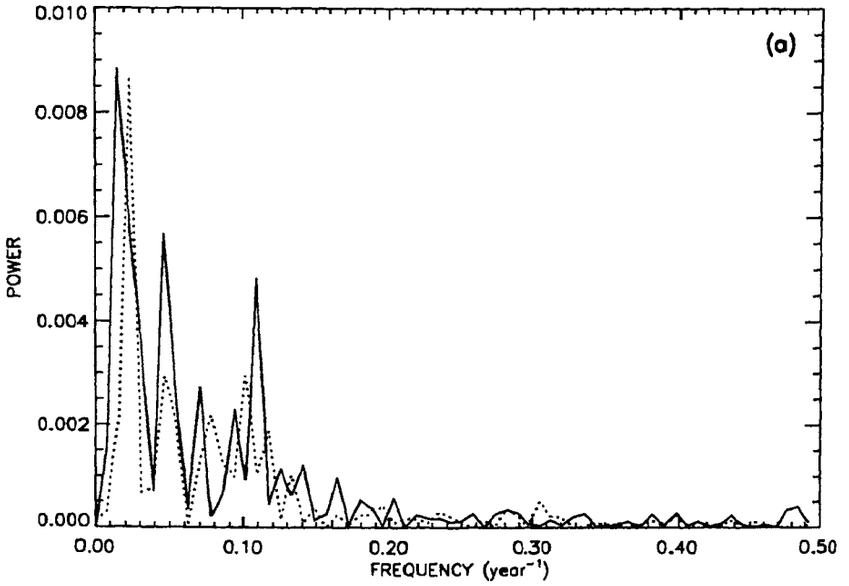

Figure 4.7(a).

Figure 4.7a–c. FFT power spectra of (a): Aa, (b): of Ba, and (c): those of $\bar{A}a$ obtained from the young groups (continuous curves) and the old groups (dotted curves) during 5-yr MTI.

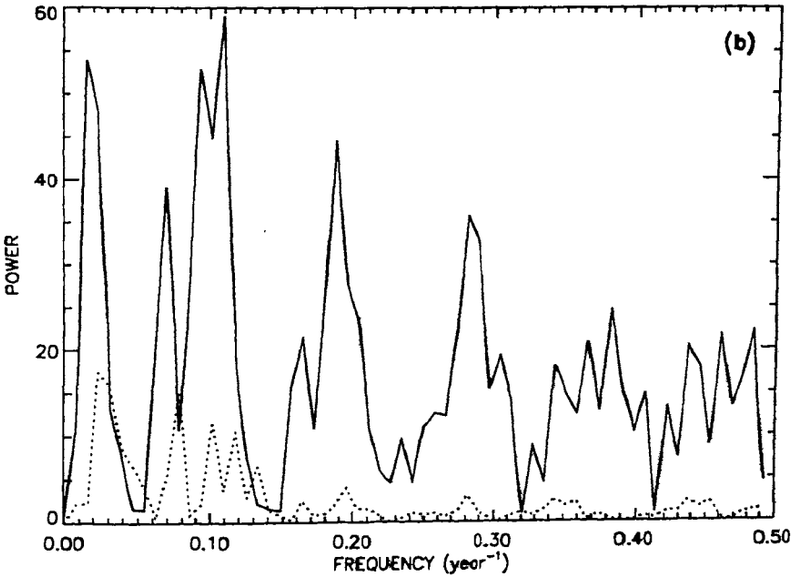

Figure 4.7(b).

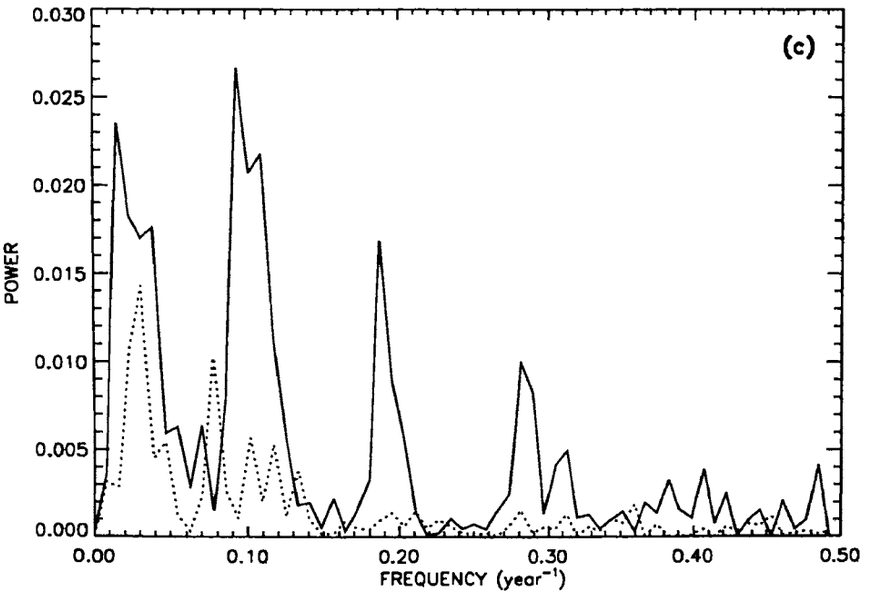

Figure 4.7(c).

the combined data. The peak at '21.3 yr' is missing in the spectrum corresponding to the young groups, whereas there is a high power concentration around the same position in the spectrum corresponding to the old groups. Thus '21.3-yr' periodicity in Ba determined in Sections 4.4.1 and 4.4.3 may be coming mainly from the temporal variation in the rotation rate of the old groups (which has to be confirmed with a better separation of young and old groups).

4.5. Periodicities Determined From the Mt. Wilson Velocity Data

Dr. R. F. Howard kindly provided with us the daily values of the A, B and C coefficients derived from Mt. Wilson Doppler velocity data measured during 1967–1994 for northern and southern hemispheres separately. We focus on observations obtained after 1981 with the reduced instrumental noise. The data reduction and analysis is same as described in Section 3.2.2 of Chapter III. The N-S asymmetries of $\bar{A}$, $\bar{B}$ and $\bar{C}$ were calculated using the formula (4.1).

Figure 4.8 shows the variations of the N-S asymmetries $\bar{A}a$, $\bar{B}a$ and $\bar{C}a$, binned into 19-day intervals of the Mt. Wilson velocity data during 1982–1994. Figures 4.9(a–c) show the FFT power spectra of the $\bar{A}a$, $\bar{B}a$ and $\bar{C}a$, respectively. The spectra $\bar{A}a$ and $\bar{C}a$ show dominant peaks at the period of 374 $\pm$ 30 day with $>$ 99.9 % confidence level. The spectrum of the N-S asymmetry of $\bar{B}$ shows peaks at the periods 374 $\pm$ 30 day, 78 $\pm$ 2 day and 49 $\pm$ 1.0 day with 99–99.8 % confidence level. In this spectrum

the two peaks at periods of 67.5 ± 1.0 day and 42.7 ± 0.3 day, and in the spectrum of $\bar{C}$ the peak at period of 44.2 ± 0.4 day are significant with 98% confidence level. In all these three spectra the peaks at the periods of ~ 11 yr are highly insignificant or absent. Influence of the 7°.17 inclination of the Sun's equator to the ecliptic may be responsible for the dominance of 374 day periodicity in the N-S asymmetries of the solar rotation and the differential rotation.

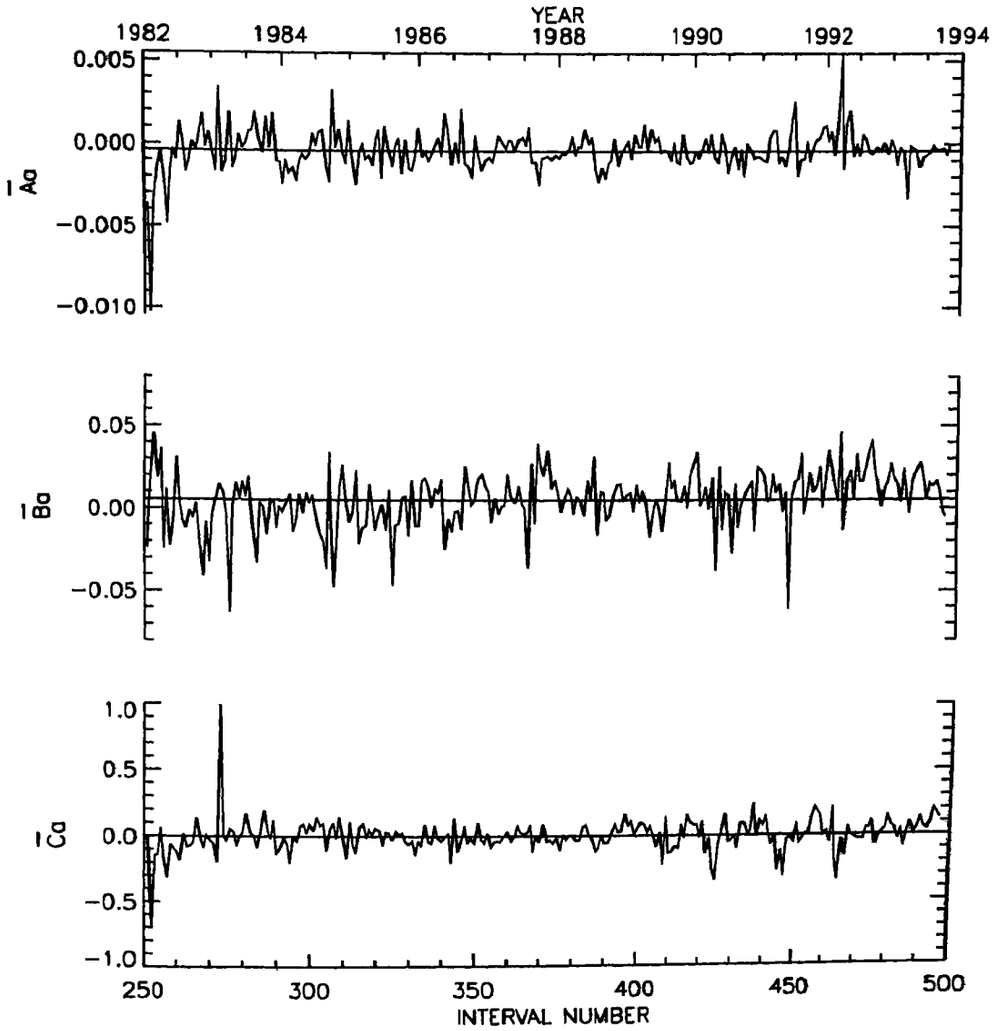

Figure 4.8. Variations of the N-S asymmetries $\bar{A}a$, $\bar{B}a$ and $\bar{C}a$ determined from Mt. Wilson velocity data during 1982–1994 rebinned into consecutive 19-day intervals. The horizontal lines represent the average values.

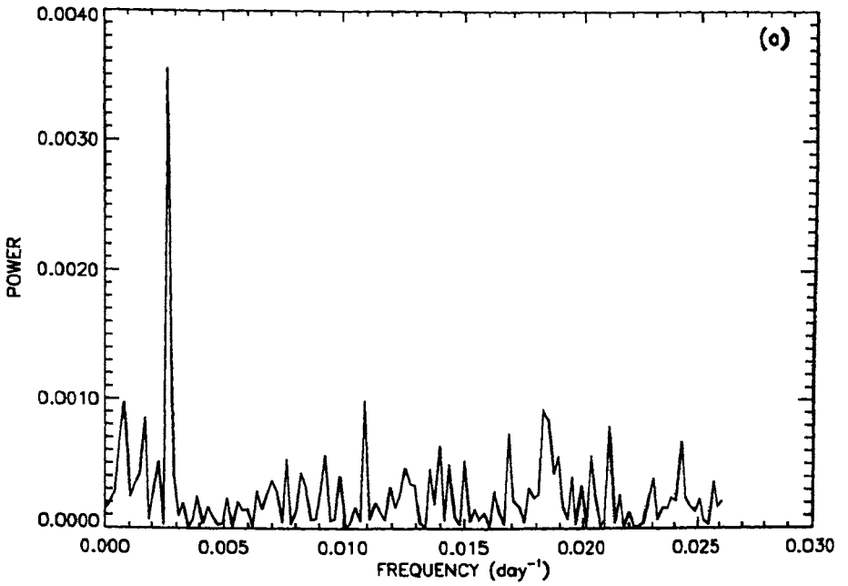

Figure 4.9(a).

Figure 4.9a–c. FFT power spectrum of (a) $\bar{A}a$, (b): of $\bar{B}a$ and (c) that of $\bar{C}a$, determined from Mt. Wilson velocity data during 1982–1994.

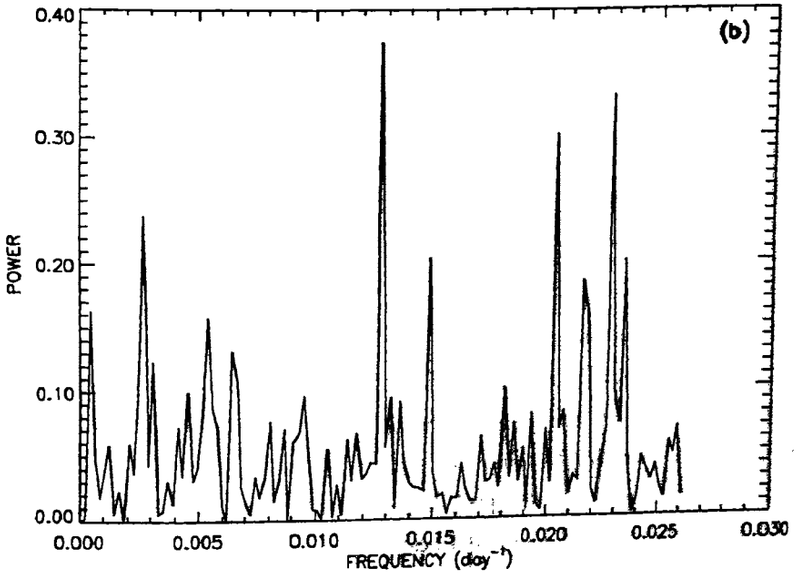

Figure 4.9(b).

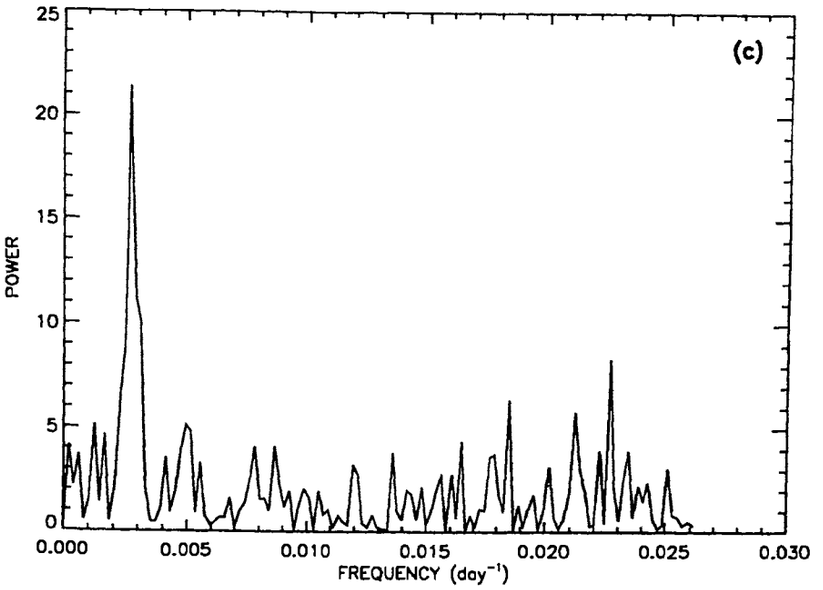

Figure 4.9(c).

4.6. Relations of Aa, Ba and $\bar{A}a$ With the Surface Magnetic Field and With Activity

4.6.1. RELATION WITH THE GLOBAL MODES IN THE MAGNETIC FIELD

Csada (1974) analyzed 8-yr magnetograms measured during 1959–1967, and found the same family of periods for both even-parity and odd-parity modes of magnetic field. Stenflo & Vogel (1986) analyzed 25-yrs of magnetograms measured during 1959–1976. They have noticed the absence of a '22-yr' periodicity in the even-parity modes. We have analyzed (Gokhale & Javaraiah 1990a; cf., Chapter II) the magnetic field inferred from the latitude distribution of sunspot activity during 1874–1976. We find a small but significant power in the '22-yr' periodicity for even parity also.

The '22-yr' oscillation in Aa, Ba and $\bar{A}a$ (determined in Section 4) might be the same as '22-yr' oscillation of even parity found in the magnetic field inferred from the sunspot data. The dominant '45-yr' periodicities in Aa, Ba and $\bar{A}a$ match with the period of so-called 'Double-Hale' solar magnetic cycle (see e.g., Fairbridge & Marcel 1977). This suggests that the periodicities in Aa, Ba and $\bar{A}a$ may represent torsional MHD oscillations of odd parity in the rotation (represented by odd terms in the Legendre polynomial fit of $\omega(\lambda)$) which correspond to even parity in the magnetic field.

Stenflo & Vogel (1986) have noticed an increase in the frequencies of the even-parity modes of the Sun's magnetic field with increase in the spherical harmonic degree. We

found that the frequencies of either even-degree modes or of the odd-degree modes are independent of their spherical harmonic degree and we have suggested that the Sun's global modes may be 'forced' by some unidentified mechanism (cf. Chapter II). The similarities in the patterns of the temporal behaviors of Aa, $(-\bar{A}a)$ and Ba seen in Section 4.2 indicate that the torsional oscillations constituting variations of these parameters may be either forced independent oscillations or components of a single oscillation which itself could be forced internally or externally. The oscillation represented by the variation of $\bar{A}a$ is in anti-phase with that represented by the variation of Ba (or $\bar{B}a$).

4.6.2. COMPARISON BETWEEN THE PERIODICITIES IN THE N-S ASYMMETRY OF AMOUNT OF SUNSPOT ACTIVITY AND THOSE OF Aa, Ba, AND $\bar{A}a$

Swinson et al. (1986), analyzed the combined data of sunspot areas and sunspot numbers from White & Trotter (1977) and Koyama (1985). They have noticed in addition to the $\sim$ 11-yr periodicity, the existence of a significant $\sim$ 22-yr periodicity in the N–S asymmetry of solar activity. The existence of '3.27-yr' and $\sim$ 80-yr periodicities in the N–S asymmetry of solar activity was also suggested from the analysis of spot group areas (see, Vizoso & Ballester 1990). Carbonell et al. (1993), using a classical and modern quantitative techniques, studied the N–S asymmetry of sunspot areas in the combined data from the GPR (1874–1983) and the United States Air Force (1983–1989). In their study only a '12.1-yr' periodicity was found to be statistically significant.

Some investigators raised doubts on the significance of the $\sim$ 11-yr periodicity in the N-S asymmetry of solar activity (Yi 1992 and references therein). According to them this periodicity might be simply an artifact of the '11-yr' cyclic variation of the total activity in the denominator of formula (4.1). Similar doubts may also be raised with respect to the $\sim$ 110-yr trend seen recently by Verma (1993) in the N–S asymmetry indices of the seven different solar activity phenomena observed during 1832–1990 (since the existence of a $\sim$ 100-yr periodicity in the total activity is well known: e.g., Cohen & Lintz 1974; Wolf 1976; Otáola & Zenteno 1983).

The doubts in the previous paragraph do not apply to the periodicities found in Aa, Ba and $\bar{A}a$ determined from sunspot data, for the following reasons. We have verified that the quantities $(An - As)$, $(Bn - Bs)$ and $(\bar{A}n - \bar{A}s)$ also show the same periodicities as in Aa, Ba and $\bar{A}a$ respectively. The low frequency ends of the spectra do not change even if the FFT spectra of the sequences of Aa, Ba and $\bar{A}a$ are calculated after subtracting their respective mean values instead of subtracting the first-order polynomial fits. Also, the correlations of Aa, Ba and $\bar{A}a$ to $(Xn - Xs)$ are found to have almost the same values as their correlations to Xa (see Section 4.3). Here Xn and Xs are the measures of sunspot activity X in the N and S hemispheres, respectively.

Thus, for the frequency resolution allowed by the data, the periodicities found in the present analysis must be really present in Aa, Ba and $\bar{A}a$ determined from spot group data.

To compare the periodicities in Aa, Ba and $\bar{A}a$ with those in the N–S asymmetry of solar activity, we have computed the FFT spectra of Xa and also that of the quantity $Xn - Xs$ (equivalent to the numerator of the Equation (4.1)) during the 3-yr MTI and 5-yr MTI. The spectra obtained from 3-yr MTI are shown in Figure 4.10. (The spectra obtained from 5-yr MTI are found to be similar, hence, not shown.) These spectra show all the dominant periodicities found in Aa, Ba and $\bar{A}a$ with similar relative magnitudes. (The FFT spectrum of Xa is much more similar to that of $\bar{A}a$ than those of Aa and Ba.)

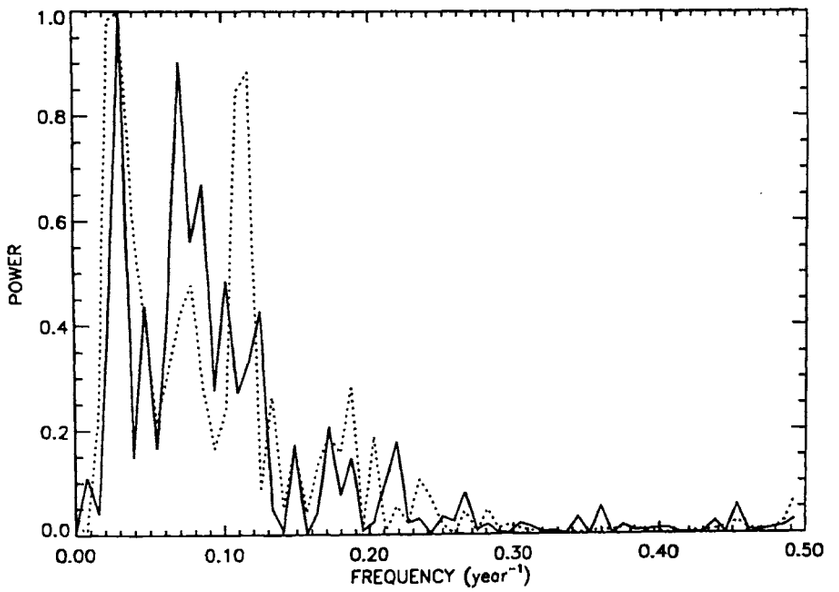

Figure 4.10. FFT power spectra of the N–S asymmetry Xa (continuous curve) of sunspot activity X and of $Xn - Xs$ (dotted curves) obtained from the values of 3-yr MTI, where Xn and Xs are the measures of sunspot activity X in northern and southern hemispheres, respectively. The power values are normalized to their respective maximum values.

[The spectrum of Xa (continuous curve) shows the presence of a dominant periodicity at '11.6-yr'. This periodicity is not dominant in the spectrum of $Xn - Xs$ (dotted curve). Hence, one may suspect that the dominance of this periodicity in Xa may be an artifact of the variation of the denominator of the Equation (4.1) as suggested by some authors (Yi 1992 and references therein). On the other hand, in the spectra of $\bar{A}a$ and Ba determined from spot group data there is a large amount of power in 10–14 years (see Section 4.4.1), hence the dominance of 10–14 yr periodicity in Xa seems

to be physical. The 11 yr periodicity is not found in $\bar{A}a$, $\bar{B}a$ and $\bar{C}a$ derived from the Mt. Wilson velocity data during 1982–994. The difference in periods determined from sunspot data and from the velocity data may be understood if the rotation rates determined from these data sets represent rotation rates at different depths in the solar convective envelope (see Section 3.7 of Chapter III).]

4.7. Comparison of Periodicities in the Solar Differential Rotation With the Periods of Planetary Configurations

The maintenance of torsional oscillations will need internal or external perturbations (either continuous or episodic), with appropriate periodicities. So far no internal source of perturbations which excite the Sun's torsional oscillations is known (see Rosner & Weiss 1992).

Influence of planetary motions on Sun's cyclic activity has been considered by a number of scientists (see Ferris 1969; Kuklin 1976; Fairbridge & Shirley 1987; Seymour et al. 1992). Some authors considered action of tidal force of planets on the Sun as a cause of sunspots (e.g., Takahashi 1968; Wood 1972; Bigg 1976; Verma 1986). Some other authors (Jose 1965; Wood & Wood 1965; Fairbridge & Shirley 1987; Landscheidt 1999) have noted that the motions of the planets cause the Sun to move irregularly around the center of mass of the solar system (barycenter) and suggested coupling of the Sun's spin and orbit motions may be responsible for the sunspot activity. Recently, Zaqarashvli (1997) suggested that the near elliptical 'path' of the Sun around the barycenter of the solar system causes weak periodic differential rotation in the interior.

In order to check whether the perturbations needed to excite the torsional oscillations could come from the solar system dynamics (SSD), we looked for the periods of planetary configurations which agree with the periods of solar differential rotation.

Most of the angular momentum of the solar system is contributed by the orbital motion of the four major planets Jupiter, Saturn, Uranus and Neptune, whose time dependent spatial configurations are responsible for irregular orbital motion of the Sun around the solar system barycenter with ~22-yr periodicity. On the other hand Mercury, Venus, Earth and Jupiter are important 'tide-raising' planets. Conjunctions of the later planets seem to be important for 'Jerks' in the Sun's orbital motion (Wood & Wood 1965). Hence, all inner as well as outer planets may be important sources of perturbations in the solar rotation, either due to their angular momentum or due to their tidal force or due to both.

Each of the significant periodicities found in the solar differential rotation seem to match with a period of configuration of two or more planets (Javaraiah & Gokhale 1995; Javaraiah 1996). We estimated the approximate values of the relative 'powers'

(approximate areas under the curve) of the significant peaks in the FFT spectra of B (Figure 3.10, Chapter III) and Ba (Figure 4.5(b), Section 4.4.1). In the spectrum of Ba, the relative values of powers of the peaks at frequencies which match with the combination frequencies $\nu_s - \nu_u$, $\nu_j - \nu_s$ and $\{(\nu_j - \nu_u),\ (\nu_j - \nu_n)\}$ were found as 1.00 ± 0.05, 0.31 ± 0.05 and 0.81 ± 0.05, respectively. Here ν_j, ν_s, ν_u and ν_n represent the orbital frequencies of Jupiter, Saturn, Uranus and Neptune, respectively. The frequencies $\nu_j - \nu_u$ and $\nu_j - \nu_n$ are considered together because the peaks at these positions are not well separated in the spectrum. The approximate values of the relative powers at the above said frequencies in the FFT spectrum of B were found as 0.71 ± 0.5, 1.00 ± 0.5 and 0.46 ± 0.05, respectively.

Thus, in B the *combination frequency* of Jupiter–Saturn pair may provide the strongest perturbation, whereas in Ba the *combination frequency* of Saturn–Uranus pair may provide the strongest perturbation. However, within Newtonian mechanics, these perturbations are quantitatively quite small.

The time dependent N–S asymmetry in the distribution of mass and angular momentum in the solar system may be the source of asymmetry of the perturbations which excite the Sun's anti-symmetric oscillations. The maximum N–S asymmetry in the distribution of mass and angular momentum in the solar system during a specific planetary configuration of planets depends upon the maximum angular distances of the planets above and below the ecliptic (or invariant plane), which in turn depends on the differences among the angular inclinations of the orbits of planets to the ecliptic (in the heliocentric co-ordinate system). Hence, we speculate that the dominance of the combination frequency of Saturn–Uranus pair in Ba may be due to large difference in the angular inclinations of the orbits of these two planets.

The main doubts about any role of the solar system dynamics in solar activity mechanism come from (i) the near absence of sunspot activity during the Maunder minimum and (ii) the variation of stellar magnetic activity along the H–R diagram and with age. Attempts have been made to explain the prolonged sunspot minima (such as Maunder minimum) using the solar system dynamics (e.g., Fairbridge & Shirley 1987). However, the role of the solar system dynamics in the basic mechanism of solar activity is still a matter of speculation.

4.8. Conclusions and Discussion

Conclusions:

From the analysis of the N–S asymmetry in the Sun's 'mean' and differential rotation obtained from 103 yr GPR data on sunspot groups and the velocity data during 1982–1994, we have drawn the following conclusions:

(1) The variation in $\bar{A}a$ is similar in character to the variation in Ba but with opposite sign. From this we suggest that the variations of $\bar{A}a$ and Ba may represent components of an anti-symmetric torsional oscillation of the Sun which are in opposite phase with each other.

(2) The temporal variations of Aa, Ba and $\bar{A}a$ have a dominant periodicity at 45.5 $\pm$ 11.5 yr and have periodicities at 21.3 $\pm$ 4.0 yr, 13.3$\pm$ 1.5 yr and 10.5$\pm$ 0.5 yr. The variations of Aa, Ba and $\bar{A}a$ may also have periodicities at '8–9 yr', '6.5 yr' and '5.6 yr'.

(3) The power spectrum of N–S asymmetry of $\bar{A}$ and that of $\bar{C}$ determined from the Mt. Wilson velocity data during 1982–1994, show peaks at the period 374 $\pm$ 30 day with $>$ 99.9 % confidence level. The spectrum of the N–S asymmetry of $\bar{B}$ shows peaks at the periods 374 $\pm$ 30 day, 78 $\pm$ 2 day and 49 $\pm$ 1 day with $\geq$ 99 % confidence level. The 7°.17 inclination of the Sun's equator to the ecliptic may be responsible for the 374 day periodicity in the N–S asymmetries of the solar rotation and the differential rotation.

(4) Almost all the periodicities of Aa, Ba and $\bar{A}a$ reported in Conclusion 2 are also seen in the variation of N–S asymmetry (Xa) of sunspot activity (X), with similar relative magnitudes.

(5) There exists a good anticorrelation between Xa and X suggesting existence of the periodicities $\sim$ 11-yr and $\sim$ 100 yr in Xa also as in X.

(6) Some of the dominant periodicities of the solar differential rotation match with the periods of configurations of dominant planets, suggesting some speculations on planetary configurations providing perturbations needed for 'torsional MHD oscillations'.

Discussion:

The average FFT power in the spectra of Aa, Ba and $\bar{A}a$ obtained from the young groups is respectively $\sim$ 2.4, $\sim$ 13 and $\sim$ 3 times higher than the average power in the corresponding spectra obtained from the old groups (see Figures 4.7(a–c)). If the young groups are anchored deeper layers than the old groups (Tuominen & Virtanen 1987; Schüssler 1987), then it seems that the asymmetry is more pronounced in the deeper layers. A similar behavior was seen in the variations of B/A obtained from the young

and the old group rotation rates (cf., Javaraiah & Gokhale 1995). The absence of '21.3-yr' periodicity in Ba as seen from the young-group data (Section 4.4) and the possibility of the existence of this periodicity in Ba as seen from the old-group data indicates that this periodicity in Ba may be connected to the rotation rate of the superficial layers (which has to be confirmed with a better separation of young and old groups).

Patterns of temporal variations of the coefficients $\bar{B}$ and $\bar{C}$ determined from Mt. Wilson magnetograph data were also found to be similar to each other (see Snodgrass & Howard 1985). This and conclusion (1) above, indicate the possibility that the Sun's torsional oscillations might be of the 'forced' variety. (As pointed out by an anonymous referee of our paper Javaraiah & Gokhale (1997a), the anticorrelation of $\bar{A}a$ and Ba may suggest an exchange of angular momentum between rigid and differential rotation.)

Since most of the frequencies (/periodicities) found in the present analysis (Conclusion 2) appear as integral multiples of one of the frequencies, they may suspiciously look like mathematical artifacts. However, they may not be mathematical artifacts since the length of the data used here is longer than double the longest period. It is more likely that the existence of these 'harmonics' and 'subharmonics' may be a consequence of the Sun's behaviour as a forced nonlinear oscillator (see also Bracewell 1988; Attolini et. al. 1990).

According to some authors (e.g., Ribes et al. 1987 and references therein) Sun was slightly more differential during the Maunder minimum (1645–1715). The activity was not totally absent and activity was more pronounced in the S-hemisphere. That is, it seems during the Maunder minimum (1645–1715) sunspot activity was not totally absent and the N–S asymmetry in the amount of activity was unusually large (see Sokoloff & Ribes 1994; Usoskin et al. 2000). There exists a good anticorrelation between the sunspot activity and its N–S asymmetry (cf., Section 4.3, Figure 4.4). However, the correlations of N–S asymmetry of activity with N–S asymmetry of A and with that of B were found to be very weak (Section 4.3). Presence of harmonics and subharmonics in the temporal variations of differential rotation determined from sunspot data may suggest nonlinear nature of Sun's torsional oscillations. So, it is interesting to investigate whether the prolonged minima such as Maunder minimum might result from the non-linearity of Sun's torsional oscillations.

Chapter V

DEPTHS OF INITIAL ANCHORING AND RISING-RATE OF SUNSPOT MAGNETIC STRUCTURES

5.1. Introduction

Statistical observations on active region size distribution, rotation and meridian flow, characteristics of growth and decay, seem to reflect regularities of the behaviour of the subsurface flux tubes through which the regions are formed (Howard 1996a). Studies of the rotation of plasma and magnetic structures on the Sun's surface are useful for understanding the magnetohydrodynamic (MHD) interactions beneath the surface. In particular, it is important to study the variations in the rotation frequencies of sunspots and sunspot groups with respect to their ages, areas and lifetimes. Several such studies have been carried out by a number of authors using Greenwich photoheliographic results (GPR) for sunspot groups (see Schröter 1985). It is believed that the rotation rate of spot groups decreases with their age (e.g., Ward 1966; Godoli & Mazzucconi 1979; Gokhale & Hiremath 1984; Balthasar et al. 1986; Tuominen & Virtanen 1987; Zappalà & Zuccarello 1991; Zuccarello 1993). This could be interpreted as an indication that the Sun's deeper layers rotate faster than the shallower layers assuming that the magnetic structures of the spot groups rise to shallower depths as the groups grow older. This interpretation supports the traditional dynamo theory (e.g., Stix 1981), but contradicts the radial gradient in the Sun's angular velocity inferred from helioseismology (e.g., Brown et al. 1989; Libbrecht 1989; Dziembowski et al. 1989; Goode et al. 1991; Tomezyk et al. 1995; Antia & Chitre 1996, Antia et al. 1998; Howe 1998). It is also known that 'large' or 'long lived' spot groups rotate *slower* than the 'small' or 'short lived' groups (e.g., Howard et al. 1984). Hence, it is possible that one obtains the larger mean angular velocity for younger spot groups because of presence of a larger percentage of 'small' and 'short-lived' groups among the sample of the 'young' groups. To verify whether it is so, it is necessary to study the rotation rates of the samples of spot groups of different life spans (lengths of life) separately. Such studies have been carried out recently by Zappalà & Zuccarello (1991) and Zuccarello (1993). In the present chapter we examine on how the rotation frequency of a spot group varies with its age (t), life span (τ) and size (area), which may help to understand motions of the magnetic structures (flux tube) of spot groups in the solar convective zone from where the magnetic structures rise (Javaraiah & Gokhale 1997b).

In Section 5.2 we describe the data reduction. In Section 5.3 we show variations

of rotation frequency of spot groups with respect to their life spans and age. In Section 5.4 we give comparison of these variations with the radial variation, ($\Omega(r)$, of the solar plasma across the convective envelope, determined from helioseismic measurements. In Section 5.5 we give estimation of the depths of the initial anchoring and the rising rate of magnetic structures of the spot groups of different life span and age. For these studies we used spot group data during 1874–1939 (Javaraiah & Gokhale 1997b). Recently, upgraded spot group data during 1874–1981 became available to us. Using this large data, in Section 5.6 we confirmed the results of these studies. In Section 5.7 we determine the area–lifetime relation of spot groups, and the distributions of spot groups with respect to life span. In Section 5.8 we summarize the conclusions and briefly discuss them.

5.2. Data and Method of Analysis

The magnetic tape of the GPR data on the sunspot groups during the years 1874–1976 which was kindly provided by Dr. H. Balthasar, included the observation time, (the date and the fraction of the day), heliographic latitude and longitude for each spot group on each day of its observation during the entire period 1874–1976. It also included the corrected whole spot area A (in mh) and central meridian longitude (CML) of spot groups for the period 1874–1939.

Let t_1, t_2,.....,t_n be the times at which a given spot group was observed and A_1, A_2, ...A_n be its corresponding area values (in mh). Considering t_1 as the time of 'birth' and t_n as the time of 'death' of the spot group, the lifetime or life span (τ, in days) and the average area A, and the maximum area A_{max} of the spot group are determined as follows:

$$\tau = t_n - t_1,$$
$$A = 1/n\Sigma A_i \ , \ i = 1, n,$$
$$A_{max} = Max\{A_i, \ i = 1, ...n\}.$$

To determine the life span of a spot group which is essential for the present study we have to ensure that we know the first and the last days of its life span without any ambiguity. For spot groups living longer than 9 days the identification of the first and the last days is possible for much fewer groups during 1940–1976 than during 1874–1939. For 1940–1976 the magnetic tape contains data on spot groups only with central meridian longitudes (CML) having absolute values $\leq 58°$. Hence, we confined our study to years 1874–1939 (later we have extended the study to a large data set). Even from the years 1874–1939, we have eliminated the entire data on those spot groups which have $|CML| > 75°$ on any day of their life. (This leads to elimination of the second and the subsequent disk passages of the recurrent spot groups.) Thus, all spot groups with identifiable first and last days, have life spans ≤ 12 days.

These spot groups are further binned into latitude intervals of width 10° each. In order to have better statistics, groups in the same latitude intervals in the northern and southern hemispheres were taken in combination. In Table 5.1 we give the total number of spot groups of different specified life spans in three latitude intervals of 10° each, deduced from the data during 1874-1939.

Table 5.1. Columns 2, 3, 4 contain the number of sunspot groups of different specified life spans (τ, in days) in different 10° latitude intervals, during 1874–1939.

τ	latitude intervals		
	$0-10^{\circ}$	$10^{\circ}-20^{\circ}$	$20^{\circ}-30^{\circ}$
1.5	183	277	109
2.5	138	217	95
3.5	107	235	62
4.5	122	201	89
5.5	123	222	81
6.5	100	292	70
7.5	92	183	65
8.5	85	159	53
9.5	84	154	52
10.5	64	142	58
11.5	16	49	26

The sidereal rotation frequency (ω) of a spot group of a specified life span in a specified latitude interval, at its age $t = (t_i + 1/2)$ *day* is computed using the epochs of its observations on the ith day (t_i) and the (i+1)th day (t_{i+1}), and the heliographic longitudes of the spot group at these epochs. Rotation frequencies between non-consecutive days were not determined. Thus the uncertainty in t is 0.5 *day*.

For each specified value of the age 't' of a spot group, the mean rotation frequency ($\omega(t)$), and the standard deviation (σ), were computed for spot groups of given life spans in given latitude bins.

For spot groups of given life span τ in a given latitude bin, the value of ω at $t = 1.5$ is defined as the mean "initial" rotation frequency $\omega_{ini}(\tau)$.

While determining the values of $\omega(t)$ and $\omega_{ini}(\tau)$ we excluded the data corresponding to the 'abnormal' motions, e.g., displacements exceeding $3^{\circ}day^{-1}$ in the longitude or $2^{\circ}day^{-1}$ in latitude. This reduces the data sample by about 3% but guards against errors in recording and in identification of small spot groups from one day to the next (Ward 1965a, 1966). This precaution substantially reduces the uncertainties in the mean rotation frequencies (cf., Javaraiah & Gokhale 1995; cf., Chapter III).

5.3. Variations of $\omega_{ini}(\tau)$ and $\omega(t)$

In Figure 5.1 we show the dependence of the "initial" rotation frequency ($\omega_{ini}(\tau)$) on the life span 'τ' of a spot group, for spot groups of life spans 2 to 12 days, in different latitude intervals, obtained from the data during 1874–1939. The 'error-bars' correspond to the uncertainties at the respective σ-levels. From this figure one can easily see that initial rotation frequencies of spot groups depend on their life span.

In Figure 5.2 we show $\omega(t)$ as a function of age t for spot groups of life spans 10–12 *days* in latitude bins $(0^\circ - 10^\circ)$, $(10^\circ - 20^\circ)$ and $(20^\circ - 30^\circ)$, obtained from data during 1874–1939. We notice the following :

(i) In each latitude interval, the rotation is accelerated during the *first* day, and in first two intervals the rotation is decelerated *after* the 9th day, and

(ii) between the 2nd and the 9th days we see the following trends : (a) in latitudes $(0^\circ - 10^\circ)$: neither acceleration nor deceleration, (b) in $(10^\circ - 20^\circ)$: slow acceleration, (c) in $(20^\circ - 30^\circ)$: slow deceleration.

We believe that the 'decreasing' trend of rotation rate with age of spot groups, reported by earlier authors was due to mixing of shorter and longer lived groups in the data sample for each given age. Such a mixture in the data sample affects largely the initial phase of $\omega(t)$. This follows from the variation of $\omega_{ini}(\tau)$ shown in Figure 5.1.

In latitudes $0^\circ - 10^\circ$ the trend in $\omega(t)$ is generally similar to that found by Zuccarello (1993) from the GPR sunspot groups with life spans of 11 *days* during 1874–1976.

5.4. Comparison of $\omega_{ini}(\tau)$ and $\omega(t)$ With $\Omega(r)$

Generally, it is believed that magnetic flux tubes of sunspots (or spot groups) are formed near the base of the convection zone and rise to the surface through buoyant forces. Hence, assuming that during the initial phases, the sunspot magnetic structures are anchored at deeper layers and subsequently rise to the surface (e.g., Schüssler 1987)), we compare $\omega_{ini}(\tau)$ and $\omega(t)$ with $\Omega(r)$.

In Figure 5.3 we show the radial variation of $\Omega(r)$, of the Sun's plasma rotation frequency (for fractional radius $\geq$ 0.65) at latitudes 5°, 15° and 25°, as provided to us by Dr. H. M. Antia, who determined it from the Big Bear Solar Observatory (BBSO) helioseismic data (Woodard & Libbrecht 1993a) by using the inversion method of Antia & Chitre (1996).

5.4.1. COMPARISON OF $\omega_{ini}(\tau)$ WITH $\Omega(r)$

From Figures 5.1 and 5.3, it can be seen that in latitude intervals $0^\circ - 10^\circ$ and $10^\circ - 20^\circ$,

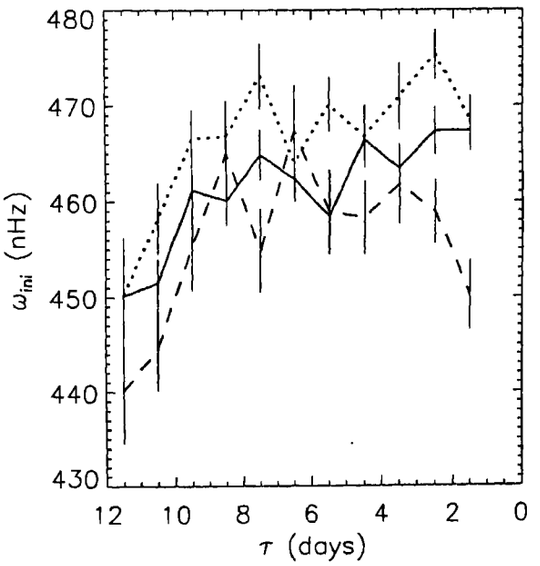

Figure 5.1. The initial rotation frequency ω_{ini} as a function of the lifespan τ, for spot groups occurring in latitude intervals $0^o - 10^o$ (dotted curve), $10^o - 20^o$ (continuous curve) and $20^o - 30^o$ (dashed curve).

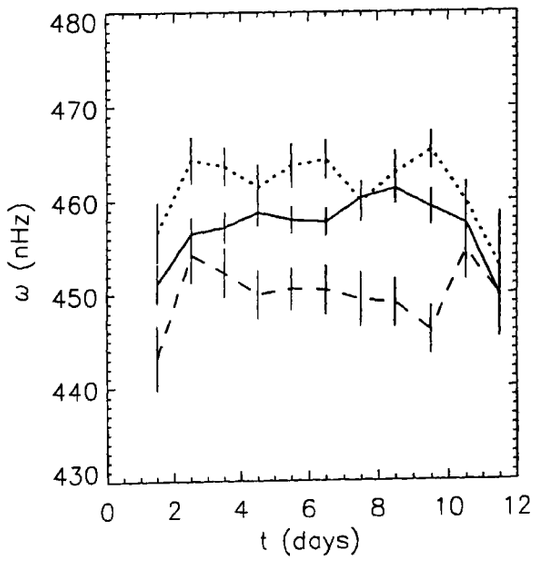

Figure 5.2. The mean rotation frequency ω as a function of the age t for spot groups with life spans of 10–12 days, occurring in latitude intervals $0^o - 10^o$ (dotted curve), $10^o - 20^o$ (continuous curve) and $20^o - 30^o$ (dashed curve).

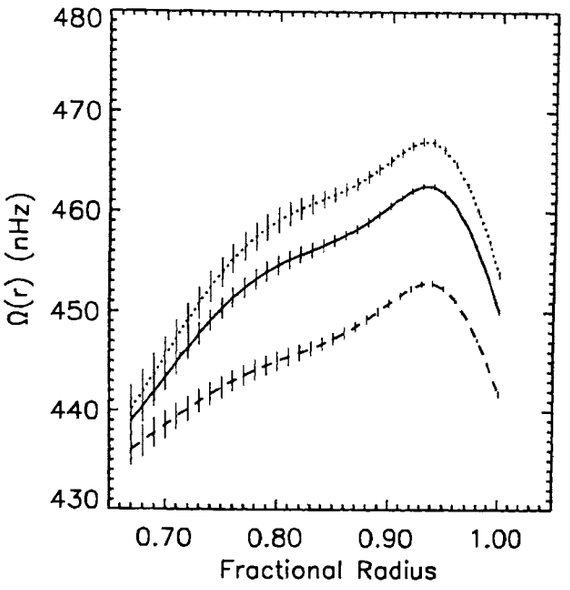

Figure 5.3. Plasma rotation frequency $\Omega(r)$ as a function of r at latitudes 5^o (dotted curve), 15^o (continuous curve) and 25^o (dashed curve) provided to us by Dr. H. M. Antia, as determined from the BBSO helioseismic data (Woodard & Libbrecht 1993) using the inversion method of Antia & Chitre (1996).

$\omega_{ini}(\tau)$ has trends similar to the trend of $\Omega(r)$, across the convective envelope. In the interval $20^o - 30^o$, there is relatively large difference between the corresponding trends of $\omega_{ini}(\tau)$ and $\Omega(r)$ which could be due to the poor statistics. However, $\omega_{ini}(\tau)$ and $\Omega(r)$ at 15^o latitude are similar. The similarity is even better for spot groups in the entire sunspot latitude belt (see Figure 5.4). In each interval, the values of $\omega_{ini}(\tau)$ are 5–15 nHz higher than the values of $\Omega(r)$. This might be due to the 'differential buoyancy' (D'Silva & Howard 1994) or difference in inclination between preceding and following wings of a rising fluxtube (Caligari et al. 1995) which might make the flux loops rotate faster than local plasma. In spite of the effects (if any) due to aforementioned factors, the similarity of trends of $\omega_{ini}(\tau)$ and $\Omega(r)$ suggests that the magnetic structures of spot groups with successively longer life spans (2–12 days), are initially anchored in successively deeper layers of the Sun.

5.4.2. COMPARISON OF $\omega(t)$ WITH $\Omega(r)$

From Figures 5.2 and 5.3, it can be seen that in each of the latitude intervals $(0^o - 10^o)$, $(10^o - 20^o)$ and $(20^o - 30^o)$, the range of values of $\omega(t)$ is similar to that of $\Omega(r)$ across the convective envelope. In the interval $10^0 - 20^o$, even the trend of $\omega(t)$ is similar to that of $\Omega(r)$ across the convective envelope at 15^o. This may be interpreted as caused

by the rise of the magnetic structures of spot groups across the convective envelope as the spot groups grow older. (This is consistent with the inference that spot groups are 'anchored' in deeper layers when they are younger and in shallower layers when they are older: e.g., Schüssler 1987).

[The similarity between $\omega(t)$ and $\Omega(r)$ depends on the statistical distribution of the magnetic structure of the sunspot groups with respect to various factors, e.g., initial field strength, total magnetic flux, drag force, magnetic tension, etc. (e.g., Fan et al. 1993, Moreno-Insertis 1997 and references therein). The lesser similarity of trends in latitude intervals $0^o - 10^o$ and $10^o - 20^o$ must be due to the effects of such factors. Which of these factors lead to maximum loss of similarity between $\omega(t)$ and $\Omega(r)$ is not clear.]

5.5. Estimation of the Depths of Initial Anchoring and the Rising–Rate of the Magnetic Structures

To estimate the initial anchoring depths and the rate of rise of the magnetic structures of spot groups, we adopt a working hypothesis that the relations between the initial radial location r_o and life span τ, and between the subsequent radial position r and age t are linear with :

$$r_o = r_1 + k_1\tau \ ,$$

$$r = r_2 + k_2 t \ ,$$

and maximize the correlations, between $\omega_{ini}(\tau)$ and $\Omega(r)$, and between $\omega(t)$ and $\Omega(r)$ as follows. We choose various combinations of trial values for the coefficients r_1 and k_1 in wide ranges around the values visually estimated from Figures 5.1 and 5.3. For each pair of trial values of r_1 and k_1, we compute the correlation between $\omega_{ini}(\tau)$ and $\Omega(r)$. The pair which yields *maximum correlation* is taken as our best estimates of r_1 and k_1. The best estimates of r_2 and k_2 are also obtained by *maximizing* in a similar way the correlation between $\omega(t)$ and $\Omega(r)$.

For the best estimates of r_1 and k_1, r_o represents the initial anchoring depth of the magnetic structures of spot groups. The best estimate of k_2 represents the rising rate of the magnetic structures.

In Figure 5.4 we show the plots of $\omega_{ini}(\tau)$ for spot groups in the entire sunspot latitude belt, $\omega(t)$ in latitude interval $10^o - 20^o$, and $\Omega(r)$ at latitude 15^o, with the maximized correlations by a dashed curve, a continuous curve and a dotted curve, respectively.

The coefficients of the maximized correlations of $\omega_{ini}(\tau)$ in the latitude intervals $0^o - 10^o$, $10^o - 20^o$ and $20^o - 30^o$ to $\Omega(r)$ at their respective midpoints, are 0.868, 0.883 and 0.725 respectively. The coefficient of the maximized correlation in the entire

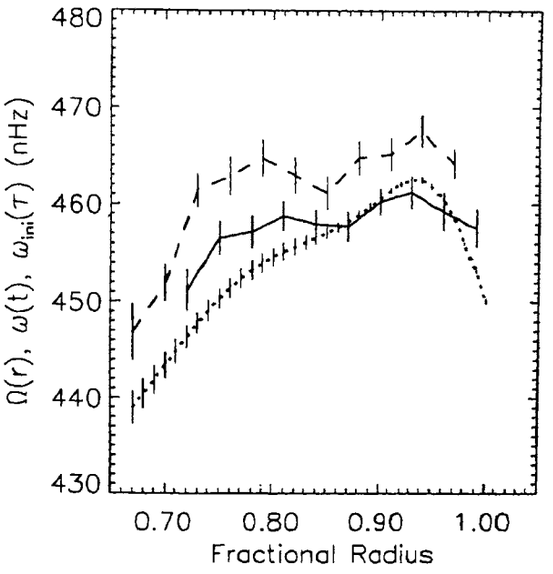

Figure 5.4. The dotted curve represents radial variation of rotation frequency of solar plasma ($\Omega(r)$) at latitude 15^o as provided to us by Dr. H. M. Antia, who determined it from the Big Bear Solar Observatory (BBSO) helioseismic data (Antia and Chitre 1996). Dashed curve represents variation of initial rotation frequency with life-span of the spot groups, $\omega_{ini}(\tau)$), in the entire sunspot latitude belt and the continuous curve represents the variation of rotation frequency with age, $\omega(t)$, of the spot groups in the latitude interval $10^o - 20^o$. The radial scales of $\omega(t)$ and $\omega_{ini}(\tau)$ are given by *maximized correlations* with $\Omega(r)$ at latitude 15^o, (the dotted curve). From left to right the values of t are 1.5, 2.5,...,10.5 days, and those of τ are 11.5, 10.5,...,1.5 days respectively (Javaraiah & Gokhale 1997b).

latitude belt, is 0.908 and the corresponding 'r_o'-'τ' relation is as follows:

$$r_o(\tau) = (696.5 \pm 0.6) - (20.9 \pm 0.1)\tau. \tag{5.1}$$

The coefficient of the maximized correlation between $\omega(t)$ of spot groups living 10–12 days in latitude interval $10^o - 20^o$ and $\Omega(r)$ at latitude 15^o is 0.863 for all 11 points and 0.911 for first 10 points. The 'r'-'t' relation corresponding the later value is as follows :

$$r(t) = (480.6 \pm 0.7) + (20.9 \pm 0.1)t. \tag{5.2}$$

Here, $r_o(\tau)$ and $r(t)$ are in megameteres (i.e., 10^3 km). The uncertainties in the coefficients in Equations (5.1) and (5.2) are nominal uncertainties corresponding to uncertainties of 0.5 *day* in age, t and lifespan, τ.

(We believe that the 87% and 88% correlations between $\omega_{ini}(\tau)$ and $\Omega(r)$ in the individual latitude intervals $0^o - 10^o$ and $10^o - 20^0$ indicate that the similarity of $\omega_{ini}(\tau)$

and $\Omega(r)$ is real. We have given here the values of r_1 and k_1 derived from the data in the entire sunspot latitude belt, because we had found that their values in individual latitude intervals do not differ by more than a few percent. We have considered the first 10 points of $\omega(t)$ because all of them represent spot groups which live for 10–12 days, but the last point is for spot groups of life spans 11–12 days which are fewer in number. In the intervals $0^\circ - 10^\circ$ and $20^\circ - 30^\circ$, the coefficients of the maximized correlations are mere 0.49 and 0.21, respectively, and for the entire sunspot latitude belt it is 0.72.)

From Equation (5.1) we infer that initially the magnetic structures of sunspot groups of life spans $\leq$ 2 *day* are anchored at $r \sim 650$ Mm, i.e., near the Sun's surface and those of spot groups with successively longer life spans between 3 and 9 *day* are anchored at successively increasing depths at the rate $\sim$ 21 Mm/*day*. The magnetic structures of the spot groups with $\tau > 9$ days are initially anchored at $r \leq 500$ Mm (near or below the base of the convective envelope).

For spot groups of life spans 10–12 days in latitudes $10^\circ - 20^\circ$, we infer from Equation (5.2) that the magnetic structures are initially anchored at $r \sim 500$ Mm (i.e. near the base of the convective envelope) and these structures rise across the envelope at the rate of $\sim$ 21 Mm/*day* (i.e., with mean speed $\sim$ 240 m/s).

5.6. Confirmation From the Larger Data set

For the reason given in Section 5.2, the data during 1940–1976 were found to be inadequate. Recently, the upgraded GPR data (1874–1976) and NOAA/UASF data (1977–1981) became available to us. These data were compiled by the National Geophysical Data Center, USA. These data included corrected whole spot area A (in mh), and central meridian longitude (CML) for each day of observation, besides other parameters, for all the spot groups observed during 1874–1981.

In Table 5.2 we give the total number (N) and the mean A of the spot groups with different specified life spans in three latitude intervals of 10° each and also in the entire sunspot latitude belt using this larger data set.

In Table 5.3 we give the values of $\omega(t)$ of spot groups of different specified life spans in three latitude intervals of 10° each, obtained by using the larger data set. (Note: Most of the differences in the day-to-day values of $\omega(t)$ are not significant for spot groups of specified life span but the overall trends of $\omega(t)$ seem to be significant.)

Using this larger data set we have confirmed the results in Sections 5.3, 5.4 and 5.5. In Section 5.5 we have used only the plasma rotation frequency $\Omega(r)$ determined from the BBSO helioseismic data (Antia & Chitre 1996, and reference therein). We have also confirmed the results using $\Omega(r)$ determined from GONG data (Antia et al. 1998, and references therein) SOHO data (Howe 1998, and references therein). The

Table 5.2. The number (N) and the average area (A, in mh) of sunspot groups with different specified life spans (τ, in days) in different 10° latitude intervals and in whole sunspot latitude belt (northern and southern hemispheres data is combined), during 1874–1981.

τ	latitude intervals							
	$0^{\circ}-10^{\circ}$		$10^{\circ}-20^{\circ}$		$20^{\circ}-30^{\circ}$		Whole belt	
	N	A	N	A	N	A	N	A
1.5	620	21.0±1.1	1119	20.9±0.7	530	19.5±0.9	2347	20.5±0.5
2.5	444	26.8±1.3	789	29.2±1.2	372	28.3±1.4	1654	28.4±0.7
3.5	339	36.6±2.2	679	35.7±1.6	284	35.9±2.0	1358	35.7 ±1.1
4.5	286	40.4±2.7	529	41.6±1.9	250	43.5±2.9	1100	41.9 ±1.4
5.5	272	56.4±5.0	469	52.0±2.7	203	53.7±6.4	979	53.7 ±2.3
6.5	224	62.4±4.3	428	61.1±3.5	176	64.0±5.7	855	61.7 ± 2.4
7.5	177	68.6±4.6	348	75.8±3.8	161	79.5±5.8	708	74.9 ±2.6
8.5	153	101.1±7.8	331	81.4±4.0	134	90.1±7.0	636	87.9 ±3.2
9.5	161	108.1±6.7	297	129.7±8.4	118	112.8±11.7	596	119.5 ±5.1
10.5	141	164.1±11.2	289	195.3±11.4	122	185.9±18.3	569	185.7 ±7.6
11.5	40	206.1±29.0	96	205.6±16.5	54	218.6±19.9	198	210.0 ±11.4

values of $\Omega(r)$ determined from GONG data were provided by Dr. H. M. Antia and those determined from SOHO data were provided by Dr. R. Howe. In Figures 5.5, 5.6 and 5.7 we show plots of $\omega_{ini}(\tau)$ and $\omega(t)$ and $\Omega(r)$, with the maximized correlations. In each of the latitude intervals, the rotation frequencies of spot groups during their initial days, i.e., the values of $\omega_{ini}(\tau)$ (dashed curves), are 10–14 nHz higher than the values of $\Omega(r)$ (dotted curves), with a maximum difference at 0.7–0.8$R_{\odot}$. Tentative explanations for this are mentioned in Section 5.4.1.

5.6.1. INFLUENCE OF SPOT GROUP AREA ON THE '$r-t$' RELATION

When the NOAA/USAF data during 1977–1981 is included, the maximized correlation between $\Omega(r)$ and $\omega(t)$ is found to be relatively lower (83–91%) for the groups in latitudes $10^{\circ}-20^{\circ}$ and a marginal increase in the correlation is also found in the intervals $0^{\circ}-10^{\circ}$ and $20^{\circ}-30^{\circ}$. We noticed that the average area (A) of spot groups of $\tau \sim$ 10–12 days is slightly (2.4%) smaller during 1874–1981 than during 1874–1976. The range of A of spot groups of life span 10–12 days is considerably wide, 110–220 mh (see Table 5.2). Hence, we repeated the calculations by excluding the data of spot groups with A smaller by 10 mh during each repetition. Improvement (about 3–7%) in the maximized correlations (obtained using $\omega(r)$ determined from BBSO, GONG and SOHO data) were found in all three latitude intervals, reached maximum when the data of spot groups whose A $<$ 130 mh were excluded (this reduces the data size by about 48%).

Table 5.3. Dependence of mean rotation frequency ($\omega(t)$, in nHz) with age (t, in days) of sunspot groups with different specified life spans (τ, in days) in different 10^o latitude intervals, determined from sunspot group data during 1874–1981.

τ		latitude intervals					
		$0-10^o$		10^o-20^o		20^o-30^o	
	t:	1.5	2.5	1.5	2.5	1.5	2.5
1.5		470.15 ± 1.39		464.99 ± 1.06		456.17 ± 1.62	
2.5		472.08 ± 1.56	468.09 ± 1.66	464.55± 1.25	461.24 ± 1.27	458.48±1.85	458.14± 1.82
3.5		469.67 ± 1.82	466.74 ±1.82	464.51±1.34	463.56 ± 1.36	459.44 ±2.15	454.16 ± 2.12
4.5		470.45 ± 1.97	467.93 ± 1.92	464.94 ±1.51	463.37 ± 1.45	457.32 ±2.29	455.95 ±2.09
5.5		471.09 ± 2.03	466.90 ±2.04	461.34 ±1.59	465.94 ± 1.59	455.41 ±2.77	456.02± 2.28
6.5		467.18 ±2.27	469.94 ± 2.24	465.60 ±1.66	464.40 ± 1.49	461.55 ±2.92	453.72 ±2.64
7.5		472.10 ±2.47	473.34 ±2.27	464.37 ±1.98	464.01 ± 1.63	461.41 ±2.99	458.879 ±2.75
8.5		466.05 ± 2.86	469.40 ± 2.54	462.56 ±1.86	463.51 ± 1.68	457.36 ±3.43	456.77 ±3.14
9.5		462.56 ±2.44	467.45 ±2.14	459.76 ±1.98	462.34 ± 1.81	461.24 ±3.33	456.94 ±3.16
10.5		458.55 ±2.48	465.36 ±1.89	451.82 ±1.83	459.43 ± 1.44	442.60 ±3.01	451.44 ±2.64
11.5		450.51 ±3.88	456.96 ± 2.65	451.05 ± 2.69	451.22 ± 2.76	437.76 ±4.46	446.82 ±3.81
	t:	3.5	4.5	3.5	4.5	3.5	4.5
3.5		463.79 ±2.06		463.88 ± 1.46		453.21 ± 2.46	
4.5		466.43 ±2.03	466.07 ±2.36	464.86 ±1.51	462.20 ± 1.64	453.66 ±2.16	452.27 ±2.50
5.5		469.84 ± 1.97	468.04 ± 2.07	461.07 ±1.50	464.70 ± 1.73	452.32 ±2.52	452.62 ± 2.75
6.5		467.94 ± 2.06	469.58 ±2.21	462.38 ±1.65	461.87 ± 1.68	457.66 ±2.52	453.60 ±2.65
7.5		468.50 ±2.31	468.52 ±2.31	462.59 ±1.69	462.60 ± 1.62	450.35 ±2.36	453.92 ± 2.63
8.5		466.62 ± 2.24	468.54 ±1.98	463.26 ±1.69	459.55 ± 1.62	452.22 ±2.82	454.92 ±2.55
9.5		466.979 ±2.27	465.92 ± 2.24	463.18 ±1.8	462.42 ± 1.82	456.52 ±3.06	456.29 ±2.91
10.5		465.52 ±2.03	462.62 ± 2.06	459.48 ±1.48	458.35 ± 1.34	450.39 ±2.35	451.83 ±2.60
11.5		461.68 ±2.58	457.89 ±2.57	455.49 ±2.69	458.93 ± 2.38	449.62 ±2.79	447.19 ±2.75
	t:	5.5	6.5	5.5	6.5	5.5	6.5
5.5		459.92 ±2.31		462.92 ±1.82		454.65 ±2.64	
6.5		467.79 ±2.25	464.64 ±2.59	462.42 ±1.77	460.97 ± 1.84	451.77 ±2.86	451.03 ±2.87
7.5		466.01 ±2.61	466.86 ±2.57	464.95 ±1.71	465.04 ± 1.79	450.07 ±2.15	457.01 ±2.88
8.5		466.55 ±2.59	467.98 ±2.19	462.94 ±1.65	459.81 ± 1.64	459.83 ±2.76	456.13 ±3.06
9.5		465.51 ±2.02	468.05 ±2.24	461.04 ±1.71	463.24 ± 1.71	455.47 ±3.03	457.70 ±2.96
10.5		460.57 ±1.85	461.07 ±2.08	459.55 ±1.47	460.95 ± 1.42	448.53 ±2.27	448.83 ±2.59
11.5		460.87 ±2.81	460.15 ± 2.82	457.97 ±2.37	455.24 ± 1.99	445.94 ±2.96	443.14 ±3.15
	t:	7.5	8.5	7.5	8.5	7.5	8.5
7.5		463.08 ± 2.70		462.42±1.79		453.01 ±3.14	
8.5		469.21 ± 2.45	465.24 ± 2.59	461.82±1.87	458.76 ± 1.77	458.79 ±3.55	453.78 ± 2.60
9.5		466.93 ± 2.26	466.87 ± 2.21	462.58±1.71	463.80 ± 1.95	452.27 ±3.40	457.35 ±2.98
10.5		461.56 ± 1.49	466.06 ± 1.90	460.35 ±1.39	459.35 ± 1.54	447.69 ±2.75	448.21 ±2.62
11.5		456.26 ±2.81	459.08 ± 2.63	458.88 ±2.06	455.75 ± 2.62	444.26 ±3.25	448.62 ±3.36
11.5		453.47 ±2.73		451.14 ±2.97		443.80 ±3.66	

Continued on the next page.

Table 5.3 is continued.

τ		latitude intervals					
		$0° - 10°$		$10° - 20°$		$20° - 30°$	
	t:	9.5	10.5	9.5	10.5	9.5	10.5
9.5		466.61 ± 2.62		462.85 ±1.86		458.91 ±2.93	
10.5		463.30 ±1.76	457.05 ± 2.17	460.57 ±1.72	459.28 ± 1.72	449.28 ±2.96	452.81±3.14
11.5		459.00 ± 2.96	464.30 ± 3.75	453.84 ±2.14	451.32 ± 2.43	443.95 ±3.25	454.81 ±2.98
	t:	11.5		11.5		11.5	
11.5		453.47 ±2.73		451.14 ±2.97		443.80 ±3.66	

Maximized correlations from data of spot groups with τ = 10–12 *days and* A $\geq$ 130 mh:

In Figures 5.5, 5.6 and 5.7 the solid curves represent $\omega(t)$ of spot groups with τ = 10–12 days and average area A $\geq$ 130 mh, and determined from the data during 1874–1981. The coefficients of the maximized correlations of $\omega(t)$ in the latitude interval $10° -$ [illegible] 0.940 for $\Omega(r)$ determined from BBSO [illegible] The corresponding 'r'–'t' relations and

BBSO data: $r(t) = (477 \pm 10) + (21 \pm 2)t$, $\chi^2 = 0.376$
GONG data: $r(t) = (470 \pm 10) + (21 \pm 2)t$, $\chi^2 = 0.183$
SOHO data: $r(t) = (516 \pm 10) + (16 \pm 2)t$, $\chi^2 = 0.016$

5.6.2. INDEPENDENCE OF '$r - t$' RELATION WITH RESPECT TO SPOT GROUP TYPE

GPR data during 1874–1976 also included indices of the types of spot groups. The spot groups were classified into 9 types, viz., single, single with few small spots, pair, pair with few small spots, stream, stream and one spot, stream and two spots, cluster or composite, pair of clusters or composites, and others. In order to check whether the rate of rise of spot group magnetic structure depends on the type (instead of area) of spot group, we maximized correlation between $\omega(t)$ and $\Omega(r)$, by excluding the data of spot groups of one type or different combinations of two or more types. Except in one case, the maximized correlation between $\omega(t)$ and $\Omega(r)$ is found to be reduced in all latitude intervals. When we excluded the spot groups of the type: few single small spots, the coefficients of the maximized correlations of $\omega(t)$, in the latitude interval $10° - 20°$, to $\Omega(r)$ at latitude 15° determined from the BBSO, GONG and SOHO data, are found to be relatively higher and the corresponding '$r - t$' relations are found to be almost same as the relation 5.2, except for minor differences in the values of the intercepts. The corresponding values of χ^2 are also found to be relatively slightly smaller. From this it seems that radial rise of a spot group magnetic structure does not depend on the type

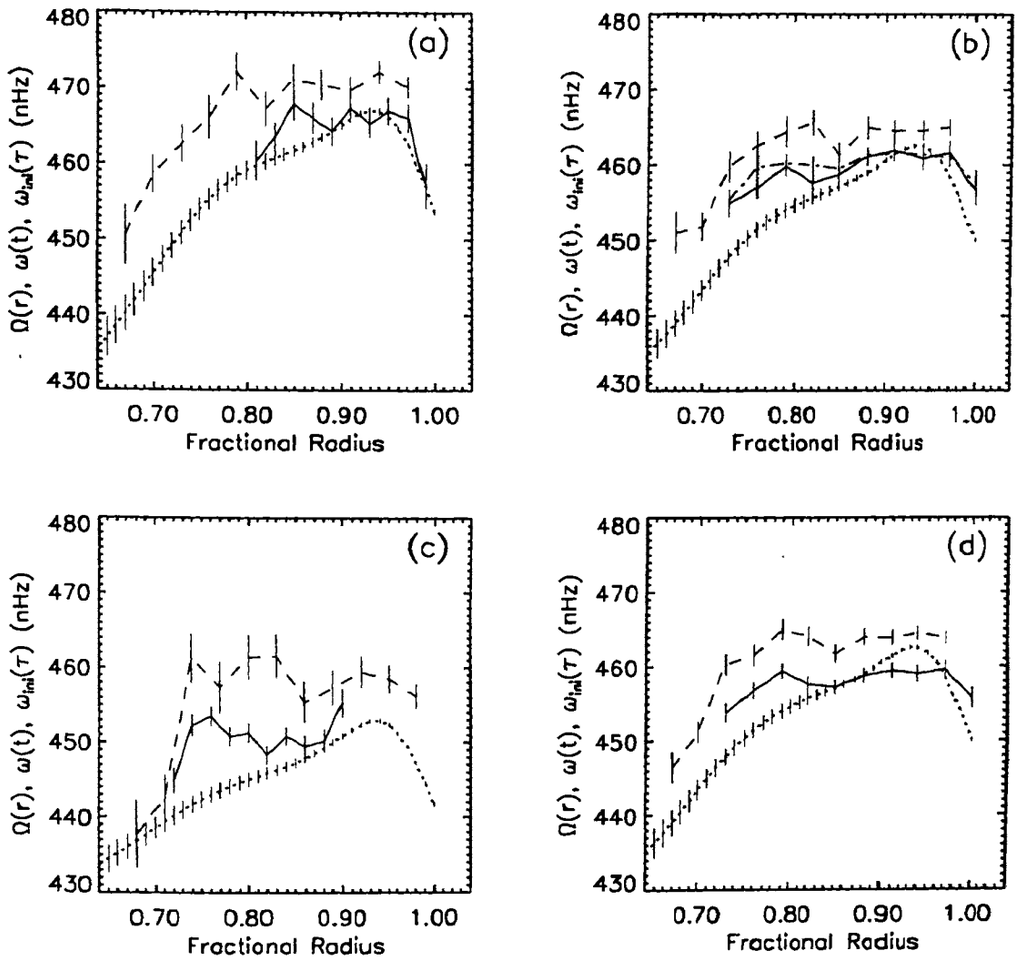

Figure 5.5. Curves $\omega_{ini}(\tau)$ and $\omega(t)$ plotted using values of r_1, k_1, r_2 and k_2 (cf., Section 5.5) which yield *maximum correlations* with $\Omega(r)$ determined from BBSO data. The dotted curves represent $\Omega(r)$. The dashed curves represent $\omega_{ini}(\tau)$ of spot groups during 1874–1981. The solid curves represent $\omega(t)$ of spot groups with τ = 10–12 days and A > 130 mh of spot groups during 1981. In latitude interval $10° - 20°$, the dotted-dashed curve represent $\omega(t)$ of spot groups with τ = 10–12 days during 1874–1976. (a) $\omega_{ini}(\tau)$ and $\omega(t)$ in latitude interval $0° - 10°$, $\Omega(r)$ at latitude 5°, (b) $\omega_{ini}(\tau)$ and $\omega(t)$ in latitude interval $10° - 20°$, $\Omega(r)$ at latitude 15°, (c) $\omega_{ini}(\tau)$ and $\omega(t)$ in latitude interval $20° - 30°$, $\Omega(r)$ at latitude 25°, and (d) $\omega_{ini}(\tau)$ and $\omega(t)$ in the entire sunspot latitude belt, $\Omega(r)$ at latitude 15°. From left to right the values of t are 1.5, 2.5,...,10.5 days, and those of τ are 11.5, 10.5,...,1.5 days respectively.

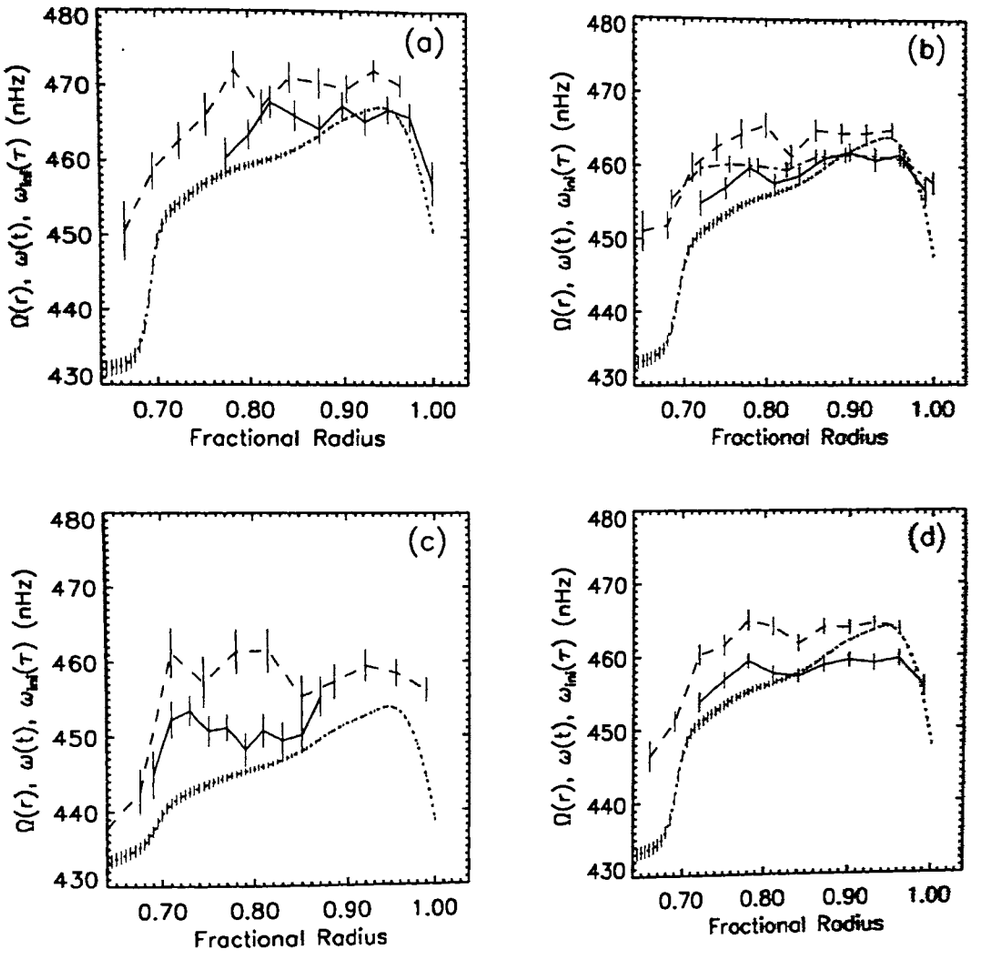

Figure 5.6. Same as Figure 5.5 except that $\Omega(r)$ was determined from GONG data.

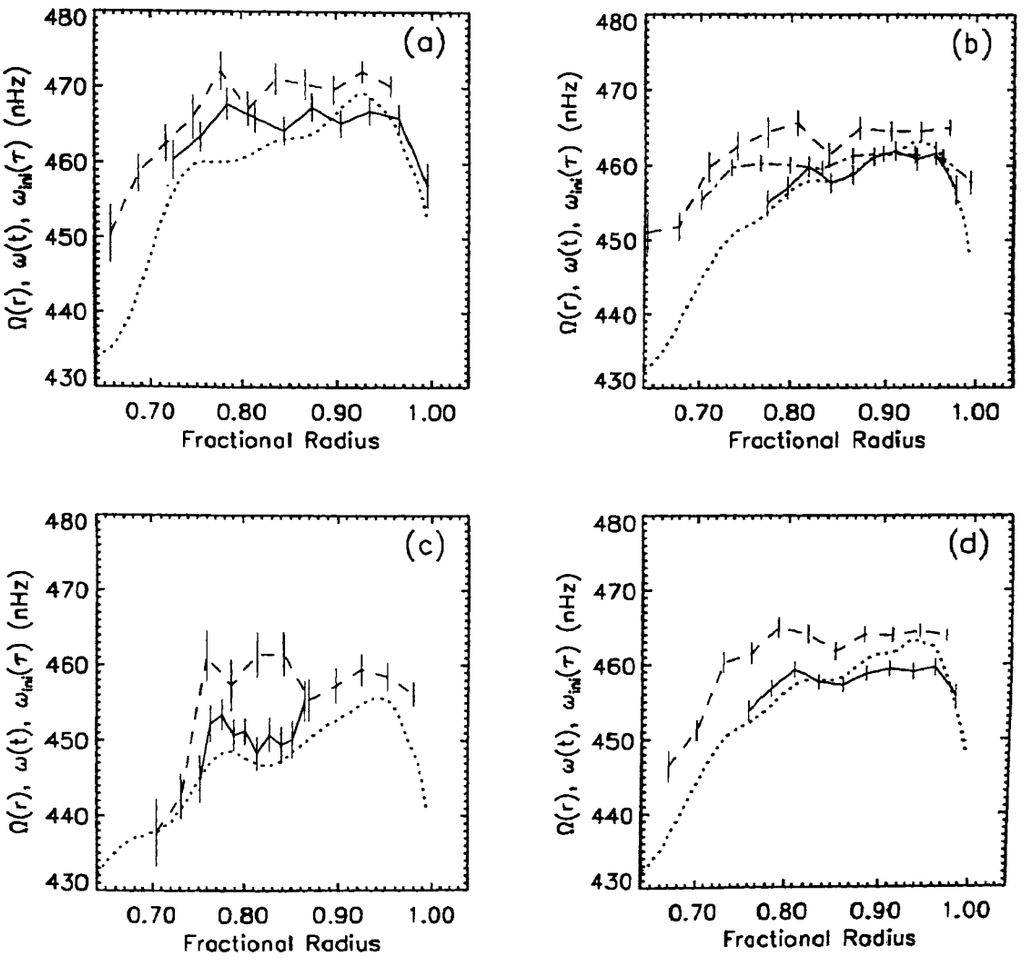

Figure 5.7. Same as Figure 5.5 except that $\Omega(r)$ was determined from SOHO data.

of spot group, except for groups of few single small spots.

5.7. Area–Lifetime Relation of Sunspot Groups

The daily area of a sunspot (or sunspot group) is one of the most important parameters used to describe the spot (or spot group) development. The area of a spot (or spot group) is closely connected with the magnetic flux of the spot (or spot group), and so the development of the spot (or spot group) area reflects the development of the magnetic field. It is well known that large spot groups also live longer. According to Waldmeier (1955) the lifetime of a spot group is related to the maximum area (attained by the rule-of-thumb) in the following way (Bray & Loughhead 1964) :

$$\tau = 0.1 A_{max} \ .$$

In Section 5.6.1, it is suggested that radial rise of magnetic structure of a spot group depends on life span and also on area of the spot group. Hence, in this section we study the area–lifetime relation of sunspot groups. We also study the distribution of spot groups with respect to life times. These studies with $r - \tau$ and $r - t$ relations, derived above, provide important information on how the magnetic structure of short lived (or small) groups is related with that of long lived (or large) groups in the convection zone. We use spot group average area because it is clear that statistically more accurate than the spot group maximum area.

Figures 5.8(a) and 5.8(b) show the correlations, (a) between Log(A) and τ and (b) between Log(N) and τ, respectively, determined from the values (given in Table 5.2.) of average area (A), life span (τ) and number (N) of spot groups. In these figures, the solid lines represent the values of Log(A) or Log(N) estimated from the linear regression analyses. The values of the corresponding intercept (a), slope (b) and correlation coefficient (R) are given in Table 5.4. The magnitudes of coefficient of correlation are high, so that the data were well fitted to the form: $Log(y(x)) = a + bx$ (see Table 5.4).

From Figures 5.8(a) and 5.8(b) and from Table 5.4, we can draw the following inferences for spot groups with life span 2–12 days, in all latitudes:

(i) the average area of a spot group increases exponentially with increasing spot group life span, (or $A(\tau) = 15.24\ exp(\tau/4.48)$),

(ii) the number of spot groups seems to decrease exponentially with increasing spot group life span, (or $N(\tau) \sim 2824\ exp(-\tau/5.38)$).

So far exponential relationship of areas of active regions to their lifetimes is not reported. Tang et al. (1984) have shown that the size distribution of active regions is close to exponential and some other authors have shown that it is close to power law

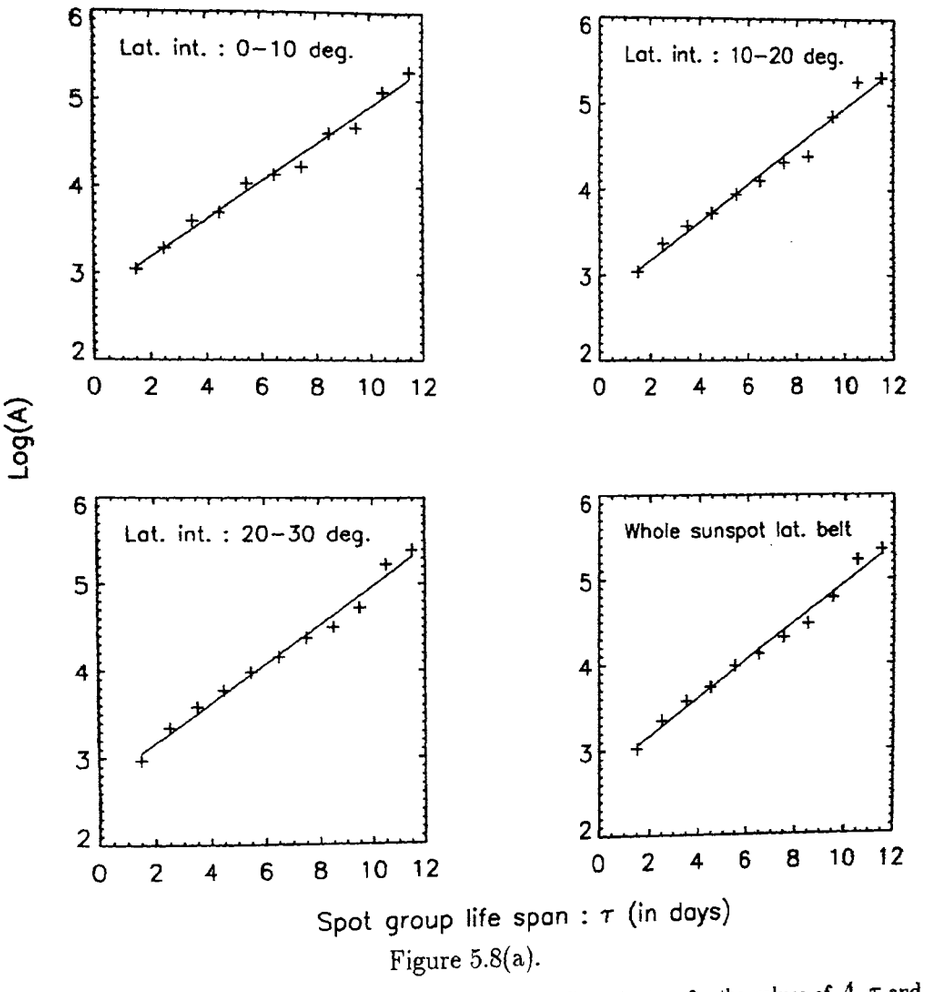

Figure 5.8(a).

Figures 5.8a b. Plots of (a) Log(A) against τ and (b) Log(N) against τ, for the values of A, τ and N given in Table 5.2. The solid lines represent the values of the Log(A) and Log(N) estimated from the linear regression analyzes (see Table 5.4).

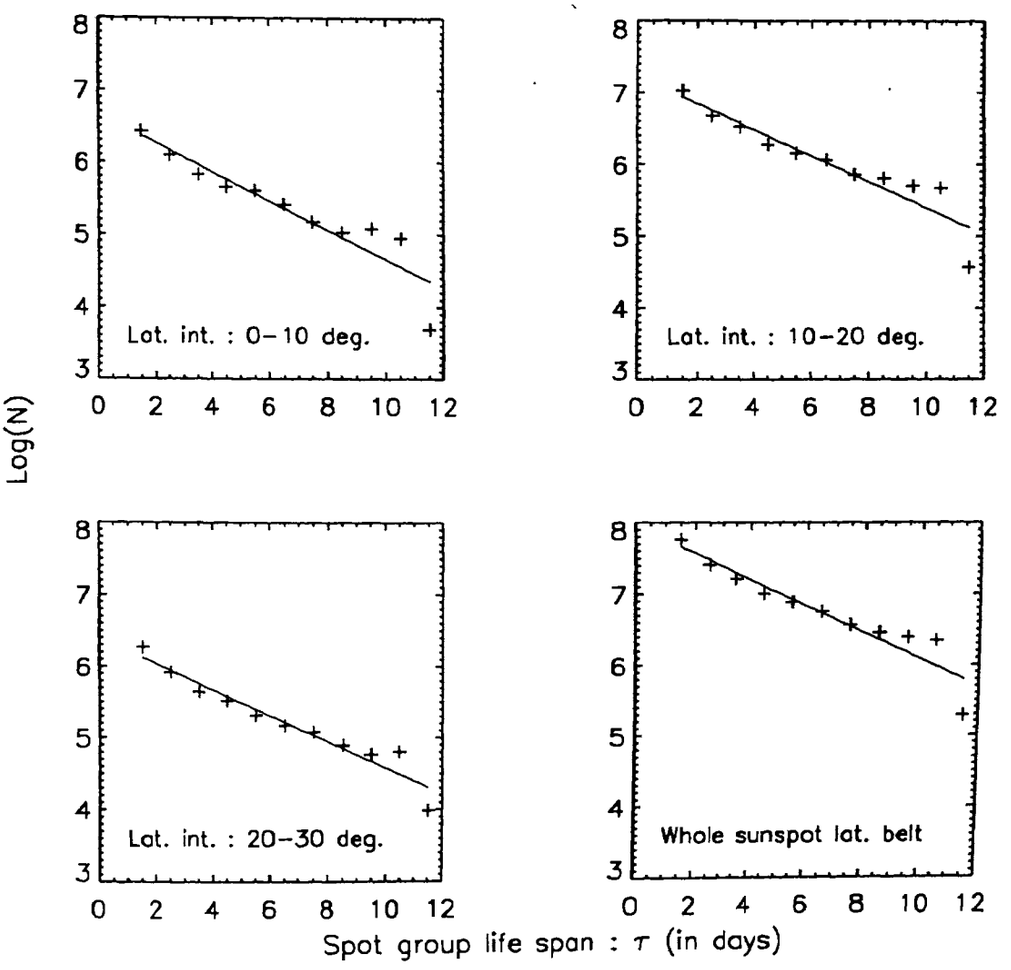
Log(N)
Lat. int. : 0–10 deg.
Lat. int. : 10–20 deg.
Lat. int. : 20–30 deg.
Whole sunspot lat. belt
Spot group life span : τ (in days)

Figure 5.8(b).

Table 5.4. Values of the coefficients (a and b) in the equation $Log(y(x)) = a + bx$, and correlation coefficient (R), determined from from the method of least-square fit to the values (given in **Table 5.2**) of the different combinations of the parameters A, τ and N taken for the x and y(x).

	latitude intervals			
	$0-10°$	$10°-20°$	$20°-30°$	Whole belt
For $x=\tau$, $y(x)=A$:				
a	2.745±0.061	2.725±0.078	2.713±0.066	2.724±0.062
b	0.217±0.008	0.224±0.011	0.226±0.009	0.223±0.008
R	0.9933	0.9896	0.9928	0.9933
For $x=\tau$, $y(x)=$ N :				
a	6.671±0.199	7.207±0.168	6.399 ±0.118	7.946 ±0.159
b	-0.202±0.027	-0.182±0.023	-0.182±0.016	-0.186±0.022
R	-0.9254	-0.9331	-0.9657	-0.9429

or log-normal distribution (Harvey & Zwaan 1993; Bogdan et al. 1988; Howard 1996). Gokhale & Sivaraman (1981) have showed that the distribution of sunspot groups with respect to maximum area may not be fitted by a simple one-parameter distribution such as single power law or an exponential law.

In the inferences (i)-(ii), above, the values of the parameters in the expressions given in brackets are determined from the data in the entire sunspot belt. In case of $A-\tau$ relation, the values of both intercept a and slope b in a given latitude interval do not significantly differ with the corresponding values in the whole belt (cf., Table 5.4). Thus, the expression given in inference (i) also holds good for all latitudes. This suggests global nature of $A-\tau$ relation.

It is interesting to note that the magnitudes of the slopes in $r-\tau$ and $r-t$ relations are equal (cf., Equations 5.1 and 5.2). Thus, for spot groups with $\tau \leq 9.5$ days

$$r_o(\tau) \approx r(10.5-\tau).$$

This means that the 'initial anchoring' of the magnetic structures of spot groups with $\tau \leq 9.5$ days is at the same depth where the anchoring of the magnetic structures of spot groups with $\tau = 10.5$ days rises in $t = 10.5-\tau$ days. Also, the linear relation of $r-\tau$ and the exponential relation of $A-\tau$, imply the exponential relation: $A \approx 130\ exp(-H/95)$, where H, in Mm, is the height above the base of the convection zone. These two facts suggest that: (i) magnetic structures (flux tubes) of spot groups with $A \geq 130$ mh might be generated around base of the convection zone, (ii) many of the magnetic structures may be fragmenting (branching) into smaller structures while rising through the solar convection zone, and (iii) magnetic structures of smaller spot groups (at least

groups with $A < 130$ mh) might be the fragmented (branched) parts of the magnetic structures of larger spot groups. These inferences are consistent with the proposals of some theoretical models (e.g., Parker 1979b). Such an inference would also account for decrease of N with τ (suggesting increase of N with H).

In Figure 5.8(b) one can see that there exist large deviations between estimated and observed values of the last 2 or 3 points (at $\tau \geq 9$ days, $A > 130$ mh or Log(A) > 4.87). In fact these points seem not to fit to the exponential forms suggested in inference (ii), above. This is because magnetic structures of spot groups with $\tau > 9$ days and $A > 130$ mh might be generated directly from the basic mechanism which generates the magnetic field for solar activity near the base of the convection zone. These structures seem to rise more radially. A reason for this may be drag force is less on these large structures (e.g., D'Silva & Howard 1994).

5.8. Conclusions and Discussion

Conclusions:

Assuming that sunspot rotation is representative of rotation at some depth in the Sun's convective zone, we infer the following:

(1) The magnetic structures of sunspot groups of life spans $\leq$ 2 *day* are anchored at $r \sim 650$ Mm, i.e., near the Sun's surface and those of spot groups with successively longer life spans between 3 and 9 *day* are anchored at successively increasing depths at the rate ~ 21 Mm/*day*. The magnetic structures of the spot groups with $\tau > 9$ days are initially anchored at $r \leq 500$ Mm.

(2) The magnetic structures of spot groups of life spans 10–12 days in latitudes $10°-20°$, are initially anchored at $r \sim 500$ Mm (i.e. near the base of the convective envelope) and these structures rise across the envelope at the rate of ~ 21 Mm/*day* (i.e., ~ 240 m/s).

(3) The radial rise of a spot group magnetic structure depends more on the size of the spot group rather than type. The conclusion (2) above, is seem to be more realistic for spot groups with $\tau = 10$–12 days and average area $A \geq 130$ mh.

(4) For spot groups living 2–12 days, the average area (A) depends exponentially on the life span (τ). The distributions of the number of spot groups (N) with respect to τ or A is nearly exponential (upto $\tau = 9$ days).

(5) From $r-\tau$, $r-t$ and $A-\tau$ relations found here, we infer the following: (i) magnetic structures (flux tubes) of spot groups with $A \geq 130$ mh might be generated around base of the convection zone, (ii) many of the magnetic structures may be fragmenting (branching) into smaller structures while rising through the solar convection zone, and

(iii) magnetic structures of smaller spot groups (at least groups with $A < 130$ mh) might be the fragmented (branched) parts of the magnetic structures of larger spot groups.

Discussion:

The Conclusion (2) above, is consistent with the conventional belief that the 'main' mechanism of solar activity, (e.g., the one that generates spot groups living longer than 10 days), operates near the base of the convective envelope (see Rosner & Weiss 1992). The rate of rise of magnetic structures of spot groups having life span 10–12 days in latitudes $10^{\circ} - 20^{\circ}$, derived by us is consistent with the conclusion of Howard & LaBonte (1981) that the magnetic flux of an active region rises on a time scale of 10 days. Incidentally, in the model of Choudhuri & D'Silva (1990), the 10 day rise of a flux tube would correspond to initial strength $\sim 10^5$ G. Conclusion (5) above consistent with the proposals of some theoretical models (e.g., Parker 1979b).

Considerable differences were found in some of the values of the correlation coefficients, slopes and intercepts obtained here using $\Omega(r)$ determined from the BBSO, GONG and SOHO data. These differences may be related to the differences in the techniques used in the inversion of these data sets (Howe 1998). The $\Omega(r)$ determined from the SOHO data yielded a drastically different r–t relation for spot groups of latitude interval $20^0 - 30^{\circ}$. It yields a rate of rise of magnetic structures is relatively slow, 7000–9000 km per day, and the rising terminates around $0.86R_{\odot}$. (In polar latitudes, the radial rise of magnetic structures might be slower and terminate at deeper layers causing absence of sunspot activity in those latitudes). This might also be related to the East West inclination of field lines in the spot group magnetic structure, which seem to depend on the emergence latitude, amount of magnetic flux, and evolution stage of spot groups (see, Caligari et al. 1995, Howard 1996b).

It must be noted that the above results represent only the average behavior of spot groups. The data used by us in determining the rotation frequencies of spot groups extends over several decades whereas the helioseismic data extends over only about 4 yr, 1985 and 1988–1990, though the internal rotation of the Sun may be varying with time besides depending upon depth and latitude (e.g., Goode & Dziembowski 1991; Gough et al. 1993; Howe et al. 2000a). Recurrent spot groups during their second and later appearances are not included in this study. It should be of interest to see how the rotation frequencies of spot groups living longer than 12 days vary in time and how their area and lifetime are related.

Chapter VI

CONFIRMATION OF 22-YEAR VARIATION IN THE SOLAR DIFFERENTIAL ROTATION AND ITS DEPTH

6.1. Introduction

It is generally accepted that Hale's 22-year magnetic cycle (cf., Section 1.2.2 of Chapter I) is the basis for all solar activity. Differential rotation plays a key role in providing toroidal magnetic fields from poloidal field (e.g., Babcock 1961). So, study of variations of the differential rotation during the solar cycle is vital for understanding the mechanism of the solar cycle and has been carried out by several authors (for references see Chapters I and III). The so-called 'torsional oscillations' have a period $\sim$ 11-yr (Howard & LaBonte 1980; LaBonte & Howard 1982a; Snadgross & Howard 1984; Komm et al. 1993a). In order to explain the difference in phase and amplitude of the torsional oscillation patterns derived from small magnetic features and from large-scale magnetic field patterns, Komm et al. (1993b) assumed that the Doppler pattern represents the surface layers, while the two magnetic patterns show the effect of layers located somewhere deeper in the convective zone. In Chapter III of this thesis, a periodicity at '18.3 $\pm$ 3-yr is found to be prominent in the differential rotation coefficient B determined from sunspot group data. Goode et al. (1991) and Goode & Dziembowski (1993) have noticed variation in the solar internal rotation derived from helioseismic data. Goode & Dziembowski (1993) suggested 22-yr solar magnetic cycle is due to the excitation of a torsional oscillation in the radiative interior. Schou (1990), Gough & Stark (1993a, b), Antia et al. (1996) have concluded the evidence for changes in the internal equatorial rotation is weak. However, Antia et al. (1996) found variation in the amplitude of the bump in the equatorial rotation near $r \approx 0.9R_\odot$ and concluded that the rotation rate near $r \approx 0.9R_\odot$ may be changing over the solar cycle. Recently, using helioseismic techniques the pattern of torsional oscillations has been measured in the outer part of the convection zone (Kosovichev & Schou 1997; Schou et al. 1998; Birch & Kosovichev 1998; Schou 1999; Basu & Antia 2000).

A number of statistical studies of solar activity suggested a physical connection between neighboring 11-yr activity cycles (Gnevyshev & Ohl 1948, 1947; Wilson 1988; Kopecký 1991, Makarov 1994; Sykora & Storini 1997; Makarov 1994; Usoskin et al. 2000). Gnevyshev & Ohl (1948) investigated the variability of the sunspot index using Zürich database (1755–1944) and found that the sum of annual Wolf numbers during an odd-numbered cycle exceeds that of the preceding even-numbered cycle (referred

as the Gnevyshev-Ohl rule). They also showed that the sum of annual Wolf numbers of an even-numbered cycle correlated well (corr. coeff. $R = +0.91 \pm 0.11$) with that of following odd-numbered cycle and the correlation is weak ($R = +0.50 \pm 0.24$) with that of preceding odd-numbered cycle. From these facts, Gnevyshev & Ohl claimed a mutual physical relation between twins of neighboring 11-yr cycles and concluded that each 22-yr cycle begins with beginning of the even cycle and ends with the end of the following odd one.

To check whether the 18.3 ± 3-yr periodicity in the differential rotation coefficient B (found in Chapter III) is related to solar magnetic cycle, we examine in the present chapter the behaviour of B in adjacent 11-yr solar cycles, i.e, in the neighboring odd numbered cycles (ONSCs) and even numbered cycles (ENSCs). In addition, using the results in Chapter V on anchoring depths of magnetic structures for spot groups of different life spans and age, we also examine the possibility of depth dependence of the periodicities in differential rotation (Javaraiah 1998).

In Section 6.2.1 we describe the data and its reduction. In Section 6.2.2 we determine mean values of the differential rotation coefficients A and B, and also show the profiles of mean differential rotation determined by averaging over 5° latitude intervals from different subsets (i.e., odd cycles, even cycles, north and south hemispheres) of sunspot group data during 1879–1975. In Section 6.2.3 we show the cycle-to-cycle variations of A and B and in Section 6.2.4 we determine variations during the solar cycle. In Section 6.2.5 we describe the correlations of A and B with amount of activity. In Section 6.3.1 we describe the data samples of the young groups and the old groups. In Section 6.3.2 we show temporal variations in B derived from the young and the old spot groups, and also from the short-lived groups. In Section 6.3.3 we show the depth dependence in the periodicities of B. In Section 6.4 we summarize the conclusions and briefly discuss them.

6.2. Long–Term Variations in A and B

6.2.1. DATA ANALYSIS

We have used the data on sunspot groups compiled from GPR during 1879–1975. This data is compiled by National Geophysical Data Center, USA and include the observation time, (the date and the fraction of the day), heliographic latitude and longitude and central meridian longitude (CML), etc., for each day of observation.

We have computed the sidereal rotation velocities (ω) for each pair of consecutive days in the life of each spot group using its longitudinal and temporal differences between these days. We fitted this data to the standard formula of differential rotation (Equation (3.2)), $\omega(\lambda) = A + Bsin^2\lambda$. We have excluded the data corresponding to

the $|CML| > 75^{\circ}$ on any day of the spot group life span and also did not use the data from non-consecutive days of spot groups life span. Further, we excluded the data corresponding to the 'abnormal' motions, e.g. displacements exceeding $3^{\circ}\ day^{-1}$ in the longitude or $2^{\circ}\ day^{-1}$ in latitude. This reduces substantially the uncertainties in A and B (see Section 3.2.3 of Chapter III).

We study variations in the equatorial rotation rate (A) and the latitudinal gradient (B) by determining them from the ONSC data and the ENSC data separately. The solar cycle variations of A and B are determined by superposing the data during 1879–1975 according to the years relative to the nearest sunspot minimum (1879, 1890, 1902, 1913, 1923, 1934, 1944, 1954, 1965, 1976).

6.2.2. MEAN VALUES OF A AND B

In Table 6.1 we give the mean values of A and those of B determined from the different subsets (e.g., odd cycles, even cycles, etc.) of the data during 1879–1975. In Figure 6.1(a) and 6.1(b) we show rotation rate determined from the ONSCs (Waldmeier cycle numbers 13, 15, 17, 19) data (circles) and ENSCs (12, 14, 16, 18, 20) data (crosses), by averaging the data over 5 degree latitude intervals. In these figures the smooth solid curves and the dashed curves represent the rotation obtained using values of A and B (given in Table 6.1) which are derived from the ONSCs data and ENSCs data, respectively. Figure 6.1(a) represents the whole sphere data whereas Figure 6.1(b) represents the separated data of northern and southern hemispheres.

Table 6.1. The values of the parameters A and B (in $\mu\ rad\ s^{-1}$) and their uncertainties $\Delta(A)$ and $\Delta(B)$ derived from the different sets data during the period 1879–1975. N represents the number of data points gone in each determination.

Data set	A	$\Delta(A)$	B	$\Delta(B)$	N
All cycles:					
Whole sphere	2.932	± 0.001	-0.536	± 0.008	112388
Southern hemisphere	2.934	± 0.001	-0.531	± 0.012	54285
Northern hemisphere	2.931	± 0.001	-0.541	± 0.011	58103
Odd numbered cycles:					
Whole sphere	2.934	± 0.001	-0.562	± 0.011	54526
Southern hemisphere	2.938	± 0.002	-0.575	± 0.017	25848
Northern hemisphere	2.932	± 0.002	-0.553	± 0.014	28678
Even numbered cycles:					
Whole sphere	2.930	± 0.001	-0.504	± 0.012	57862
Southern hemisphere	2.931	± 0.002	-0.484	± 0.017	28437
Northern hemisphere	2.930	± 0.002	-0.526	± 0.017	29425

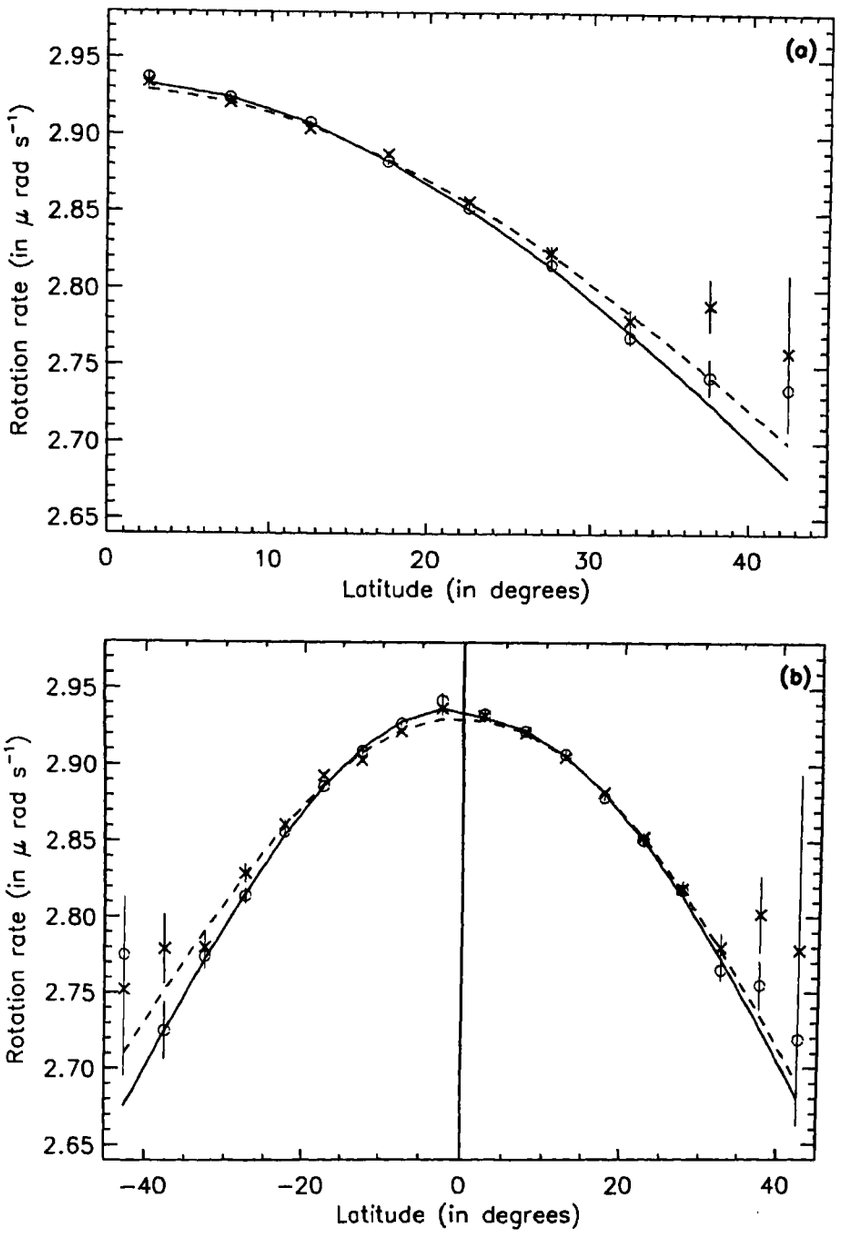

Figure 6.1. Differential rotation determined from the ONSCs (13, 15, 17, 19) data (circles) and of ENSCs (12, 14, 16, 18, 20) data (crosses), by averaging the data over 5 degree latitude intervals. The smooth solid curves and the dashed curves represent the rotation rate at different latitudes obtained using values of A and B (given in Table 6.1) derived from the ONSCs data and ENSCs data, respectively. (a) Represents the whole sphere whereas (b) represents the northern hemisphere (positive latitudes) and southern hemisphere (negative latitudes).

From the Table 6.1 and Figures 6.1(a) and 6.1(b) it can be seen that the rotation is significantly more differential in the ONSCs than in the ENSCs. The difference in the magnitude of B is about 5 times larger then their respective uncertainties (ΔB values). However, this difference is mainly contributed from the southern hemisphere. In the northern hemisphere the difference is marginal (about 1.6 times larger than their respective ΔB values). North–south asymmetry in B (cf., Chapter IV) is considerably significant (2.6 times the corresponding values of ΔB) in the ENSCs and it is less significant (1.6 times ΔB) in ONSCs. In ENSCs and ONSCs the behaviour seems to be opposite in the northern and southern hemispheres, i.e, in ENSCs the rotation is more differential in the northern hemisphere than in the southern hemisphere and it is opposite in the ONSCs.

The equatorial rotation rate A is also significantly larger in the ONSCs than in the ENSCs. In general, southern hemisphere seems to be rotating (near equator) faster than the northern hemisphere. The north–south asymmetry in A seems to be large in ONSCs.

6.2.3. CYCLE TO CYCLE VARIATIONS OF A AND B

Figures 6.2(a) and 6.2(b) show the cycle–to–cycle variations of A and B, respectively. In Figure 6.2(a), there is a big jump in the values of A from cycle 13 to cycle 14. This large decrease in A was already noticed by Tuominen & Kyrölāinen (1981) and Balthasar et al. (1986) from the analysis of GPR data. There is a suggestion of gradual increase in A from cycle 14 to cycle 17 and a sudden decrease from cycle 17 to cycle 18. The time gap between this jump and the previous big jump is about 55 years. Yoshimura & Kambry (1993) have detected a 55 year grand cycle in A using NAOJ spot group data during 1948–1987. The overall trend in Figure 6.2(a) suggests existence of a dominant long periodicity of the order of 100 year in A.

In Figure 6.2(b), there exists a systematic cycle–to–cycle variation in B, suggesting existence of 22-yr modulation in B. If we exclude the first data point (belongs to the cycle 12), the remaining data suggest that the magnitude of B in each of ONSCs is somewhat larger than that in its neighboring ENSCs. Such a systematic behaviour in A can also be seen in Figure 6.2(a) but it is not as well defined as that of B. In Figure 6.3 we show the correlation between B of ONSCs and that of following ENSCs (cycle 12 is not included). The good (96.3%) correlation confirms the aforementioned systematic behaviour in B and also suggests existence of long term variation in B. (The correlation between B of ENSCs and that of following ONSCs is found be better. However, the number of data points are reduced to 3.) In Figure 6.2(b), there is a suggestion of ~ 80 year variation (Gleissberg cycle) in B, whose amplitude ($\sim 0.07\ \mu\ rad\ s^{-1}$) seems to be considerably larger than that (maximum $\sim 0.04\ \mu\ rad\ s^{-1}$) of the 22-yr modulation. In fact, the $\sim$ 22-yr modulation seems to be superimposed on the $\sim$ 80-yr modulation.

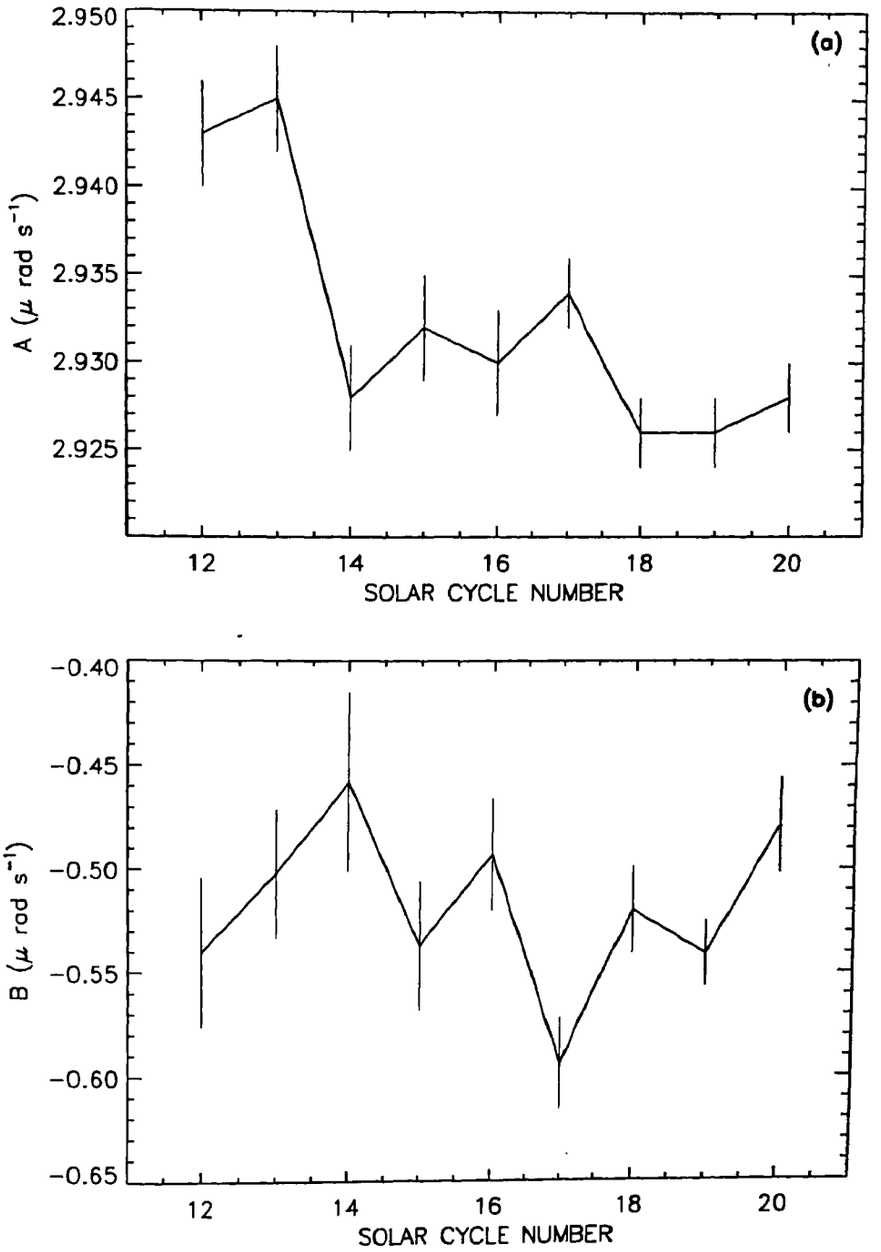

Figure 6.2 . . Cycle-to-cycle variations of A and B.

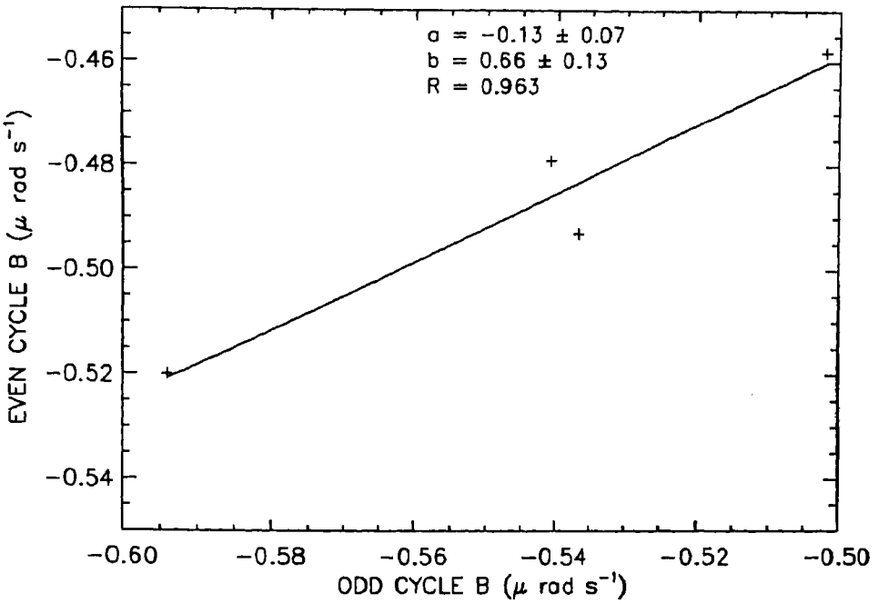

Figure 6.3. Plot of values (in Figure 6.2(b)) of B during odd cycles verses that during the 'following' even cycles. The solid line represents the values of even cycles B obtained from the linear regression analysis (the values of the intercept (a), slope (b) and the correlation coefficient R are also shown).

6.2.4. VARIATIONS DURING THE SOLAR CYCLE

Figures 6.4(a) and 6.4(b) show the mean variations of A and B with phase of sunspot cycle determined by superposed epoch analysis of the spot group data during 1879–1975. Figures 6.5(a) and 6.5(b) show the mean variations of A and B during the ONSCs (Waldmeier cycle numbers 13, 15, 17, 19)(dashed curves) and the ENSCs (12, 14, 16, 18, 20) (dotted curves). From Figures 6.4(a) and 6.4(b) it can seen that A and B vary significantly during the solar cycle. However, from Figure 6.5(a) it can be seen that the variation in A is significant only in the ONSCs, with amplitude $\sim 0.01\ \mu\ rad\ s^{-1}$, at minimum years. The variation in B is quite significant in both ONSCs and ENSCs with amplitude $\sim 0.05\ \mu\ rad\ s^{-1}$. Also, there exists a good anticorrelation between the dashed and dotted curves (in Figure 6.5(b)) suggesting existence of a '22-yr' periodicity in B. However, the amplitude of the anticorrelation between odd and even cycles B depends on the phase of the solar cycle. The value of the correlation coefficient (R) is only -0.33 from all the 6 points. Exclusion of the last point (average value of 11th and 12th year) yielded $R = -0.53$. The exclusion of last two points yielded $R = -0.93$ and this is shown in Figure 6.6. The regression line shown in this figure (solid line) suggests existence of a good inverse linear relationship between the B of ONSCs and that of ENSCs, in the first eight years of the cycles. However, it has to be confirmed by using more data points. (These results are reported in Javaraiah 2000.)

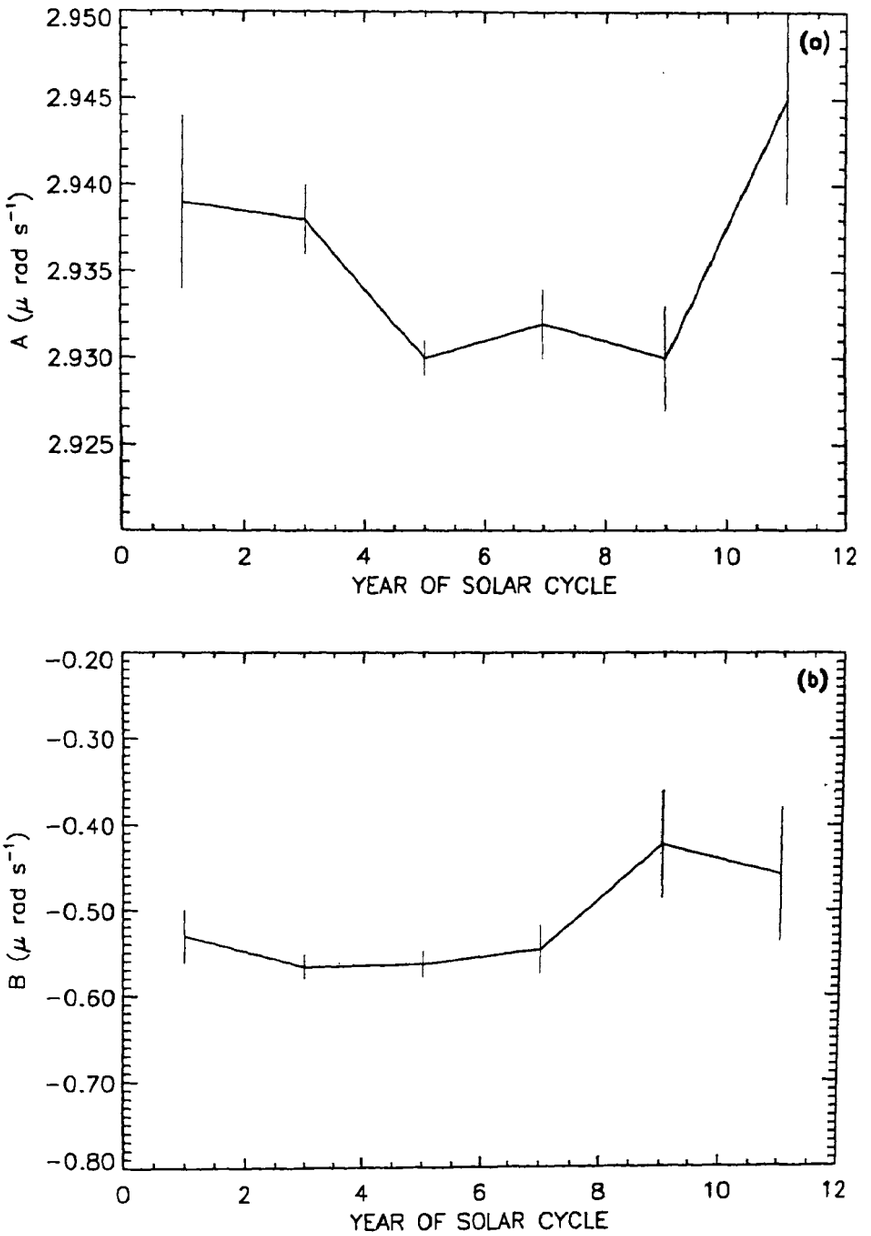

Figure 6.4. The mean variations of A and B during the solar cycle determined by superposing the data during 1879–1975 according to the years relative to the nearest sunspot minimum (1879, 1890, 1902, 1913, 1923, 1934, 1944, 1954, 1965, 1976). Averages taken over 2-yr intervals. Activity maximum is around 4–5 years.

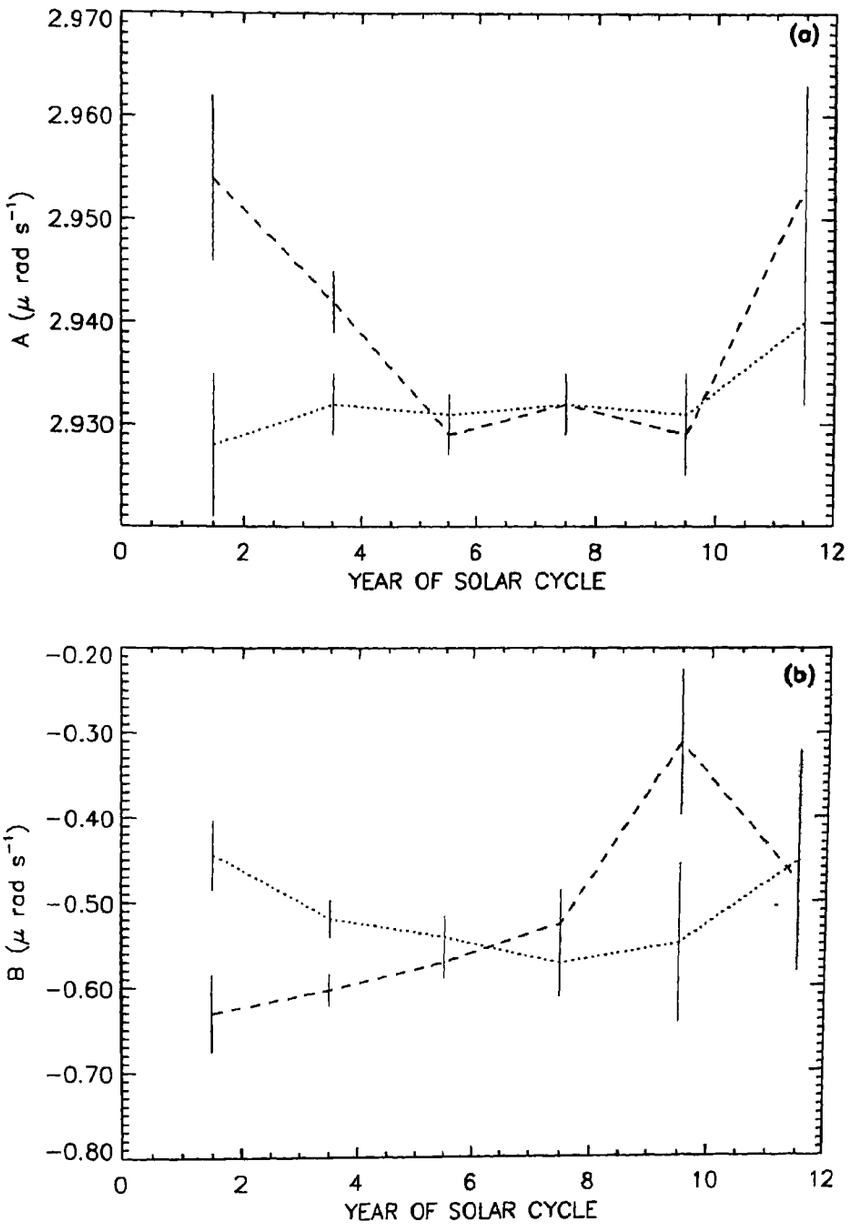

Figure 6.5. The mean variations of A and B during ONSCs (dashed curves) and ENSCs (dotted curves). Averages taken over 2-yr intervals. Activity maximum is around 4–5 years.

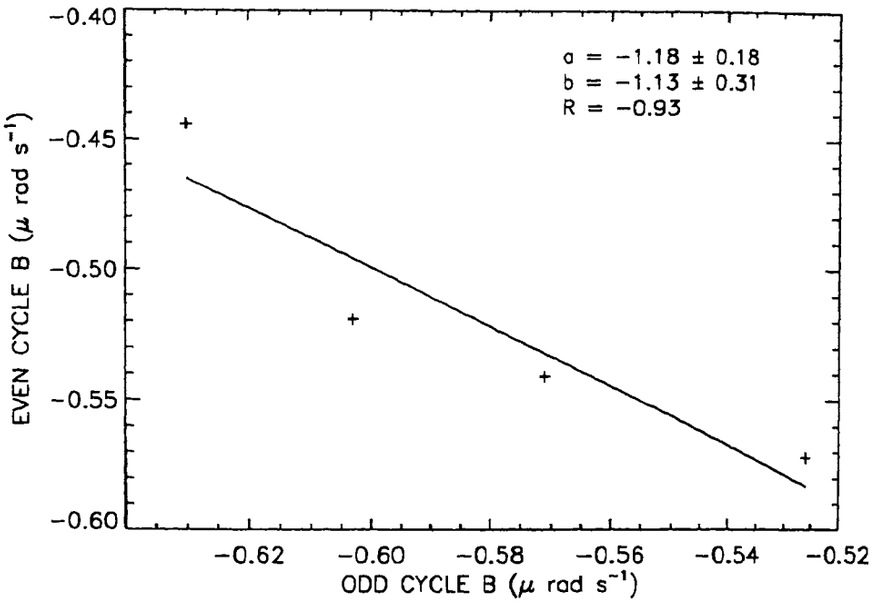

Figure 6.6. Correlation between B of ONSCs and that of ENSCs during the first eight years of the cycles. The solid line represent the values of B of ENSCs obtained from the linear regression analysis. The values of intercept a, slope b and correlation coefficient R are also given.

[Note: as already pointed out in Chapter III (Section 3.4.2), the substantial decrease in the magnitude of B at 9.5 year in Figure 6.4(b) is mainly coming from the data in the year 1962. The exclusion of the year 1962 yielded the value -0.474 for B at 9.5 year, whose magnitude is even greater than the corresponding value at 11.5 year. The exclusion of the year 1962 yielded the value -0.389 for B of ONSCs at 9.5 year in Figure 6.5(b). However, still the pattern of the dashed curve remains almost same.]

6.2.5. CORRELATIONS OF A AND B WITH THE ACTIVITY

From the pattern of cycle-to-cycle variation of B shown in Figure 6.2(b) (described in Section 6.2.3, above) it seems that the known Gnevyshev & Ohl rule (Gnevyshev & Ohl 1948) rule of solar activity (see Section 6.1) may be applicable also to B. We also found 94% correlation between the ratios A_{2n}/A_{2n+1} and X_{2n}/X_{2n+1}, and 91% correlation between ratios B_{2n}/B_{2n+1} and X_{2n}/X_{2n+1}, where X is the mean sunspot activity of given cycle (calculated from the yearly means taken from web page:

http://www.astro.oma.be/SIDC/DATA/yearssn.dat)

and the subscripts represent the cycle numbers with $n = 7, 8, 9$. The ratios of preceding odd cycle and the following even cycle combinations yielded only 40%-50% anticorrelation. One may interpret these correlations as follows: Each 22-yr cycle may begin with

beginning of the even cycles and may end with the end of the following odd one, as suggested by Gnevyshev & Ohl (1948) from the analysis of sunspot activity. However the aforementioned correlations are derived from only 3-4 points. The exact physical reason for better correlations of preceding even cycle and the following odd cycles ratios of A and B with corresponding ratios of X and the low (and negative) correlations of the 'preceding odd cycle-following even' combinations is yet be found.

6.3. Depth dependence of periodicities in the solar differential rotation

6.3.1. SAMPLES OF THE DATA ON THE YOUNG AND OLD SUNSPOT GROUPS

We have analysed GPR spot group data during 1879–1939 (the data was provided by H. Balthasar). The data reduction is the same as in Section 6.2.1 but here we have used only data on spot groups living 2–12 days (the data on second and subsequent appearances of recurrent spot groups are excluded).

In view of the relationships found in Chapter V between the rotation frequencies of spot groups and the life span and age of spot groups, we considered separately the following data samples defined as follows: (i) YLSG: *young long-lived sunspot groups* (YLSG1: $t = 2$, $\tau = 7$–12, or YLSG2: $t < 4$, $\tau = 10$–12), where τ and t represent respectively life span and age of a sunspot group in days, (ii) SLSG: *short-lived sunspot groups* ($\tau = 2$–4) and (iii) OLSG: *old long-lived sunspot groups* ($t > 4$, $\tau = 10$–12).

For these well separated data we fitted the standard formula of differential rotation, $\omega(\lambda) = A + Bsin^2\lambda$. For each of the above data sets, we determined variations of the differential rotation coefficient, B, during 5-yr moving time intervals successively displaced by 1 yr (5-yr MTI) (the data sizes in the intervals < 5-yr are inadequate).

6.3.2. TEMPORAL VARIATIONS OF B DETERMINED FROM YLSG, OLSG AND SLSG

Figure 6.7 shows the variations of the differential rotation coefficient, B, during 5-yr MTI of YLSG1, YLSG2, OLSG and SLSG. In this figure it can be seen that the uncertainty bars are sufficiently small for seeing the variations of B on time scales 10–20 years.

Figure 6.8 shows the FFT spectra of B determined from the YLSG1, YLSG2, OLSG and SLSG for 5-yr MTI during 1879–1976. (For longer interval lengths the uncertainties in B will be smaller. However, the peaks corresponding to the higher frequencies will be washed out, and the peaks at lower frequencies will be broader.) The FFT spectra of B determined from the YLSG show existence of a periodicity at $\sim$ 21 yr. This periodicity is absent (or insignificant), and a $\sim$ 11 yr periodicity is dominant in the spectra of B determined from the OLSG and SLSG.

To check whether the positions and significance levels of the peaks in the FFT

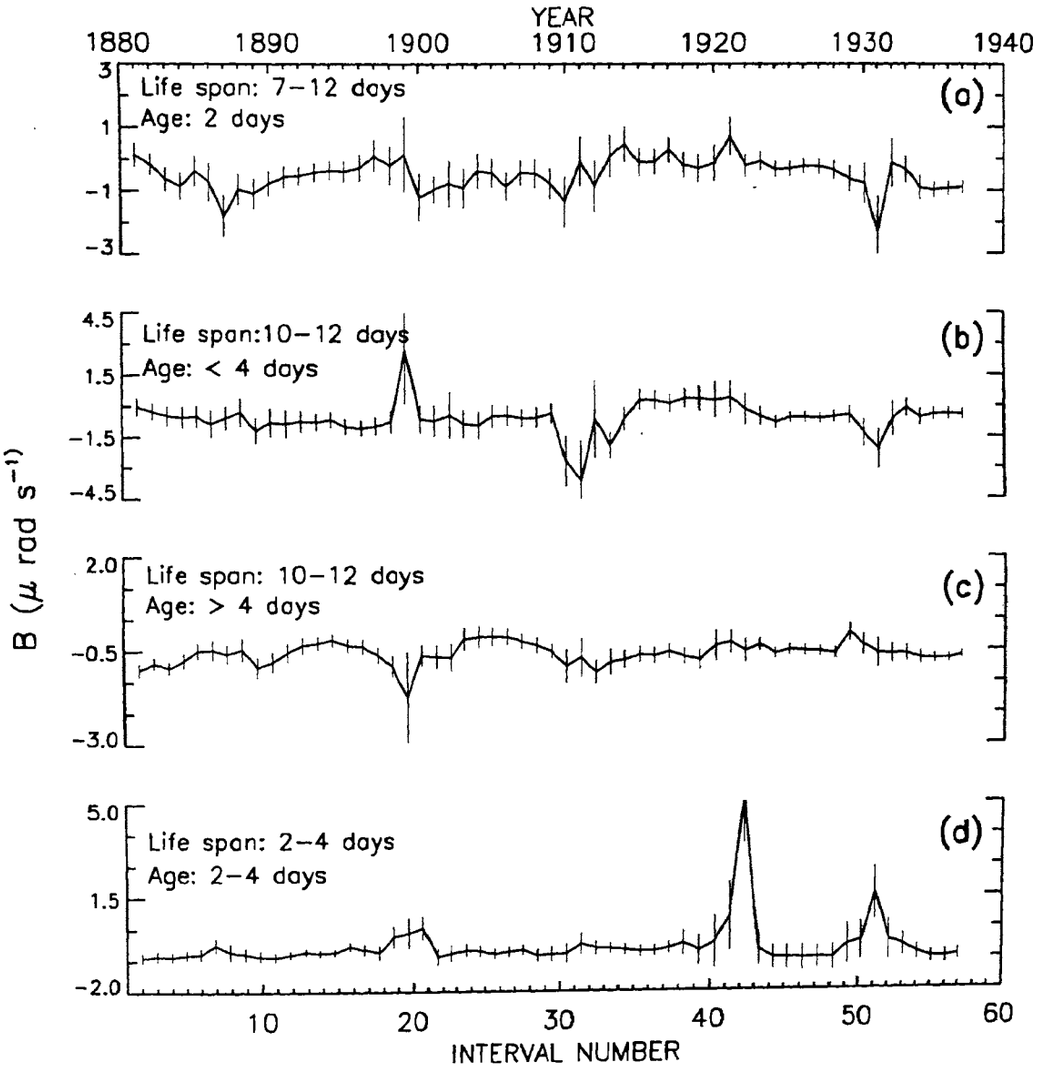

Figure 6.7. Variation of the differential rotation coefficient B determined from the two subsets (a) YLSG1 and (b) YLSG2 of YLSG: *young long-lived sunspot groups*, (c) OLSG: *old long-lived sunspot groups* and (d) SLSG: *short-lived sunspot groups* (cf., Javaraiah 1998). The successive 5-yr intervals 1879–1883, 1880–1884, ..., 1935–1939 are denoted by the interval numbers 1, 2, ..., 57 respectively, shown on the bottom scale. The middle years of these intervals are shown in the top scale.

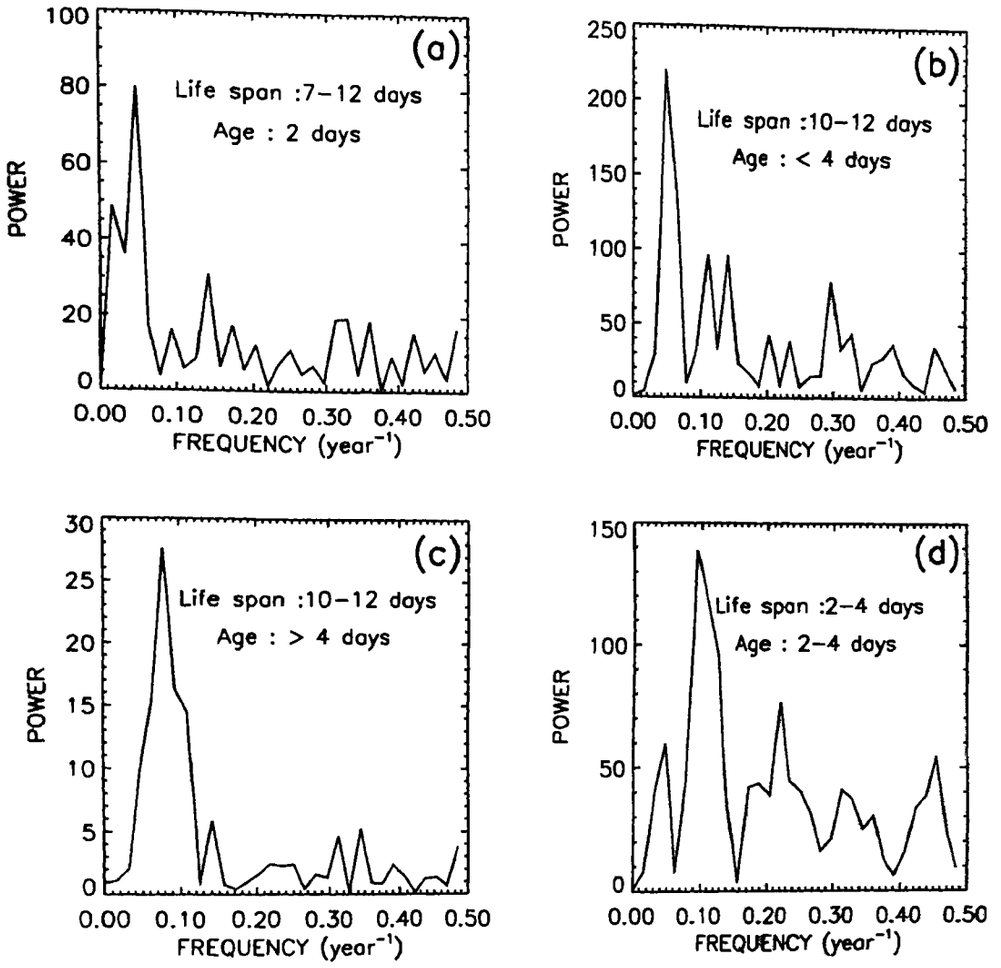

Figure 6.8. FFT spectra of B determined from the (a) YLSG1, (b) YLSG2, (c) OLSG and (d) SLSG.

spectra of B are reliable in spite of the uncertainties (standard deviations) in the values of B, we used the following method which we have already used in Chapters III and IV. We generated 'simulated' time series B' of B by varying each value of B in the time series by adding to it a random number whose magnitude is equal or less than the corresponding uncertainty. FFT analyzes were then done for the simulated series of B'. In both spectra of B and B' determined from given data set, the positions of the peaks are found to be the same. Thus, even if the 'correct' values of B were any where within their respective standard deviations, the positions of the peaks in FFT spectra would be unaltered. Hence, the peaks in the FFT spectra of B represent the true variations of B.

6.3.3. DEPTH DEPENDENCE OF ROTATION FREQUENCIES OF THE YLSG, OLSG AND SLSG

In Figure 6.9, we compare the average rotation frequencies (ω) of YLSG, OLSG and SLSG with the radial dependence ($\Omega(r)$) of plasma rotation frequency determined from helioseismology. From this figure we infer that the average rotation frequency determined from the YLSG represents the average rotation frequency of magnetic structures of YLSG which are initially anchored (or born) in deeper layers (near the base of the convective envelope, $r/R_\odot \sim 0.73$), whereas the average rotation frequencies determined from the OLSG and SLSG represent the average rotation frequency of magnetic structures which are anchored at $r/R_\odot > 0.95$.

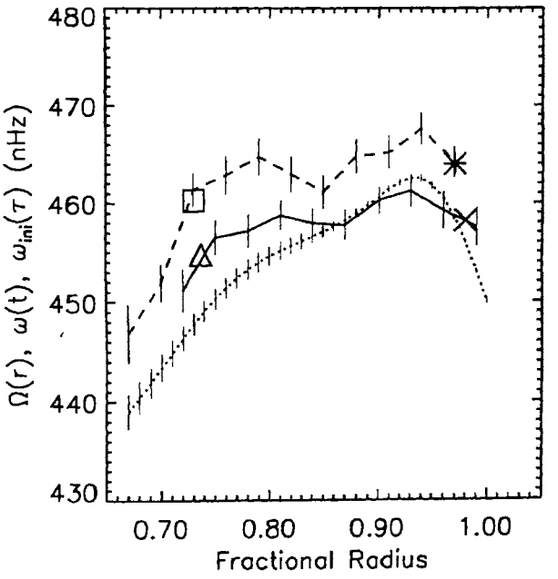

Figure 6.9. Same as the Figure 5.4 of Chapter V except that here we have also showed the average rotation frequencies of the YLSG1, YLSG2 and OLSG and SLSG (represent by the symbols □, △, × and ∗, respectively) and they were determined from, data during entire period 1874–1939.

6.4. Summary of Conclusions and Discussion

Summary:

The main conclusions of the above study are as follows:

(1) The equatorial rotation rate A is significantly larger in the ONSCs than in the ENSCs. The north-south asymmetry in the A seems to be large in the ONSCs and less in the ENSCs.

(2) The rotation is significantly more differential in the ONSCs than in the ENSCs and the difference is mainly contributed from the southern hemisphere. In the northern hemisphere the difference is marginal.

(3) North-south asymmetry in B is significant in the ENSCs and it is not significant in ONSCs. In ONSCs the rotation is more differential in the northern hemisphere than in the southern hemisphere and it is in opposite sense in the ENSCs.

(4) There exists a systematic cycle-to-cycle variation in B, i.e., the magnitude of B in each of the ONSCs is larger than that in its neighboring ENSCs, suggesting existence of 22-yr modulation in B. (Such a systematic behaviour can also be seen in the cycle-to-cycle variation of A but it is not as well defined as that of B).

(5) Existence of $\sim$ 80-yr cycle (Gleissberg cycle) in B is seen in the cycle-to-cycle variation of B. The weak 22-yr modulation in B seems to be superposed on the relatively strong 80-yr modulation.

(6) The A varies significantly only during ONSCs with amplitude $\sim 0.01\ \mu\ rad\ s^{-1}$, at minimum years. There exists a good anticorrelation between the variations of B derived from the ONSCs and ENSCs, suggesting existence of a '22-yr' periodicity in B. The amplitude of variation of B is $\sim 0.05\ \mu\ rad\ s^{-1}$.

(7) It seems the known Gnevyshev & Ohl rule (Gnevyshev & Ohl 1948) of solar activity is applicable also to B. (The pattern of correlations of A and B with activity also suggest that the each 22-yr cycle begin with beginning of the even cycles and ends with the end of the following odd one, as suggested by Gnevyshev & Ohl (1948) from the analysis of sunspot numbers.)

(8) The periodicities $\sim$ 21 yr and $\sim$ 11 yr in B may be dominant in the rotational perturbations in the Sun's deeper layers (near base of the convective envelope, $r \sim 0.73 R_\odot$) and in the shallower layers ($\sim\ r > 0.95 R_\odot$), respectively.

(9) The average rotation frequency of YLSG may represent the rotation of their magnetic structures which are initially anchored near the base of the convective envelope, whereas the average rotation frequencies of OLSG and SLSG may represent the rotation

frequencies of their magnetic structures anchored in shallower layers near the surface.

(10) From conclusions (8) and (9) we conclude that (i) the $\sim$ 22 yr and $\sim$ 11 yr periodicities in B may be dominant in the rotational perturbations in the deeper layers (near base of the convective envelope, $r \sim 0.73 R_\odot$) and in the shallower layers of the Sun ($\sim\ r > 0.95 R_\odot$), respectively.

Discussion:

Existence of anticorrelation in the variations of B during ONSCs and ENSCs (Conclusion (6), above) indicate that the solar cycle variations in B found here is not an artifact of influence of latitudinal distribution of sunspot activity in the course of solar cycle (Butterfly diagram). We have used superposition of 5 or 10 cycles data. So, the magnitude of variation of B during some single solar cycles may be larger than that is found here.

It has been claimed that the torsional pattern is present in sunspot motions (Godoli & Mazzucconi 1982; Tuominen et al. 1983; Ternullo 1990), although the results are marginally significant, judging from the errors. Tuominen et al. (1993) analyzed longitudinal and latitudinal motions of recurrent sunspot groups using Greenwich spot group data during 1974–1976. Although their time resolution was course, they found some evidence for the 11-yr oscillation in the sunspot zones with an amplitude of a few m s^{-1}. Gilman & Howard (1984) have observed faster and slower bands, but with no clear migratory character. Ternullo (1990) has discovered evidence of equatorward moving bands through a careful study of the sunspot drawings made during cycle 21 at Catania Astrophysical Observatory. It is interesting note that Ternullo used for each spot group only the data collected from the 4th day of observation until the last observation available (i.e., the data on old spot group). From the Conclusion (10), above, we confirm that 11-yr period 'torsional oscillations' (Howard & LaBonte 1980; LaBonte & Howard 1982; Snodgrass & Howard 1985; Komm et al. 1993a) may be strong in the rotational perturbations in the shallower layers of the Sun ($\sim\ r > 0.95 R_\odot$). Similar suggestions are also found in the recent helioseismic measurements (e.g., Howe et al. 2000b; Basu & Antia 2000).

Results/conclusions (1)–(10) above, confirm: (i) existence of '22-yr' periodicity in B, (ii) its validity near the base of the convection zone, (ii) its relation to solar magnetic cycle.

Chpater VII

VARIATION OF THE SUN'S MERIDIONAL FLOW DURING THE SOLAR CYCLE

7.1. Introduction

Many solar physicists believe that the Sun's meridional flow can transfer angular momentum and magnetic flux across the solar latitudes and can even maintain the observed differential rotation (e.g., Schröter 1985 and references therein). So far the meridional velocity determined from tracers like sunspots or sunspot groups, faculae and plages suggest a flow of only a few m s^{-1} and the direction is either north or south from the mean latitude (e.g., Balthasar et al. 1986; Howard & Gilman 1986; Howard 1991, 1996a; Lustig & Wöhl 1991; Nesme-Ribes et al. 1993; Meunier et al. 1997). The velocities determined from Dopplergrams and magnetograms suggest a poleward flow of 10–20 m s^{-1} (Duvall 1979; LaBonte & Howard 1982b; Ulrich et al. 1988; Cavallini et al. 1992; Komm et al. 1993c; Snodgrass & Dailey 1996). Recently, helioseismological measurements of the near-surface and subsurface properties of meridional flows (Duvall et al. 1993; Hathaway 1996; Hathaway et. al. 1996; Giles et al. 1997; Braun & Fan 1998) also suggest a poleward flow in the range 10–20 m s^{-1}. The reason for the discrepancy in the results derived from tracers and from Doppler velocity measurements, and also in the results obtained from different tracers, is not yet known. However, this might be due to difficulties in obtaining adequate homogeneous samples of identical tracers (for example, sunspots or sunspot groups with same life span, age, area etc.). The homogeneity of the samples might also help in interpreting the results in terms of the anchoring depths of the magnetic structures of the tracers (cf., Chapters V and VI). Variability of the meridional motion through the solar cycle would provide valuable information on the dynamics controlling the differential rotation, which is responsible for the dynamo mechanism. Because the amplitude of meridional motion is small, it is difficult to measure its variability. In the present chapter we discuss the dependence of the meridional motions of sunspot group on life spans and age of the groups and on the phase of the solar cycle, through the analysis of the large data on sunspot groups.

The outline of this chapter is as follows: In Section 7.2 we describe the data and the method of analysis. In Section 7.3.1 we describe the mean meridional motions of sunspot groups of different life spans. In Section 7.3.2 we show the variation of initial meridional velocities of spot groups with life span τ in range 2–12 days and the variation of the mean meridional velocity of long lived (τ = 10–12 days) spot groups with age

t. In Section 7.3.3 we derive the 'surface plasma meridional flows' from spot groups which lived 10 12 days. In Section 7.4.1 we show variations in the mean meridional velocity of sunspot groups during the solar cycle. The variations in the 'surface plasma meridional velocity' during the solar cycle is determined in Section 7.4.2. In Section 7.5 we determine the correlation between the solar cycle variations of the mean meridional motion of spot groups and the solar differential rotation. In Section 7.6 we summarize and interpret the results and also discuss briefly the source of uncertainties.

7.2. Data and Analysis

We have used the data on sunspot groups compiled from *Greenwich Photoheliographic Results* (1874–1976) and from NOAA/USAF for the years 1977–1981. The method of data reduction is the same as in Chapters V and VI. In Table 7.1 we give the total number of the spot groups of different specified life spans in three latitude intervals of 10° each and for northern and southern hemispheres separately.

Table 7.1 The number of sunspot groups of different specified life spans (τ, in days) in different 10° latitude intervals, during 1874–1981.

	North hemisphere			South hemisphere		
	Latitude intervals			Latitude intervals		
τ	$0° - 10°$	$10° - 20°$	$20° - 30°$	$0° - 10°$	$10° - 20°$	$20° - 30°$
1.5	289	571	247	331	548	283
2.5	223	378	205	221	411	167
3.5	178	324	143	161	355	141
4.5	145	277	132	141	252	118
5.5	137	248	100	135	221	103
6.5	105	190	109	119	238	67
7.5	78	177	87	99	171	74
8.5	75	166	77	78	165	57
9.5	75	166	70	86	131	48
10.5	73	145	65	68	144	57
11.5	24	49	27	16	47	27

The meridional velocity (daily latitudinal drift), v, of a spot group of a specified life span, and in a specified latitude interval, at its age $t = (n + 1/2)$ *day* is computed using the epochs of its observations on the (n)th and the (n+1)th day, and the heliographic latitudes of the spot group at these epochs. Non-consecutive days were not used for determining v. Thus the uncertainty in t is ≤ 0.5 *day*. We adopt the following convention: a positive value of v indicates poleward flow in either hemisphere.

For each specified value of the age 't' of a spot group, the mean meridional velocity ($v(t)$), and the standard deviation (σ), were computed for spot groups of given life span in given latitude bin. For spot groups of given life span τ in a given latitude bin, the value of v at $t = 3/2$ day is defined as the mean "initial" meridional velocity $v_{ini}(\tau)$.

The variation in the mean meridional motion of the spot groups during the solar cycle is determined using the method of superposed epoch analysis (cf. Chapter VI). In this case the calculations were repeated with and without including the second and subsequent disk passages of the recurrent spot groups. Each disk passage of a recurrent group is treated as a separate spot group.

7.3. Variation of Meridional Motions of Sunspot Groups During Their Life span

7.3.1. MERIDIONAL MOTIONS OF SUNSPOT GROUPS OF DIFFERENT LIFE SPANS AVERAGED OVER THEIR LIFE

In Figure 7.1 we show the "mean" meridional velocities, $< v > (\tau)$, of the spot groups of different specified life spans in three latitude intervals of 10° each, during the entire period 1874 -1981 (data in northern and southern hemispheres were folded by adopting the convention mentioned in Section 7.2, i.e, in either hemisphere the positive and negative values of v indicate poleward and equatorward motions, respectively). For spot groups of given life span (τ) in any given latitude interval, the values of $< v > (\tau)$ were computed by taking the data during the entire life span of spot groups, i.e.,

$$< v > (\tau) \; = 1/\tau \sum_{t=1}^{\tau} v(t).$$

In Figure 7.1 one can see that for spot groups of any specified life span and in all the three latitude intervals the magnitudes of $< v > (\tau)$ are only a few m s^{-1} and most of them are of the same order (or less than) their respective standard deviations. Thus, $< v > (\tau)$ is neither significant nor it exhibits particular trend with increasing τ.

7.3.2. VARIATIONS OF $v_{ini}(\tau)$ AND $v(t)$

In Figure 7.2(a) we show variation in the 'initial' meridional velocity ($v_{ini}(\tau)$) with life span τ of spot groups of life spans 2 to 12 days in different latitude intervals, obtained from data during 1874 -1981. The variations of $v_{ini}(\tau)$ derived separately from northern hemisphere data (solid curves) and southern hemisphere data (dotted curves) are shown in Figure 7.2(b). The error bars represent plus/minus one standard deviation.

In Figure 7.3(a) we show variation in the mean meridional motion $v(t)$ with age t of sunspot groups of life span 10–12 days in different latitude intervals, obtained from the data during 1874 -1981. In Figure 7.3(b) we show the variations in $v(t)$ derived

separately from northern hemisphere data (solid curves) and southern hemisphere data (dotted curves).

[Note: In view of the relations of the life spans (τ) and (t) of spot groups with the anchoring depths of sunspot magnetic structures derived earlier, (cf., Chapters V), we have chosen the scales of abscissa of Figure 7.2 in the reverse order. This helps to compare the variation of $v_{ini}(\tau)$ with τ and that of $v(t)$ with t.]

In Figures 7.2 and 7.3 one can see the following:

(i) In each latitude interval, the values of $v_{ini}(\tau)$ and $v(t)$ (10–20 m s^{-1}) often differ from zero significantly. (The values of $v_{ini}(\tau)$ of spot groups of life span $\tau \leq 5$ *day* do not differ from zero significantly.)

(ii) The variations of $v_{ini}(\tau)$ and $v(t)$ determined from the spot groups data in the entire sunspot latitude belt seem to be largely similar to the corresponding variations of $v_{ini}(\tau)$ and $v(t)$ in the latitude interval $20° - 30°$. This could be due to the fact that in the interval $20° - 30°$, the amplitudes of $v_{ini}(\tau)$ and $v(t)$ are 5–10 m s^{-1} larger than those in the intervals $0° - 10°$ and $10° - 20°$.

(iii) In the latitude interval $20° - 30°$, the variations of $v_{ini}(\tau)$ and $v(t)$ are systematic and mutually similar, and the north-south similarities of $v_{ini}(\tau)$ and $v(t)$ are more pronounced than in the other two intervals (Note: the first value of $v(t)$ is the average of first three values of $v_{ini}(\tau)$). The form of $v(t)$ suggests existence of periodic variation in the meridional motion of magnetic structures of spot groups with period 4-day and amplitude 10–20 m s^{-1}. The similarity in the forms of $v(t)$ and $v_{ini}(\tau)$ suggests presence of this periodicity in solar meridional flow.

7.3.3. SURFACE PLASMA MERIDIONAL FLOW

In Table 7.2, we give the values of meridional velocity, $v_e(t)$, determined from the last few days (t : 10–12 days) data of the spot groups which live 10–12 days. In latitude interval $20° - 30°$ the values of $v_e(t)$ differ from zero more than 2σ in the northern hemisphere, more than 1σ in the southern hemisphere and around 3σ in the average value of north and south hemispheres. In latitude intervals $0° - 10°$ and $10° - 20°$ the values are small and they are not significant. In order to have adequate data, we used $10°$ latitude intervals. We also confirmed the characteristic properties of the aforementioned results for the intervals $5° - 15°$, $15° - 25°$ and $25° - 35°$ and the values of $v_e(t)$ in these intervals are also given in Table 7.2. We obtained ~ 6 m s^{-1} higher velocity in the latitude interval $25° - 35°$ than that in $20° - 30°$ (however, in the former interval statistics is relatively poor). In Table 7.2, the general characteristics of $v_e(t)$ are similar to the characteristics of meridional flow determined from Doppler velocity measurements and small magnetic features (e.g., Komm et al. 1993c; Snodgrass & Dailey 1996; Hathaway

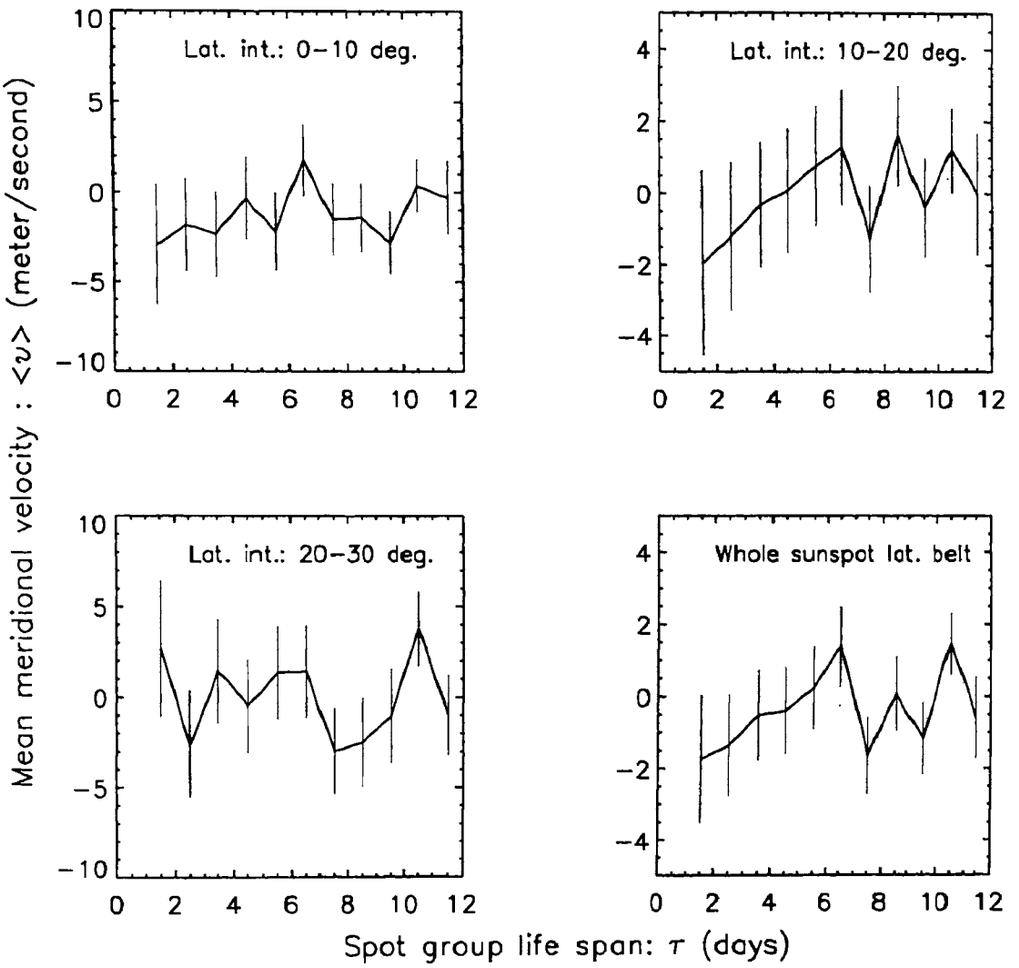

Figure 7.1. Variation in the mean meridional velocity, $< v > (\tau)$, with life span τ of spot groups of life spans 2 to 12 days in different latitude intervals , obtained from the data during 1874–1981. Northern and southern hemispheres' data were folded. (In either hemisphere, the positive values of the velocity indicate poleward motions and negative values indicate equatorward motions.)

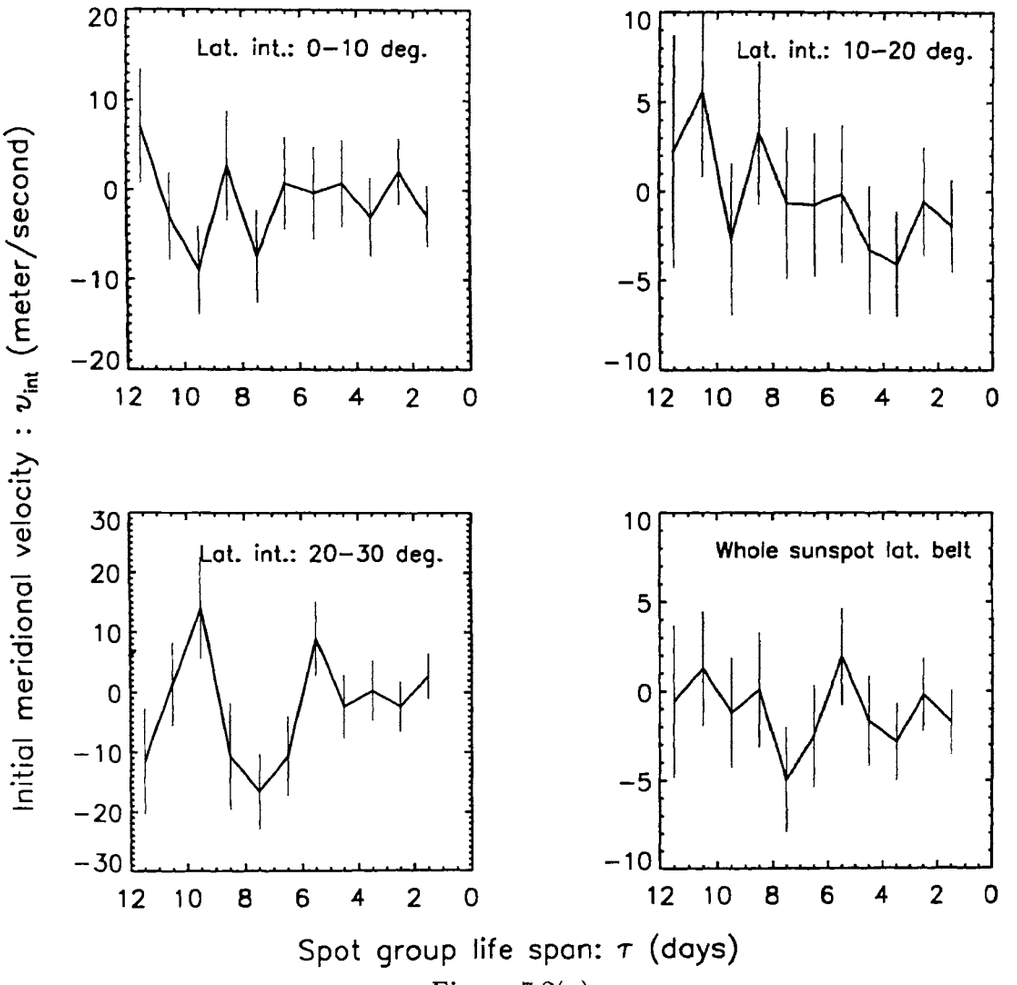

Figure 7.2(a).

Figure 7.2(a). Variation in the 'initial' meridional velocity, $v_{ini}(\tau)$), with life span τ of spot groups of life spans 2 to 12 days in different latitude intervals, obtained from the data during 1874–1981. Northern and southern hemispheres' data were folded. (The sign convention is same as mentioned in the caption of Figure 7.1.)

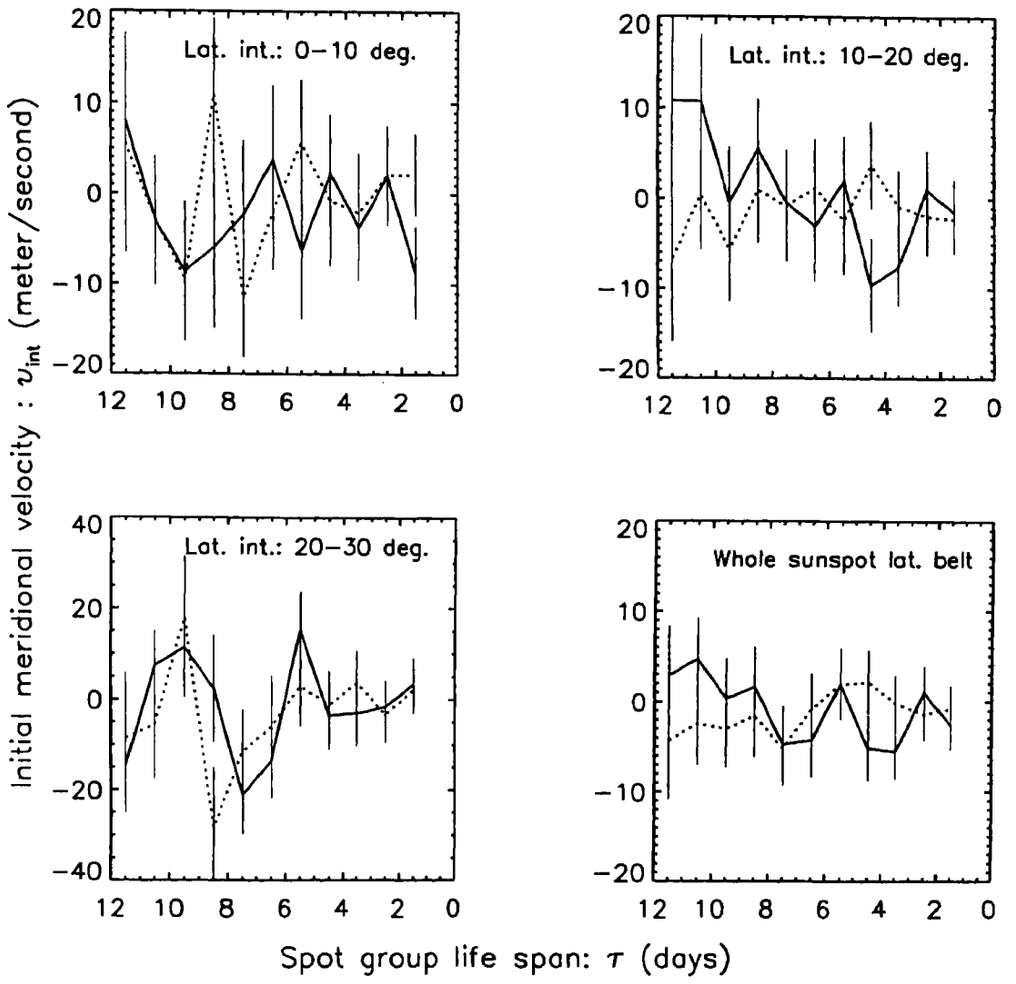

Figure 7.2(b). Same as Figure 7.2(a) except that the variations in $v_{ini}(\tau)$ derived separately from northern hemisphere data (solid curves) and southern hemisphere data (dotted curves).

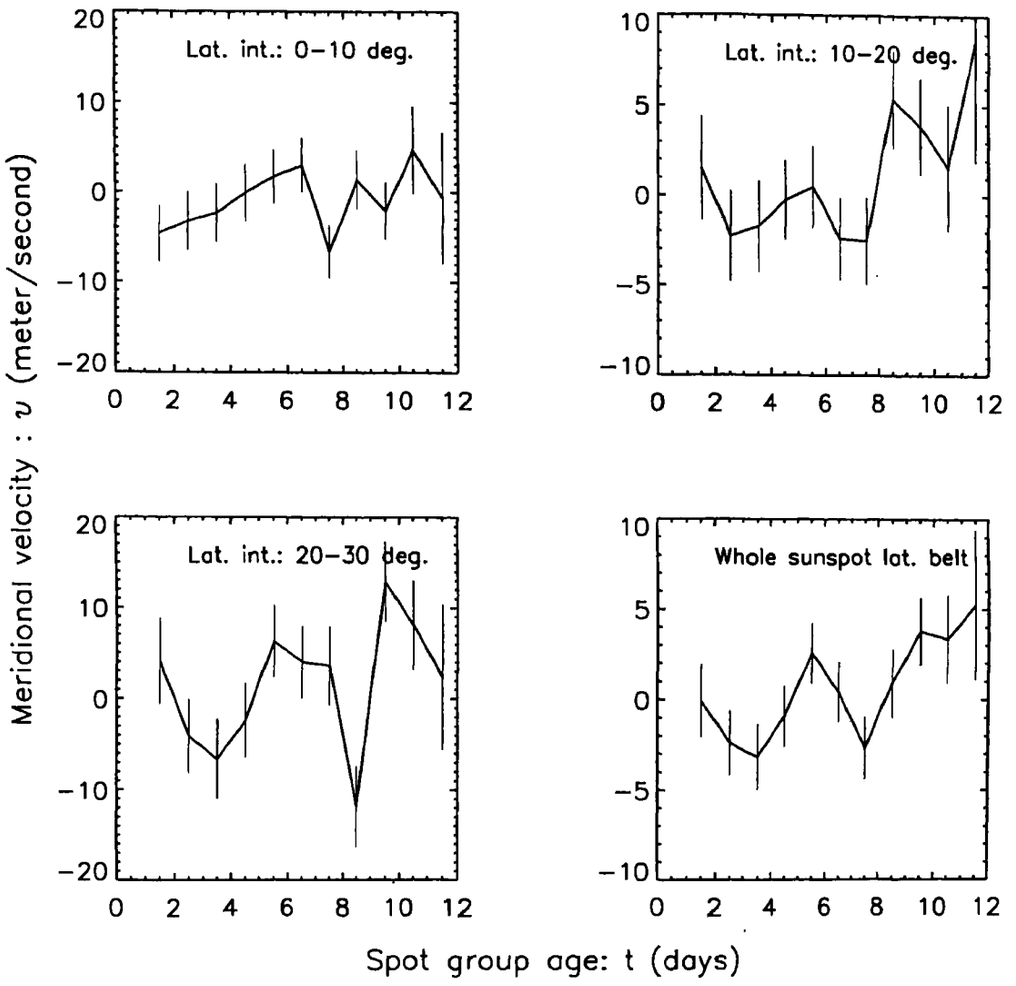

Figure 7.3(a). Variations in the mean meridional velocity, $v(t)$, with age t of sunspot groups of life span 10–12 days in different latitude intervals, obtained from data during 1874–1981. Northern and southern hemispheres' data were folded. (The sign convention is same as mentioned in the caption of Figure 7.1.)

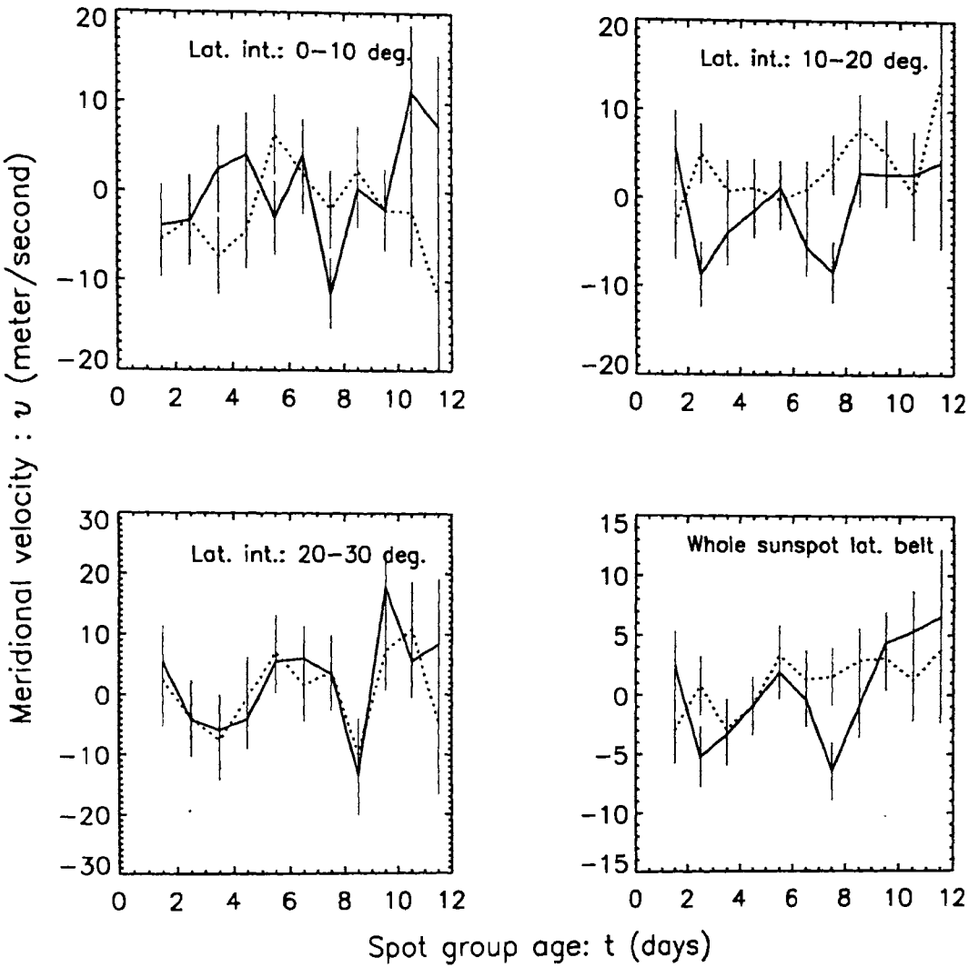

Figure 7.3(b). Same as Figure 7.3(a) except that the variations in $v(t)$ derived separately from northern hemisphere data (solid curves) and southern hemisphere data (dotted curves).

Table 7.2. The values of surface meridional velocity ($v_e(t)$, in m s^{-1}) with their uncertainties (σ) determined from the last few days (age t: 10–12 days) data of the spot groups of life span (τ) 10–12 days. The number of observations (N) gone in each determination is also given. In either hemisphere, the positive values of the velocity indicate poleward motions and negative values indicate equatorward motions.

Lat. interval	north			south			north+south		
	v_e	σ	N	v_e	σ	N	v_e	σ	N
$0° - 10°$	3.14	3.69	267	-2.72	3.4	256	0.272	2.53	523
$10° - 20°$	2.82	2.80	585	4.14	2.90	547	3.46	2.01	1132
$20° - 30°$	12.71	4.12	267	7.19	4.61	236	10.12	3.08	503
$5° - 15°$	5.00	4.28	217	0.11	3.75	204	2.63	2.86	421
$15° - 25°$	0.774	4.01	260	10.46	4.55	265	5.66	3.04	525
$25° - 35°$	18.75	7.47	85	13.61	9.11	85	16.17	5.88	170
Whole belt	4.84	1.93	1170	2.53	2.02	1071	3.74	1.40	2241

1996), i.e., the motions (in general) are poleward in each hemisphere with amplitude 10–20 m s^{-1} in middle latitudes. (Note: the average of all the 11 points of $v_{ini}(\tau)$ and that of $v(t)$ are found to be only a few m s^{-1}, cf. Sections 7.3.1. and 7.3.2.)

Doppler velocity measurements and small magnetic features suggest a weak (or non-existence) north-south asymmetry in the surface meridional flow (Komm et al. 1993c; Snodgrass & Dailey 1996). In $v_e(t)$ there is a suggestion of north-south asymmetry. In latitude interval $15° - 25°$, the asymmetry seems to be substantially large.

7.4. Variation in the Sunspot Meridional Motion During the Solar cycle

7.4.1. VARIATIONS OF THE MEAN MERIDIONAL MOTION OF SPOT GROUPS

In order to have better statistics here we have used the data during entire life spans of the spot groups with life spans 2–12 days. The calculations were repeated with and without inclusion of second and subsequent disk passages of the recurrent spot groups. Each disk passage of a recurrent group is treated as a separate group. Since the mean meridional velocities, $< v > (\tau)$, of spot groups seem to be almost independent of the life spans (τ) of spot groups (cf. Section 7.3.1, Figure 7.1), variations in the mean value

(say v'), i.e.,

$$v' = 1/11 \sum_{\tau=2}^{\tau=12} < v > (\tau) \quad ,$$

of $< v > (\tau)$ of spot groups represents the variations in the meridional velocity of the solar plasma averaged over thickness of the convection zone. The variations are determined by superposing the data during 1874–1981 according to the years relative to the nearest sunspot minimum (1867, 1879, 1890, 1902, 1913, 1923, 1934, 1944, 1954, 1965, 1976, 1986). Figure 7.4(a) shows the solar cycle variations of the mean meridional velocity v' of all recurrent and non-recurrent spot groups in different latitude intervals, during the solar cycle. Figure 7.4(b) shows the variations derived separately from the data in the northern hemisphere (solid curves) and southern hemisphere (dotted curves). Figure 7.4(c) shows the variations derived separately from the data in the odd numbered (Waldmeier cycle numbers 11, 13, 15, 17, 19, 21) cycles (solid curves) and even numbered (12, 14, 16, 18, 20) cycles (dotted curves).

In Figure 7.4(a) it can be seen that in all latitude intervals the velocity is not significantly different from zero during the rising phase of the solar cycle and there is suggestion of poleward motion only in the declining end. Especially in the ending years the velocity values (a few m s^{-1} at lower latitudes and $\sim$ 15 m s^{-1} at higher latitudes) differ from zero significantly. In latitude interval $20° - 30°$, the exclusion of the data on the second and subsequent disk passages of the recurrent spot groups yielded poleward motion of about 40 m s^{-1} around 9th–10th year of the cycle. (It is interesting to note here that there are rapid changes in the variation of the solar differential rotation coefficient around 1–2 year before the cycle minima (cf., Chapter III). In Figure 7.4(b) it can be seen that in all latitudes there is a suggestion on existence of north-south asymmetry, but the velocity values have large uncertainties. The strength of the asymmetry seems to be depending on phase of the solar cycle. On the average (during $\frac{3}{4}$ of the cycle) the velocity seems to be poleward in southern hemisphere and equatorward in the northern hemisphere (in the ending years the motion is poleward in both hemispheres).

In Figure 7.4(c), there is a suggestion that in the beginning of the cycles, the velocity is equatorward in the odd numbered cycles and it is poleward in the even numbered cycles, mainly in latitude interval $0° - 10°$. Around 9th–10th year the velocity seems to be larger in the even numbered cycle than that in the odd numbered cycle, but the velocity values have large uncertainties. The aforementioned differences of the meridional motions of spot groups in the odd and even numbered cycles may suggest existence of 22-yr modulation in the solar meridional flow (Tuominen 1952; Richardson & Schwarzschild 1953).

[In Chapter III (Section 3.4.2) and Chapter VI (Section 6.2.4) we have observed the abnormal behaviour in the data during 1962. Exclusion of this data increased the value of v' (to $\sim$ 20.72 m s^{-1}) at 9.5 year in latitude interval 20°–30° shown in Figure 7.4(a).

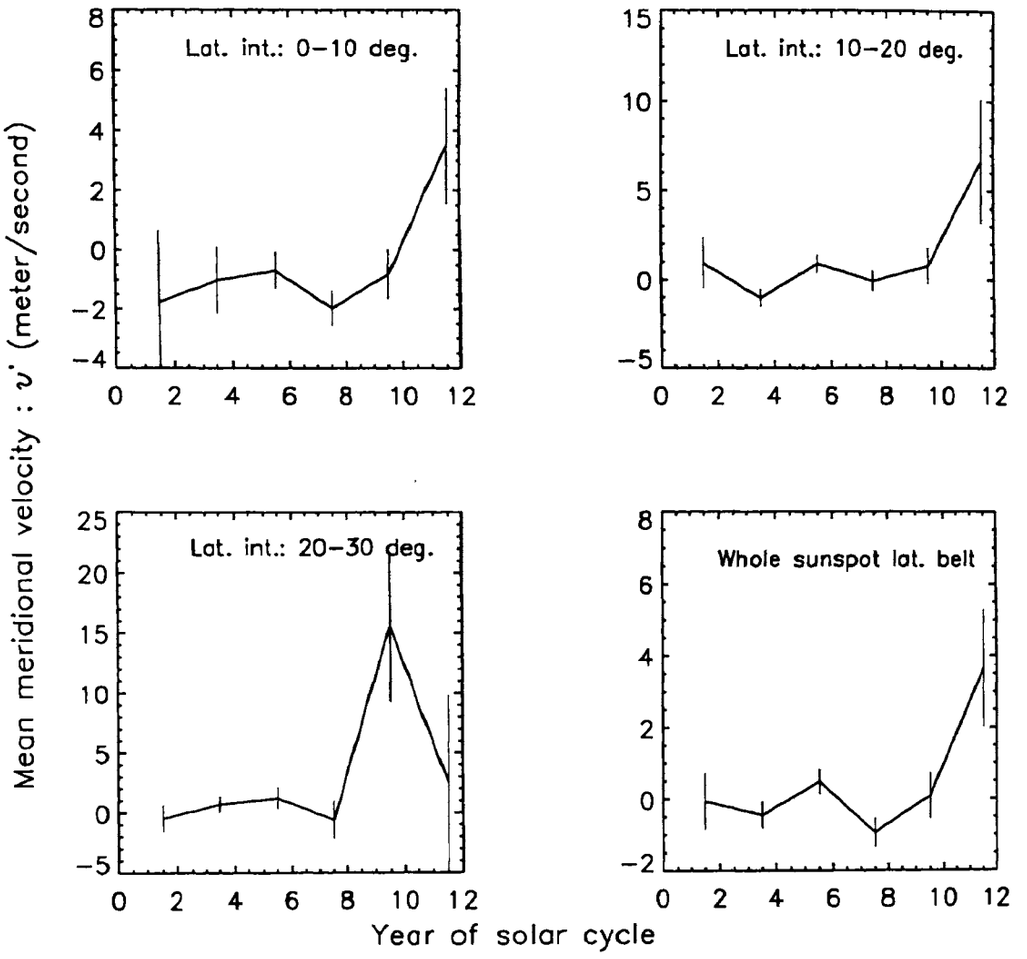

Figure 7.4(a). Variations of the mean meridional velocity, v', of 2–12 days living sunspot groups during the solar cycle. (Note: each disk passage of the recurrent spot group is treated as a separate group and its data are also used here.) Averages taken over 2-yr intervals. Activity maximum is around 4–5 years. Northern and southern hemispheres' data were folded. (The sign convention is same as mentioned in the caption of Figure 7.1.)

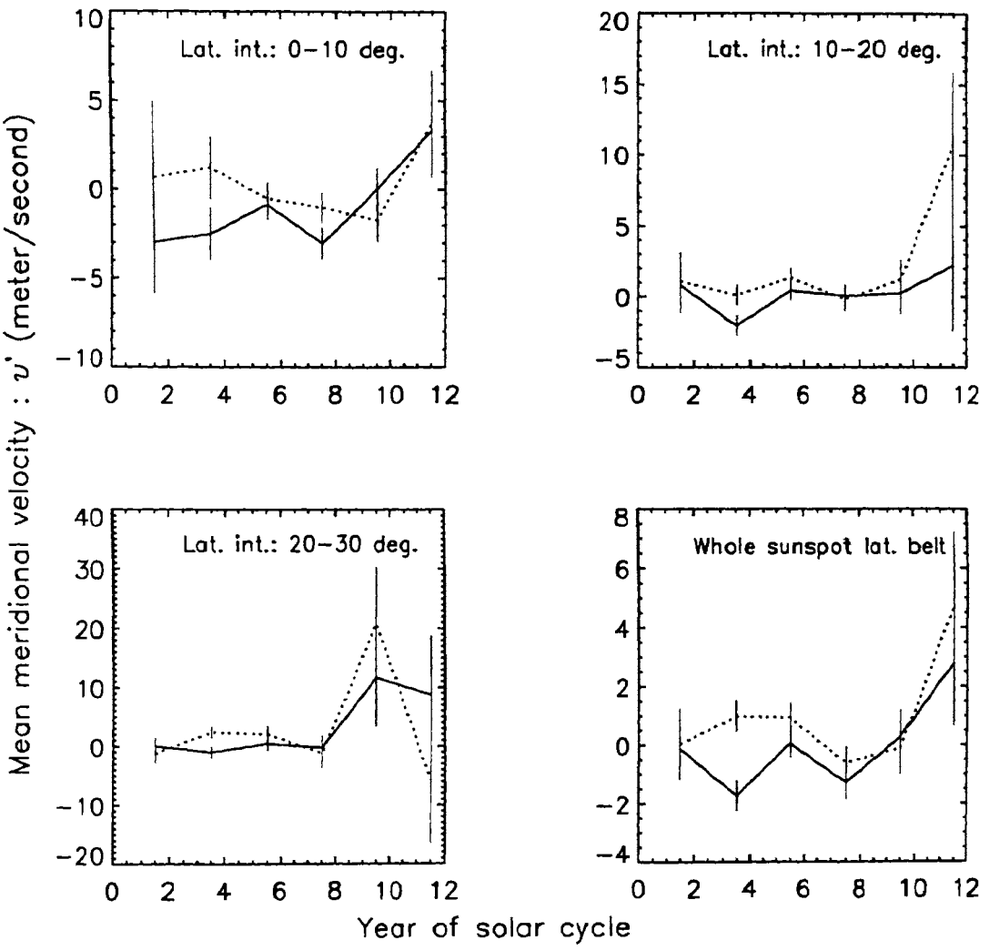

Figure 7.4(b). Same as Figure 7.4(a) except that the variations determined separately from the northern hemisphere data (solid curve) and southern hemisphere data (dotted curve).

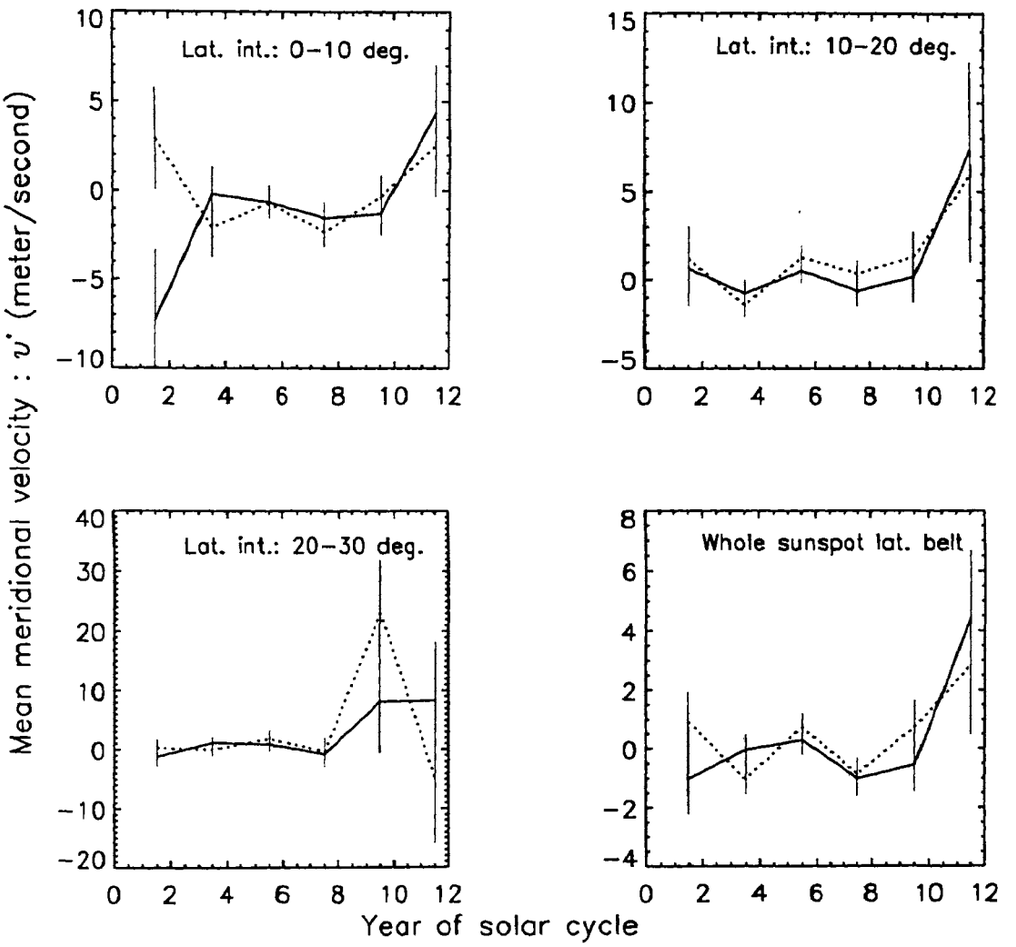

Figure 7.4(c). Same as Figure 7.4(a) except that the variations determined separately from the odd numbered cycles data (solid curves) and even numbered cycles data (dotted curves).

The gap between the values of odd-even cycles at the same position in Figure 7.4(b) is found to be reduced. This does not affect on the aforementioned conclusions.]

7.4.2. VARIATIONS OF THE SURFACE PLASMA MERIDIONAL FLOW

In latitude interval $20° - 30°$, the 'surface' meridional velocity, $v_e(t)$ (defined in Section 7.3.3), is found to be $\sim$ 20 m s^{-1} poleward during the maximum years (around 5th year) and it is equatorward at declining end of the cycle by about the same magnitude. In latitude intervals $0° - 10°$ and $10° - 20°$, the values of $v_e(t)$ are found to be not significantly different from zero throughout the cycle, i.e., the variation can not be recognized because of the large uncertainties.

[In Figure 7.4(a), even in the latitude interval $20° - 30°$, the average velocity determined from all spot groups is not significantly different from zero during the maximum years. This could be due to the dependence of meridional motions of long living spot groups with their age. The mean velocity of a spot group of given life span is only a few m s^{-1}.]

7.5. Correlation Between the Solar Cycle Variation of the Average Meridional Velocity and the Differential Rotation

Theoretical models which attempt to explain observed torsional pattern argue that the meridional flows have an important role in generation of torsional oscillations (e.g., see Snodgrass 1992 and references therein). We determined correlations of the solar cycle variation of meridional motion v' averaged over the entire sunspot belt with those of the equatorial rotation rate A, the latitude gradient of the rotation B and the 'mean' rotation rate $\bar{A}$ (cf., Chapter III). The v', A, B and $\bar{A}$ were determined from data of all recurrent and non-recurrent spot groups. We find 68% correlation between v' and A, 52% correlation between v' and B, and 74% correlation between v' and $\bar{A}$. These correlations suggest existence of coupling in the latitudinal and longitudinal motions (in the Suns convection zone over the depths to which the sunspot magnetic structures were extended).

7.6. Summary and Discussion

Conclusions:

From the analysis of a large set of sunspot group data we have drawn the following conclusions:

1. The mean meridional velocities, $< v > (\tau)$, of sunspot groups with life spans 2-12 days (over entire life span) are only a few m s^{-1} and independent of the life spans of spot groups. However, the initial meridional velocities, $v_{ini}(\tau)$, of spot groups depend

on their life spans (τ) and the velocities of long lived spot groups depend on their age (t).

2. In latitude interval $20° - 30°$, the variations of $v_{ini}(\tau)$ and $v(t)$ are similar and the form of $v(t)$ suggests existence of periodic variation in the meridional motion of magnetic structures with period 4-day and amplitude 10–20 m s^{-1}.

3. Meridional flows ($v_e(t)$) determined from the data during the last few days (age t: 10–12 days) of spot groups of life spans 10–12 days are found to have magnitudes (10–20 m s^{-1}) and directions (poleward) similar to those of the surface (and near to the surface) plasma meridional flows determined earlier from the Dopplergrams and magnetograms.

4. Existence of north-south asymmetry in the 'surface meridional plasma flow' is suggested. In the latitude interval $15° - 25°$, the asymmetry seems to be substantially large.

5. The mean meridional motion (v') of sunspot groups seems to vary with the phase of the solar cycle. The velocity is not significantly different from zero during the rising phase of the cycle and there is a suggestion of poleward motion (a few m s^{-1} at lower latitude and $\sim$ 15 m s^{-1} at higher latitudes) during the declining end of the cycle.

6. Existence of north-south asymmetry in the solar cycle dependence of the mean meridional motion of sunspot groups is suggested. The strength of the asymmetry depends on the phase of the cycle. On the average, during $\frac{3}{4}$ of the cycle, the velocity seems to be poleward in the southern hemisphere and equatorward in the northern hemisphere.

7. In latitude interval $20° - 30°$ the 'surface plasma meridional motion', $v_e(t)$, is found to be poleward around maximum years ($v_e(t) \sim 20$ m s^{-1} at 4th–5th year) and equatorward around the declining end of the cycle (about the same magnitude).

8. There exists a reasonable correlation between the solar cycle variation of the average meridional motion v' and coefficients of the differential rotation A, B and $\bar{A}$, suggesting existence of coupling in the latitudinal and longitudinal motions, some where in the convection zone.

Discussion:

In latitude interval $20° - 30°$, the magnitudes of $v_e(t)$ obtained from the northern hemisphere data and also those obtained from combined data set of northern and southern hemispheres, are $\sim$ 1.5–2 times larger than the estimated relative error in the measurements of heliographic coordinates of mass centers of spot groups (see Section 1.2.3 of Chapter I). In the southern hemisphere, the values of $v_e(t)$ are of the same

order or slightly grater than the estimated error. This is because in this hemisphere N is relatively less. In the intervals $0^\circ - 10^\circ$ and $10^\circ - 20^\circ$ the meridional speed itself is low and hence it is not possible to arrive at any conclusion on the significance of the velocity values in these intervals.

In latitude interval $20^\circ - 30^\circ$, the relative variations in $v_{ini}(\tau)$ and $v(t)$ (Figures 7.2 and 7.3) are slightly greater than the estimated relative errors of heliographic positions. In this interval, the variations of $v_{ini}(\tau)$ and $v(t)$ obtained from the combined data set of the northern and southern hemispheres as well as from the separate data sets are mutually similar. This suggests that the variation in $v(t)$ is not an artifact of the evolution of the spot groups producing a shifts of the spot groups centers in latitude. Existence of a 4-day periodicity in the total solar irradiance is reported by some authors (Froelich & Pap 1989, Nikonova et al. 1998). In view of all these factors and conclusion 3 above, the 4-day periodic variation seen in $v(t)$ seems to be of solar origin. Using the anchoring depths of magnetic structures for spot groups of different τ and t, estimated earlier (cf. Chapters V), we suggest that the patterns of $v_{ini}(\tau)$ and $v(t)$ may represent radial variation of meridional flow in the Sun's convection zone, rather than temporal variation of the flow. So, the discrepancy in the magnitudes and directions of the solar meridional flow determined from sunspot data and direct Doppler velocity measurements might be due to the dependence of meridional motions of sunspots or sunspot groups on their life spans and age, i.e., due to depth dependence of the meridional flow.

It must be noted that the results obtained here may represent only the average behavior of many spot groups. The meridional velocity of any single spot group might be affected by several factors such as splittings, expansions, etc. The data used in the determination of $v_{ini}(\tau)$ and $v(t)$ extends over 10 decades and we have used superposition of 5 or 10 cycles data in the determination of the solar cycle dependence of meridional velocity. So, the magnitude of variation of the meridional velocity during some single solar cycles may be larger than that is found here.

Ward (1965a) analyzed Greenwich data (1935–1944) and showed for the first time the existence of a positive correlation between latitudinal and longitudinal motions of sunspot groups. Coffey & Gilman (1969) and Paternó et al. (1991) found a similar correlation. Belvedere et al. (1976) were also found similar correlation using facular data covering a four-year interval. Howard (1991, 1996a) using Mt. Wilson measurements found a strong correlation between meridional drift and residual rotation velocity of sunspot groups (from 1917–1985) and of plages (from 1967–1985). Nesme-Ribes et al. (1993) using Meudon observations covering the cycle 21, found no significant covariance from sunspot data. Recently, Komm et al. (1994) using the small-scale magnetic field data deduced from Kitt Peak magnetograms covering the years 1987–1990, and Meunier et al. (1997) using the photospheric facular data during cycle 19 (1957–1962), found a very small covariance.

Theoretical models (e.g., Gilman 1986) predict the observed correlation between the surface latitudinal and longitudinal motions as reflection of equatorial angular momentum transport from Reynolds stresses and argued that the Sun's differential rotation could be maintained using Reynolds stresses near the surface. Reynolds stress is produced by interaction of convective elements and the Coriolis force, which causes a correlation between longitudinal and latitudinal velocity components of the convective elements. The smaller the Rossby number $Ro = u/(2\Omega l)$ (where u is a typical velocity in the non-axisymmetric eddies, l a typical cell size, and Ω the angular velocity), the more efficient this interaction, i.e, the correlation (Reynolds stress) depends on the size l and the velocity u of the convective elements present in the convection zone. Hence, the angular momentum transport by Reynolds stresses is more efficient with supergranulation than with granulation. The giant meridional cells (if exist) should also be more efficient than supergranulation. So, if the convective elements are large and have small velocities, the Reynolds stress produced can be large enough to maintain the equatorial angular momentum transport and thus the differential rotation against viscosity. The sizes of the granular and super granular cells seem to be smaller at solar maximum than at solar minimum (Muller 1985; Singh & Bappu 1981). So, the increase in the equatorial rotation rate (cf., Section 6.2.4 of Chapter VI) and the magnitude of the meridional motion (Conclusion (1), above) during the solar minimum phase may relate to the enhancement of the Coriolis force and in turn efficiency of the Reynolds stress during the cycle minimum phase.

There have been criticisms of the theoretical explanations of the equatorial acceleration of the Sun as being due to equatorial angular momentum transport from Reynolds stresses which are reflected in the correlations of latitudinal and longitudinal motions shown in the surface motion data. These criticisms are on the basis that the observed motions may result from the well-known expansion and contraction of sunspots along the tilted magnetic axes of the sunspot groups. These axes are inclined in such a way (leading spots equatorward of following spots) as to lead to the correlation that is seen (RB Leighton 1965, unpublished manuscript). Gilman & Howard (1984), argued that because the effect could be observed for whole sunspot groups, at least some fraction of the observed correlation must be due to Reynolds stresses near the solar surface and that this amount was sufficient to account for the angular momentum transport required to maintain the solar differential rotation.

Chapter VIII

CONCLUSIONS AND FUTURE PROSPECTS

In this chapter first I summarize the conclusions from Chapters II to VII and then provide some overall interpretations of the results in Chapters II–VII. I also list in the end some important investigations to be undertaken.

8.1. Summary of the Conclusions in Chapters II–VII

We inferred the rate of emergence of toroidal magnetic flux above the Sun's surface, per unit latitude interval and per unit time during 1874–1976, using sunspot group data and Hale's Law of magnetic polarities. Though the sunspot data comes only from latitudes $< 35^{o}$, the superposition of the main LF terms in the estimated rate of emergence of toroidal magnetic flux not only *reproduces* the butterfly diagrams, but also *predicts* the following large scale characteristics of the weak fields in latitudes $> 35^{o}$: (i) the migrations of neutral lines from latitudes $\sim 35^{o}$ *upto* $\sim 90^{o}$, and (ii) polar field reversals at the correct phase of the cycle. This suggests that the buoyant toroidal magnetic flux tubes, whose emergence above the Sun's surface produces 'sunspot' activity as well as the 'quiet sun' activity, may be created in the Sun by interference of 'global' MHD oscillations /waves represented by the dominant LF terms. The structure of the LF spectrum of these oscillations/waves and its approximate 'steadiness' suggest that these oscillations are resonating with frequencies forced by some permanent sources of excitation.

In the photospheric 'mean rotation' $\bar{A}$, determined from the Mt. Wilson velocity data during 1982–1994, we found periods: 6.7–4.4 yr, 2.2 ± 0.4 yr, 1.2 ± 0.2 yr, and 243 ± 10 day (with a $\geq 99.9\%$ confidence level), which are similar to the periods found in other indicators of solar activity suggesting that they are of solar origin. The 11-yr periodicity is found to be insignificant or absent in $\bar{A}$. In the differential rotation parameters $\bar{B}$ and $\bar{C}$, determined from the same data set, we found only the ~ 11 yr period with a $\geq 99.9\%$ confidence level.

The time series of $\bar{A}$ determined from the yearly sunspot group data obtained during 1879–1976 is found to be similar to the corresponding time series of $\bar{B}$. After correcting for data with large error bars (occuring during cycle minima), we have found periods of 18.3 ± 3.0 yr and 7.5 ± 0.5 yr in $\bar{A}$ and these and a few other short periods (e.g., 3.0 ± 0.1 yr, etc.) in $\bar{B}$. We found considerable differences in the periodicities of

$\bar{A}$ and $\bar{B}$ determined from the velocity data and those determined from the spot group data. Presence of these differences may be understood if the rotation rates determined from sunspot data represent the rotation rates of the Sun's deeper layers.

Recently a number of authors reported existence of $\sim$ 160 day periodicity in several solar activity indices. We have also found a $\sim$ 163 day periodicity in the ratio B/A determined from Mt. Wilson velocity data during 1969–1982. However, it is not found in the data during 1983–1994. Hence, whether this periodicity comes from the errors in the velocity data before 1982 or due to some other reason is yet be confirmed.

In the North–south (N–S) asymmetry of $\bar{A}$ and also that of $\bar{B}$ determined from the spot group data we have detected the periodicities : 45 $\pm$11.5 yr, 21.3 $\pm$ 4.5 yr, 13.3 $\pm$ 1.5 yr and 10.5 $\pm$ 0.5 yr. We have also found similar periodicities in the N–S asymmetry of sunspot activity. For the velocity data we focused on observations obtained after 1981 with the reduced instrumental noise. Power spectra of N–S asymmetries of $\bar{A}$ and $\bar{C}$ determined from the velocity data during 1982–1994, show peaks at the period 374 $\pm$ 30 day with $>$ 99.9 % confidence level. The spectrum of the N–S asymmetry of $\bar{B}$ shows peaks at the periods 374 $\pm$ 30 day, 78 $\pm$ 2 day and 49 $\pm$ 1 day with $\geq$ 99 % confidence level. The 7°.17 inclination of the Sun's equator to the ecliptic may be responsible for the 374 day periodicity in the N–S asymmetries of the solar rotation and the differential rotation.

Some of the dominant periodicities of the solar differential rotation and its N-S asymmetry happen to match with periods of configurations of dominant planets. Hence, I present some speculations on possibility of planetary configurations providing perturbations needed for 'torsional MHD oscillations'.

Assuming that during the initial phases of the active regions magnetic structures are anchored at deeper layers (e.g, Foukal 1972; Schüssler 1987), we compared the dependence of the mean rotation frequency of a spot group on its age (t), and the dependence of the 'initial rotation' of a spot group on its life span (τ), with the dependence of plasma rotation frequency ($\Omega(r)$) on the radial distance (r) at different latitudes (λ) as determined from helioseismology. This comparison brings out the following important possibility : (i) The magnetic structures of spot groups which live successively longer by 1 day are initially anchored in layers successively deeper by $\sim$ 21 Mm. (ii) Structures which yield spot groups with life spans 10–12 days are initially anchored near the base of the convective envelope. (iii) For a spot group which lives 10–12 days in latitudes $10° - 20°$ the 'anchoring layer' of its magnetic structure also rises at a rate approximately 21 Mm per day, as the spot group ages.

The result (iii) above, is found to be more realistic for spot groups with life spans 10–12 days and average area $A \geq 130$ millionth of the solar hemisphere. For spot groups living 2–12 days, we find a well defined exponential dependence of the average

area (A) on the life span (τ). We also find that the distribution of the number of spot groups (N) with respect to τ is nearly exponential, in the range 2-9 days. From these relations and the equality of the slopes of $r-\tau$ and $r-t$ relations we have drawn (in Chapter V) the following tentative inferences : (i) magnetic structures (flux tubes) of spot groups with $A \geq 130$ mh might be generated around base of the convection zone, (ii) many of the magnetic structures may be fragmenting (branching) into smaller structures while rising through the solar convection zone, and (iii) magnetic structures of spot groups (at least groups with $A < 130$ mh) might be the fragmented (branched) parts of the magnetic structures of larger spot groups. These inferences are consistent with the proposals of some theoretical models (e.g., Parker 1979b).

Using the spot group data during the whole period 1879–1975 we find the equatorial rotation rate A is significantly larger in the odd numbered solar cycles (ONSCs) than in the even numbered solar cycles (ENSCs). The N–S asymmetry in the A seems to be large in the ONSCs and less in the ENSCs. The rotation is significantly more differential in the ONSCs than in the ENSCs and the difference is mainly contributed from the southern hemisphere. In the northern hemisphere the difference is marginal. N–S asymmetry in B is significant in the ENSCs and it is not significant in ONSCs. In ONSCs the rotation is more differential in the northern hemisphere than in the southern hemisphere and it is in opposite sense in the ENSCs.

There exists a systematic cycle–to–cycle variation in B, i.e., the magnitude of B in each of the ONSCs is larger than that in its neighboring ENSCs, suggesting existence of 22-yr modulation in B. Such a systematic behaviour can also be seen in the cycle–to–cycle variation of A but it is not as well defined as that of B. The trend of variation of A suggests existence of a long periodicity of the order of 100-yr in A. Existence of $\sim$ 80-yr cycle (Gleissberg cycle) in B is seen in the cycle–to–cycle variation of B. The weak 22-yr modulation in B seems to be superposed on the relatively strong 80-yr modulation.

The coefficient A varies significantly only during ONSCs with amplitude ~ 0.01 $\mu\ rad\ s^{-1}$, at minimum years. There exists a good anticorrelation between the variations of B derived from the ONSCs and ENSCs, suggesting existence of a '22-yr' periodicity in B. The amplitude of variation of B is ~ 0.05 $\mu\ rad\ s^{-1}$. It seems the known Gnevyshev & Ohl rule (Gnevyshev & Ohl 1948) of solar activity is applicable also to B. The pattern of correlations of A and B with activity also suggests that the each 22-yr "episode" begin with the beginning of an even cycle and ends with the end of the following odd one, as suggested by Gnevyshev & Ohl (1948) from the analysis of sunspot numbers.

In the differential rotation coefficient B determined from the long–lived young groups '22-yr' periodicity is dominant whereas that determined from the long–lived old

groups and the short lived groups, the dominant periodicity is '11-yr'. From comparing the mean rotation frequencies of the young, the old and the short lived spot groups with the $\Omega(r)$ determined from helioseismology, it is suggested that the periodicities $\sim$ 21 yr and $\sim$ 11 yr in B are dominant in the rotational perturbations in Sun's deeper layers ($r \sim 0.73 R_\odot$) and shallower layers ($\sim\ r > 0.95 R_\odot$), respectively.

In the latitude interval $20^o - 30^o$, the forms of 'initial' meridional motion, $v_{ini}(\tau)$, of sunspot groups and mean meridional motion, $v(t)$, are largely systematic and mutually similar in both north and south hemispheres. In $v(t)$ there is a suggestion of existence of periodic variation in the meridional motion with period 4-day and amplitude 10–20 m s^{-1}. The meridional flows ($v_e(t)$) determined from the data during the last few days of spot groups of life spans 10–12 days are found to have magnitudes and directions similar to those of the surface meridional plasma flows determined from Dopplergrams and magnetograms. Existence of N–S asymmetry in $v_e(t)$ is suggested. Using the anchoring depths of magnetic structures for spot groups of different τ and t estimated in Chapter V, I suggest that the patterns of $v_{ini}(\tau)$ and $v(t)$ may represent the spatial structure of the meridional flow in the Sun's convection zone, rather than its temporal variation.

The mean meridional motion (v') of sunspot groups seems to vary with the phase of the solar cycle. The velocity is not significantly different from zero during the rising phase of the cycle and there is a suggestion of poleward motion (a few m s^{-1} at lower latitude and $\sim$ 15 m s^{-1} at higher latitudes) during the declining end of the cycle. Existence of N–S asymmetry in the solar cycle dependence of the mean meridional motion of sunspot groups is suggested. The strength of the asymmetry depends on the phase of the cycle. On the average, during $\frac{3}{4}$ of the cycle, the velocity seems to be poleward in the southern hemisphere and equatorward in the northern hemisphere. In latitude interval $20^\circ - 30^\circ$ the 'surface plasma meridional motion', $v_e(t)$, is found to be poleward around maximum years ($v_e(t) \sim 20$ m s^{-1} at 4th–5th year) and equatorward around the declining end of the cycle (about the same magnitude). There exists a reasonable correlation between the solar cycle variation of the average meridional motion v' and that of A, between v' and B, and between v' and $\bar{A}$, suggesting existence of coupling in the latitudinal and longitudinal motions, somewhere in the convection zone.

8.2. Overall Summary of the Thesis

To conclude, the summary of this thesis is as follows:

The LF analysis of sunspot group data suggests that the solar activity may be created in the Sun by some kind of 'slow' MHD waves constituting 'global MHD oscillations' (Chapter II). The periodicities in the rotation parameters, the depth dependence of the rotation of sunspot groups (and its temporal variations), and the temporal variations in the meridional motions of sunspot groups (Chapters III–VII) suggest existence of couplings between the spatial (radial, latitudinal and longitudinal) and temporal (few days to few decades) variations of Sun's magnetic field, rotation, and meridional flow. This supports the suggestion that the oscillations found in Chapter II are 'global MHD oscillations'. The substantial variations in the differential rotation, whose periodicities and parity suggest that these oscillations are torsional in nature.

8.3 Future Work

More work will be necessary to acquire further insight into the real mechanism of solar cycle. For this purpose we list the following important investigations to be undertaken in the near future:

1. Physical explanation for the observed amplitude spectrum of the odd degree axisymmetric modes determined from the magnetic field inferred from sunspot data.

2. Estimation of the depths of initial anchoring and rising rates of sunspot magnetic structures during different phases of the solar cycle using the more accurate data set of measurements of individual sunspots from Kodaikanal and Mt. Wilson observatories (Sivaraman et al. 1993).

3. Finding relationship between the meridional and rotational flows.

4. Spherical-Harmonic-Fourier analysis of the magnetic field from high resolution GONG and SOHO magnetograms for detecting high frequency 'global MHD oscillations' if any.

5. Identification of physical relations (if any) between the solar system dynamics and the torsional MHD oscillations.

REFERENCES

Abarbanell C., Wöhl H., 1981, Solar Phys. **70**, 197
Alfvén, H.:1943, *Arkiv. Math. Astr. Fys.* **29A**, No. 12
Altrock R.C., 1997, Solar Phys. **170**, 411
Antia H.M., Chitre S.M., 1996, BASI **24**, 321
Antia H.M., Chitre S.M., Thompson M.J., 1996, A&A **308**, 656
Antia H.M., Basu S., Chitre S.M., 1998, MNRAS **298**, 543
Antonucci E., Hoeksema J.T., Scherrer P.H., 1990, ApJ **360**, 296
Arévalo M.J., Gomez R., Vázquez M., Balthasar H., Wöhl H., 1982, A&A **111**, 266
Attolini M.R., Cecchini S., Galli M., Nanni T., 1990, Il Nuovo Cimento **13C**, 131
Babcock H.D., 1959, ApJ **130**, 364
Babcock H.W., 1961, ApJ **133**, 572
Babcock H.W., Babcock H.D., 1955, ApJ **121**, 349
Becker U., 1955, Z. Astrophys. **37**, 47
Bai T., 1994, Solar Phys. **150**, 385
Bai T., Sturrock P.A., 1991, Nature **350**, 141
Balthasar H., Wöhl H., 1980, A&A **92**, 111
Balthasar H., Vázquez M., Wöhl H., 1986, A&A **155**, 87
Basu S., Antia H.M., 2000, in Proc. IAU Colloquium 179, J. Astron. Astrophys. (submitted).
Becker U., 1955, Z. Astrophys. **37**, 47
Belvedere G., Lanzafame G., 1997, Mem. S.A.It. **68–2**, 415
Belvedere G., Godoli G., Motta S., Paternò L., Zappalà R.A., 1976, Solar Phys. **46**, 23
Bigg, E.K., 1976, Astron. J. **72**, 463
Birch A.C., Kosovichev A.G., 1998, ApJ **503**, L187
Bracewell R.N., 1988, MNRAS **230**, 535
Bogart R.S., 1987, Solar Phys. **110**, 23
Bogdan T.J., Gilman P.A., Lerche I., Howard R., 1988, ApJ **327**, 451
Bray R.J., Loughhead R.E., 1964, Sunspots, Chapman and Hall, London
Braun D.C., Fan Y., 1988, ApJ **508**, L105
Brault J.W., White O.R., 1971, A&A **13**, 169
Brown T.M., Christensen-Dalsgaard J., Dziembowski W., Goode P.R., Gough D.O., Morrow C.A., 1989, ApJ **343**, 526
Caligari P., Moreno-Insertis F., Schüssler M., 1995, ApJ **441**, 886
Carbonell M., Ballester J. L., 1992, A&A **255**, 350.
Carbonell M., Oliver R., Ballester J.L., 1993, A&A **274**, 497
Carrington R.C., 1863, Observations of the Spots on the Sun, Williams and Norgate, London
Cavallini F., Ceppatelli G., Righini A., 1992, A&A **254**, 381
Choudhuri A.R., D'Silva S., 1990, A&A **239**, 326
Christensen-Dalsgaard J., Thompson M.J., 1999, Current Science **77**, 1460
Clark D.H., Yallop B.D., Richard S., Emerson B., Rudd P.J., 1979, Nature **280**, 299
Coffey H.E., Gilman P.A., 1969, Solar Phys. **9**, 423
Cohen T.J., Lintz P. R., 1974, Nature **250**, 398
Cowling T.G., 1981, ARA&A **19**, 115
Csada I.K., 1974, Solar Phys. **35**, 325
Delache P., Laclare F., Sadsaoud H., 1985, Nature **317**, 416
DeLuca E.E., Gilman P.A., 1991, in Cox A.N., Livingston W.C., Matthews (eds.), Solar Interior and Atmosphere, The University of Arizona Press, Tucson, P.275

Di Mauro M.P., Dziembowski W.A., Paternó L., 1998, in: Korzennik S.G., Wilson A. (eds.) Structure and Dynamics of the Interior of the Sun and Sun-Like Stars, ESA SP-418, P.759
Deubner F. L., Gough D. O.,1984, ARAA **44**, 371
Dicke R.H., 1970, ARAA **8**, 297
Dicke R.H., 1979, Nature **276**, 676
Dikpati M., Charbonneau P., 1999, ApJ **518**, 508
Ding Youji, 1978, Bulletin of Chinese Sciences **2**, 35
D'Silva S., Howard R., 1994, Solar Phys. **151**, 213
Duchlev P.I., Dermendjiev V.N., 1996, Solar Phys. **168**, 205
Duvall T.L., Jr., 1979, Solar Phys. **63**, 3
Duvall T.L., Jr., Kosovichev A.G., Scherrer P.H., 1998, in Provost J., Schimider F-X. (eds.), Sounding Solar and Stellar Interiors, IAU Symp. **181** (Poster Volume), P. 169
Duvall T.L., Jr., Jefferies S.M., Harvey J.W., Pomerantz M. A., 1988, Nature **362**, 430
Duvall T.L., Jr. et.al., 1997, Solar Phys. **170**, 63
Dziembowski W.A., Goode, P.R., 1989, ApJ **376**, 547
Dziembowski W.A., Goode, P.R., Libbrecht K.G., 1989, ApJ **337**, L53
Eddy J.A., 1976, Science **192**, 1189
Eddy J.A., Gilman P.A., Tortter D.E., 1976, Solar Phys. **46**, 3
Eddy J.A., 1978, The New Solar Physics, AAAS Selected Symposium 17, Westview Press, Colorado, P. 11
Fairbridge R.W., Marcel C.H., 1977, Nature **268**, 413
Fairbridge R.W., Shirley J.H., 1987, Solar Phys. **110**, 191
Fan Y., Fisher G.H. and DeLuca E.E., 1993, ApJ **405**, 390
Ferraro V. C. A., Memory D. J., 1952, MNRAS **199**, 53
Ferris G.A.J., 1969, J. Brit. Astron. Assoc. **79**, 385
Froelich C., Pap J., 1989, A&A **220**, 272
Foukal P., 1972, ApJ **173**, 439
Gibson E.G., 1973, The Quiet Sun, NASA SP-303, U.S. Government Printing Offic, Washington, D.C.
Giles P. M., Duvall T.L., Jr., 1998, Deubner F.L. et al (eds.) New Eyes to See Inside the Sun and Stars, IAU Symp. **185**, P. 149
Giles P.M., Duvall T.L., Jr., Scherrer P.H., Bogart R.S., 1997, Nature **390**, 52
Gilman P.A., 1974, ARAA **12**, 70
Gilman P.A., 1976, in Bumba V., Kleczek J. (eds.) Basic Mechanisms of Solar Activity, IAU Symp. **71**, Reidel, Hingham, P. 207
Gilman P.A., 1980, Highlights of Astronomy **5**, 91
Gilman P.A., 1986, in Sturrock P.A., Holzer T.E, Mihalas D.M, Ulrich R.K. (eds.) Physics of the Sun, Vol. 1, (Dordrecht: D. Reidel), P. 95
Gilman P.A., 1992, in Harvey K.L. (ed.) The Solar cycle, ASP Conf. Series., **27**, P. 241
Gilman P.A., Howard R., 1984, ApJ **283**, 385
Gilman P.A., Howard R., 1986, ApJ **303**, 480
Gnevyshev M.N., Ohl A.I., 1948, Astron. Zh. **25(1)**, 18
Godoli G., Mazzuconi F., 1979, Solar Phys. **64**, 247
Godoli G., Mazzuconi F., 1982, A&A **116**, 188
Gokhale M.H., Sivaraman K.R, 1981, J. Astrophys. Astron. **2**, 365.
Gokhale M.H., Hiremath K.M., 1984, BASI **12**, 398
Gokhale M.H., Hiremath K.M., 1993, ApJ **407**, 366
Gokhale M.H., Javaraiah J., 1990a, MNRAS **243**, 241
Gokhale M.H., Javaraiah J., 1990b, in: Priest E.R., Krishan V. (eds.) Basic Plasma Process on the Sun, IAU Symp. **142**, 119

Gokhale M.H., Javaraiah J., 1992, Solar Phys. **138**, 399
Gokhale M.H., Javaraiah J.,1995, Solar Phys. **156**, 157
Gokhale M.H., Javaraiah J., Hiremath K.M., 1990, in: Stenflo J.O.(ed.) Solar Photosphere: Structure, Convection and Magnetic fields, IAU Symp. **138**, 375
Gokhale M.H., Javaraiah J., Kutty K.N., Varghese B.A., 1992, Solar Phys. **138**, 35
Goode P.R., Dziembowski W.A., 1991, Nature **349**, 223
Goode P.R., Dziembowski W.A., 1993 in: Brown T.M. (ed.) Seismic Investigation of the Sun and Stars, ASP Conf. Series **42**, 217
Goode P. R., Dziembowski W. A., Korzennik S. G., Rhodes E.J., Jr., 1991, ApJ **367**, 649
Gough D.O., Stark P.B., 1993a, in: Brown T.M. (ed.) Seismic Investigation of the Sun and Stars, ASP Conf. Series **42**, 221
Gough D.O., Stark P.B., 1993b, ApJ **415**, 376
Gough D.O., Kosovichev A.G., Sekii T., Libbrecht K.G., Woodard M.F., 1993, in: Werner W.W., Baglin A. (eds.) Inside the Stars, IAU Coll. 137, ASP Conf. Series., **40**, 93
Gupta S.S., 1994, Ph D. Thesis, Ravishankar University
Gupta S.S., Sivaraman K.R., Howard R.F., 1999, Solar Phys. **188**, 225
Hale G.E., Ellerman F., Nicholson S.B., Joy A.H., 1919, ApJ **49**, 153
Hanslmeier A., Lustig G., 1986, A&A **154**, 227
Hathaway D.H., 1996, ApJ **460**, 1027
Hathaway D.H., 1998, Balasubramaniam K.S., Harvey J.W., Rabin D. M. (eds.), Synoptic Solar Physics, ASP Conf. Series **140**, 47.
Hathaway D.H., Wilson R.M., 1990, ApJ **357**, 271.
Hathaway D.H., Gilman P.A., Harvey J.W., Hill F., Howard R.F., Jones H.P., Kasher J.C., Leibacher J.W., Pinter J.A., Simon G.W., 1996, Science **272**, 1306
Harvey K.L., Zwaan C., 1993, Solar Phys. **148**, 85
Hill F., 1990, Solar Phys. **128**, 321
Hill F., 1998, Balasubramaniam K.S., Harvey J.W., Rabin D. M. (eds.), Synoptic Solar Physics, ASP Conf. Series **140**, 33.
Hiremath K.M., 1995, Ph D. Thesis, Bangalore University
Hiremath K.M., Gokhale M. H., 1995, ApJ **155**, 295
Howard R., 1978, Rev. Geophys. Space Phys. **16**, 721
Howard R., 1974, Solar Phys. **38**, 283
Howard R., 1984, ARAA **22**, 131
Howard R.F., 1991, Solar Phys. **135**, 43
Howard R., 1996a, ARAA **34**, 75
Howard R., 1996b, Solar Phys. **169**, 293
Howard R., Harvey J., 1970, Solar Phys. **12**, 23
Howard R., LaBonte B.J., 1980, ApJ **239**, L33
Howard R., LaBonte B.J., 1981, Solar Phys. **74**, 131
Howard R., LaBonte J., 1983, in: Stenflo J.O. (ed.) Solar and Stellar Magnetic Fields: Origin and Coronal Effects, IAU Symp. **102**, 101
Howard R.F., Gilman P.A., 1986, ApJ **307**, 389
Howard R., Gilman P.A., Gilman P.I., 1984, ApJ **283**, 373
Howard R.F., Gupta S.S., Sivaraman K.R., 1999, Solar Phys. **186**, 25
Howard R., Boyden J.E., Bruning D.H., Clark M.K., Crist H.W., LaBonte B.J., 1983, Solar Phys. **87**, 195
Howard R.F., Kichatinov L.L., Bogart R.S., Ribes E., 1991, in Cox A.N., Livingston W.C., Matthews (eds.), Solar Interior and Atmosphere, The University of Arizona Press, Tucson, P. 748

Howe R., 1998, in: Korzennik S.G., Wilson A. (eds.) Structure and Dynamics of the Interior of the Sun and Sun-Like Stars, ESA SP-418, P. 669
Howe R., Christensen-Dalsgaard J., Hill F., Komm R.W., Larsen R.M., Schou J., Thompson M.J., Toomre J., 2000a, Science **287**, 2456
Howe R., Christensen-Dalsgaard J., Hill F., Komm R.W., Larsen R.M., Schou J., Thompson M.J., Toomre J., 2000b, ApJ **533**, L163
Ichimoto K., Kubota J., Suzuki M., Tohmura I., Kurokawa H., 1985, Nature **316**, 422
Javaraiah J., 1996, BASI **24**, 351
Javaraiah J., 1998, in: Korzennik S.G., Wilson A. (eds.) Structure and Dynamics of the Interior of the Sun and Sun-Like Stars, ESA SP-418, P. 809
Javaraiah J., 1999, Solar Phys. **189**, 289
Javaraiah J., 2000, J. Astrophys. Astron. (accepted).
Javaraiah J., Gokhale M.H., 1995, Solar Phys. **158**, 173
Javaraiah J., Gokhale M.H., 1997a, Solar Phys. **170**, 389
Javaraiah J., Gokhale M.H., 1997b, A&A **327**, 795
Javaraiah J., Komm R.W., 1999, Solar Phys. **184**, 41
Jose P.D., 1965, Astron. J. **70**, 193
Kambry M.A., Nishikawa J., 1990, Solar Phys. **126**, 89
Kliorin N.I., Ruzmaikin A.A., 1984, AZh, **10**, 826 (Soviet Astron. Lett., **10**, 390)
Komm R. W., 1995, Solar Phys. **156**, 17
Komm R.W, Howard R.F., Harvey J.W., 1993a, Solar Phys. **143**, 19
Komm R.W, Harvey J.W., Howard R.F., 1993b, in: Brown T.M. (ed.) Seismic Investigation of the Sun and Stars, ASP Conf. Series **42**, 269
Komm R.W, Howard R.F., Harvey J.W., 1994, Solar Phys. **151**, 15
Komm R.W., Howard R.F., Harvey J.W., 1993c, Solar Phys. **147**, 207
Kosovichev A.G., 1996, ApJ **469**, L61
Kosovichev A.G., Schou J., 1997, ApJ **482**, L207
Kosovichev A.G., Duvall T.L., Jr., 1999, Current Science **77**, 1467
Koyama H., 1985, Observation of Sunspots 1947-1984, kawadeshoboshinsha, Tokyo.
Kuklin G.V., 1976, in: Bumba V., Kleczek J. (eds.) Basic Mechanisms of Solar Activity, IAU Symp. **71**, Reidel, Hingham, P. 147
LaBonte B.J., Howard R.F., 1982a, Solar Phys. **75**, 161
LaBonte B.J., Howard R.F., 1982b, Solar Phys. **80**, 361
Landscheidt T., 1999, Solar Phys. **189**, 415
Layzer D., Rosner R., Doyle H. T., 1979, ApJ **229**, 1126
Li Y., 1997, Solar Phys. **170**, 437
Li K., 1999, A&A **345**, 1006
Libbrecht K.G., 1989, ApJ **336**, 1092
Libbrecht K.G., Morrow C.A., 1991, in Cox A.N., Livingston W.C., Matthews (eds.), Solar Interior and Atmosphere, The University of Arizona Press, Tucson, P. 479
Liritzis I., 1995, Solar Phys. **161**, 29
Livingston W.C., 1969, Solar Phys. **9**, 448
Lustig G., 1983, A&A **125**, 355
Lustig G., Dvorak R., 1984, A&A **141**, 105
Lustig G., Wöhl H., 1991, A&A **249**, 528
Makarov V.I., 1994, Solar Phys. 150, 359
Makarov V.I., Sivaraman K.R., 1983, Solar Phys. **85**, 215
Makarov V.I., Sivaraman K.R., 1986, Soln. Dann. **No. 9**, 64
Makarov V.I., Sivaraman K.R., 1989, Solar Phys. **123**, 367
Maunder E.W., 1922, Brit. Astron. Assoc. J. **32**, 140.

Merzlyakov V.L., 1997, Solar Phys. **170**, 425
Mestel L., Weiss N.O., 1987, MNRAS **226**, 123
Meunier N., Nesme-Ribes E., Collin B., 1997, A&A **319**, 683
Moreno-Insertis F., 1997, Mem. S.A.It. **68–2**, 491
Muller R., 1985, Solar Phys. **100**, 237
Nesme-Ribes E., Ferreira E.N., Vince I., 1993, A&A **276**, 211
Nesme-Ribes E., Ferreira E.N., Sadourny R., Le Treut H. Li Z.X., 1993, J. Geophys. Res. **98**, 18 923
Nesme-Ribes E., Baliunas S.L., Sokoloff D., August 1996, Scientific American, P. 31
Newton H.W., Nunn M.L., 1951, MNRAS **111**, 413
Nikonova M. V., Klochek N.V., Palamarchuk L.E., 1998, in: Deubner F.L. et al. (eds.) New Eyes to See Inside the Sun and Stars, IAU Symp. **185**, P. 119
Oliver R., Ballester J.L., 1995, Solar Phys. **156**, 145
Otáola J.A., Zenteno G., 1983, Solar Phys. **89**, 209
Parker E.N., 1979a, Cosmic Magnetic Field, Clarendon Press, Oxford
Parker E.N., 1979b, ApJ **232**, 282
Parker E.N.,1987, in Durney B.R., Sofia S. (eds.), 'The Internal Solar Angular Velocity', Astrophysics and Space Science Library **137**, 289
Parker E.N., 1993, ApJ **408**, 707
Paternó I., 1978, Proc. Workshop on Solar Rotation, Publ. Catania No. 162, P. 11
Paternó I., Spadaro D., Zappalá R.A., Zuccarello F., 1991, A&A **252**, 337
Piddington J.H., 1976, in: Bumba V., Kleczek J. (eds.) Basic Mechanisms of Solar Activity, IAU Symp. **71**, Reidel, Hingham, P. 389
Pierce A.K., Lopresto J.C., 1984, Solar Phys. **93**, 155
Polygiannakis J.M., Moussas X., Sonett C.P., 1996, Solar Phys. **163**, 193
Priest E.R., 1982, Solar magnetic hydrodynamics, D. Riedel Publishing Company, Dordrecht, Holland
Ribes J.C., Nesme-Ribes E., 1994, A&A **276**, 549
Ribes E., Mein P., Mangeny A., 1985, Nature **318**, 170
Ribes E., Ribes J.C., Barthalot R., 1987, Nature **326**, 52
Roberts P.H., 1972, Phil. Trans. of the Royal Soc. of London, Ser. A272, 663
Richardson R.S., Schwarschild M., 1953, *Acad. Naz. Linc. Fond. Ales. Volta. Atti Conv.* **11**, 228
Rosner R., Weiss N.O., 1992, in: Harvey K.L. (ed.) The Solar cycle, ASP Conf. Series. **27**, 511
Rüdiger G., Kichatinov L.L., 1990, A&A **236**, 503
Sakurai K., 1977, Nature **269**, 401
Schou J., 1990, in Gough D., Toomre J. (eds.), Challenges to Theories of the Structure of Moderate - Mass Stars, Lecture Notes in Physics, Springer **388**, 81
Schou J., 1998, ApJ **505**, 390
Schou J., 1999, ApJ **523**, L181
Schröter E.H., 1985, Solar Phys. **100**, 141
Schröter E.H., Wöhl H. 1978, Proc. Workshop on Solar Rotation, Publ. Catania No. 162, P.35
Schröter E.H., Soltan D., Wöhl H., Vázques M., 1978, Proc. Workshop on Solar Rotation, Publ. Catania No. 162, P. 180
Schüssler M., 1981, A&A **94**, L17
Schüssler M., 1987, in: Durney B.R., Sofia S. (eds.) The Internal Solar Angular Velocity, Astrophysics and Space Science Library **137**, 303
Sheeley N.R., Jr., Nash A.G., Wang Y.-M., 1987, ApJ **319**, 481
Singh J., Bappu M.K.V., 1981, Solar Phys. **71**, 161

Sivaraman K.R., Guptha S.S., Howard R. F., 1993, Solar Phys. **146**, 27
Snodgrass H.B., 1983, ApJ **270**, 288
Snodgrass H.B., 1984, Solar Phys. **94**, 13
Snodgrass H.B., 1991, ApJ **383**, L85
Snodgrass H.B., 1992, in: Karen L. Harvey (ed.) The Solar Cycle, ASP Conf. Series **27**, 205.
Snodgrass H.B., Dailey S.B., 1996, Solar Phys. **163**, 21
Snodgrass H.B., Howard R., 1985, Solar Phys. **95**, 221
Snodgrass H.B., Wilson P.R., 1987, Nature **328**, 696
Snodgrass H.B., Howard R., Webster L., 1984, Solar Phys. **90**, 199
Sokoloff D., Ribes E.N., 1994, A&A **288**, 293
Spruit H.C., 1990, in : Berthomiu G., Crivier M. (eds.), Inside the Sun, Kluwer Academic Publ., Dordrecht, Holland, P. 415
Seymore P.A.H., Willmott M. Turner A., 1992, Vistas Astro. **35**, 39
Stenflo J.O., 1974, Solar Phys. **36**, 495
Stenflo J.O., 1977, A&A **61**, 797
Stenflo J.O., 1989, A&A **210**, 403
Stenflo J.O., 1988, Astrophys. Space Sci. **144**, 321
Stenflo J.O., 1992, in: Karen L. Harvey (ed.) The Solar Cycle, ASP Conf. Series **27**, 421
Stenflo J.O., Vogel M., 1986, Nature **319**, 285
Stix M., 1981, A&A **93**, 339
Stix M., 1991. Geophys. Astrophys. Fluid Dyn. **62**, 211
Swinson D.B., Koyama H. Saito T., 1986, Solar Phys. **106**, 35
Sýkora J., Storini M., 1997, Hvar Obs. Bull. **21(1)**, 21
Takahashi K., 1968, Solar Phys. **3**, 598
Tang F., Howard R., Adkins J.M., 1984, Solar Phys. **91**, 75
Ternullo M., 1990, Solar Phys. **127**, 29
Ternullo M., Zappalà R.A., Zuccarello F., 1981, Solar Phys. **74**, 111
Tomczyk S., Schou J., Thompson M.J., 1995, ApJ **448**, L57
Tuominen J., 1952, Z. Astrophys. **30**, 261
Tuominen J., Kyöläinen J., 1981, Solar Phys. **74**, 153
Tuominen J., Kyöläinen J., 1982, Solar Phys. **79**, 161
Tuominen I., Virtanen H., 1987, in: Durney B.R., Sofia S. (eds.) The Internal Solar Angular Velocity, Astrophysics and Space Science Library **137**, P. 83
Tuominen J. Tuominen I., Kyöläinen J., 1983, MNRAS **205**, 691
Thomson D.J., 1990, Phil. Trans. of the Royal Soc. of London, Ser. **A330**, 601
Ulrich R.K., Bertello L., 1996, ApJ **465**, L65
Ulrich R.K., Boyden J.E., Webster L., Snodgrass H. B., Padilla, S.P., Gilman P., Shieber T., 1988, Solar Phys. **117**, 291
Ulrych T.J., Bishop T.N., 1975, Rev. Geophys. Space Phys. **13**, 183
Usoskin I.G., Mursula K., Kovaltsov G.A., 2000, A&A **354**, L33
Verma S.D., 1986, in: Bhatnagar K.B. (ed), Space Dynamics and Celestial Mechanics, D. Reidel Publishing Company, P. 143
Verma V.K., 1993, ApJ **403**, 797
Vizoso G., Ballester J.L., 1990, A&A **229**, 540.
Waldmeier M., 1955, Ergebnisse und Probleme der Sonnenforschung, 2. Aufl., Akad. Verlagsges., Leipzig.
Waldmeier M., 1961, The Sunspot Activity in the Years 1610-1960, Schulthess and Co. AG, Zürich.
Walther G., 1998, Phys. Rev. Lett. **79**, 4522
Wang Y.-M., Sheeley N.R., Jr., 1989, Solar Phys. **124**, 81

Ward, F.: 1964, Pure Appl. Geophys. **58**, 157
Ward, F.: 1965a, ApJ **141**, 534
Ward, F.: 1965b, Pure Appl. Geophys. **60**, 126
Ward F., 1966, ApJ **145**, 416
White O.R., Trotter D.E., 1977, ApJ Suppl. **33**, 391
Wilcox J.M., Howard R., 1970, Solar Phys. **13**, 251
Wilcox J.M., Schatten K.H., Tannenbaum A.S., Howard R., 1970, Solar Phys. **14**, 255
Wilson P.R., 1987, Solar Phys. **110**, 59
Wilson R.M., 1988, Solar Phys. **117**, 269
Wilson P.R., Altrock R.C., Harvey K.L., Martin S.F., Snodgrass H.B., 1988, Nature **333**, 748
Wittmann A.D., Xu Z.T., 1987, A&AS **70**, 83
Wolf C.L., 1976, ApJ **205**, 612
Wolf R., 1852, Acad. Sci. Compt. Rend. **35**,704
Wodd K.D., 1972, Nature **240**, 91
Wood R.M., Wood K.D., 1965, Nature **208**, 129
Woodard M. F., Libbrecht K. G., 1993a, ApJ **402**, L77
Woodard M. F., Libbrecht K. G., 1993b, Science **260**, 1778
Yi W., 1992, J. The Royal Astron. Soc. Canada **86**, 635
Yoshimura H., 1981, ApJ **247**, 1102
Yoshimura H., Kambry M.A., 1993, Solar Phys. **143**, 205
Yule G.D., Kendall M.G., 1957, An Introduction to the Theory of Statistics, 14th Edition (Third impression), Charles Griffin & Co., London, P. 470
Zappalà R.A., Zuccarello F., 1991, A&A **242**, 480
Zaqarashvili T.V., 1997, ApJ **487**, 930
Zirin H., 1966, The Solar Atmosphere, Blaisdell Publishing Company, printed in USA
Zuccarello F., 1993, A&A **272**, 587